JSCSEN 89(1)1-140(2024)

ISSN 1820-7421(Online)

Journal of the Serbian Chemical Society

VOLUME 89

No 1

BELGRADE 2024

Available on line at

www.shd.org.rs/JSCS/

The full search of JSCS is available through DOAJ DIRECTORY OF OPEN ACCESS JOURNALS www.doaj.org

The **Journal of the Serbian Chemical Society** (formerly Glasnik Hemijskog društva Beograd), one volume (12 issues) per year, publishes articles from the fields of chemistry. The **Journal** is financially supported by the **Ministry of Education, Science and Technological Development of the Republic of Serbia.**

Articles published in the **Journal** are indexed in **Clarivate Analytics products: Science Citation Index-Expanded™** – accessed *via* **Web of Science®** and **Journal Citation Reports®**.

Impact Factor announced on 28 June, 2023: **1.000; 5-year Impact Factor**: **1.100**.

Articles appearing in the **Journal** are also abstracted by: **Scopus, Chemical Abstracts Plus (CAplus℠), Directory of Open Access Journals, Referativnii Zhurnal (VINITI), RSC Analytical Abstracts, EuroPub, Pro Quest** and **Asian Digital Library.**

Publisher:	**Serbian Chemical Society**, Karnegijeva 4/III, P. O. Box 36, 1120 Belgrade 35, Serbia tel./fax: +381–11–3370–467, E-mails: **Society** – shd@shd.org.rs; **Journal** – jscs@shd.org.rs Home Pages: **Society** – http://www.shd.org.rs/, **Journal** – http://www.shd.org.rs/JSCS/
Internet Service:	Contents, Abstracts and full papers (from Vol 64, No. 1, 1999) are available in the electronic form at the Web Site of the **Journal** (http://www.shd.org.rs/JSCS/).
Former Editors:	**Nikola A. Pušin** (1930–1947), **Aleksandar M. Leko** (1948–1954), **Panta S. Tutundžić** (1955–1961), **Miloš K. Mladenović** (1962–1964), **Đorđe M. Dimitrijević** (1965–1969), **Aleksandar R. Despić** (1969–1975), **Slobodan V. Ribnikar** (1975–1985), **Dragutin M. Dražić** (1986–2006).
Editor-in-Chief:	BRANISLAV Ž. **NIKOLIĆ**, Serbian Chemical Society (E-mail: jscs-ed@shd.org.rs)
Deputy Editor:	DUŠAN **SLADIĆ**, Faculty of Chemistry, University of Belgrade
Sub editors:	
Organic Chemistry	DEJAN **OPSENICA**, Institute of Chemistry, Technology and Metallurgy, University of Belgrade JÁNOS **CSANÁDI**, Faculty of Science, University of Novi Sad
Biochemistry and Biotechnology	OLGICA **NEDIĆ**, INEP – Institute for the Application of Nuclear Energy, University of Belgrade
Inorganic Chemistry	MILOŠ **ĐURAN**, Serbian Chemical Society
Theoretical Chemistry	IVAN **JURANIĆ**, Serbian Chemical Society
Physical Chemistry	LJILJANA **DAMJANOVIĆ-VASILIĆ**, Faculty of Physical Chemistry, University of Belgrade
Electrochemistry	SNEŽANA **GOJKOVIĆ**, Faculty of Technology and Metallurgy, University of Belgrade
Analytical Chemistry	RADA **BAOŠIĆ**, Faculty of Chemistry, University of Belgrade
Polymers	BRANKO **DUNJIĆ**, Faculty of Technology and Metallurgy, University of Belgrade
Thermodynamics	MIRJANA **KIJEVČANIN**, Faculty of Technology and Metallurgy, University of Belgrade
Chemical Engineering	TATJANA **KALUĐEROVIĆ RADOIČIĆ**, Faculty of Technology and Metallurgy, University of Belgrade
Materials	RADA **PETROVIĆ**, Faculty of Technology and Metallurgy, University of Belgrade
Metallic Materials and Metallurgy	ANA **KOSTOV**, Mining and Metallurgy Institute Bor, University of Belgrade
Environmental and Geochemistry	VESNA **ANTIĆ**, Faculty of Agriculture, University of Belgrade
History of and Education in Chemistry	DRAGICA **TRIVIĆ**, Faculty of Chemistry, University of Belgrade
English Language Editors:	LYNNE **KATSIKAS**, Serbian Chemical Society VLATKA **VAJS**, Serbian Chemical Society JASMINA **NIKOLIĆ**, Faculty of Technology and Metallurgy, University of Belgrade
Technical Editors:	VLADIMIR **PANIĆ**, Institute of Chemistry, Technology and Metallurgy, University of Belgrade, MARIO **ZLATOVIĆ**, Faculty of Chemistry, University of Belgrade
Journal Manager & Web Master:	MARIO **ZLATOVIĆ**, Faculty of Chemistry, University of Belgrade
Office:	VERA **ĆUŠIĆ**, Serbian Chemical Society

Editorial Board

From abroad: **R. Adžić**, Brookhaven National Laboratory (USA); **A. Casini**, University of Groningen (The Netherlands); **G. Cobb**, Baylor University (USA); **D. Douglas**, University of British Columbia (Canada); **G. Inzelt**, Etvos Lorand University (Hungary); **J. Kenny**, University of Perugia (Italy); **Ya. I. Korenman**, Voronezh Academy of Technology (Russian Federation); **M. D. Lechner**, University of Osnabrueck (Germany); **S. Macura**, Mayo Clinic (USA); **M. Spiteller**, INFU, Technical University Dortmund (Germany); **M. Stratakis**, University of Crete (Grecce); **M. Swart**, University de Girona (Cataluna, Spain); **G. Vunjak-Novaković**, Columbia University (USA); **P. Worsfold**, University of Plymouth (UK); **J. Zagal**, Universidad de Santiago de Chile (Chile).

From Serbia: **B. Abramović**, **V. Antić**, **R. Baošić**, **V. Beškoski**, **J. Csanadi**, **Lj. Damjanović-Vasilić**, **A. Dekanski**, **V. Dondur**, **B. Dunjić**, **M. Đuran, S. Gojković**, **I. Gutman**, **B. Jovančićević**, **I. Juranić**, **T. Kaluđerović Radoičić**, **L. Katsikas**, **M. Kijevčanin**, **A. Kostov**, **V. Leovac**, **S. Milonjić**, **V.B. Mišković-Stanković**, **O. Nedić**, **B. Nikolić**, **J. Nikolić**, **D. Opsenica**, **V. Panić**, **M. Petkovska**, **R. Petrović**, **I. Popović**, **B. Radak**, **S. Ražić**, **D. Sladić**, **S. Sovilj**, **S. Šerbanović**, **B. Šolaja**, **Ž. Tešić**, **D. Trivić**, **V. Vajs, M. Zlatović**.

Subscription: The annual subscription rate is **150.00 €** including postage (surface mail) and handling. For Society members from abroad rate is **50.00 €**. For the proforma invoice with the instruction for bank payment contact the Society Office (E-mail: shd@shd.org.rs) or see JSCS Web Site: http://www.shd.org.rs/JSCS/, option Subscription.

Godišnja pretplata: Za članove SHD: **2.500,00 RSD**, za penzionere i studente: **1000,00 RSD**, a za ostale: **3.500,00 RSD**:za organizacije i ustanove: **16.000,00 RSD**. Uplate se vrše na tekući račun Društva: **205-13815-62**, poziv na broj **320**, sa naznakom "pretplata za JSCS".

Nota: Radovi čiji su svi autori članovi SHD prioritetno se publikuju.

Odlukom Odbora za hemiju Republičkog fonda za nauku Srbije, br. 66788/1 od 22.11.1990. godine, koja je kasnije potvrđena odlukom Saveta Fonda, časopis je uvršten u kategoriju međunarodnih časopisa (**M-23**). Takođe, aktom Ministarstva za nauku i tehnologiju Republike Srbije, 413-00-247/2000-01 od 15.06.2000. godine, ovaj časopis je proglašen za publikaciju od posebnog interesa za nauku. **Impact Factor** časopisa objavljen 28. juna 2023. godine je **1,000**, a petogodišnji **Impact Factor 1,100**.

Journal of the Serbian Chemical Society
JSCS-info@shd.org.rs • www.shd.org.rs/JSCS

J. Serb. Chem. Soc. Vol. 89, No. 1 (2024)

CONTENTS*

Organic Chemistry

M. S. Nešić, *M. D. Nešić* and *N. S. Radulović*: Assignment of NMR spectral data of diastereomeric tetrahydrofuranyl acetals directly from their mixture by spectral simulation 1

Biochemistry and Bioengineering

S. M. Stajčić, *L. L. Pezo*, *G. S. Ćetković*, *J. M. Čanadanović-Brunet*, *A. I. Mandić*, *V. T. Tumbas Šaponjac*, *J. J. Vulić*, *V. N. Travičić* and *M. M. Belović*: Antioxidant activity according to bioactive compounds content in dried pumpkin waste 13

Inorganic Chemistry

L. Todan, *D. C Culita*, *M. E. Soare*, *R. M. Ion*, *R. C. Fierascu* and *M. Maganu*: Immobilization of natural betalain pigments in inorganic hosts 29

Theoretical Chemistry

C.-W. Liu, *M.-H. Liu*, *T.-M. Wang*, *C.-L. Chen* and *T.-H. Ting*: Study of the metal ion adsorption capacity of palygorskite by computer simulation 39

Physical Chemistry

R. K. Allabergenova, *D. A. Bobkova*, *E. M. Borodina*, *T. A. Kryuchkova*, *E. B. Markova*, *T. F. Sheshko*, *N. N. Lobanov* and *A. G. Cherednichenko*: Synthesis, characterization, and catalytic properties of $GdCoO_3$ for dry reforming of methane 51

Elecrochemistry

H. D. Tran, *U. P. N. Tran* and *D. Q. Nguyen*: [BMIm][PF6]/silicon oil/multi-walled carbon nanotubes paste electrode: Electrochemical properties and application for lead and cadmium ion determinations 63

Polymers

N. M. Edres, *I. A. Buniyat-Zadeh*, *S. B. Aliyeva*, *S. M. Turp* and *R. M. Alosmanov*: Structure and thermal stability of phosphochlorinated polybutadiene/carbon black composite synthesized *via* oxidative chlorophosphorylation reaction 79

Materials

R. Brahmi, *K. Diaf*, *Z. Elbahri* and *M. Baitiche*: Preparation and *in-vitro* evaluation of single and bi-layered beeswax-based microparticles for colon-specific delivery of mesalamine 91

Chemical Engineering

S. Toufouki, *A. Ali*, *Y. Wang*, *R. Li*, *Y. Cao* and *S. Yao*: Deep eutectic solvents formed by pharmaceutical ingredients and their potential influences on solid preparations 107

Environmental

R. Zein, *H. Fathony*, *P. Ramadhani* and *D. Deswati*: Facile chemical activation process of kapok husk as a low-cost biosorbent for removal methylene blue dye in aqueous solution 123

Published by the Serbian Chemical Society
Karnegijeva 4/III, P.O. Box 36, 11120 Belgrade, Serbia
Printed by the Faculty of Technology and Metallurgy
Karnegijeva 4, P.O. Box 35-03, 11120 Belgrade, Serbia

* For colored figures in this issue please see electronic version at the Journal Home Page: http://www.shd.org.rs/JSCS/

Journal of the Serbian Chemical Society
JSCS@tmf.bg.ac.rs • www.shd.org.rs/JSCS

J. Serb. Chem. Soc. *89* (1) 1–11 (2024)
JSCS–5701

Original scientific paper
Published 12 February 2024

Assignment of NMR spectral data of diastereomeric tetrahydrofuranyl acetals directly from their mixture by spectral simulation

MILAN S. NEŠIĆ, MILICA D. NEŠIĆ and NIKO S. RADULOVIĆ*#

Department of Chemistry, Faculty of Science and Mathematics, University of Niš, Višegradska 33, 18000 Niš, Serbia

(Received 14 June, revised 3 August, accepted 27 August 2023)

Abstract: In this study, an NMR spectral analysis of the mixture of diastereomeric acetals, synthesized from 2,3-dihydrofurane and a racemic mixture of citronellol, was performed. ^{1}H-NMR full spin analysis was achieved by manually adjusting δ_H and J values (previously calculated using the Spartan software) to fit the experimentally available values, followed by further optimization using MestreNova software. The simulated ^{1}H- and ^{13}C-NMR spectra of individual diastereomers, as well as their superimposed and summed spectra, were compared with the obtained experimental spectra. Spin simulation of proton signals was particularly useful for the assignment of the diastereotopic protons of tetrahydrofuranyl moiety and diastereomer discrimination. The NMR spectral data of individual diastereomers – chemical shifts, coupling constants, HMBC and NOESY interactions were systematized in appropriate tables and schemes. To the best of our knowledge, this is for the first time that the complete assignment of tetrahydrofuranyl moiety was performed, and the data obtained herein may be of great importance for the utilization of this protecting group in the future.

Keywords: tetrahydrofuran; citronellol; spectral assignment; spin simulation; diastereomers; mixture.

INTRODUCTION

The acetal moiety can be found in many natural, as well as synthetic, organic compounds, thus a lot of research is focused on the development of synthetic procedures for the conversion of alcohols and aldehydes into acetals.[1–3] In addition to being protective groups for alcohols and aldehydes, acetals can also be transformed into a range of other functionalities, making them valuable synthetic intermediates. They can be allylated,[4] undergo substitution,[5–7] and other trans-

* Corresponding author. E-mail: nikoradulovic@yahoo.com
# Serbian Chemical Society member.
https://doi.org/10.2298/JSC230614054N

formations,[8,9] and some, such as tetrahydrofuranyl (THF) and tetrahydropyranyl (THP) acetals,[10–12] can undergo reductive ring cleavage,[13] a synthetically very useful transformation.

Tetrahydrofuranyl (THF) and tetrahydropyranyl (THP) acetals exhibit remarkable stability in the presence of strong bases (*e.g.*, LDA, *terc*-BuOK, HMDS), reducing agents (*e.g.*, H_2/Rh, H_2/Ni, H_2/Pd; $NaBH_4$, $LiAlH_4$, Na/NH_3), organometallics (*e.g.*, RLi, RMgX, RCuLi), certain electrophilic reagents (*e.g.*, RCHO, RX) and specific oxidizing reagents (*e.g.*, $KMnO_4$, OsO_4).[1,2] One of the main advantages of THF and THP acetals, unlike the other alcohol-protecting groups, is their great stability under basic and neutral conditions combined with very easy deprotection under mildly acidic conditions, such as diluted acetic acid in aqueous tetrahydrofuran.[14,15] These can be selectively removed in the presence of other alcohol-protecting groups, such as benzyl ethers, various esters and *t*-butyldiphenylsilyl ethers, which can also be selectively removed using H_2,Pd/C or Na/NH_3,[16,17] basic conditions[1,18] and fluoride-containing reagents,[1,18,19] respectively, the conditions under which THF and THP acetals are stable.[1] These acetals display different reactivity compared to other acetals, such as benzylidene acetals used for diol protection, which can be selectively removed using H_2/ /$Pd(OH)_2$,[16] and dimethyl acetals, which exhibit slightly higher stability under mildly acidic conditions.[20,21] THF acetals also find utility in protecting other functional groups, such as amine and thiol groups in peptides.[22,23] Subtle distinctions in the stability of THP and THF acetals indicate the potential for THF acetals to be hydrolyzed under slightly gentler conditions compared to THP acetals.[14]

Citronellol (**1**, Fig. 1) is an acyclic monoterpene alcohol known for its distinctive rose-like scent, found in the essential oils of various plant species, and valued for its diverse pharmacological activities.[24] It is widely used as a fragrance ingredient in the perfume industry and in formulations targeting mosquito repellency.[25] Derivatives of citronellol, including rose-oxide (**2**, Fig. 1) with a herbal-floral odor, obtained through the photooxidation of citronellol,[26] and acetaldehyde methyl-citronellyl acetal (**3**, Fig. 1) with a refreshing floral-citrus fragrance, obtained through the transacetalization of acetaldehyde dimethyl acetal with citronellol,[27] have also found significant applications in the fragrance industry.

The tetrahydrofuranyl acetal of citronellol is characterized by an intense, warm, floral-honey fragrance reminiscent of the fragrance of linden bee honey.[27] Due to its attractive smell, simplicity of preparation, and stability in neutral and elevated pH environments,[1,2] it can find practical use as a component of a fragrance composition intended for perfuming soaps, detergents, and cosmetics.[27]

Despite such great application and convenience in synthesis and industry, THP and THF acetals are less preferred or even avoided in some cases. One of

the reasons may be that the NMR spectra of these acetals are very complex, especially the part of the spectrum originating from the THF or THP group, which is difficult to analyze. Also, considering that the chemical shifts are around 2 and 4 ppm in the ^{1}H-NMR, and in the range of 20–70 ppm in the ^{13}C-NMR spectrum, they can overlap (^{1}H-NMR) or be very close (^{13}C-NMR) to the signals originating from the rest of the molecule which can make the spectral assignment of these acetals uncertain. In addition, commercially available monoterpene alcohols often represent a mixture of enantiomers, thus the obtained tetrahydrofuranyl acetals of these alcohols will represent a mixture of chromatographically difficult-to-separate diastereomers, due to the newly formed chiral center on the tetrahydrofuran moiety. In order to address primarily the difficulties in the NMR assignment of THF acetals, more specifically those of compound **4** (Fig 1), directly from a mixture of diastereomers, herein we performed a detailed analysis of the corresponding NMR spectra of **4**, and utilizing molecular modeling and spectral simulation tools, this resulted in the complete assignment of ^{1}H- and ^{13}C--NMR spectra of **4**. The data provided could be generally used for the assignments of other THF acetals, significantly facilitating future work on this protecting group.

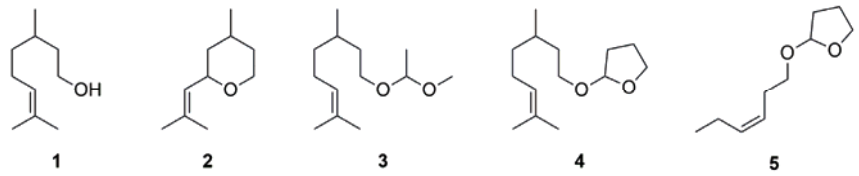

Fig. 1. Citronellol (**1**) and its derivatives: rose oxide (**2**), acetaldehyde methyl-citronellyl acetal (**3**), tetrahydrofuranyl acetal of citronellol (**4**) and tetrahydrofuranyl acetal of *cis*-3-hexen-1-ol (**5**).

EXPERIMENTAL

General procedures

All herein used reagents (citronellol, 2,3-dihydrofuran, *cis*-3-hexen-1-ol, *p*-toluenesulfonic acid) and solvents (hexane and diethyl-ether) were obtained from commercial sources (Sigma–Aldrich; Merck; Carl Roth, Karlsruhe, Germany) and used as received.

Gas chromatography/mass spectrometry (GC/MS) analysis was performed on a Hewlett––Packard 6890N gas chromatograph equipped with a fused silica capillary column DB-5MS (5 % polydiphenylsiloxane, 95 % polydimethylsiloxane, 30 m×0.25 mm, film thickness 0.25 μm; Agilent Technologies, Santa Clara, CA, USA) and coupled with a 5975B mass selective detector from the same company. The injector and interface were operated at 250 and 320 °C, respectively. The oven temperature was raised from 70 to 315 °C at a heating rate of 5 °C/min and then isothermally held for 30 min. As a carrier gas helium was used with a flow of 1.0 ml/min. The samples, 1 μl of the sample solutions in diethyl ether (10 mg dissolved in 1 ml), were injected in a split mode (split ratio 40:1). Mass selective detector was operated at the ionization energy of 70 eV, in the 35–850 amu range and scanning speed of 0.34 s. The relat-

ive abundance of the reaction mixture components was calculated from the peak areas without the use of correction factors. Retention indices (*RI*s) were determined using a mixture of *n*-alkanes from C8−C40. Analytical TLC separations were done on coated Al silica gel plates (Kieselgel 60 F254, 0.2 mm, Merck, Darmstadt, Germany). TLC plates were initially visualized by UV light (254 nm) and then sprayed with 50 mass % aqueous H_2SO_4 followed by heating. Infrared (IR) measurements (attenuated total reflectance) were carried out using a Thermo Nicolet 6700 FTIR spectrometer (Thermo Fisher Scientific, Waltham, MA, USA). Microanalysis of carbon and hydrogen were carried out on a Carlo Erba 1106 microanalyzer (Carlo Erba Strumentazione, Italy). High-resolution mass spectrometry (HRMS) analysis was performed using an MStation JMS-700 mass spectrometer (JEOL, Peabody, MA, USA) with an ionization energy of 70 eV, an ionization trap current of 300 μA, and a source temperature of 230 °C.

The ^{1}H- and ^{13}C-NMR spectra were recorded on a Bruker Avance III 400 MHz NMR spectrometer (Fällanden, Switzerland; ^{1}H at 400 MHz, ^{13}C at 100.6 MHz), equipped with a 5 mm dual ^{13}C/^{1}H probe head. All NMR spectra were recorded at 20 °C in deuterated chloroform with TMS as the internal standard. Chemical shifts (δ) are reported in ppm and referenced to TMS (δ_H = 0.00 ppm) in ^{1}H- and to the (residual) solvent signal in ^{13}C-NMR and heteronuclear 2D spectra (residual $CHCl_3$ δ_H = 7.26 ppm and $^{13}CDCl_3$ δ_C = 77.16 ppm). Scalar couplings are reported in Hz. The sample (30 mg of the acetal mixture) was dissolved in 1 mL of deuterated chloroform, and 0.7 mL of the solution was transferred into a 5 mm Wilmad, 528-TR-7 NMR tube.

Analytical and spectral data of the compounds are given in Supplementary material to this paper.

Synthetic procedure

*Preparation of 2-((3,7-dimethyloct-6-en-1-yl)oxy)tetrahydrofuran (**4**)*. In a flask equipped with a stirrer and a thermometer, 5 g (32 mmol) of citronellol 40 ml methylene chloride, and 0.025 g (0.145 mmol) of *p*-toluenesulfonic acid were added. Then, 2.4 g (35 mmol) of 2,3-dihydrofuran was added dropwise, and stirring was continued for 3 h at room temperature. The reaction mixture was basified with an aqueous solution of Na_2CO_3 and washed with water to pH 8. After drying with anhydrous $MgSO_4$ and removing the solvent under *vacuum*, the residue of 7.5 g (containing about 88 % of **4**, GC–MS analysis) was subjected to purification by silica gel column chromatography using a mixture of hexane and diethyl ether as the eluent. 4.5 g (62 %) of a colorless product was obtained, containing 99 % (GC analysis) of compound **4**, characterized by an intense, warm, floral-honey fragrance.

*Preparation of (Z)-2-(hex-3-en-1-yloxy)tetrahydrofuran (**5**)*. The same procedure was used as described for the preparation of **4**. 3.2 g of *cis*-3-hexen-1-ol was used, and 3.49 g (64 %) of **5** was obtained.

Quantum-mechanical calculations

Conformational search, geometry optimization, and NMR calculation details. Searches for the lowest energy conformers of THF acetals and calculation of the coupling constant were performed using a multi-step conformation method incorporated in Wavefunction's Spartan '20 software. Initially, a maximum number of meaningful conformers are considered, and their energies are calculated using the MM2 force field method (over 4000, in the case of **4**). Then, in subsequent steps, which included the energy calculation and geometry optimization, the energy window was narrowed, leading to a reduction in the number of conformers. Simultaneously, the level of theory is elevated, also using a more complex basis set, and with it the

precision of the calculation increased, ensuring more accurate results (for more details see Supplementary material, Figs. S-14–S-17). The final energy calculations were performed employing WB97X-V density functional with 6-311+G(2DF,2P)[6-311G*] basis set on the pool of around 50 conformers, making up the 99.99 % Boltzmann population. In the first case, referred to as "Spartan-NMR", the energy calculation, geometry optimization, and calculation of coupling constants using the method incorporated in Wavefunction's Spartan 20 software did not account for solvent effects. In the second case, referred to as "Spartan–Karplus" the solvent effects were considered through energy calculations and geometry optimizations, utilizing a method implemented within the software. However, the calculation of coupling constants involved the utilization of a dihedral angle and the incorporation of substituent effects through the modified Karplus equation.[32-34] The copies of the reports from this software, including the Cartesian coordinates for the lowest energy conformers (one per compound), are provided in the Supplementary material (Figs. S-14–S-17). The obtained 3D structures were used in the appropriate figures within the manuscript.

^{1}H-NMR full spin analysis

^{1}H-NMR full spin analysis of tetrahydrofuranyl acetal of citronellol was performed by manually adjusting δ_H and J values to fit the experimentally available values and further optimized using MestReNova 11.0.3 software (tools/spin simulation). This procedure led to a systematic refinement of all calculated NMR parameters until the simulation outcome was in excellent agreement (*NRMSD* < 0.05 %) with the experimental data of the synthesized compounds.

RESULTS AND DISCUSSION

Tetrahydrofuranyl acetal of citronellol (**4**, Fig. 1) was obtained by a modified procedure described in Patent PL224652.[27] The target acetal contains two chiral centers giving rise to 4 possible stereoisomers, two pairs of enantiomers (Fig. 2). The TIC chromatogram, obtained by GC–MS analysis of the isolated product (Supplementary material, Figs. S-7 and S-8), contained two almost completely overlapping peaks – each corresponding to one of the enantiomeric pairs, with a relative ratio of 1:1, based on TIC peak integration. A combination of 1D- and 2D-NMR experiments (Supplementary material, Figs. S-3–S-6), homonuclear selective decoupling experiments were initially employed to perform an approximate assignment of ^{1}H- and ^{13}C-NMR spectra directly from the mixture without any separation.

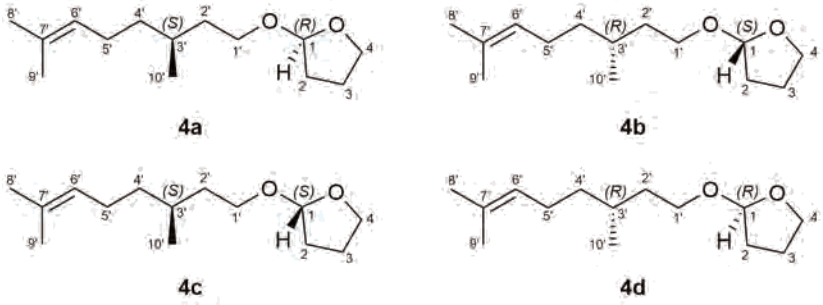

Fig 2. Structures of diastereomeric tetrahydrofuranyl acetals of citronellol.

Calculation of coupling constants and chemical shifts from 3D models has found application in the stereochemical assignment of molecules having complex NMR spectra, or higher order multiplets.[28–31] Unfortunately, the straightforward application is limited to conformationally rigid molecules, due to the fact that in these cases all parameters can be usually calculated based on only one structure/ /conformer. In order to apply such an approach to conformationally flexible molecules, an additional parameter had to be considered - the energy of the conformers, and thus their Boltzmann population, under the assumption that these are in fast equilibrium (see Experimental). Based on these parameters, numerous conformers were selected for each diastereomer, comprising well over 99 % of the total population. Coupling constants were then calculated for these conformers using two different methods. The first method utilized the built-in functionality of Wavefunction's Spartan 20 software (Table I, Spartan-NMR columns), while the second method employed a modified Karplus equation (Table I,

TABLE I. The comparison of the calculated coupling constants of **4** and **5**, and the ones obtained by spin simulation; designations "r" and "s" of hydrogen atoms refer to the prochirality of these hydrogens

J_{H-H}	Tetrahydrofuranyl group (from **5**)			Tetrahydrofuranyl acetal of citronellol (**4**)					
	Spartan--NMR	Spartan––Karplus	Spin simulation	Spartan-NMR		Spartan–Karplus		Spin simulation	
				SS(RR)	SR(RS)	SS(RR)	SR(RS)	SS(RR)	SR(RS)
1 - 2r	6.6	4.5	5	4.7	5.3	4.9	5.7	5.3	5.3
1 - 2s	0.8	1.5	1.5	1.2	0.7	1.3	1.9	0.9	0.9
2r - 3r	12.1	7.8	8.3	13.1	12.6	11.2	7.9	8.3	8.3
2r - 3s	6.2	5.9	10	8	7.3	7.1	8.1	10	10
2s - 3r	2.3	7.6	8.5	7.7	7.7	7.4	8.3	8.5	8.5
2s - 3s	12.2	7.6	4	0	0.5	2.0	4.4	4	4
3r - 4r	10.2	5.8	7.3	10.8	9.4	9.2	8.7	7.3	7.3
3r - 4s	2.2	4.3	5.6	10.3	9.4	9.1	6.1	5.6	5.6
3s - 4r	7.8	5.2	6.2	0.7	1.1	2.4	5.7	6.2	6.2
3s - 4s	9	6.0	7.5	7.6	7.8	9.0	8.8	7.5	7.5
1'r - 2'r	–	–	–	6.1	3.9	6.8	8.2	6.2	7.9
1'r - 2's	–	–	–	1.1	2.2	5.9	3.6	7.9	5.5
1's - 2'r	–	–	–	13.1	12	3.9	4.7	6.2	7.7
1's - 2's	–	–	–	3.8	1.6	6.9	8.1	7.9	6.9
2'r - 3'	–	–	–	4.1	1.5	11.4	8.0	8.5	6.5
2's - 3'	–	–	–	11.4	12.4	4.6	7.2	6.5	8.5
3' - 4'r	–	–	–	12	12.3	10.5	6.0	9.2	6.0
3' - 4's	–	–	–	4	1.7	4.8	7.0	5	6.2
4'r - 5'r	–	–	–	3.5	3.6	4.0	3.9	2.3	5.9
4'r - 5's	–	–	–	4.4	3.2	11.2	11.0	7.6	9.8
4's - 5'r	–	–	–	4.6	3.2	11.2	11.0	7.4	8.1
4's - 5's	–	–	–	13.5	13.1	4.1	4.4	5.6	4.2
5'r - 6'	–	–	–	11.6	4.1	8.2	7.5	7.6	7.6
5's - 6'	–	–	–	5	11.4	8.2	8.0	6.6	6.6

Spartan–Karplus columns).[32–34] In the latter approach, the calculation was based on the dihedral angle obtained from the Spartan software, as well as the attached substituents. The resulting coupling constants were multiplied by the relative abundance of each conformer and summed.

These parameters were employed in the initial spin simulation, which was followed by manual iterative adjustments to accurately reproduce the original ^{1}H--NMR spectrum. However, achieving a complete spin simulation proved challenging due to signal overlap in the ^{1}H-NMR spectrum of compound **4** (protons in positions 3 and 5'). To overcome this, a tetrahydrofuranyl acetal of a non--chiral alcohol, *cis*-3-hexen-1-ol, was synthesized and used for proton assignment of the tetrahydrofuranyl moiety, as in this case, appropriate signals do not overlap (Supplementary material, Figs. S-9–S-13, Table S-II). The chemical shifts and coupling constants, obtained from the spin simulation (Table I and Fig. 3) of ^{1}H--NMR spectrum of this acetal were then utilized in the spin simulation of the tetrahydrofuranyl acetal of citronellol. The coupling constants derived from the calculations were compared to the coupling constants obtained after the iterative adjustments and are presented in Table I.

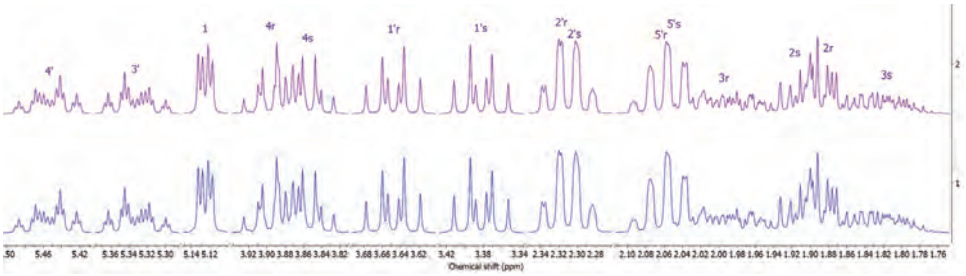

Fig. 3. Upper trace: simulated ^{1}H-NMR (400 MHz) spectrum of **5**; lower trace: ^{1}H-NMR (400 MHz, $CDCl_3$) spectrum of **5**.

Table S-I of the Supplementary material provides the assigned NMR chemical shifts of ^{1}H signals for the tetrahydrofuranyl acetals of citronellol, along with an interpretation of the couplings. The NMR chemical shifts ^{13}C signals, HMBC and NOESY interactions relevant to the assignment are summarized in Table S-I (Supplementary material), while Fig. S-2 (Supplementary material) highlights the key interactions used in the assignment process. The final result of the simulation of ^{1}H-NMR spectrum of the sample confirmed that it consisted of an equimolar mixture of stereoisomers **4a**–**d**.

The differences in chemical shifts and coupling constants between the analogous hydrogens of diastereomers of **4** are small but can be brought into connection with the spatial arrangement of the groups within these molecules. Fig. 4 shows important coupling constants between hydrogens in positions 1’ to 5’, as well as the appearance of signals of 1’ and 4’. The differences in the dihedral

angles between these hydrogens in the highest abundant conformers of each diastereomer (shown in Fig. 4) are in agreement with the value of the couplings obtained by simulation.

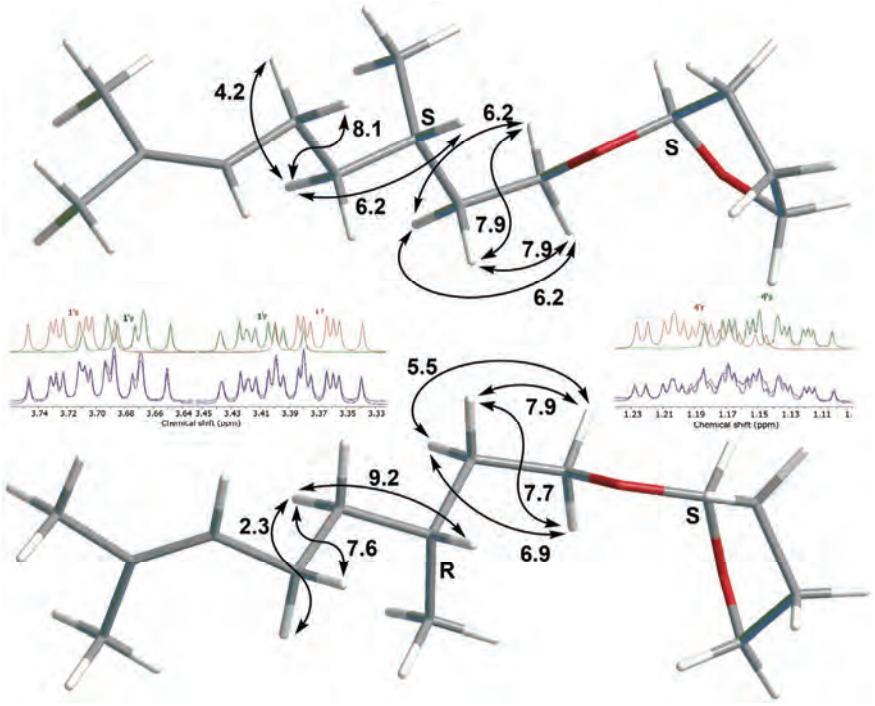

Fig. 4. The most stable conformers of the diastereomerers of **4**. Important coupling constants between hydrogens in positions 1' to 5', and the appearance of signals of 1' and 4'. Upper spectra represent spin simulations, while the bottom ones represent a comparison of the added simulated spectrum and the experimental one.

CONCLUSION

In conclusion, this study successfully performed an NMR spectral analysis of diastereomeric acetals derived from 2,3-dihydrofurane and a racemic mixture of citronellol, as well as corresponding acetal of *cis*-3-hexen-1-ol. Conformational analysis and calculation of coupling constants were done using Spartan software and Karplus equation, followed by manual adjustments to correspond to experimental values, using MestreNova software. Spin simulation of proton signals allowed the assignment of the diastereotopic protons of tetrahydrofuranyl moiety and diastereomer discrimination. The assignment of the tetrahydrofuranyl moiety was achieved for the first time, providing valuable data for the future utilization of this protecting group.

SUPPLEMENTARY MATERIAL

Additional data and information are available electronically at the pages of journal website: https://www.shd-pub.org.rs/index.php/JSCS/article/view/12436, or from the corresponding author on request.

Acknowledgments. This work was supported by the Ministry of Science, Technological Development and Innovation of Serbia (Grant No. 451-03-47/2023-01/200124). This work is a part of the Ph.D. dissertation of Milan S. Nešić under the supervision of Niko Radulović.

И З В О Д

АСИГНАЦИЈА NMR СПЕКТРАЛНИХ ПОДАТАКА ДИЈАСТЕРЕОМЕРНИХ ТЕТРАХИДРОФУРАНИЛ-АЦЕТАЛА СПЕКТРАЛНОМ СИМУЛАЦИЈОМ ДИРЕКТНО ИЗ ЊИХОВЕ СМЕШЕ

МИЛАН С. НЕШИЋ, МИЛИЦА Д. НЕШИЋ и НИКО С. РАДУЛОВИЋ

Департман за хемију, Природно-математички факултет, Универзитет у Нишу, Вишеградска 33, 18000 Ниш

У овом раду извршена је НМР спектрална анализа смеше дијастереомерних тетрахидрофуранил-ацетала синтетисаних из 2,3-дихидрофурана и рацемске смеше цитронелола. Потпуна ^{1}H-NMR спинска анализа је остварена итеративним подешавањем вредности δ_H и J (израчунатих помоћу софтвера Spartan) до поклапања са експерименталним вредностима коришћењем софтвера MestreNova. Извршено је поређење симулираних ^{1}H-NMR спектара сваког дијастереомера понаособ, као и њихових преклопљених и сумираних спектара са експериментално добијеним спектрима. Спинска симулација сигнала водоника омогућила је асигнацију протона тетрахидрофуранил-групе, као и одређивање релативне конфигурације хиралних центара. Хемијска померања, константе купловања, HMBC и NOESY интеракције систематизовани су у одговарајућим табелама и шемама. Ово је први пут да је извршена потпуна асигнација протона на тетрахидрофуранил-групи, а добијени резултати могу бити од великог значаја за већу будућу примену ове заштитне групе.

(Примљено 14. јуна, ревидирано 3. августа. прихваћено 27. августа 2023)

REFERENCES

1. P. G. M. Wuts, T. W. Greene, *Greene's Protective Groups in Organic Synthesis*, John Wiley & Sons, Inc., Hoboken, NJ, 2006 (https://dx.doi.org/10.1002/0470053488)
2. B. Kumar, M. A. Aga, A. Rouf, B. A. Shah, S. C. Taneja, *RSC Adv.* **4** (2014) 21121 (https://dx.doi.org/10.1039/c4ra02093f)
3. N. S. Radulović, M. S. Nešić, *RSC Adv.* **6** (2016) 93068 (https://dx.doi.org/10.1039/C6RA19980A)
4. M. Barbero, S. Bazzi, S. Cadamuro, S. Dughera, C. Piccinini, *Synthesis* **2** (2010) 315 (https://dx.doi.org/10.1055/s-0029-1217093)
5. H. Fujioka, T. Okitsu, T. Ohnaka, R. Li, O. Kubo, K. Okamoto, Y. Sawama, Y. Kita, *J. Org. Chem.* **72** (2007) 7898 (https://dx.doi.org/10.1021/jo071187g)
6. C. V. T. Vo, T. A. Mitchell, J. W. Bode, *J. Am. Chem. Soc.* **133** (2011) 14082 (https://dx.doi.org/10.1021/ja205174c)
7. L. S. Li, S. Das, S. C. Sinha, *Org. Lett.* **6** (2004) 127 (https://dx.doi.org/10.1021/ol030108u)

8. S. Yoshioka, M. Oshita, M. Tobisu, N. Chatani, *Org. Lett.* **7** (2005) 3697 (https://dx.doi.org/10.1021/ol0513138)
9. L. Lemiègre, R. L. Stevens, J. C. Combret, J. Maddaluno, *Org. Biomol. Chem.* **3** (2005) 1308 (https://dx.doi.org/10.1039/B419381D)
10. A. Fürstner, T. Gastner, *Org. Lett.* **2** (2000) 2467 (https://dx.doi.org/10.1021/ol0061236)
11. A. Robinson, V. K. Aggarwal, *Angew. Chem. Int. Ed.* **49** (2010) 6673 (https://dx.doi.org/10.1002/anie.201003236)
12. N. Hama, T. Matsuda, T. Sato, N. Chida, *Org. Lett.* **11** (2009) 2687 (https://dx.doi.org/10.1021/ol900799e)
13. E. L. Eliel, B. E. Nowak, R. A. Daignault, V. G. Badding, *J. Org. Chem.* **30** (1962) 2441 (https://dx.doi.org/10.1021/jo01018a082)
14. L. J. Lambert, M. J. Miller, P. W. Huber, *Org. Biomol. Chem.* **13** (2015) 2341 (https://dx.doi.org/10.1039/C4OB02212B)
15. E. J. Corey, N. M. Weinshenker, T. K. Schaaf, W. Huber, *J. Am. Chem. Soc.* **91** (1969) 5675 (https://dx.doi.org/10.1021/ja01048a062)
16. H. Kusama, R. Hara, S. Kawahara, T. Nishimori, H. Kashima, N. Nakamura, K. Morihira, I. Kuwajima, *J. Am. Chem. Soc.* **122** (2000) 3811 (https://dx.doi.org/10.1021/ja9939439)
17. T. Mukaiyama, I. Shiina, H. Iwadare, M. Saitoh, T. Nishimura, N. Ohkawa, H. Sakoh, K. Nishimura, Y.-I. Tani, M. Hasegawa, K. Yamada, K. Saitoh, *Chem. Eur. J.* **5** (1991) 121 (https://dx.doi.org/10.1002/(SICI)1521-3765(19990104)5:1<121::AID-CHEM121>3.0.CO;2-O)
18. J. D. Winkler, M. B. Rouse, M. F. Greaney, S. J. Harrison, Y. T. Jeon, *J. Am. Chem. Soc.* **124** (2002) 9726 (https://dx.doi.org/10.1021/ja026600a)
19. G. Stork, A. Yamashita, J. Adams, G. R. Schulte, R. Chesworth, Y. Miyazaki, J. J. Farmer, *J. Am. Chem. Soc.* **131** (2009) 11402 (https://dx.doi.org/10.1021/ja9038505)
20. B. Liu, S. Thayumanavan, *J. Am. Chem. Soc.* **139** (2017) 2306 (https://dx.doi.org/10.1021/jacs.6b11181)
21. S. J. Danishefsky, J. J. Masters, W. B. Young, J. T. Link, L. B. Snyder, T. V Magee, D. K. Jung, R. C. A. Isaacs, W. G. Bornmann, C. A. Alaimo, C. A. Coburn, M. J. di Grandi, *J. Am. Chem. Soc.* **118** (1996) 2843 (https://dx.doi.org/10.1021/ja952692a)
22. I. Ramos-Tomillero, H. Rodriguez, F. Albericio, *Org. Lett.* **17** (2015) 1680 (https://dx.doi.org/10.1021/acs.orglett.5b00444)
23. 23. A. Sharma, I. Ramos-Tomillero, A. El-Faham, E. Nicolas, H. Rodriguez, B. G. de la Torre, F. Albericio, *ChemistryOpen* **6** (2017) 168 (https://dx.doi.org/10.1002/open.201600156)
24. P. L. Santos, J. P. S. C. F. Matos, L. Picot, J. R. G. S. Almeida, J. S. S. Quintans, L. J. Quintans-Júnior, *Food Chem. Toxicol.* **123** (2019) 459 (https://dx.doi.org/10.1016/j.fct.2018.11.030)
25. W. S. Hsu, J. H. Yen, Y. S. Wang, *J. Environ. Sci. Health., B* **48** (2013) 1014 (https://dx.doi.org/10.1080/03601234.2013.816613)
26. N. Monnerie, J. Ortner, *J. Sol. Energy Eng.* **123** (2001) 171 (https://dx.doi.org/10.1115/1.1354996)
27. Jozef Kula, Aleksandra Wojciechowska, PL224652 (2017)
28. N. S. Radulović, S. I. Filipović, M. S. Nešić, N. M. Stojanović, K. V. Mitić, M. Z. Mladenović, V. N. Randelović, *J. Nat. Prod.* **83** (2020) 3554 (https://dx.doi.org/10.1021/acs.jnatprod.0c00585)

29. N. S. Radulović, M. Z. Mladenović, N. M. Stojanović, P. J. Randjelović, P. D. Blagojević, *J. Nat. Prod.* **82** (2019) 1874 (https://dx.doi.org/10.1021/acs.jnatprod.9b00120)
30. N. Radulović, M. Stevanović, M. Nešić, N. Stojanović, P. Ranelović, V. Ranelović, *J. Nat. Prod.* **83** (2020) 2902 (https://dx.doi.org/10.1021/acs.jnatprod.0c00437)
31. M. Nesic, N. Radulovic, *Facta Univ., Ser.: Phys., Chem. Technol.* **19** (2021) 69 (https://dx.doi.org/10.2298/FUPCT2102069N)
32. H. Gunther, *NMR Spectroscopy; Basic Principles, Concepts and Application in Chemistry Third Edition*, Wiley-VCH, Weinheim, 2013 (ISBN: 978-3-527-33000-3)
33. C. A. G. Haasnoot, F. A. A. M. de Leeuw, C. Altona, *Tetrahedron* **36** (1980) 2783 (https://dx.doi.org/10.1016/0040-4020(80)80155-4)
34. L. A. Donders, F. A. A. M. De Leeuwt, C. Altonaz, *Magn. Reson. Chem.* **27** (1989) 556 (https://dx.doi.org/10.1002/mrc.1260270608).

Journal of the Serbian Chemical Society
JSCS@tmf.bg.ac.rs • www.shd.org.rs/JSCS
J. Serb. Chem. Soc. *89* (1) S1–S51 (2024) *Supplementary material*

SUPPLEMENTARY MATERIAL TO

Assignment of NMR spectral data of diastereomeric tetrahydrofuranyl acetals directly from their mixture by spectral simulation

MILAN S. NEŠIĆ, MILICA D. NEŠIĆ and NIKO S. RADULOVIĆ*

Department of Chemistry, Faculty of Science and Mathematics, University of Niš, Višegradska 33, 18000 Niš, Serbia

J. Serb. Chem. Soc. *89* (1) (2024) 1–11

EXPERIMENTAL AND ANALYTICAL DATA

2-((3,7-Dimethyloct-6-en-1-yl)oxy)tetrahydrofuran (***4***). ^{1}H NMR (400 MHz, $CDCl_3$) and ^{13}C (100.6 MHz, $CDCl_3$) for each diastereomer are given in Table S-I; FTIR (neat, cm^{-1}) 2912, 1025; MS (70 eV): *m*/*z* (%): 226 (0.2), 154 (4.4), 123 (2.5), 95 (4.5), 81 (5.5), 71 (100), 69 (14.1), 67 (5.9), 55 (5.8), 41 (13.8); (+)ESI-HRMS (**m**/**z**): calculated for $[C_{14}H_{26}O_2]^+$ 226.1933, observed 226.1929; Elemental analysis for $C_{14}H_{26}O_2$: Calculated. C 74.28, H 11.58, O 14.14; found C 74.26, H 11.59. RI (DB-5MS) 1553 and 1554 for each diastereomer.

(Z)-2-(Hex-3-en-1-yloxy)tetrahydrofuran (***5***). ^{1}H- (400 MHz, $CDCl_3$) and ^{13}C-NMR (100.6 MHz, $CDCl_3$) are given in Table S-II; FTIR (neat, cm^{-1}) 2911, 1022; MS (70 eV): *m*/*z* (%): 170 (0.04), 101 (6.2), 87 (6.2), 82 (5.6), 71 (100), 67 (8.9), 55 (12.7), 43 (19.7), 41 (20,1), 39 (9.9); (+)ESI-HRMS (**m**/**z**): calculated for $[C_{10}H_{18}O_2]^+$ 170.1307, observed 170.1310; Elemental analysis for $C_{14}H_{26}O_2$: Calculated. C 70.55, H 10.66, O 18.79; found C 70.57, H 10.65.

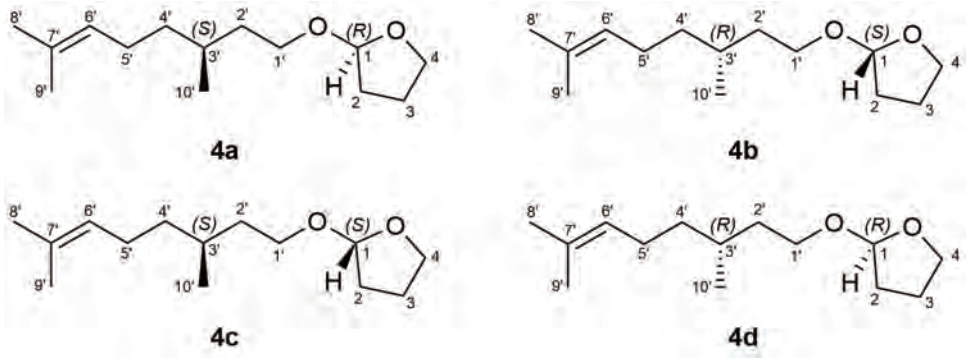

Fig. S-1. Atom numbering scheme of tetrahydrofuranyl acetals of citronellol (**4a**-**4d**).

* Corresponding author. E-mail: nikoradulovic@yahoo.com

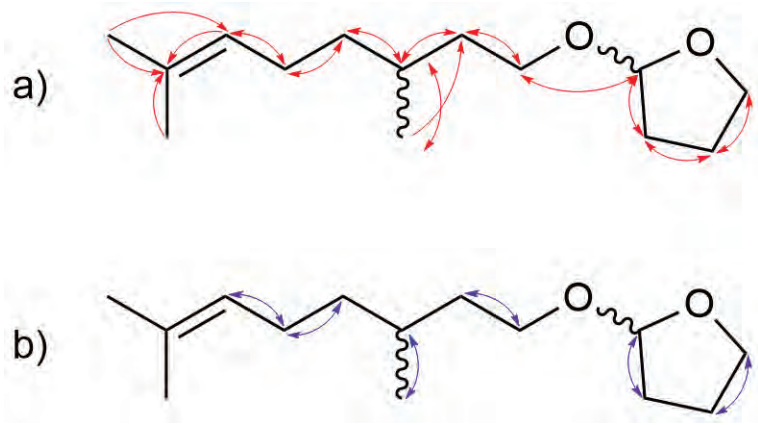

Fig. S-2. Key HMBC (a) and NOESY (b) interactions.

Table S-I. ^{1}H (400 MHz) and ^{13}C (100.6 MHz) NMR data of tetrahydrofuranyl acetals of citronellol ($CDCl_3$, NMR parameters are derived from manual iterative full spin analysis

Position	4c/4d		4a/4b		HMBC[b]	NOESY[c]
	δ_H (m, *J* (Hz), Integral)[a]	δ_C	δ_H (m, *J* (Hz), Integral)	δ_C		
1	5.1072 (dd, $^{3}J_{1,2r}$ = 5.3, $^{3}J_{1,2s}$ = 0.9, 1 H)	103.80	5.1032 (dd, $^{3}J_{1,2r}$ = 5.3, $^{3}J_{1,2s}$ = 0.9, 1 H)	103.99	2, 3, 4, 1'	2r, 2s
2r	1.9160 (dddd, $^{2}J_{2r,2s}$ = -11.5, $^{3}J_{2r,3r}$ = 8.3, $^{3}J_{2r,3s}$ = 10.0, $^{3}J_{1,2r}$ = 5.3, 1 H)	23.66	1.9160 (dddd, $^{2}J_{2r,2s}$ = -11.5, $^{3}J_{2r,3r}$ = 8.3, $^{3}J_{2r,3s}$ = 10.0, $^{3}J_{1,2r}$ = 5.3, 1 H)	23.66	1, 3, 4	1
2s	1.8710 (dddd, $^{2}J_{2r,2s}$ = -11.5, $^{3}J_{2s,3r}$ = 8.5, $^{3}J_{2s,3s}$ = 4.0, $^{3}J_{1,2s}$ = 0.9, 1 H)		1.8710 (dddd, $^{2}J_{2r,2s}$ = -11.5, $^{3}J_{2s,3r}$ = 8.5, $^{3}J_{2s,3s}$ = 4.0, $^{3}J_{1,2s}$ = 0.9, 1 H)			
3r	1.9720 (ddddd, $^{2}J_{3r,3s}$ = -11.4, $^{3}J_{2r,3r}$ = 8.3, $^{3}J_{3r,4r}$ = 7.3 $^{3}J_{2s,3r}$ = 8.5, $^{3}J_{3r,4s}$ = 5.6, 1 H)	32.47	1.9720 (ddddd, $^{2}J_{3r,3s}$ = -11.4, $^{3}J_{2r,3r}$ = 8.3, $^{3}J_{3r,4r}$ = 7.3 $^{3}J_{2s,3r}$ = 8.5, $^{3}J_{3r,4s}$ = 5.6, 1 H)	32.46	2, 4	4r, 4s
3s	1.8158 (ddddd, $^{2}J_{3r,3s}$ = -11.4, $^{3}J_{3s,4s}$ = 7.5, $^{3}J_{2r,3s}$ = 10.0, $^{3}J_{3s,4r}$ = 6.2, $^{3}J_{2s,3s}$ = 4.0, 1 H)		1.8158 (ddddd, $^{2}J_{3r,3s}$ = -11.4, $^{3}J_{3s,4s}$ = 7.5, $^{3}J_{2r,3s}$ = 10.0, $^{3}J_{3s,4r}$ = 6.2, $^{3}J_{2s,3s}$ = 4.0, 1 H)			

4r	3.8897 (ddd, $^2J_{4r,4s}$ = -8.1, $^3J_{3r,4r}$ = 7.3, $^3J_{3s,4r}$ = 6.2, 1 H)	66.91	3.8897 (ddd, $^2J_{4r,4s}$ = -8.1, $^3J_{3r,4r}$ = 7.3, $^3J_{3s,4r}$ = 6.2, 1 H)	66.91	1, 3	3r, 3s
4s	3.8570 (ddd, $^2J_{4r,4s}$ = -8.1, $^3J_{3s,4s}$ = 7.5, $^3J_{3r,4s}$ = 5.6, 1 H)		3.8570 (ddd, $^2J_{4r,4s}$ = -8.1, $^3J_{3s,4s}$ = 7.5, $^3J_{3r,4s}$ = 5.6, 1 H)			
1'r	3.3694 (ddd, $^2J_{1'r,1's}$ = -9.6, $^3J_{1'r,2's}$ = 7.9, $^3J_{1'r,2'r}$ = 6.2, 1 H)	65.72	3.4089 (ddd, $^2J_{1'r,1's}$ = -9.7, $^3J_{1'r,2'r}$ = 7.9, $^3J_{1'r,2's}$ = 5.5, 1 H)	65.58	1, 2', 3'	2'r, 2's
1's	3.7168 (ddd, $^2J_{1'r,1's}$ = -9.6, $^3J_{1's,2's}$ = 7.9, $^3J_{1's,2'r}$ = 6.2, 1 H)		3.6801 (ddd, $^2J_{1'r,1's}$ = -9.7, $^3J_{1's,2'r}$ = 7.7, $^3J_{1's,2's}$ = 6.9, 1 H)			
2'r	1.3886 (dddd, $^2J_{2'r,2's}$ = -13.2, $^3J_{2'r,3'}$ = 8.5, $^3J_{1'r,2'r}$ = $^3J_{1's,2'r}$ = 6.2, 1 H)	36.71	1.6008 (dddd, $^2J_{2'r,2's}$ = -13.6, $^3J_{1'r,2'r}$ = 7.9, $^3J_{1's,2'r}$ = 7.7, $^3J_{2'r,3'}$ = 6.5, 1 H)	36.83	1', 3', 4', 10'	1'r, 1's
2's	1.6145 (dddd, $^2J_{2'r,2's}$ = -13.2, $^3J_{1's,2's}$= $J_{1'r,2's}$= 7.9, $^3J_{2's,3'}$ = 6.5, 1 H)		1.3846 (dddd, $^2J_{2'r,2's}$ = -13.6, $^3J_{2's,3'}$ = 8.5, $^3J_{1's,2's}$= 6.9, $J_{1'r,2's}$= 5.5, 1 H)			
3'	1.5332 (ddqdd, $^3J_{3',4'r}$ = 9.2, $^3J_{2'r,3'}$ = 8.5, $^3J_{3',10'}$ = 6.7, $^3J_{2's,3'}$ = 6.5, $^3J_{3',4's}$ = 5.0, 1 H)	29.70	1.5359 (dqddd, $^3J_{2's,3'}$ = 8.5, $^3J_{3',10'}$ = 6.7, $^3J_{2'r,3'}$ = 6.5, $^3J_{3',4's}$ = 6.2, $^3J_{3',4'r}$ = 6.0, 1 H)	29.74	1', 2', 4', 5', 10'	10'
4'r	1.1885 (dddd, $^2J_{4'r,4's}$ = -14.3, $^3J_{3',4'r}$ = 9.2, $^3J_{4'r,5's}$ = 7.6, $^3J_{4'r,5'r}$ = 2.3, 1 H)	37.36	1.3336 (dddd, $^2J_{4'r,4's}$ = -14.3, $^3J_{4'r,5's}$ = 9.8, $^3J_{3',4'r}$ = 6.0, $^3J_{4'r,5'r}$ = 5.9, 1 H)	37.18	2', 3', 5', 6', 10'	5'r, 5's
4's	1.3422 (dddd, $^2J_{4'r,4's}$ = -14.3, $^3J_{4's,5'r}$ = 7.4, $^3J_{4's,5's}$ = 5.6, $^3J_{3',4's}$ = 5.0, 1 H)		1.1448 (dddd, $^2J_{4'r,4's}$ = -14.3, $^3J_{4's,5'r}$ = 8.1, $^3J_{3',4's}$ = 6.2, $^3J_{4's,5's}$ = 4.2, 1 H)			
5'r	1.9617 (dddd, $^2J_{5'r,5's}$ = -14.3, $^3J_{5'r,6'}$ = 7.6, $^3J_{4's,5'r}$ = 7.4, $^3J_{4'r,5'r}$ = 2.3, 1 H)	25.58	2.0006 (dddd, $^2J_{5'r,5's}$ = -14.3, $^3J_{4's,5'r}$ = 8.1, $^3J_{5'r,6'}$ = 7.6, $^3J_{4'r,5'r}$ = 5.9, 1 H)	25.58	3', 4', 6', 7'	4'r, 4's, 6'
5's	2.0107 (dddd, $^2J_{5'r,5's}$ = -14.3, $^3J_{4'r,5's}$ = 7.6, $^3J_{5's,6'}$ = 6.6, $^3J_{4's,5's}$		1.9635 (dddd, $^2J_{5'r,5's}$ = -14.3, $^3J_{4'r,5's}$ = 9.8, $^3J_{5's,6'}$ = 6.6, $^3J_{4's,5's}$ = 4.2, 1 H)			

	= 5.6, 1 H)					
6'	5.0946 (ddqq, $^3J_{5'r,6'}$ = 7.6, $^3J_{5's,6'}$ = 6.6, $^4J_{6',8'}$ = $^4J_{6',9'}$ = -1.4, 1 H)	124.97	5.0946 (ddqq, $^3J_{5'r,6'}$ = 7.6, $^3J_{5's,6'}$ = 6.6, $^4J_{6',8'}$ = $^4J_{6',9'}$ = -1.4, 1 H)	124.97	4', 5', 8', 9'	5'r, 5's
7'	/	131.22	/	131.21	/	/
8'	1.6790 (dq, $^4J_{6',8'}$ = -1.4, $^4J_{8',9'}$ = -0.8, 3 H)	25.85	1.6790 (dq, $^4J_{6',8'}$ = -1.4, $^4J_{8',9'}$ = -0.8, 3 H)	25.85	4', 6', 7', 9'	/
9'	1.5996 (dq, $^4J_{6',9'}$ = -1.4, $^4J_{8',9'}$ = -0.8, 3 H)	17.75	1.5996 (dq, $^4J_{6',9'}$ = -1.4, $^4J_{8',9'}$ = -0.8, 3 H)	17.75	5', 6', 7', 8'	/
10'	0.8898 (d, $^3J_{3',10'}$ = 6.7, 3 H)	19.57	0.8898 (d, $^3J_{3',10'}$ = 6.7, 3 H)	19.72	2', 3', 4'	3'

[a]Coupling constant values were initially inferred from ^{1}H homonuclear selective decoupling NMR experiments and afterward refined through a manual iterative full spin analysis. [b]gHMBC correlations observed between the hydrogen in this row and the carbon in the listed position. [c]Cross-peaks observed in the NOESY spectrum

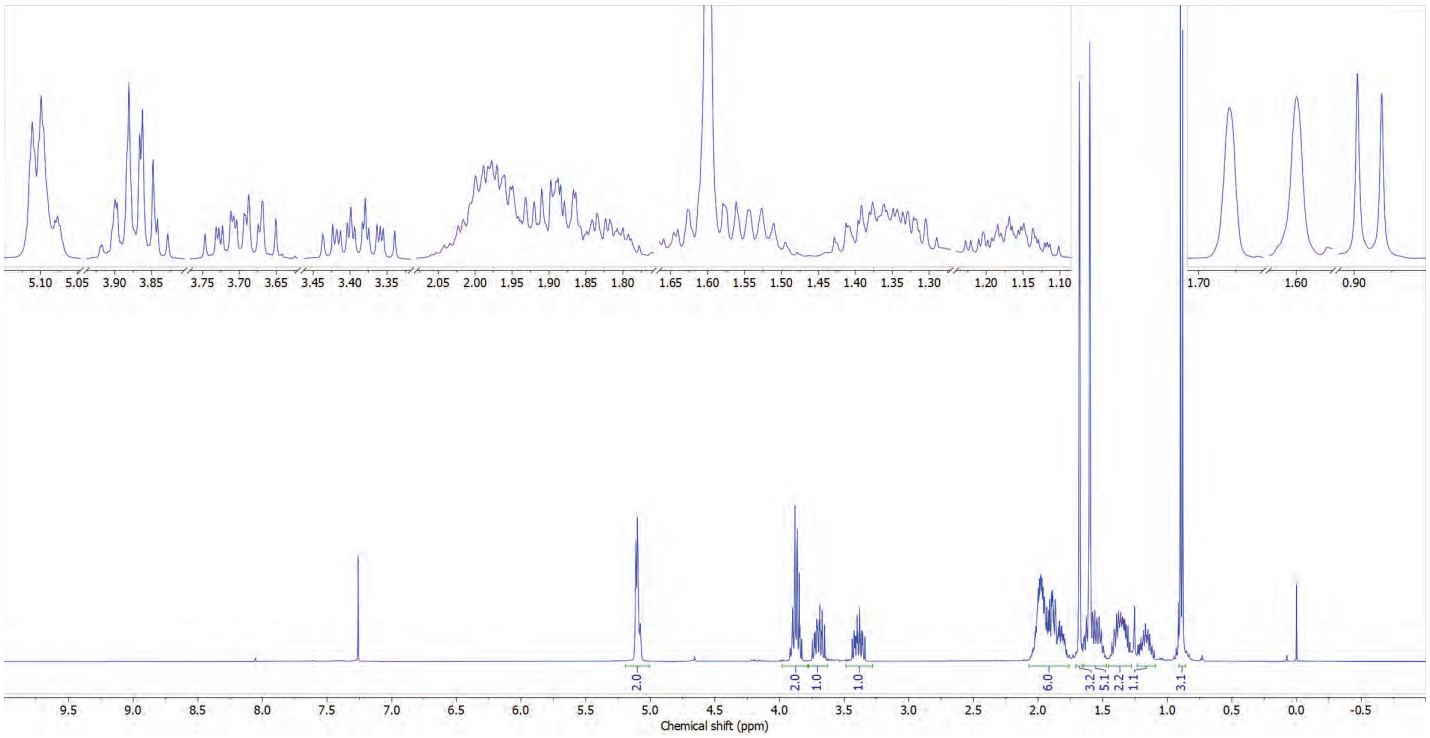

Fig. S-3. ^{1}H-NMR (400 MHz, $CDCl_3$) spectrum of mixture of tetrahydrofuranyl acetals of citronellol (**4a-4d**) and the corresponding expansions.

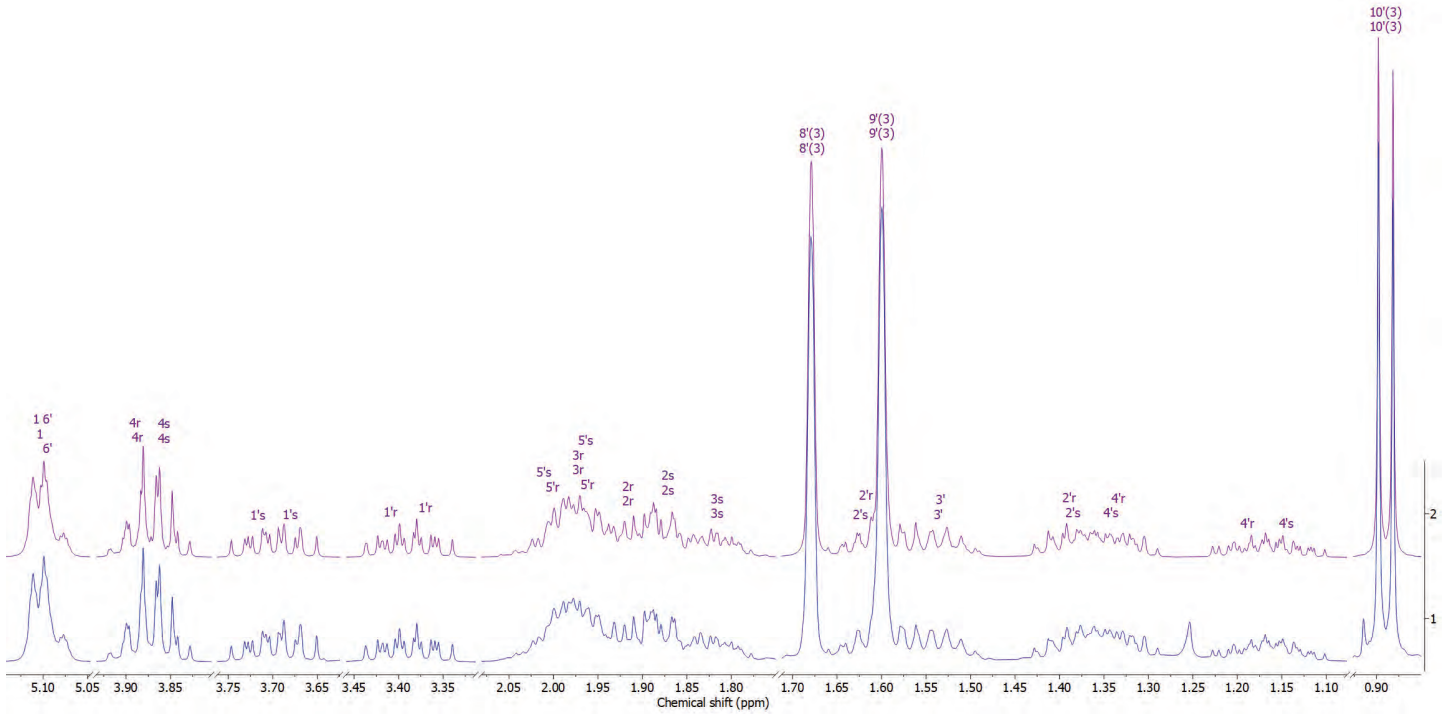

Fig.S-4. Upper trace: simulated ^{1}H NMR (400 MHz) spectrum of equimolar mixture of **4a**-**4d**; lower trace: ^{1}H NMR (400 MHz, $CDCl_3$) spectrum of equimolar mixture of **4a**-**4d**.

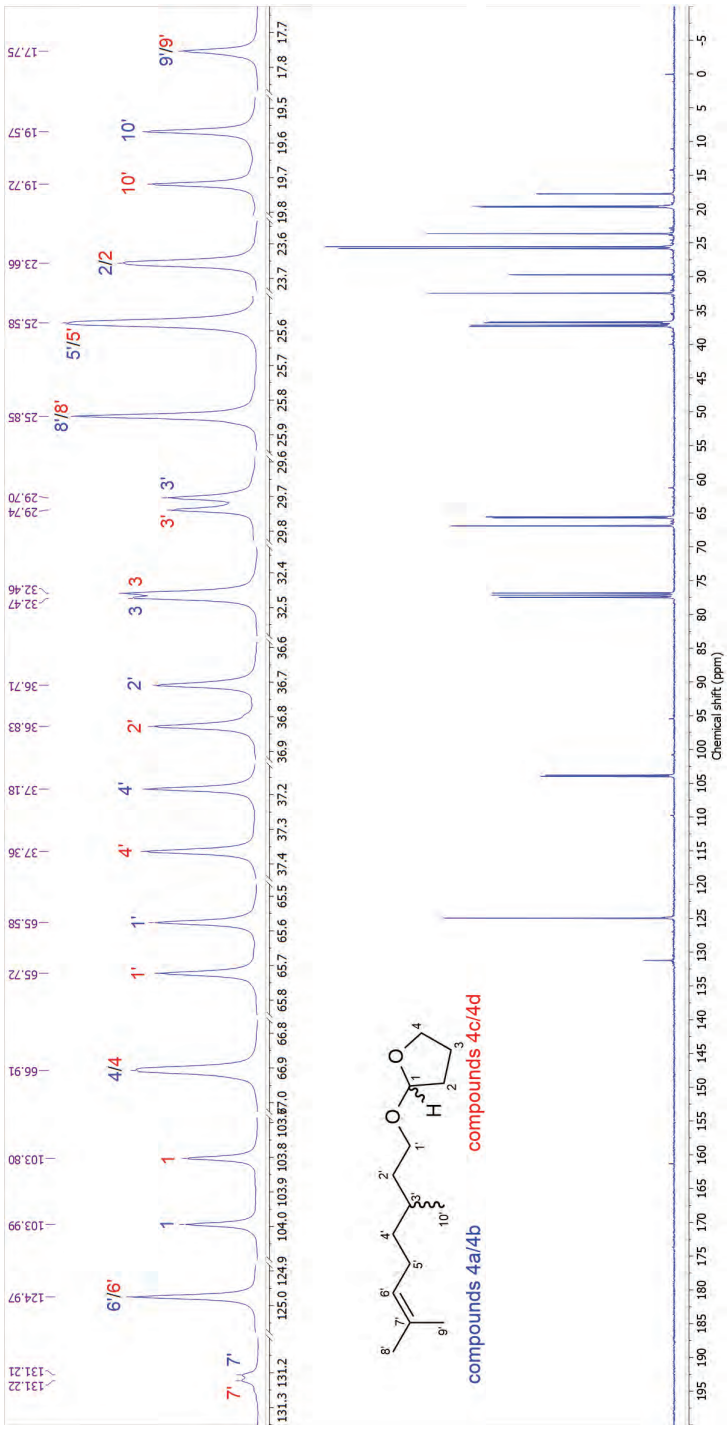

Fig. S.5. ^{13}C NMR (100.6 MHz, $CDCl_3$) spectrum of equimolar mixture of **4a–4d**, and the corresponding expansion.

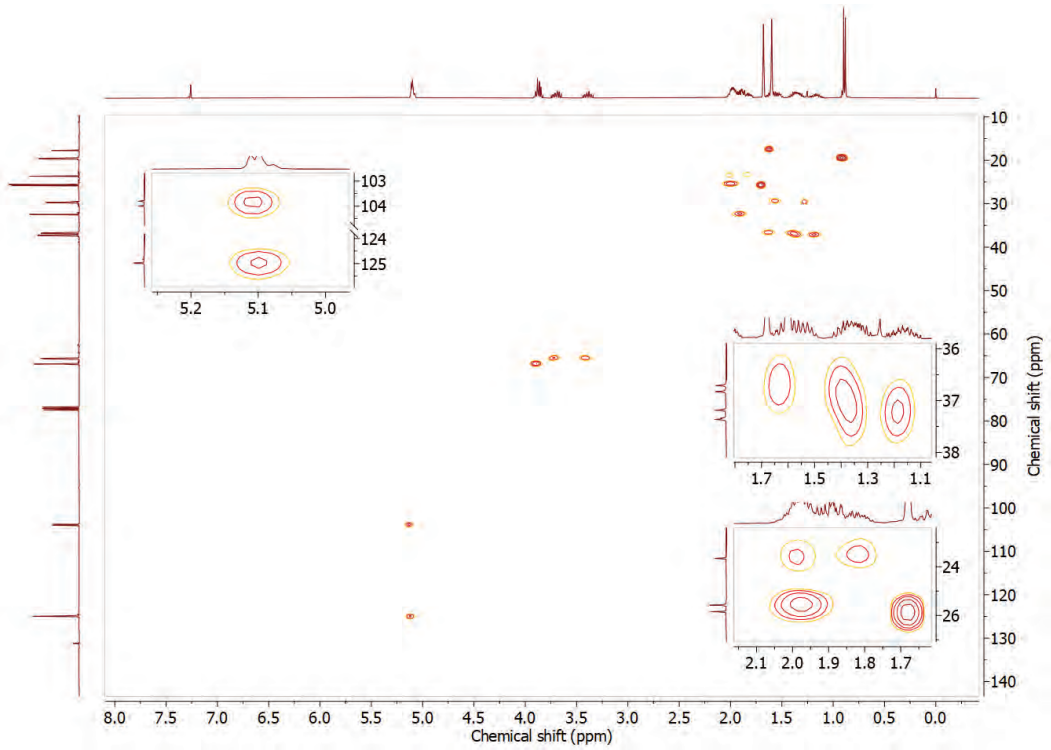

Fig. S-6. grHSQC spectrum of an equimolar mixture of **4a**-**4d**, and the corresponding expansions.

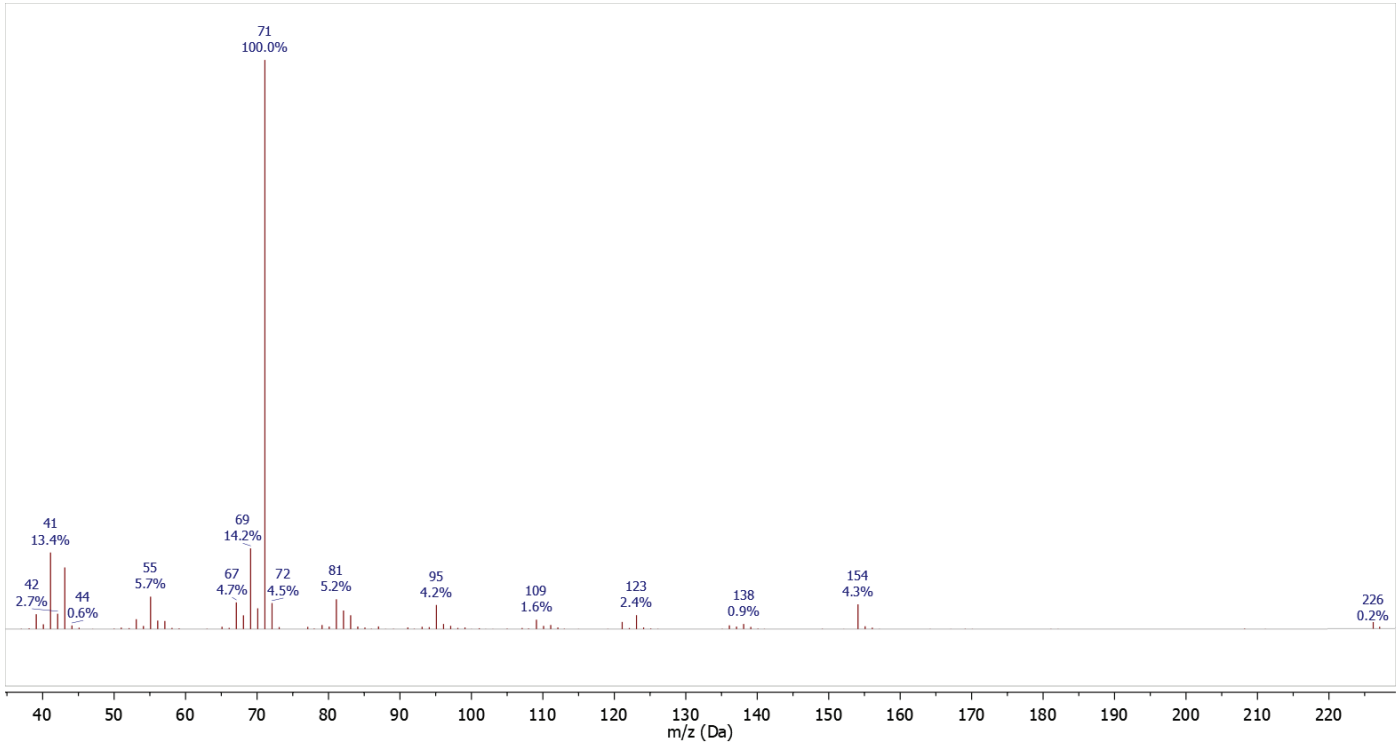

Fig. S-7. EI (70 eV) Mass spectrum of a diastereomer of **4** (RI 1553).

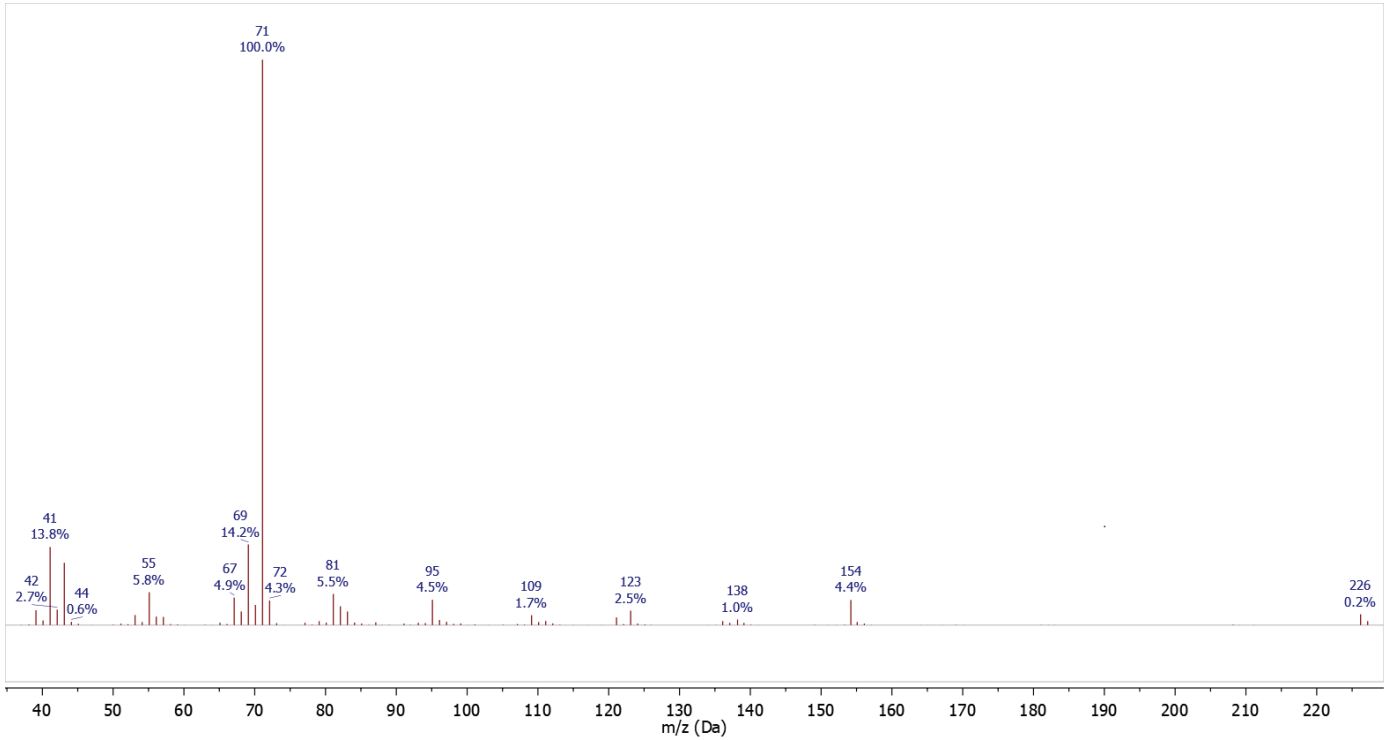

Fig. S-8. EI (70 eV) Mass spectrum of a diastereomer of **4** (RI 1554).

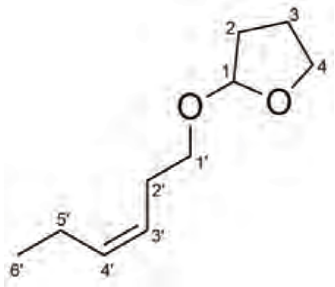

Fig. S-9. Atom numbering scheme of tetrahydrofuranyl acetal of *cis*-3-hexen-1-ol (**5**)

Table S-II. ^{1}H (400 MHz) and ^{13}C (100.6 MHz) NMR data of tetrahydrofuranyl acetal of *cis*-3-hexen-1-ol

Position	**System 1**	
	δ_H (m, *J* (Hz), Integral)[a]	δ_C
1	5.1248 (dd, $^{3}J_{1,2r}$ = 5.0, $^{3}J_{1,2s}$ = 1.5, 1 H)	103.84
2r	1.9170 (dddd, $^{2}J_{2r,2s}$ = -13.1, $^{3}J_{2r,3s}$ = 10.0, $^{3}J_{2r,3r}$ = 8.3, $^{3}J_{1,2r}$ = 5.0, 1 H)	23.58
2s	1.8800 (dddd, $^{2}J_{2r,2s}$ = -13.1, $^{3}J_{2s,3r}$ = 8.5, $^{3}J_{2s,3s}$ = 4.0, $^{3}J_{1,2s}$ = 1.5, 1 H)	
3r	1.9940 (ddddd, $^{2}J_{3r,3s}$ = -13.2, $^{3}J_{2s,3r}$ = 8.5, $^{3}J_{2r,3r}$ = 8.3, $^{3}J_{3r,4r}$ = 7.3, $^{3}J_{3r,4s}$ = 5.6, 1 H)	32.43
3s	1.8165 (ddddd, $^{2}J_{3r,3s}$ = -13.2, $^{3}J_{2s,3s}$ = 4.0, $^{3}J_{3s,4s}$ = 7.5, $^{3}J_{3s,4r}$ = 6.2, $^{3}J_{2r,3s}$ = 10.0, 1 H)	
4r	3.8958 (ddd, $^{2}J_{4r,4s}$ = -8.2, $^{3}J_{3r,4r}$ = 7.3, $^{3}J_{3s,4r}$ = 6.2, 1 H)	66.92
4s	3.8553 (ddd, $^{2}J_{4r,4s}$ = -8.2, $^{3}J_{3s,4s}$ = 7.5, $^{3}J_{3r,4s}$ = 5.6, 1 H)	
1'r	3.3826 (ddd, $^{2}J_{1'r,1's}$ = -9.5, $^{3}J_{1'r,2'r}$ = 7.2, $^{3}J_{1'r,2's}$ = 7.0, 1 H)	66.89
1's	3.6472 (ddd, $^{2}J_{1'r,1's}$ = -9.5, $^{3}J_{1's,2's}$ = 7.2, $^{3}J_{1's,2'r}$ = 7.0, 1 H)	
2'r	2.3170 (dddddd, $^{2}J_{2'r,2's}$ = -21.0, $^{3}J_{2'r,3'}$ = 7.3, $^{3}J_{1'r,2'r}$ = 7.2, $^{3}J_{1's,2'r}$ = 7.0, $^{4}J_{2'r,4'}$ = 1.5, 1 H)	27.96
2's	2.3030 (dddddd, $^{2}J_{2'r,2's}$ = -21.0, $^{3}J_{2's,3'}$ = 7.3, $^{3}J_{1's,2's}$ = 7.2, $J_{1'r,2's}$= 7.0, $^{4}J_{2's,4'}$ = 1.5, 1 H)	

3'	5.3325 (ddddd, $^{3}J_{3',4'} = 10.8$, $^{3}J_{2'r,3'} = {}^{3}J_{2's,3'} = 7.3$, $^{4}J_{3',5'r} = {}^{4}J_{3',5's} = 1.5$, 1 H)	125.03
4'	5.4535 (ddddd, $^{3}J_{3',4'} = 10.8$, $^{3}J_{4',5'r} = {}^{3}J_{4',5's} = 7.3$, $^{4}J_{2'r,4'} = {}^{4}J_{2's,4'} = 1.5$, 1 H)	133.63
5'r	2.0630 (dqdd, $^{2}J_{5'r,5's} = -20.0$, $^{3}J_{5'r,6'} = 7.5$, $^{3}J_{4',5'r} = 7.3$, $^{4}J_{3',5'r} = 1.5$, 1 H)	20.71
5's	2.0490 (dqdd, $^{2}J_{5'r,5's} = -20.0$, $J_{5's,6'} = 7.5$, $^{3}J_{4',5's} = 7.3$, $^{4}J_{3',5's} = 1.5$, 1 H)	
6'	0.9600 (dd, $^{3}J_{5'r,6'} = {}^{3}J_{5's,6'} = 7.5$, 3 H)	14.35

[a]Coupling constant values were initially inferred from ^{1}H homonuclear selective decoupling NMR experiments and afterward refined through a manual iterative full spin analysis.

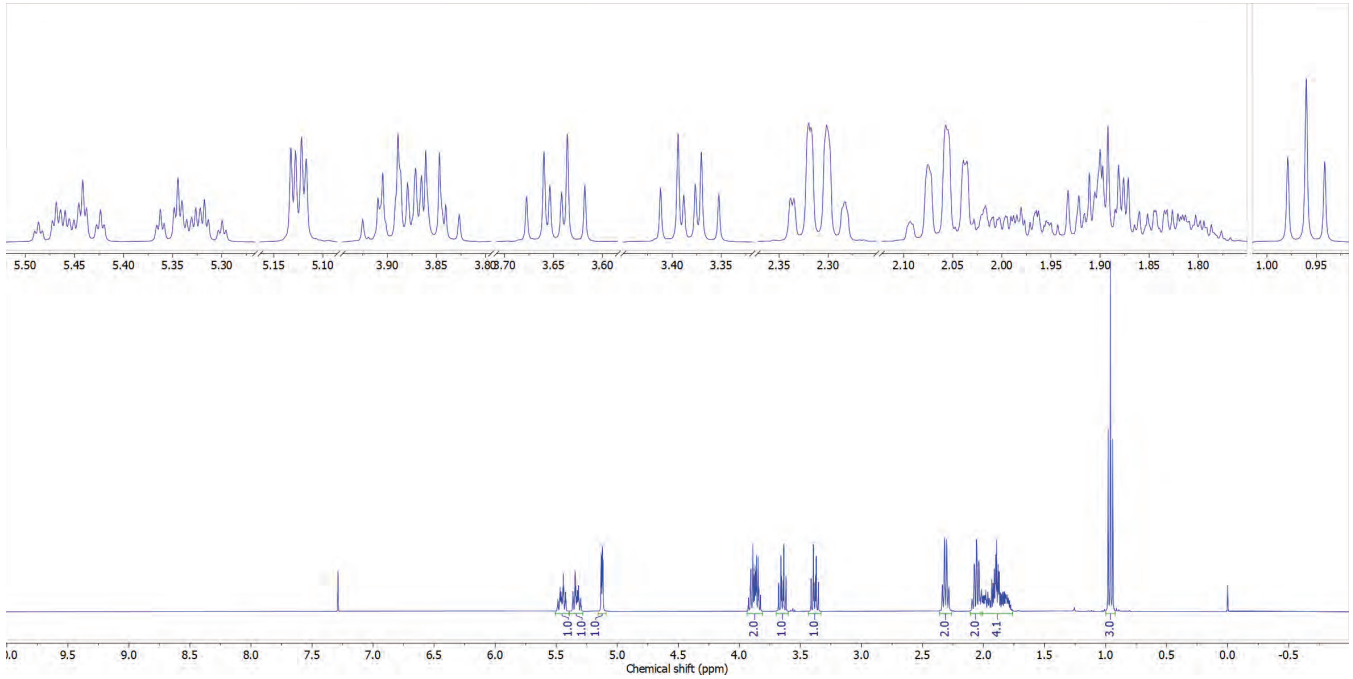

Fig. S-10. ^{1}H-NMR (400 MHz, $CDCl_3$) spectrum of tetrahydrofuranyl acetal of *cis*-3-hexen-1-ol and the corresponding expansions.

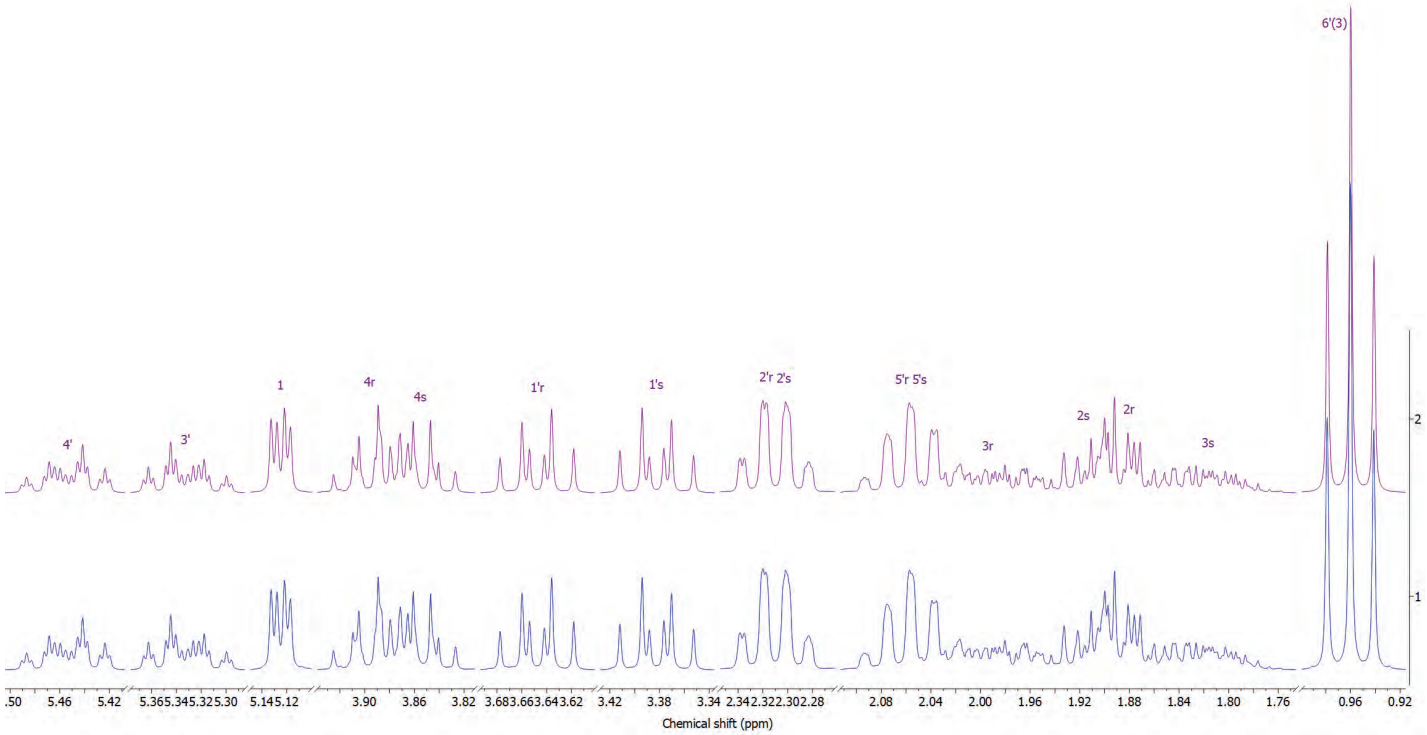

Fig. S-11. Upper trace: simulated ^{1}H NMR (400 MHz) spectrum of **5**; lower trace: ^{1}H NMR (400 MHz, $CDCl_3$) spectrum of **5**.

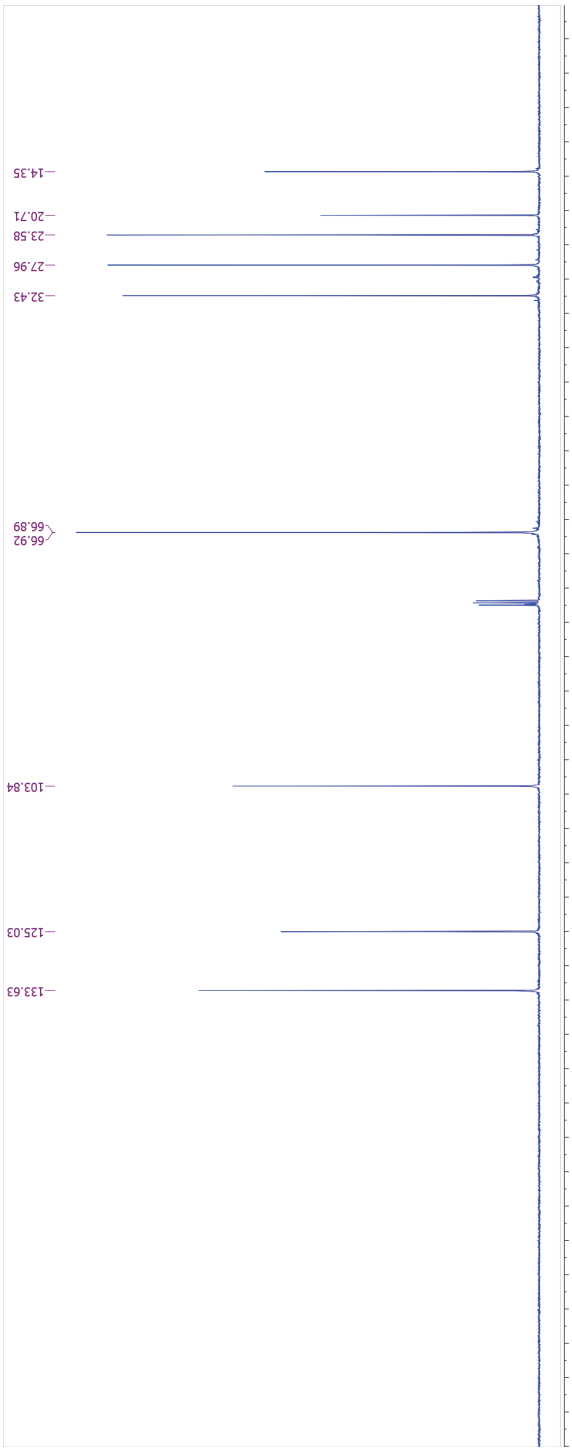

Fig. S-12. ^{13}C-NMR (100.6 MHz, $CDCl_3$) spectrum of **5**.

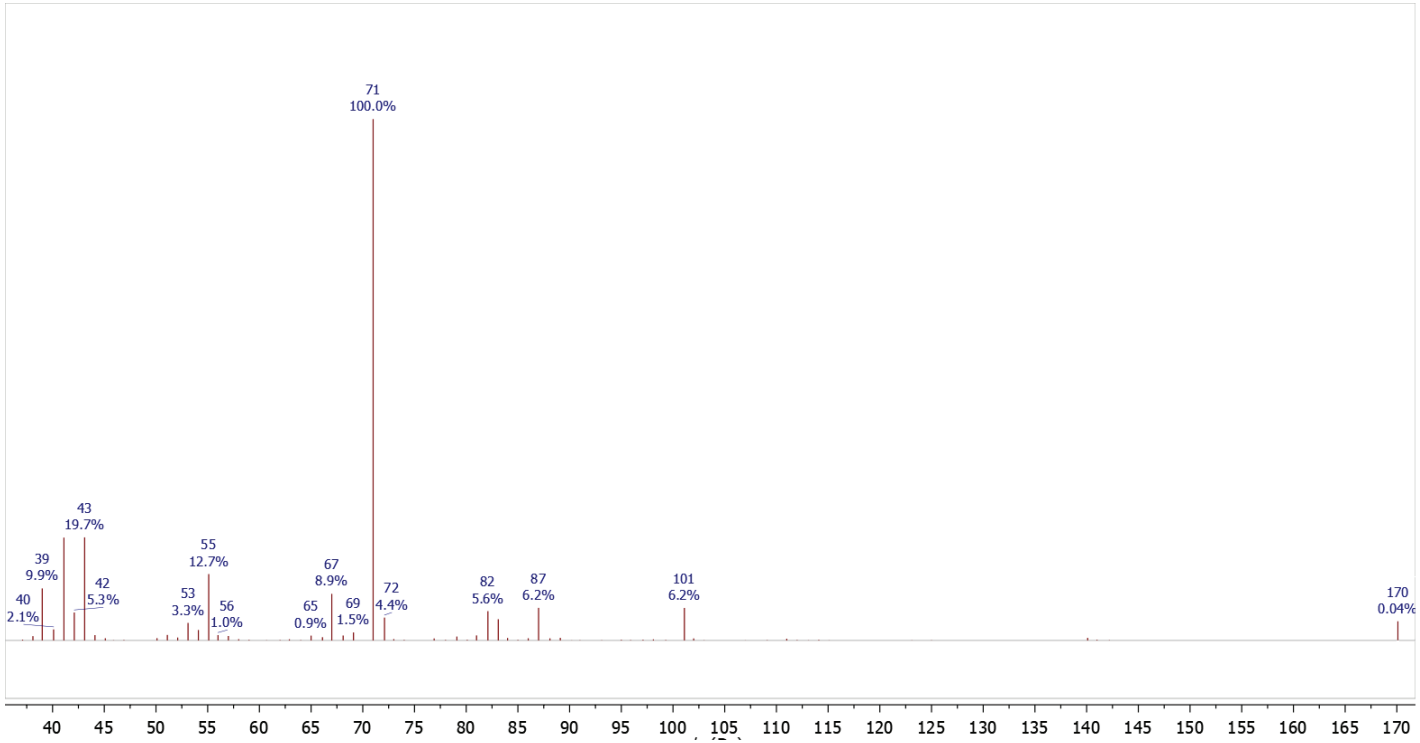

Fig. S-13. EI (70 eV) Mass spectrum of **5**.

Table S-III. Calculated vicinal coupling constants (from H-1 to H-6')

	1 -2r	1 -2s	2r - 3r	2r - 3s	2s - 3r	2s - 3s	3r - 4r	3r - 4s	3s - 4r	3s - 4s	1'r - 2'r	1'r - 2's	1's - 2'r	1's - 2's	2'r-3'	2's-3'	3'-4'r	3'-4's	4'r - 5'r	4'r - 5's	4's - 5'r	4's - 5's	5'r - 6'	5's - 6'
SS new 311	7.73	2.01	11.63	7.38	7.71	2.04	9.61	9.49	2.46	9.40	8.25	7.28	5.28	8.34	11.90	4.75	10.89	4.99	4.15	11.64	11.62	4.26	8.52	8.55
SR new 311	8.87	2.98	8.20	8.41	8.61	4.61	9.08	6.35	5.92	9.16	9.71	4.93	6.09	9.63	8.34	7.49	6.23	7.28	4.09	11.46	11.48	4.59	7.81	8.38
	1 -2r	1 -2s	2r - 3r	2r - 3s	2s - 3r	2s - 3s	3r - 4r	3r - 4s	3s - 4r	3s - 4s	1'r - 2'r	1'r - 2's	1's - 2'r	1's - 2's	2'r-3'	2's-3'	3'-4'r	3'-4's	4'r - 5'r	4'r - 5's	4's - 5'r	4's - 5's	5'r - 6'	5's - 6'
SS new cor	4.95	1.29	11.16	7.09	7.40	1.95	9.22	9.11	2.37	9.02	6.80	5.87	3.94	6.88	11.42	4.56	10.46	4.79	3.98	11.17	11.16	4.09	8.18	8.21
SR new cor	5.68	1.91	7.87	8.08	8.27	4.43	8.71	6.09	5.68	8.80	8.20	3.61	4.73	8.12	8.00	7.19	5.98	6.99	3.93	11.01	11.02	4.41	7.50	8.04

Table S-IV. Dihedral angles between vicinal hydrogens (from H-1 to H-6') for every conformer of **4a**/**4b**

4c/4d (SS/RR)																										
	boletzmen	energy	1-2r	1-2s	2r-3r	2r-3s	2s-3r	2s-3s	3r-4r	3r-4s	3s-4r	3s-4s	1'r-2'r	1'r-2's	1's-2'r	1's-2's	2'r-3'	2's-3'	3'-4'r	3'-4's	4'r-5'r	4'r-5's	4's-5'r	4's-5's	5'r-6'	5's-6'
M0007	-1825208.81	0.206	-695183119.00	-35.85	84.77	159.88	38.54	36.53	-84.80	-28.14	-146.15	98.07	-24.84	56.61	173.40	-59.94	54.84	177.39	61.12	175.73	-68.73	-59.84	-175.11	-174.16	70.06	-161.96	-45.74
M0031	-1825209.01	0.149	-695184813.00	-35.98	84.64	159.78	38.49	36.40	-84.88	-22.65	-145.71	98.56	-24.50	174.28	-70.36	54.54	169.59	179.12	62.54	-179.91	-64.63	-58.22	-174.16	-179.06	71.00	-160.10	-43.77
M0027	-1825208.53	0.123	-695184633.00	-36.00	84.61	158.89	37.70	35.57	-85.62	-21.16	-144.15	99.93	+23.06	172.84	-71.94	53.08	168.39	173.90	56.86	63.58	178.77	-71.63	172.60	179.44	57.67	43.99	160.21
M0009	-1825208.49	0.121	-695184618.00	-36.23	84.45	159.87	38.53	36.48	-84.86	-22.52	-145.56	98.66	-24.38	59.20	174.27	-59.12	55.65	179.54	63.32	179.68	-64.95	-60.68	-176.45	-175.47	68.76	36.50	152.72
M0032	-1825208.43	0.118	-695184599.00	-36.00	84.63	159.86	38.55	36.47	-84.85	-22.70	-145.73	98.49	-24.53	174.52	-70.12	54.78	170.13	177.13	60.54	176.24	-68.32	-61.27	-177.07	-176.29	67.91	44.12	160.34
M0013	-1825206.11	0.046	-695183711.00	-36.08	84.56	159.42	38.13	36.05	-85.24	-22.12	-145.07	99.05	-23.90	58.31	173.04	-60.30	54.42	178.79	62.47	-179.51	-64.19	57.88	-56.96	-56.96	-171.90	64.13	-179.36
M0008	-1825206.00	0.044	-695183668.00	-36.91	83.86	158.92	37.71	35.52	-85.69	-20.36	-143.10	100.74	-22.01	-52.67	62.57	-171.79	-56.55	-60.13	-176.44	-177.58	-61.58	-58.27	-174.06	-173.22	71.00	-170.88	-54.37
M0062	-1825204.27	0.022	-695183008.00	-35.94	84.63	160.22	38.86	36.81	-84.55	-23.45	-146.54	97.84	-25.24	-171.57	-56.53	69.12	-175.84	-57.53	-173.80	-52.35	62.46	-63.87	-179.77	-178.11	65.99	41.72	157.74
M0033	-1825204.22	0.022	-695182990.00	-36.99	83.57	156.71	35.82	33.37	-87.52	-16.27	-139.01	104.43	-18.31	-60.51	59.82	-179.15	-64.82	-154.25	69.17	77.40	-167.06	-63.34	-178.61	-178.45	66.28	44.87	160.84
M0021	-1825204.15	0.021	-695182962.00	-36.28	84.44	160.29	38.89	36.91	-84.49	-23.37	-146.42	97.89	-25.16	58.89	173.72	-59.78	55.05	179.43	63.02	-178.98	-62.74	58.91	-55.67	-56.31	-170.89	-147.84	-32.18
M0024	-1825203.75	0.018	-695182810.00	-35.75	84.92	160.17	38.79	36.85	-84.53	-23.76	-146.79	97.57	-25.47	174.19	-70.35	54.37	170.03	174.41	57.26	60.85	173.89	170.76	55.76	55.71	-59.30	178.45	-65.04
M0028	-1825203.69	0.017	-695182788.00	-36.43	84.24	158.51	37.42	35.11	-85.98	-20.17	-143.03	100.91	-21.96	-76.62	88.01	164.68	-80.69	178.86	62.76	-177.77	-62.46	-58.06	-178.89	-177.68	71.42	-152.44	-36.13
M0023	-1825203.55	0.016	-695182735.00	-36.85	84.84	159.47	38.21	36.00	-85.25	-21.84	-144.69	99.52	-23.53	173.51	-71.13	53.81	169.17	177.69	61.04	175.58	-65.16	57.46	-57.49	-57.60	-172.54	62.84	179.31
M0047	-1825202.93	0.013	-695182499.00	-35.75	84.86	159.62	38.32	36.22	-85.06	-22.59	-145.62	98.62	-24.41	174.87	-69.74	55.26	170.65	-179.93	63.45	-177.65	-62.15	58.80	-55.69	-56.55	-171.04	-147.19	-31.64
M0001	-1825202.43	0.010	-695182307.00	-36.55	84.16	160.12	38.72	36.69	-84.71	-22.68	-145.89	98.33	-24.68	65.53	-179.89	-54.06	60.52	-165.14	77.57	63.89	179.47	166.37	51.87	51.13	-63.37	42.20	157.78
M0015	-1825202.27	0.010	-695182246.00	-36.44	84.38	161.07	39.59	37.61	-83.87	-24.66	-147.59	96.64	-26.29	-53.84	61.01	-172.94	-58.09	-54.22	-170.32	-55.77	59.13	-68.92	175.02	176.53	60.47	43.05	159.13
M0056	-1825201.92	0.009	-695182113.00	-35.93	84.73	160.35	38.95	36.91	-84.49	-23.69	-146.73	97.54	-25.49	-167.38	-52.15	73.02	-171.76	-59.99	-176.44	-174.27	-56.22	58.56	-56.07	-56.64	-171.28	-144.51	-28.79
M0018	-1825201.19	0.006	-695181838.00	-36.68	84.06	159.62	38.35	36.23	-85.04	-22.00	-145.05	99.18	-23.87	77.96	-167.99	-40.86	73.19	-60.20	-175.74	-56.01	59.46	-64.26	178.99	-179.32	63.93	50.91	168.12
M0014	-1825201.06	0.006	-695181787.00	-36.70	83.93	158.91	37.74	35.61	-85.56	-20.57	-143.60	100.50	-22.53	63.70	177.77	-54.65	59.42	-87.06	156.55	174.15	-70.33	57.25	-57.34	-58.52	-173.60	63.23	179.58
M0003	-1825200.48	0.005	-695181566.00	-36.67	83.89	152.22	31.48	29.02	-91.73	-8.74	-131.47	111.86	-10.87	-62.58	52.59	177.70	-67.12	-75.90	167.32	179.16	-70.96	-64.62	178.80	-179.25	65.17	51.21	147.15
M0067	-1825200.04	0.004	-695181399.00	-0.33	118.51	100.46	-21.15	-21.48	-143.09	36.91	-87.33	157.59	33.34	60.88	175.16	-58.30	56.48	-176.62	66.40	-57.85	57.19	-65.00	176.92	-179.61	64.32	-150.98	-34.99
M0058	-1825199.52	0.003	-695181200.00	-36.18	84.48	159.21	37.98	35.83	-85.39	-21.48	-144.50	99.67	-23.35	-178.04	-63.05	61.86	176.84	58.75	-57.47	176.46	-67.59	56.26	-56.68	-58.75	-173.69	63.11	179.71
M0075	-1825197.91	0.002	-695180587.00	-1.59	117.27	101.55	-20.00	-20.35	-141.90	36.40	-87.86	156.99	32.74	173.29	-71.53	53.43	168.62	174.01	57.02	61.11	176.44	170.52	55.99	55.19	-59.34	29.70	145.25
M0054	-1825196.97	0.001	-695180229.00	-37.09	83.58	156.88	33.95	33.49	-87.43	-16.57	-139.49	104.23	-18.69	-59.89	54.46	-178.78	-64.44	-150.86	92.19	71.91	-172.55	174.54	59.85	59.23	-55.47	30.23	145.57
M0012	-1825196.20	0.001	-695179937.00	-35.45	84.96	155.32	34.51	32.18	-88.82	-15.84	-138.76	104.77	-18.16	60.45	175.10	-58.50	56.16	-174.91	68.21	69.77	-174.95	173.38	58.26	58.53	-56.80	-168.81	-52.28
M0006	-1825196.20	0.001	-695179936.00	-38.13	82.62	153.33	32.60	29.90	-90.84	-8.68	-132.09	112.08	-11.33	-63.06	51.80	177.48	-67.65	-76.87	166.65	169.97	-74.37	45.43	-69.47	-69.48	175.60	45.30	160.80
M0037	-1825195.73	0.001	-695179758.00	-0.89	118.08	100.53	-21.13	-21.47	-143.13	37.21	-86.95	157.91	33.75	-55.73	59.14	-174.98	-60.11	-56.92	-173.10	-55.64	59.33	-65.03	178.75	-179.47	64.31	-155.43	-39.01
M0036	-1825195.44	0.001	-695179647.00	-35.88	84.61	158.76	37.51	35.46	-85.78	-20.95	-148.95	100.16	-22.85	73.81	-172.01	-44.26	69.92	-75.53	168.49	175.87	-68.75	57.15	-57.66	-58.45	-173.26	-141.52	-26.06
M0069	-1825195.36	0.001	-695179614.00	-36.70	84.16	160.37	39.00	36.94	-84.43	-23.25	-146.19	98.02	-24.93	-57.26	57.91	-176.46	-61.29	-71.31	172.22	168.98	-65.42	176.43	62.10	61.93	-52.40	32.68	151.61
M0035	-1825195.10	0.001	-695179517.00	-36.18	84.45	157.94	36.84	34.58	-86.52	-18.25	-142.86	101.81	-21.30	-50.37	63.41	-168.94	-55.17	-60.39	-175.26	-53.16	61.75	-63.75	-179.87	-178.19	65.66	-157.14	-40.99
M0042	-1825194.81	0.000	-695179404.00	-36.41	84.26	157.66	36.59	34.31	-86.76	-18.21	-141.21	102.79	-20.20	172.38	-71.64	53.90	169.88	-81.00	162.37	161.30	-62.88	47.25	-68.07	-67.89	178.79	45.86	162.07
M0064	-1825194.62	0.000	-695179334.00	-36.78	83.74	153.18	32.41	29.97	-90.81	-9.76	-133.04	110.80	-12.48	-55.34	59.80	-174.52	-59.38	-64.70	178.82	-176.69	-60.71	55.06	-59.64	-60.04	-174.74	-164.14	-48.19
M0052	-1825194.41	0.000	-695179253.00	-36.65	84.19	160.48	39.04	37.00	-84.44	-22.89	-145.72	98.26	-24.55	-73.61	60.97	167.27	-78.15	55.61	-60.30	176.35	-68.77	-61.91	-177.95	-176.36	67.59	-157.28	-40.92
M0071	-1825194.00	0.000	-695179098.00	-5.59	113.34	104.78	-16.68	-17.17	-138.62	35.19	-89.01	155.70	31.50	-65.21	49.17	176.23	-69.38	-165.20	78.51	-175.07	-59.46	57.81	-56.84	-57.50	-172.15	-145.90	-30.19
M0049	-1825192.91	0.000	-695178682.00	-36.88	83.86	158.39	37.35	35.01	-86.03	-19.50	-142.20	101.53	-21.18	-69.70	44.64	171.49	-74.17	60.67	-55.00	-179.47	-64.60	57.44	-57.38	-57.49	-172.31	65.53	-178.07
M0002	-1825192.46	0.000	-695178512.00	-36.90	84.49	160.98	39.53	37.61	-83.84	-24.16	-147.35	97.02	-26.17	-51.37	63.58	-170.17	-55.22	-51.95	-168.00	-57.12	57.58	-72.74	170.68	172.66	56.08	-160.65	-43.58
M0066	-1825192.29	0.000	-695178446.00	-35.62	85.02	159.50	38.28	36.17	-85.07	-22.73	-145.43	98.46	-24.23	-63.80	51.92	177.37	-67.41	-73.11	170.06	139.84	-104.15	175.49	60.50	61.09	-53.90	-168.60	-51.96
M0034	-1825191.57	0.000	-695178171.00	-36.85	83.85	154.86	34.04	31.54	-89.27	-12.60	-135.59	108.18	-14.80	167.15	-77.51	47.80	163.14	173.01	57.76	58.79	173.96	169.85	54.86	54.66	-60.33	179.46	-64.03
M0004	-1825191.03	0.000	-695177947.00	-35.72	84.90	159.25	38.01	35.88	-83.36	-21.67	-144.68	99.49	-23.72	176.97	-66.91	57.50	173.72	-177.41	65.75	61.98	177.09	167.70	52.76	52.69	-62.26	-179.76	-63.36
M0005	-1825190.29	0.000	-695177685.00	-36.35	84.26	156.78	35.77	33.48	-87.33	-16.86	-140.01	104.06	-19.09	-175.15	-58.91	65.68	-178.08	-57.67	-173.75	-49.83	65.07	-67.35	176.39	178.36	62.11	-161.78	-45.41
M0010	-1825190.02	0.000	-695177562.00	-36.23	84.30	159.95	38.16	36.79	-90.06	-11.53	-134.53	109.23	-13.76	-178.27	-63.33	62.20	177.14	52.87	-63.45	60.03	174.83	173.62	60.31	60.97	-54.38	177.77	-65.69
M0011	-1825189.79	0.000	-695177496.00	-36.84	84.03	160.38	39.09	36.93	-84.85	-22.21	-145.85	99.11	-24.03	52.09	167.72	-66.02	49.61	179.18	62.39	171.24	-73.21	51.63	-63.57	-63.46	-178.86	51.16	167.37
M0068	-1825189.72	0.000	-695177466.00	-36.78	84.04	160.30	38.93	36.83	-84.54	-23.00	-145.85	98.20	-24.65	-56.44	58.60	-175.70	-60.66	-61.16	-177.32	-44.33	69.90	54.41	-59.50	-59.64	-173.55	67.47	-177.12
M0041	-1825189.69	0.000	-695177454.00	-35.48	85.36	162.28	40.82	38.56	-82.60	-27.24	-150.21	94.12	-28.85	60.53	175.80	-57.91	57.36	-170.02	72.51	74.83	-170.45	-175.88	69.46	69.20	-45.46	76.76	-167.30
M0025	-1825187.98	0.000	-695176804.00	-36.50	84.22	159.23	38.00	35.87	-85.35	-20.55	-143.34	100.47	-22.33	70.70	-174.95	-46.99	57.36	-70.58	173.27	-177.62	-62.67	59.08	-55.92	-56.15	-171.16	66.23	-177.34
M0060	-1825182.90	0.000	-695174671.00	-34.99	85.55	159.83	38.62	36.81	-84.60	-23.22	-146.12	97.83	-25.07	66.45	-178.99	-50.96	63.58	-79.08	164.31	176.46	-67.96	57.63	-57.16	-58.39	-173.18	-140.28	-24.72
M0046	-1825182.77	0.000	-695174622.00	-36.75	84.07	160.43	39.01	36.99	-84.43	-23.10	-146.04	98.14	-24.79	-52.03	62.99	-170.87	-55.86	-56.60	-172.88	-62.65	51.54	-179.94	66.24	65.67	-48.16	-164.14	136.07
M0059	-1825182.24	0.000	-695174618.00	-0.01	118.75	100.30	-21.44	-21.58	-143.32	37.66	-86.42	158.43	34.34	54.65	170.19	-63.41	52.12	179.29	62.53	168.90	-75.17	49.39	-65.77	-65.90	178.94	48.58	164.58
M0030	-1825178.91	0.000	-695173851.00	-35.60	85.00	159.34	38.07	36.02	-85.25	-21.96	-144.95	99.34	-23.74	176.24	-67.93	56.97	172.60	-65.23	178.61	-58.58	55.17	-178.00	68.13	68.27	-45.80	168.08	-76.80
M0026	-1825170.56	0.000	-695170171.00	-34.00	86.10	153.59	32.83	30.67	-90.09	-13.58	-136.35	106.76	-16.01	-72.53	40.57	169.46	-77.44	68.48	-45.82	-70.60	43.90	-70.63	173.45	174.99	59.07	-139.40	-22.32

Table S-V. Calculated vicinal coupling constants (from H-1 to H-6') for every conformer of **4a**/**4b**

boltzmen	1-2r	1-2s	2r-3r	2r-3s	2s-3r	2s-3s	3r-4r	3r-4s	3s-4r	3s-4s	1'r-2'r	1'r-2's	1's-2'r	1's-2's	2'r-3'	2's-3'	3'-4'r	3'-4's	4'r-5'r	4'r-5's	4's-5'r	4's-5's	5'r-6'	5's-6'
0.206	7.76	1.99	11.76	7.34	7.65	1.99	9.54	9.73	2.34	9.32	4.18	12.86	4.01	4.74	12.98	3.85	12.94	2.95	4.09	12.92	12.89	2.82	10.38	6.79
0.149	7.74	1.99	11.74	7.34	7.67	1.99	9.59	9.65	2.37	9.37	12.90	2.79	4.78	12.68	13.00	3.67	13.00	3.41	4.25	12.89	12.85	2.73	10.20	7.08
0.123	7.74	1.99	11.66	7.47	7.80	1.98	9.76	9.38	2.47	9.55	12.84	2.66	5.01	12.57	12.88	4.44	3.53	13.00	2.68	12.83	12.86	4.33	7.05	10.21
0.121	7.70	2.00	11.75	7.34	7.66	1.99	9.61	9.63	2.38	9.39	4.07	12.90	4.12	4.62	13.00	3.57	13.00	3.37	3.91	12.96	12.93	2.95	8.16	9.39
0.118	7.74	1.99	11.75	7.33	7.66	1.99	9.59	9.66	2.37	9.37	12.90	2.82	4.75	12.69	12.97	3.93	12.95	3.00	3.33	12.97	12.96	3.04	7.03	10.23
0.046	7.72	2.00	11.70	7.40	7.73	1.99	9.66	9.54	2.40	9.44	4.23	12.85	3.96	4.80	13.00	3.67	13.00	3.46	4.28	4.43	4.43	12.79	4.24	11.20
0.044	7.56	2.01	11.64	7.47	7.81	1.96	9.85	9.19	2.53	9.67	5.07	3.66	12.78	4.49	3.98	12.96	12.98	3.79	4.24	12.89	12.85	2.73	10.98	5.52
0.021	7.75	1.99	11.80	7.28	7.61	2.00	9.50	9.79	2.32	9.28	12.77	4.49	3.91	12.94	4.35	12.88	5.12	3.68	3.50	13.00	12.99	3.25	7.39	9.97
0.022	7.56	2.01	11.36	7.76	8.14	1.98	10.26	8.45	2.87	10.06	3.93	4.89	13.00	3.38	11.01	1.99	2.26	12.47	3.56	12.99	12.99	3.22	6.92	10.27
0.021	7.69	2.00	11.80	7.28	7.59	2.00	9.51	9.77	2.33	9.29	4.15	12.87	4.03	4.71	13.00	3.60	12.99	3.64	4.15	4.62	4.52	12.74	8.76	8.76
0.018	7.77	1.99	11.79	7.30	7.60	2.00	9.46	9.84	2.31	9.25	12.89	2.79	4.78	12.69	12.90	4.38	3.89	12.95	12.73	4.60	4.61	4.10	11.19	4.13
0.017	7.67	2.00	11.59	7.51	7.87	1.98	9.87	9.18	2.55	9.67	2.30	7.42	12.27	2.10	12.99	3.64	12.98	3.68	4.28	12.88	12.83	2.70	9.36	8.21
0.016	7.68	2.00	11.71	7.39	7.74	1.99	9.71	9.48	2.44	9.49	12.87	2.72	4.90	12.63	12.98	3.86	13.00	3.34	4.36	4.35	4.34	12.82	4.39	11.20
0.013	7.77	1.99	11.72	7.37	7.70	1.99	9.60	9.64	2.37	9.38	12.92	2.85	4.68	12.72	13.00	3.55	12.98	3.72	4.17	4.61	4.49	12.75	8.67	8.83
0.010	7.65	2.00	11.78	7.31	7.63	1.99	9.57	9.68	2.35	9.35	3.30	13.00	4.86	3.93	12.31	2.25	3.50	13.00	12.42	5.19	5.31	3.56	7.32	9.97
0.010	7.67	2.00	11.89	7.17	7.48	2.01	9.35	9.97	2.25	9.14	4.88	3.86	12.84	4.27	4.83	12.70	4.60	4.12	2.93	12.92	12.96	3.94	7.19	10.11
0.009	7.75	1.99	11.81	7.27	7.59	2.00	9.47	9.83	2.30	9.25	12.50	5.15	2.56	12.78	4.00	12.96	12.90	4.25	4.20	4.56	4.47	12.76	8.30	9.21
0.006	7.63	2.00	11.72	7.37	7.70	1.99	9.67	9.54	2.41	9.45	2.23	12.55	6.96	2.55	3.97	12.94	4.57	4.07	3.45	13.00	13.00	3.49	6.02	10.84
0.006	7.63	2.01	11.64	7.46	7.80	1.98	9.83	9.28	2.51	9.61	3.52	12.98	4.77	4.08	1.98	11.33	12.89	2.80	4.39	4.30	4.20	12.87	4.34	11.20
0.005	7.63	2.01	10.71	8.42	8.77	2.04	10.78	7.05	3.76	10.66	3.66	5.08	12.98	3.12	2.33	12.48	12.85	2.74	3.41	13.00	13.00	3.34	8.89	8.67
0.004	11.00	4.76	2.51	9.77	9.73	9.19	7.59	1.98	11.47	8.14	3.95	12.93	4.24	4.50	12.96	3.20	4.30	4.39	3.36	13.00	13.00	3.44	9.18	8.37
0.003	7.71	2.00	11.68	7.42	7.76	1.98	9.73	9.44	2.45	9.51	12.99	3.60	3.75	12.97	4.17	4.35	12.96	3.07	4.53	4.18	4.17	12.87	4.36	11.20
0.002	10.99	4.56	2.60	9.89	9.85	8.98	7.67	1.96	11.39	8.23	12.86	2.69	4.95	12.59	12.89	4.42	3.85	12.96	12.72	4.57	4.69	4.09	9.09	8.41
0.001	7.57	2.01	11.38	7.74	8.12	1.98	10.23	8.54	2.85	10.03	4.01	4.80	13.00	3.43	10.50	2.05	2.65	12.82	12.90	4.02	4.11	4.65	9.02	8.45
0.001	7.82	1.99	11.17	7.97	8.32	1.98	10.29	8.41	2.90	10.08	3.94	12.92	4.21	4.54	12.92	3.01	2.85	12.92	12.86	4.24	4.20	4.48	10.88	5.82
0.001	7.40	2.04	10.88	8.25	8.63	2.02	10.78	7.16	3.79	10.63	3.60	5.21	12.98	3.07	2.29	12.44	12.88	2.46	6.22	2.88	2.88	12.94	6.83	10.27
0.001	11.00	4.69	2.52	9.77	9.73	9.20	7.55	1.98	11.51	8.06	4.61	4.12	12.92	3.99	4.43	12.85	4.70	4.02	3.36	13.00	13.00	3.45	9.71	7.79
0.001	7.75	1.99	11.62	7.50	7.82	1.98	9.79	9.35	2.49	9.57	2.50	12.80	6.41	2.84	2.37	12.58	12.95	2.95	4.40	4.33	4.21	12.86	7.87	9.54
0.001	7.63	2.00	11.81	7.26	7.59	2.00	9.52	9.73	2.33	9.32	4.38	4.29	12.96	3.83	2.71	12.81	10.10	2.18	12.96	3.72	3.74	5.11	8.25	9.26
0.001	7.71	2.00	11.52	7.60	7.96	1.98	9.97	9.06	2.62	9.75	5.43	3.56	12.61	4.69	3.95	12.93	5.00	3.79	3.51	13.00	12.99	3.28	9.90	7.50
0.000	7.67	2.00	11.48	7.64	8.00	1.98	10.07	8.85	2.71	9.87	12.82	2.68	4.88	12.68	2.09	12.04	11.92	2.03	5.93	3.02	3.04	12.97	6.77	10.38
0.000	7.61	2.01	10.86	8.28	8.64	2.02	10.73	7.34	3.62	10.56	4.67	4.03	12.90	4.08	3.40	13.00	12.96	3.90	4.71	4.05	3.99	12.91	10.56	6.42
0.000	7.63	2.00	11.33	7.26	7.58	2.00	9.57	9.65	2.35	9.36	2.51	6.95	12.48	2.22	4.63	3.96	12.96	2.95	3.75	12.99	12.96	3.07	9.92	7.51
0.000	10.91	3.97	2.91	10.22	10.17	8.38	7.86	1.99	11.22	8.42	3.34	5.62	12.95	2.89	12.31	2.20	12.92	4.07	4.31	4.44	4.35	12.80	8.50	9.03
0.000	7.60	2.01	11.57	7.52	7.89	1.98	9.94	9.03	2.60	9.76	2.86	6.35	12.77	2.47	3.91	4.72	13.00	3.41	4.36	4.37	4.35	12.81	4.08	11.19
0.000	7.69	2.00	11.86	7.18	7.48	2.01	9.41	9.93	2.27	9.16	5.27	3.53	12.69	4.68	5.18	12.55	4.40	4.34	2.58	12.72	12.83	4.56	10.26	7.11
0.000	7.80	1.99	11.71	7.38	7.71	1.99	9.58	9.60	2.36	9.40	3.57	5.19	12.98	3.09	2.55	12.69	8.60	2.84	12.94	3.93	3.85	4.88	10.86	5.87
0.000	7.60	2.01	11.10	8.04	8.41	1.99	10.55	7.82	3.29	10.38	12.48	2.25	5.84	12.12	12.92	4.31	4.17	12.88	12.67	4.74	4.77	3.96	11.20	4.25
0.000	7.78	1.99	11.68	7.42	7.75	1.98	9.71	9.51	2.44	9.47	12.97	3.16	4.35	12.87	12.98	3.28	3.74	12.97	12.52	5.06	5.07	3.70	11.20	4.33
0.000	7.68	2.00	11.36	7.77	8.12	1.98	10.20	8.64	2.83	9.99	12.92	4.15	3.28	12.99	4.33	12.88	5.52	3.36	3.10	12.96	12.99	3.72	10.36	6.84
0.000	7.70	2.00	10.97	8.17	8.53	2.00	10.62	7.62	3.41	10.46	12.99	3.57	3.71	12.97	5.04	3.55	4.00	12.91	12.94	3.96	3.87	4.82	11.19	4.06
0.000	7.60	2.00	11.81	7.23	7.59	2.00	9.63	9.59	2.41	9.43	5.16	12.52	3.25	5.33	13.00	3.68	12.76	2.55	5.23	3.54	3.55	12.99	5.98	10.80
0.000	7.61	2.00	11.81	7.27	7.61	2.00	9.55	9.68	2.35	9.35	4.50	4.19	12.94	3.91	3.84	12.98	6.40	2.84	4.81	4.07	4.05	12.87	3.86	11.18
0.000	7.82	1.98	12.03	6.97	7.28	2.04	9.02	10.40	2.12	8.80	3.93	12.94	4.29	4.37	12.68	2.60	2.46	12.71	12.95	2.88	2.91	6.22	3.05	10.78
0.000	7.66	2.00	11.65	7.42	7.76	1.98	9.83	9.24	2.51	9.63	2.76	12.92	5.97	3.10	2.77	12.86	12.98	3.65	4.13	4.58	4.55	12.75	4.00	11.18
0.000	7.89	1.98	11.75	7.32	7.64	1.99	9.58	9.72	2.32	9.50	3.20	13.00	5.33	3.58	2.17	12.23	12.96	3.03	4.33	4.40	4.22	12.85	7.69	9.70
0.000	7.62	2.00	11.82	7.26	7.58	2.00	9.54	9.71	2.34	9.33	5.17	3.61	12.74	4.59	4.48	12.84	3.65	5.25	13.00	3.22	3.29	5.78	10.94	7.06
0.000	11.00	4.79	2.50	9.73	9.72	9.23	7.48	1.98	11.58	7.99	4.77	12.70	3.56	5.16	13.00	3.67	12.61	2.39	5.59	3.27	3.26	13.00	6.36	10.59
0.000	7.80	1.99	11.69	7.41	7.73	1.99	9.69	9.52	2.43	9.46	12.95	3.04	4.43	12.84	3.34	12.99	4.20	4.66	12.99	3.02	3.00	6.20	10.83	3.05
0.000	8.04	1.98	10.92	8.22	8.54	2.00	10.48	7.96	3.12	10.28	2.60	7.01	12.65	2.26	2.98	6.16	2.77	6.47	2.77	12.86	12.92	4.13	7.56	9.96

Table S-VI. The product of multiplying the Boltzman weights and Calculated vicinal coupling constants (from H-1 to H-6') for every conformer of **4a**/**4b**

1-2r	1-2s	2r-3r	2r-3s	2s-3r	2s-3s	3r-4r	3r-4s	3s-4r	3s-4s	1'r-2'r	1'r-2's	1's-2'r	1's-2's	2'r-3'	2's-3'	3'-4'r	3'-4's	4'r-5'r	4'r-5's	4's-5'r	4's-5's	5'r-6'	5's-6'
1.60	0.41	2.42	1.51	1.58	0.41	1.96	2.00	0.48	1.92	0.86	2.65	0.83	0.98	2.67	0.79	2.67	0.61	0.84	2.66	2.66	0.58	2.14	1.40
1.15	0.30	1.75	1.09	1.14	0.30	1.43	1.44	0.35	1.40	1.92	0.42	0.71	1.89	1.94	0.55	1.94	0.51	0.63	1.92	1.91	0.41	1.52	1.06
0.95	0.25	1.43	0.92	0.96	0.24	1.20	1.15	0.30	1.17	1.58	0.33	0.62	1.55	1.58	0.55	0.43	1.60	0.33	1.58	1.58	0.53	0.87	1.26
0.93	0.24	1.42	0.89	0.93	0.24	1.16	1.16	0.29	1.14	0.49	1.56	0.50	0.56	1.57	0.43	1.57	0.41	0.47	1.57	1.57	0.36	0.99	1.14
0.91	0.24	1.39	0.87	0.90	0.23	1.13	1.14	0.28	1.11	1.52	0.33	0.56	1.50	1.53	0.46	1.53	0.35	0.45	1.53	1.53	0.36	0.83	1.21
0.36	0.09	0.54	0.34	0.36	0.09	0.44	0.44	0.11	0.43	0.19	0.59	0.18	0.22	0.60	0.17	0.60	0.16	0.20	0.20	0.20	0.59	0.19	0.52
0.33	0.09	0.51	0.33	0.34	0.09	0.43	0.40	0.11	0.43	0.22	0.16	0.56	0.20	0.18	0.57	0.57	0.17	0.19	0.57	0.57	0.12	0.48	0.24
0.17	0.04	0.26	0.16	0.17	0.04	0.21	0.22	0.05	0.20	0.28	0.10	0.06	0.28	0.10	0.28	0.11	0.08	0.08	0.29	0.29	0.07	0.16	0.22
0.17	0.04	0.25	0.17	0.18	0.04	0.23	0.19	0.06	0.22	0.09	0.11	0.29	0.07	0.24	0.04	0.05	0.27	0.08	0.29	0.29	0.07	0.15	0.23
0.16	0.04	0.25	0.15	0.16	0.04	0.20	0.21	0.05	0.20	0.09	0.27	0.08	0.10	0.27	0.08	0.27	0.08	0.09	0.10	0.09	0.27	0.18	0.18
0.14	0.04	0.21	0.13	0.14	0.04	0.17	0.18	0.04	0.17	0.23	0.05	0.09	0.23	0.23	0.08	0.07	0.23	0.23	0.08	0.08	0.07	0.20	0.07
0.13	0.03	0.20	0.13	0.13	0.03	0.17	0.16	0.04	0.16	0.04	0.13	0.21	0.04	0.22	0.06	0.22	0.06	0.07	0.22	0.22	0.05	0.16	0.14
0.12	0.03	0.19	0.12	0.12	0.03	0.16	0.15	0.04	0.15	0.21	0.04	0.08	0.20	0.21	0.06	0.21	0.05	0.07	0.07	0.07	0.21	0.07	0.18
0.10	0.03	0.15	0.10	0.10	0.03	0.12	0.13	0.03	0.12	0.17	0.04	0.06	0.17	0.17	0.05	0.17	0.05	0.05	0.06	0.06	0.17	0.11	0.11
0.08	0.02	0.12	0.07	0.08	0.02	0.10	0.10	0.02	0.09	0.03	0.13	0.05	0.04	0.12	0.02	0.03	0.13	0.12	0.05	0.05	0.04	0.07	0.10
0.08	0.02	0.12	0.07	0.07	0.02	0.09	0.10	0.02	0.09	0.05	0.04	0.13	0.04	0.05	0.13	0.05	0.04	0.03	0.13	0.13	0.04	0.07	0.10
0.07	0.02	0.11	0.07	0.07	0.02	0.09	0.09	0.02	0.08	0.11	0.05	0.02	0.12	0.04	0.12	0.12	0.04	0.04	0.04	0.04	0.11	0.07	0.08
0.05	0.01	0.07	0.04	0.05	0.01	0.06	0.06	0.01	0.06	0.01	0.08	0.04	0.02	0.02	0.08	0.03	0.02	0.02	0.08	0.08	0.02	0.04	0.07
0.05	0.01	0.07	0.04	0.05	0.01	0.06	0.06	0.02	0.06	0.02	0.08	0.03	0.02	0.01	0.07	0.08	0.02	0.03	0.03	0.03	0.06	0.03	0.07
0.04	0.01	0.05	0.04	0.04	0.01	0.05	0.04	0.02	0.05	0.02	0.03	0.06	0.02	0.01	0.06	0.06	0.01	0.02	0.06	0.06	0.02	0.04	0.04
0.04	0.02	0.01	0.04	0.04	0.04	0.03	0.01	0.05	0.03	0.02	0.05	0.02	0.02	0.05	0.01	0.02	0.02	0.01	0.05	0.05	0.01	0.04	0.03
0.02	0.01	0.04	0.02	0.02	0.01	0.03	0.03	0.01	0.03	0.04	0.01	0.01	0.04	0.01	0.01	0.04	0.01	0.01	0.01	0.01	0.04	0.01	0.03
0.02	0.01	0.01	0.02	0.02	0.02	0.02	0.00	0.02	0.02	0.03	0.01	0.01	0.03	0.03	0.01	0.01	0.03	0.03	0.01	0.01	0.01	0.02	0.02
0.01	0.00	0.01	0.01	0.01	0.00	0.01	0.01	0.00	0.01	0.00	0.00	0.01	0.00	0.01	0.00	0.00	0.01	0.01	0.00	0.00	0.00	0.01	0.01
0.01	0.00	0.01	0.01	0.01	0.00	0.01	0.01	0.00	0.01	0.00	0.01	0.00	0.00	0.01	0.00	0.00	0.01	0.01	0.00	0.00	0.00	0.01	0.01
0.01	0.00	0.01	0.01	0.01	0.00	0.01	0.01	0.00	0.01	0.00	0.01	0.01	0.00	0.00	0.01	0.01	0.00	0.01	0.00	0.00	0.01	0.01	0.01
0.01	0.00	0.00	0.01	0.01	0.01	0.00	0.00	0.01	0.01	0.00	0.00	0.01	0.00	0.00	0.01	0.00	0.00	0.00	0.01	0.01	0.00	0.01	0.01
0.01	0.00	0.01	0.01	0.01	0.00	0.01	0.01	0.00	0.01	0.00	0.01	0.01	0.00	0.00	0.01	0.01	0.00	0.00	0.00	0.00	0.01	0.01	0.01
0.01	0.00	0.01	0.01	0.01	0.00	0.01	0.01	0.00	0.01	0.00	0.00	0.01	0.00	0.00	0.01	0.01	0.00	0.01	0.00	0.00	0.01	0.01	0.01
0.01	0.00	0.01	0.01	0.01	0.00	0.01	0.01	0.00	0.01	0.01	0.00	0.01	0.00	0.00	0.01	0.00	0.00	0.00	0.01	0.01	0.00	0.01	0.01
0.00	0.00	0.00	0.00	0.00	0.00	0.00	0.00	0.00	0.00	0.00	0.00	0.00	0.00	0.00	0.00	0.00	0.00	0.00	0.00	0.00	0.00	0.00	0.00
0.00	0.00	0.00	0.00	0.00	0.00	0.00	0.00	0.00	0.00	0.00	0.00	0.00	0.00	0.00	0.00	0.00	0.00	0.00	0.00	0.00	0.00	0.00	0.00
0.00	0.00	0.00	0.00	0.00	0.00	0.00	0.00	0.00	0.00	0.00	0.00	0.00	0.00	0.00	0.00	0.00	0.00	0.00	0.00	0.00	0.00	0.00	0.00
0.00	0.00	0.00	0.00	0.00	0.00	0.00	0.00	0.00	0.00	0.00	0.00	0.00	0.00	0.00	0.00	0.00	0.00	0.00	0.00	0.00	0.00	0.00	0.00
0.00	0.00	0.00	0.00	0.00	0.00	0.00	0.00	0.00	0.00	0.00	0.00	0.00	0.00	0.00	0.00	0.00	0.00	0.00	0.00	0.00	0.00	0.00	0.00
0.00	0.00	0.00	0.00	0.00	0.00	0.00	0.00	0.00	0.00	0.00	0.00	0.00	0.00	0.00	0.00	0.00	0.00	0.00	0.00	0.00	0.00	0.00	0.00
0.00	0.00	0.00	0.00	0.00	0.00	0.00	0.00	0.00	0.00	0.00	0.00	0.00	0.00	0.00	0.00	0.00	0.00	0.00	0.00	0.00	0.00	0.00	0.00
0.00	0.00	0.00	0.00	0.00	0.00	0.00	0.00	0.00	0.00	0.00	0.00	0.00	0.00	0.00	0.00	0.00	0.00	0.00	0.00	0.00	0.00	0.00	0.00
0.00	0.00	0.00	0.00	0.00	0.00	0.00	0.00	0.00	0.00	0.00	0.00	0.00	0.00	0.00	0.00	0.00	0.00	0.00	0.00	0.00	0.00	0.00	0.00
0.00	0.00	0.00	0.00	0.00	0.00	0.00	0.00	0.00	0.00	0.00	0.00	0.00	0.00	0.00	0.00	0.00	0.00	0.00	0.00	0.00	0.00	0.00	0.00
0.00	0.00	0.00	0.00	0.00	0.00	0.00	0.00	0.00	0.00	0.00	0.00	0.00	0.00	0.00	0.00	0.00	0.00	0.00	0.00	0.00	0.00	0.00	0.00
0.00	0.00	0.00	0.00	0.00	0.00	0.00	0.00	0.00	0.00	0.00	0.00	0.00	0.00	0.00	0.00	0.00	0.00	0.00	0.00	0.00	0.00	0.00	0.00
0.00	0.00	0.00	0.00	0.00	0.00	0.00	0.00	0.00	0.00	0.00	0.00	0.00	0.00	0.00	0.00	0.00	0.00	0.00	0.00	0.00	0.00	0.00	0.00
0.00	0.00	0.00	0.00	0.00	0.00	0.00	0.00	0.00	0.00	0.00	0.00	0.00	0.00	0.00	0.00	0.00	0.00	0.00	0.00	0.00	0.00	0.00	0.00
0.00	0.00	0.00	0.00	0.00	0.00	0.00	0.00	0.00	0.00	0.00	0.00	0.00	0.00	0.00	0.00	0.00	0.00	0.00	0.00	0.00	0.00	0.00	0.00
0.00	0.00	0.00	0.00	0.00	0.00	0.00	0.00	0.00	0.00	0.00	0.00	0.00	0.00	0.00	0.00	0.00	0.00	0.00	0.00	0.00	0.00	0.00	0.00
0.00	0.00	0.00	0.00	0.00	0.00	0.00	0.00	0.00	0.00	0.00	0.00	0.00	0.00	0.00	0.00	0.00	0.00	0.00	0.00	0.00	0.00	0.00	0.00
0.00	0.00	0.00	0.00	0.00	0.00	0.00	0.00	0.00	0.00	0.00	0.00	0.00	0.00	0.00	0.00	0.00	0.00	0.00	0.00	0.00	0.00	0.00	0.00
0.00	0.00	0.00	0.00	0.00	0.00	0.00	0.00	0.00	0.00	0.00	0.00	0.00	0.00	0.00	0.00	0.00	0.00	0.00	0.00	0.00	0.00	0.00	0.00

Table S-VII. Dihedral angles between vicinal hydrogens (from H-1 to H-6') for every conformer of **4c**/**4d**

4a/4b (SR/RS)																													
Label	E (kJ/mol)	energy	boltzmann	1'-2r	1'-2s	2r-3r	2r-3s	2s-3r	2s-3s	3r-4r	3r-4s	3s-4r	3s-4s	1'r-2'r	1'r-2's	1's-2'r	1's-2's	2'r-3'	2's-3'	3'-4'r	3'-4's	4'r-5'r	4'r-5's	4's-5'r	4's-5's	5'r-6'	5's-6'
M0082	-1825218.06	-695188263.00	0.145	34001.00	122.01	97.12	-24.50	-24.74	-146.36	93.13	-85.55	159.06	35.33	-56.63	58.28	-175.41	-60.50	-63.69	-179.95	66.49	-178.14	-70.23	173.56	174.90	58.70	58.59	169.99
M0018	-1825217.79	-695188158.00	0.130	-37.48	83.52	159.27	98.01	35.82	-85.43	-21.08	-143.47	99.97	-22.41	178.12	-67.32	58.38	172.94	177.44	61.22	-59.90	54.54	-63.68	179.77	-177.91	65.54	-171.88	-55.33
M0027	-1825217.38	-695188001.00	0.110	-37.48	83.53	159.29	98.04	35.84	-85.41	-21.04	-143.37	100.03	-22.30	178.50	-66.92	58.80	173.38	177.71	61.48	-61.36	53.10	-66.82	176.68	178.96	62.46	53.85	170.12
M0015	-1825216.90	-695187818.00	0.090	-5.26	113.89	104.29	-16.97	-17.54	-138.81	35.01	-88.70	155.49	31.77	59.75	174.31	-56.93	55.63	-178.83	65.20	53.35	179.30	-70.46	173.93	174.61	58.40	55.85	172.31
M0017	-1825214.95	-695187077.00	0.041	-37.86	83.37	157.99	96.87	34.64	-86.48	-18.56	-140.96	102.42	-19.99	-52.57	61.70	-170.96	-56.69	-60.94	-176.69	178.30	-66.60	-58.63	-174.91	-173.42	70.30	-172.06	-55.64
M0021	-1825214.58	-695186938.00	0.036	-37.72	83.33	157.53	96.49	34.12	-86.91	-17.75	-140.14	103.18	-19.20	-172.52	-57.40	67.88	-177.00	-64.79	178.59	176.12	-68.79	-58.58	-175.84	-174.47	69.27	-172.04	-55.60
M0020	-1825214.35	-695186926.00	0.035	-37.74	83.31	157.91	96.79	34.49	-86.63	-18.24	-140.64	102.74	-19.66	-172.40	-57.30	67.97	-176.93	-63.99	179.40	177.03	-67.90	-58.17	-175.44	-174.05	69.66	-172.03	-55.58
M0072	-1825214.19	-695186786.00	0.030	-37.48	83.53	158.76	97.57	35.34	-85.85	-20.18	-142.54	100.85	-21.51	-175.64	-61.58	64.13	178.19	61.08	-54.45	-177.74	-63.10	53.43	-61.60	-60.80	-173.83	68.59	-173.14
M0030	-1825214.02	-695186723.00	0.028	-37.86	83.22	158.60	97.43	35.17	-86.00	-19.23	-141.64	101.78	-20.63	177.21	-67.88	57.53	172.43	-176.05	68.16	63.74	179.45	-70.54	173.24	174.70	58.47	55.32	171.79
M0025	-1825213.94	-695186692.00	0.027	-37.74	83.30	157.76	96.69	34.35	-86.72	-18.02	-140.39	102.92	-19.45	-172.95	-57.88	67.47	-177.46	-66.40	177.01	174.16	-70.73	-62.52	-178.79	-177.44	66.26	56.96	173.40
M0081	-1825213.91	-695186680.00	0.027	-37.40	83.58	158.90	97.70	35.48	-85.72	-20.51	-142.85	100.51	-21.82	-176.37	-61.29	63.43	177.52	60.70	-54.31	-177.72	-63.06	53.40	-61.63	-60.81	-175.85	68.80	-174.94
M0086	-1825213.84	-695186656.00	0.026	-7.00	112.14	105.97	-15.20	-15.85	-137.02	34.03	-89.68	154.45	30.75	60.90	175.30	-57.81	56.59	176.27	60.36	-59.74	54.54	-63.58	179.91	-177.69	63.60	-172.63	-56.43
M0003	-1825213.83	-695186649.00	0.026	-37.32	83.65	159.28	98.00	35.89	-85.39	-21.24	-143.65	99.84	-22.57	178.26	-67.01	58.26	173.00	178.04	61.95	149.08	-65.56	-65.79	178.36	179.89	64.04	-171.56	-55.30
M0078	-1825213.34	-695186465.00	0.022	-4.52	114.66	103.56	-17.71	-18.28	-139.55	35.36	-88.31	155.87	32.21	-171.31	-56.56	63.82	-176.43	-64.08	179.40	88.54	-176.44	176.04	61.10	61.42	-59.32	177.64	-66.24
M0089	-1825213.05	-695186354.00	0.019	-0.79	118.29	100.26	-21.18	-21.55	-142.99	36.87	-86.88	157.55	33.86	-58.32	56.58	-177.05	-62.16	-68.52	174.43	-56.92	57.77	-63.62	179.82	-178.27	65.17	-172.12	-55.80
M0070	-1825212.83	-695186270.00	0.018	-7.76	111.40	106.78	-14.38	-15.06	-136.22	33.56	-90.10	153.96	30.30	178.65	-66.69	58.71	173.37	-174.25	69.34	67.10	-177.52	175.06	60.10	60.70	-54.29	176.20	-67.58
M0042	-1825212.20	-695186031.00	0.014	-36.52	84.45	160.31	98.94	36.90	-84.47	-23.33	-145.81	97.80	-24.68	-176.86	-62.03	63.86	178.69	179.19	62.71	-62.79	51.64	-64.92	178.48	-179.15	64.25	57.37	173.84
M0060	-1825211.94	-695185929.00	0.012	-37.72	83.33	157.42	96.34	34.04	-87.04	-17.52	-139.90	103.40	-18.98	-174.02	-58.87	66.41	-178.44	-67.81	175.99	66.79	-178.16	174.95	60.00	60.29	-54.65	176.00	-67.77
M0031	-1825211.86	-695185899.00	0.012	-4.62	114.54	103.86	-17.43	-17.93	-139.22	34.95	-88.70	155.48	31.83	-68.17	45.94	173.93	-71.96	-166.93	77.18	70.63	-173.87	-66.80	176.84	177.82	61.45	-174.47	-58.10
M0050	-1825211.75	-695185858.00	0.011	-37.67	83.35	157.52	96.46	34.14	-86.92	-17.61	-139.97	103.32	-19.04	-172.94	-57.83	67.46	-177.44	-65.58	177.80	175.52	-69.61	54.11	-60.86	-60.43	-173.42	66.52	-177.86
M0034	-1825211.67	-695185827.00	0.011	-37.75	83.29	157.91	96.78	34.53	-86.59	-18.26	-140.63	102.70	-19.67	-173.29	-58.24	67.14	-177.81	-66.28	177.09	174.95	-70.17	53.58	-61.39	-60.98	-175.95	65.60	-178.29
M0046	-1825211.58	-695185794.00	0.011	-37.75	83.30	157.76	96.68	34.37	-86.71	-18.01	-140.40	102.94	-19.45	177.47	-67.67	57.83	172.70	-174.88	69.29	65.66	-178.92	174.31	59.56	60.13	-54.82	175.50	-68.26
M0066	-1825211.53	-695185774.00	0.010	-37.70	83.34	157.91	96.80	34.53	-86.57	-18.34	-140.75	102.62	-19.80	-56.71	57.68	-175.09	-60.69	-70.08	173.91	-56.73	57.96	-63.62	179.81	-178.23	65.19	-172.36	-55.98
M0051	-1825211.41	-695185729.00	0.010	-37.56	83.46	158.84	97.64	35.41	-85.78	-20.24	-142.61	100.78	-21.39	179.21	-66.12	59.18	173.85	178.89	62.74	146.21	-58.59	47.83	-67.69	-66.22	178.26	64.15	-179.60
M0062	-1825211.31	-695185692.00	0.010	-37.79	83.28	157.71	96.61	34.30	-86.80	-17.81	-140.23	103.12	-19.30	-176.46	-61.24	64.13	179.34	-71.92	171.26	-58.64	56.16	-66.06	177.36	179.15	62.57	55.32	171.75
M0033	-1825211.29	-695185684.00	0.009	-19.46	100.00	120.66	0.07	-1.37	-121.96	23.79	-99.50	143.80	20.50	-54.09	60.38	-172.19	-57.98	-63.50	-178.81	88.24	-175.36	-67.07	176.72	178.06	61.85	-173.44	-56.96
M0035	-1825211.27	-695185671.00	0.009	-10.15	108.98	108.40	-11.63	-12.38	-133.41	31.92	-91.65	152.21	28.64	67.82	-178.74	-50.28	63.16	53.74	-61.14	-178.08	-62.45	-57.88	-174.26	-178.57	70.05	179.99	-68.10
M0069	-1825211.05	-695185592.00	0.009	-37.71	83.35	158.41	97.26	35.00	-86.15	-19.16	-141.54	101.84	-20.54	177.43	-67.74	58.05	172.83	177.76	62.11	-60.06	54.32	-64.02	179.44	-178.21	65.24	-171.96	-55.64
M0040	-1825210.94	-695185548.00	0.008	-37.73	83.34	157.92	96.82	34.51	-86.60	-18.29	-140.69	102.66	-19.73	178.54	-66.64	59.14	173.96	178.51	62.63	-61.12	53.29	-66.43	177.05	179.37	62.85	56.61	172.91
M0016	-1825210.43	-695185357.00	0.007	-9.25	110.00	108.42	-12.63	-13.44	-134.49	32.60	-91.08	152.93	29.25	-53.09	61.20	-171.48	-57.18	-60.86	-176.61	178.21	-66.69	-58.73	-175.02	-178.51	70.20	-172.35	-55.93
M0058	-1825209.90	-695185136.00	0.005	-37.37	83.68	158.90	97.73	35.58	-85.60	-20.42	-142.83	100.63	-21.78	65.70	-179.61	-53.16	61.53	-177.52	66.14	127.74	-118.86	46.67	-59.04	-67.30	176.99	60.40	177.13
M0004	-1825209.66	-695185062.00	0.005	-37.66	83.35	157.32	96.30	33.90	-87.13	-17.30	-139.69	103.62	-18.78	-177.06	-62.67	63.02	177.41	61.03	-54.21	-177.89	-62.91	-61.22	-177.40	-175.87	67.95	55.64	172.09
M0006	-1825209.64	-695185056.00	0.005	-37.70	83.36	158.18	97.04	34.75	-86.39	-18.72	-141.11	102.26	-20.13	-176.84	-62.46	63.25	177.63	61.20	-54.00	-177.82	-62.84	-61.36	-177.34	-176.01	67.80	56.19	172.68
M0028	-1825209.21	-695184889.00	0.004	-37.56	120.22	99.00	-22.52	-22.84	-144.36	37.46	-86.31	158.17	34.40	-175.74	-60.47	64.92	-179.81	-67.17	173.93	67.39	-177.25	-67.29	176.41	177.66	61.36	-173.33	-56.85
M0012	-1825209.06	-695184836.00	0.004	-37.66	83.42	158.24	97.11	34.80	-86.32	-18.83	-141.23	102.15	-20.25	-177.53	-61.80	62.48	177.22	57.86	-57.60	70.57	-173.49	-68.40	175.52	176.68	60.59	55.56	172.08
M0029	-1825208.76	-695184719.00	0.003	-1.77	117.32	101.55	-19.84	-20.27	-141.66	36.26	-87.48	156.84	33.10	173.92	-70.95	54.58	169.71	-178.04	65.28	63.13	178.77	-71.39	172.41	173.88	57.67	54.66	171.08
M0009	-1825208.50	-695184619.00	0.003	-37.73	120.71	98.63	-22.93	-23.22	-144.77	37.63	-86.14	158.36	34.59	-174.01	-58.77	66.66	-178.10	-63.31	179.33	177.70	-67.22	-58.65	-174.86	-178.54	70.25	-171.21	-54.83
M0023	-1825208.39	-695184580.00	0.003	-0.18	118.91	100.08	-21.39	-21.75	-143.22	36.99	-86.77	157.64	33.88	174.70	-70.21	55.32	170.41	-176.76	66.54	64.87	-179.47	-68.86	174.87	176.37	60.10	-173.70	-57.17
M0022	-1825208.35	-695184562.00	0.003	0.32	119.42	99.62	-21.86	-22.22	-143.70	37.20	-86.57	157.89	34.12	174.68	-70.23	55.30	170.39	-177.08	66.22	64.96	-179.98	-69.01	174.72	176.22	59.85	-173.90	-57.37
M0013	-1825208.10	-695184468.00	0.003	-1.24	117.83	101.13	-20.31	-20.69	-142.13	36.52	-87.25	157.14	33.37	-178.61	-63.45	62.29	177.45	-74.12	168.55	169.23	-75.41	-65.51	178.44	179.52	63.47	54.32	170.66
M0005	-1825206.91	-695184013.00	0.002	-37.03	121.58	97.94	-23.62	-23.90	-145.46	37.87	-85.96	158.61	34.78	-176.85	-62.02	63.88	178.71	179.28	62.78	-62.75	51.68	-64.97	178.45	-179.18	64.23	57.10	173.56
M0039	-1825206.32	-695183791.00	0.001	-37.72	83.31	157.66	96.58	34.26	-86.82	-17.76	-140.15	103.18	-19.22	-176.59	-62.07	63.46	177.97	61.11	-53.97	-177.32	-62.67	54.23	-60.66	-60.01	-174.89	70.64	-173.14
M0084	-1825206.24	-695183758.00	0.001	-7.28	111.85	106.33	-14.83	-15.52	-136.68	33.94	-89.80	154.36	30.62	-56.98	57.47	-175.54	-60.85	-69.86	-179.54	-57.56	57.15	-65.49	-177.66	-179.55	-61.88	58.71	-171.66
M0026	-1825206.13	-695183719.00	0.001	0.66	119.73	99.50	-22.00	-22.32	-143.83	37.25	-86.54	157.93	34.14	-176.94	-61.84	63.85	178.95	-76.19	166.55	168.92	-75.25	48.71	-66.52	-66.14	178.53	57.87	173.76
M0088	-1825206.08	-695183698.00	0.001	0.70	119.31	99.38	-22.11	-22.46	-143.95	37.25	-86.53	157.93	34.15	178.95	-66.13	59.74	174.66	178.16	61.59	-61.43	53.98	-64.62	178.78	-178.80	64.60	-170.89	-54.50
M0067	-1825205.56	-695183512.00	0.001	1.00	120.10	99.13	-22.38	-22.72	-144.23	37.35	-86.49	158.04	34.27	179.46	-65.65	60.22	175.11	178.35	61.79	-61.42	53.98	-64.67	178.73	-178.86	64.54	-171.02	-54.65
M0057	-1825205.07	-695183313.00	0.001	-37.03	83.98	158.59	97.39	35.15	-86.04	-20.08	-142.59	100.91	-21.59	-176.86	-61.45	63.37	178.79	62.74	-52.44	-179.30	-58.77	55.71	-59.16	-58.55	-173.42	70.19	-173.60
M0002	-1825205.00	-695183285.00	0.001	-37.03	83.97	158.89	97.66	35.49	-85.74	-20.64	-143.13	100.36	-22.13	-176.44	-61.01	63.61	179.25	62.95	-52.26	-179.17	-58.74	55.66	-59.20	-58.60	-173.46	70.06	-173.74
M0036	-1825201.07	-695181791.00	0.000	-0.66	118.41	100.71	-20.72	-20.96	-142.39	36.59	-87.15	157.23	33.49	63.30	178.19	-54.75	60.13	-179.48	64.17	137.42	-107.22	44.61	-71.34	-69.44	174.61	59.49	176.10
M0079	-1825197.90	-695180582.00	0.000	-37.46	83.54	157.74	96.64	34.39	-86.71	-18.13	-140.51	102.81	-19.37	-179.69	-64.52	60.87	175.54	56.95	-58.59	176.04	-69.79	-172.74	73.15	73.43	-60.69	163.64	-60.67
M0081	-1825196.99	-695180237.00	0.000	-37.25	83.77	157.70	96.59	34.34	-86.77	-18.21	-140.88	102.73	-19.74	173.57	-72.04	53.68	168.07	38.04	-76.77	-58.26	55.89	-67.99	174.93	177.73	60.85	60.83	177.40

Table S-VIII. Calculated vicinal coupling constants (from H-1 to H-6') for every conformer of **4c**/**4d**

boltzmen	1-2r	1-2s	2r-3r	2r-3s	2s-3r	2s-3s	3r-4r	3r-4s	3s-4r	3s-4s	1'r-2'r	1'r-2's	1's-2'r	1's-2's	2'r-3'	2's-3'	3'-4'r	3'-4's	4'r-5'r	4'r-5's	4's-5'r	4's-5's	5'r-6'	5's-6'
0.145	11.89	5.34	2.28	9.37	9.34	9.76	7.39	1.98	11.66	7.84	4.48	4.24	12.93	3.93	3.53	13.00	3.19	12.99	2.81	12.87	12.92	4.18	5.63	10.94
0.130	7.50	2.01	11.68	7.42	7.76	1.98	9.77	9.26	2.47	9.62	12.99	3.10	4.22	12.84	12.98	3.84	4.01	4.79	3.52	13.00	12.99	3.30	11.02	5.38
0.110	7.50	2.01	11.68	7.42	7.76	1.98	9.78	9.24	2.48	9.63	12.99	3.14	4.17	12.86	12.98	3.80	3.82	5.00	3.16	12.96	13.00	3.68	5.59	10.95
0.090	10.92	4.05	2.86	10.19	10.14	8.42	7.89	1.98	11.19	8.38	4.03	12.90	4.15	4.62	13.00	3.34	3.56	13.00	2.78	12.86	12.91	4.22	5.31	11.05
0.041	7.48	2.02	11.52	7.60	7.95	1.98	10.04	8.81	2.68	9.89	5.09	3.77	12.74	4.47	3.87	12.96	12.99	3.18	4.19	12.92	12.86	2.80	11.04	5.34
0.036	7.47	2.02	11.46	7.66	8.03	1.98	10.12	8.66	2.75	9.97	12.82	4.36	3.04	12.97	3.39	12.99	12.95	2.95	4.06	12.94	12.90	2.90	11.04	5.35
0.035	7.46	2.02	11.51	7.61	7.97	1.98	10.07	8.73	2.71	9.93	12.82	4.38	3.03	12.97	3.48	13.00	12.97	3.04	4.11	12.93	12.89	2.86	11.03	5.35
0.030	7.50	2.01	11.62	7.48	7.84	1.98	9.87	9.09	2.54	9.73	12.94	3.79	3.47	12.99	3.85	4.80	12.98	3.59	4.95	3.79	3.89	12.94	3.75	11.14
0.028	7.44	2.02	11.60	7.51	7.86	1.98	9.97	8.93	2.62	9.82	12.98	3.04	4.35	12.82	12.95	3.01	3.52	13.00	2.78	12.85	12.91	4.21	5.38	11.02
0.027	7.46	2.02	11.49	7.63	7.99	1.98	10.09	8.71	2.72	9.95	12.84	4.30	3.09	12.98	3.20	12.97	12.89	2.76	3.67	13.00	12.98	3.21	5.16	11.09
0.027	7.52	2.01	11.64	7.47	7.82	1.98	9.84	9.15	2.52	9.69	12.96	3.70	3.55	12.98	3.91	4.74	12.98	3.60	4.96	3.78	3.89	12.95	3.72	11.13
0.026	10.86	3.80	3.03	10.35	10.29	8.08	8.04	1.99	11.04	8.53	3.88	12.93	4.31	4.48	12.96	3.95	4.04	4.79	3.53	13.00	12.99	3.29	11.06	5.23
0.026	7.53	2.01	11.68	7.42	7.75	1.98	9.76	9.29	2.46	9.60	12.99	3.13	4.24	12.84	12.99	3.74	10.22	2.19	3.27	12.99	13.00	3.48	11.01	5.39
0.022	10.94	4.16	2.78	10.12	10.07	8.55	7.84	1.98	11.24	8.31	12.76	4.49	2.94	12.96	3.47	13.00	2.97	12.96	12.95	3.85	3.81	4.94	11.19	4.00
0.019	11.00	4.72	2.50	9.76	9.72	9.18	7.60	1.98	11.47	8.07	4.23	4.48	12.97	3.71	2.97	12.90	4.43	4.31	3.59	13.00	12.99	3.34	11.04	5.32
0.018	10.83	3.70	3.12	10.41	10.36	7.93	8.11	2.00	10.97	8.59	12.99	3.17	4.18	12.86	12.89	2.89	3.13	12.98	12.92	3.99	3.91	4.82	11.16	3.85
0.014	7.65	2.00	11.81	7.27	7.60	2.00	9.51	9.67	2.32	9.35	12.97	3.73	3.50	12.99	13.00	3.64	3.63	5.23	3.37	12.99	13.00	3.45	5.10	11.10
0.012	7.47	2.02	11.45	7.68	8.04	1.98	10.14	8.62	2.77	10.00	12.89	4.16	3.20	12.99	3.05	12.95	3.16	12.99	12.92	4.00	3.96	4.77	11.16	3.83
0.012	10.94	4.14	2.81	10.15	10.10	8.49	7.90	1.98	11.19	8.37	3.01	6.14	12.88	2.65	12.46	2.27	2.77	12.88	3.16	12.97	12.98	3.81	11.12	5.00
0.011	7.47	2.02	11.46	7.66	8.02	1.98	10.13	8.63	2.76	9.99	12.84	4.30	3.09	12.98	3.30	12.98	12.94	2.87	4.85	3.88	3.94	12.93	3.97	11.18
0.011	7.46	2.02	11.51	7.61	7.96	1.98	10.07	8.73	2.70	9.93	12.86	4.24	3.12	12.98	3.22	12.97	12.92	2.81	4.93	3.81	3.87	12.95	4.07	11.19
0.011	7.46	2.02	11.49	7.63	7.99	1.98	10.09	8.71	2.73	9.95	12.98	3.06	4.30	12.83	12.92	2.90	3.29	13.00	12.90	4.06	3.98	4.74	11.15	3.78
0.010	7.47	2.02	11.51	7.61	7.96	1.98	10.06	8.77	2.70	9.91	4.46	4.32	12.92	3.91	2.82	12.88	4.46	4.28	3.53	13.00	12.99	3.34	11.05	5.29
0.010	7.49	2.02	11.63	7.48	7.83	1.98	9.86	9.11	2.54	9.72	13.00	3.23	4.11	12.83	13.00	3.64	9.74	2.37	5.84	3.06	3.22	12.99	4.23	11.20
0.010	7.45	2.02	11.49	7.64	8.00	1.98	10.11	8.68	2.74	9.96	12.96	3.83	3.47	13.00	2.65	12.76	4.19	4.54	3.24	12.98	13.00	3.66	5.38	11.02
0.009	9.95	2.48	5.11	11.00	10.99	5.33	9.46	2.44	9.32	9.34	4.86	3.95	12.82	4.28	3.54	13.00	2.90	12.93	3.13	12.97	12.99	3.75	11.09	5.16
0.009	10.71	3.38	3.44	10.61	10.56	7.41	8.36	2.04	10.71	8.83	3.05	12.99	5.44	3.59	4.91	3.85	12.99	3.68	4.30	12.89	12.87	2.82	11.20	4.36
0.009	7.47	2.02	11.58	7.54	7.89	1.98	9.98	8.91	2.63	9.83	12.98	3.06	4.27	12.84	12.98	3.72	3.99	4.82	3.48	13.00	12.99	3.34	11.03	5.34
0.008	7.46	2.02	11.51	7.61	7.97	1.98	10.07	8.76	2.70	9.92	12.99	3.18	4.12	12.88	12.99	3.63	3.85	4.98	3.20	12.97	13.00	3.63	5.20	11.07
0.007	10.73	3.51	3.31	10.55	10.49	7.61	8.25	2.02	10.82	8.74	5.01	3.84	12.77	4.40	3.88	12.96	12.99	3.17	4.18	12.92	12.87	2.81	11.05	5.30
0.005	7.52	2.01	11.64	7.46	7.80	1.98	9.83	9.15	2.52	9.69	3.28	13.00	5.00	3.80	12.98	3.23	6.36	4.46	6.02	2.92	3.10	12.97	4.70	11.18
0.005	7.47	2.02	11.44	7.69	8.06	1.98	10.16	8.58	2.79	10.02	12.97	3.65	3.60	12.98	3.86	4.84	12.99	3.62	3.84	12.98	12.95	3.03	5.34	11.04
0.005	7.47	2.02	11.55	7.57	7.93	1.98	10.02	8.84	2.66	9.88	12.97	3.68	3.58	12.98	3.84	4.87	12.98	3.63	3.82	12.98	12.95	3.05	5.26	11.06
0.004	2.40	5.04	2.40	9.61	9.57	9.42	7.51	1.98	11.55	7.98	12.94	3.94	3.37	13.00	3.12	12.95	3.09	12.98	3.10	12.96	12.98	3.82	11.08	5.17
0.004	7.48	2.02	11.55	7.56	7.92	1.98	10.01	8.86	2.65	9.86	12.98	3.63	3.67	12.98	4.30	4.34	2.77	12.57	2.99	12.94	12.96	3.92	5.35	11.04
0.003	10.99	4.57	2.60	9.91	9.86	8.94	7.70	1.98	11.37	8.18	12.88	2.74	4.78	12.66	12.99	3.33	3.59	13.00	2.70	12.82	12.88	4.33	5.48	10.99
0.003	9.35	5.12	2.38	9.56	9.53	9.49	7.48	1.98	11.57	7.95	12.89	4.17	3.17	12.99	3.57	13.00	12.98	3.11	4.19	12.92	12.87	2.80	11.00	5.45
0.003	11.00	4.82	2.48	9.74	9.70	9.22	7.58	1.98	11.48	8.06	12.91	2.81	4.67	12.71	12.97	3.19	3.38	13.00	2.84	12.92	12.96	3.98	11.10	5.13
0.003	11.00	4.90	2.45	9.69	9.64	9.30	7.55	1.98	11.51	8.03	12.91	2.81	4.67	12.71	12.97	3.22	3.44	13.00	2.92	12.91	12.95	4.01	11.10	5.10
0.003	11.00	4.65	2.57	9.86	9.82	9.02	7.65	1.98	11.41	8.14	12.99	3.55	3.70	12.98	2.48	12.58	12.63	2.38	3.30	12.99	13.00	3.55	5.53	10.97
0.002	2.34	5.27	2.33	9.48	9.44	9.61	7.44	1.98	11.60	7.92	12.97	3.73	3.50	12.99	13.00	3.63	3.64	5.22	3.37	12.99	13.00	3.46	5.14	11.09
0.001	7.47	2.02	11.48	7.65	8.00	1.98	10.12	8.66	2.75	9.97	12.96	3.73	3.55	12.99	3.65	4.87	12.98	3.65	4.83	3.91	4.00	12.91	3.55	11.08
0.001	10.85	3.77	3.07	10.38	10.32	8.02	8.05	2.00	11.03	8.55	4.42	4.35	12.93	3.88	2.83	12.88	4.34	4.40	3.27	12.98	13.00	3.61	5.25	11.06
0.001	11.00	4.96	2.44	9.67	9.63	9.32	7.54	1.98	11.51	8.02	12.97	3.74	3.48	13.00	2.33	12.48	12.61	2.55	5.69	3.19	3.23	12.99	5.03	11.10
0.001	11.00	4.97	2.43	9.66	9.62	9.35	7.54	1.98	11.51	8.02	13.00	3.23	4.04	12.91	12.98	3.79	3.81	5.02	3.41	13.00	13.00	3.41	10.98	5.50
0.001	11.00	5.02	2.41	9.63	9.59	9.39	7.52	1.98	11.53	8.00	13.00	3.29	3.97	12.92	12.99	3.76	3.81	5.02	3.40	12.99	13.00	3.42	10.99	5.48
0.001	7.37	2.01	11.60	7.52	7.87	1.98	9.88	9.10	2.55	9.72	12.97	3.81	3.56	13.00	3.64	5.11	12.86	4.17	4.61	4.12	4.20	12.86	3.59	11.09
0.001	7.37	2.01	11.64	7.48	7.81	1.98	9.82	9.20	2.50	9.65	12.96	3.86	3.51	13.00	3.61	5.13	12.86	4.17	4.62	4.11	4.19	12.86	3.60	11.10
0.000	11.00	4.74	2.53	9.81	9.79	9.07	7.64	1.98	11.42	8.12	3.57	12.99	4.75	3.98	13.00	3.46	8.16	3.17	6.36	2.70	2.88	12.91	4.82	11.16
0.000	7.51	2.01	11.49	7.64	7.98	1.98	10.08	8.73	2.71	9.94	13.00	3.42	3.95	12.94	4.43	4.19	12.95	2.85	12.83	2.55	2.53	6.99	10.52	2.83
0.000	7.54	2.01	11.49	7.64	7.99	1.98	10.07	8.76	2.71	9.92	12.87	2.64	4.92	12.55	7.42	2.29	4.24	4.61	3.03	12.92	12.98	3.91	4.84	11.18

Table S-IX. The product of multiplying the Boltzman weights and Calculated vicinal coupling constants (from H-1 to H-6') for every conformer of **4c**/**4d**

1-2r	1-2s	2r-3r	2r-3s	2s-3r	2s-3s	3r-4r	3r-4s	3s-4r	3s-4s	1'r-2'r	1'r-2's	1's-2'r	1's-2's	2'r-3'	2's-3'	3'-4'r	3'-4's	4'r-5'r	4'r-5's	4's-5'r	4's-5's	5'r-6'	5's-6'
1.72	0.77	0.33	1.36	1.35	1.42	1.07	0.29	1.69	1.14	0.65	0.61	1.88	0.57	0.51	1.88	0.46	1.88	0.41	1.87	1.87	0.61	0.82	1.59
0.98	0.26	1.52	0.96	1.01	0.26	1.27	1.20	0.32	1.25	1.69	0.40	0.55	1.67	1.69	0.50	0.52	0.62	0.46	1.69	1.69	0.43	1.43	0.70
0.83	0.22	1.29	0.82	0.85	0.22	1.08	1.02	0.27	1.06	1.43	0.35	0.46	1.41	1.43	0.42	0.42	0.55	0.35	1.43	1.43	0.40	0.61	1.20
0.98	0.36	0.26	0.92	0.91	0.76	0.71	0.18	1.01	0.75	0.36	1.16	0.37	0.42	1.17	0.30	0.32	1.17	0.25	1.16	1.16	0.38	0.48	0.99
0.31	0.08	0.47	0.31	0.33	0.08	0.41	0.36	0.11	0.41	0.21	0.15	0.52	0.18	0.16	0.53	0.53	0.13	0.17	0.53	0.53	0.11	0.45	0.22
0.27	0.07	0.41	0.28	0.29	0.07	0.36	0.31	0.10	0.36	0.46	0.16	0.11	0.47	0.12	0.47	0.47	0.11	0.15	0.47	0.46	0.10	0.40	0.19
0.26	0.07	0.40	0.27	0.28	0.07	0.35	0.31	0.09	0.35	0.45	0.15	0.11	0.45	0.12	0.45	0.45	0.11	0.14	0.45	0.45	0.10	0.39	0.19
0.23	0.06	0.35	0.22	0.24	0.06	0.30	0.27	0.08	0.29	0.39	0.11	0.10	0.39	0.12	0.14	0.39	0.11	0.15	0.11	0.12	0.39	0.11	0.33
0.21	0.06	0.32	0.21	0.22	0.06	0.28	0.25	0.07	0.28	0.36	0.09	0.12	0.36	0.36	0.08	0.10	0.36	0.08	0.36	0.36	0.12	0.15	0.31
0.20	0.05	0.31	0.21	0.22	0.05	0.27	0.24	0.07	0.27	0.35	0.12	0.08	0.35	0.09	0.35	0.35	0.07	0.10	0.35	0.35	0.09	0.14	0.30
0.20	0.05	0.31	0.20	0.21	0.05	0.27	0.25	0.07	0.26	0.35	0.10	0.10	0.35	0.11	0.13	0.35	0.10	0.13	0.10	0.11	0.35	0.10	0.30
0.28	0.10	0.08	0.27	0.27	0.21	0.21	0.05	0.29	0.22	0.10	0.34	0.11	0.12	0.34	0.10	0.10	0.12	0.09	0.34	0.34	0.09	0.29	0.14
0.20	0.05	0.30	0.19	0.20	0.05	0.25	0.24	0.06	0.25	0.34	0.08	0.11	0.33	0.34	0.10	0.27	0.06	0.09	0.34	0.34	0.09	0.29	0.14
0.24	0.09	0.06	0.22	0.22	0.19	0.17	0.04	0.25	0.18	0.28	0.10	0.06	0.29	0.08	0.29	0.07	0.29	0.28	0.08	0.08	0.11	0.25	0.09
0.21	0.09	0.05	0.19	0.18	0.17	0.14	0.04	0.22	0.15	0.08	0.09	0.25	0.07	0.06	0.25	0.08	0.08	0.07	0.25	0.25	0.06	0.21	0.10
0.19	0.07	0.06	0.19	0.19	0.14	0.15	0.04	0.20	0.15	0.23	0.06	0.08	0.23	0.23	0.05	0.06	0.23	0.23	0.07	0.07	0.09	0.20	0.07
0.11	0.03	0.17	0.10	0.11	0.03	0.13	0.14	0.03	0.13	0.18	0.05	0.05	0.18	0.18	0.05	0.05	0.07	0.05	0.18	0.18	0.05	0.07	0.16
0.09	0.02	0.14	0.09	0.10	0.02	0.12	0.10	0.03	0.12	0.15	0.05	0.04	0.16	0.04	0.16	0.04	0.16	0.16	0.05	0.05	0.06	0.13	0.05
0.13	0.05	0.03	0.12	0.12	0.10	0.09	0.02	0.13	0.10	0.04	0.07	0.15	0.03	0.15	0.03	0.03	0.15	0.04	0.16	0.16	0.05	0.13	0.06
0.08	0.02	0.13	0.08	0.09	0.02	0.11	0.09	0.03	0.11	0.14	0.05	0.03	0.14	0.04	0.14	0.14	0.03	0.05	0.04	0.04	0.14	0.04	0.12
0.08	0.02	0.13	0.08	0.09	0.02	0.11	0.10	0.03	0.11	0.14	0.05	0.03	0.14	0.04	0.14	0.14	0.03	0.05	0.04	0.04	0.14	0.04	0.12
0.08	0.02	0.13	0.08	0.09	0.02	0.11	0.10	0.03	0.11	0.14	0.03	0.05	0.14	0.14	0.03	0.04	0.14	0.14	0.04	0.04	0.05	0.12	0.04
0.07	0.02	0.12	0.08	0.08	0.02	0.10	0.09	0.03	0.10	0.04	0.04	0.13	0.04	0.03	0.13	0.04	0.04	0.04	0.13	0.13	0.03	0.11	0.05
0.07	0.02	0.12	0.07	0.08	0.02	0.10	0.09	0.03	0.10	0.13	0.03	0.04	0.13	0.13	0.04	0.10	0.02	0.06	0.03	0.03	0.13	0.04	0.11
0.07	0.02	0.11	0.08	0.08	0.02	0.10	0.09	0.03	0.10	0.13	0.04	0.03	0.13	0.03	0.13	0.04	0.05	0.03	0.13	0.13	0.04	0.05	0.11
0.09	0.02	0.05	0.10	0.10	0.05	0.09	0.02	0.06	0.09	0.04	0.04	0.12	0.04	0.03	0.12	0.03	0.12	0.03	0.12	0.12	0.03	0.10	0.05
0.10	0.03	0.03	0.10	0.10	0.07	0.08	0.02	0.10	0.08	0.03	0.12	0.05	0.03	0.04	0.03	0.12	0.03	0.04	0.12	0.12	0.03	0.10	0.04
0.07	0.02	0.10	0.07	0.07	0.02	0.09	0.08	0.02	0.09	0.12	0.03	0.04	0.12	0.12	0.03	0.04	0.04	0.03	0.12	0.12	0.03	0.10	0.05
0.06	0.02	0.09	0.06	0.06	0.02	0.08	0.07	0.02	0.08	0.10	0.03	0.03	0.10	0.10	0.03	0.03	0.04	0.03	0.10	0.10	0.03	0.04	0.09
0.08	0.02	0.02	0.07	0.07	0.05	0.06	0.01	0.08	0.06	0.04	0.03	0.09	0.03	0.03	0.09	0.09	0.02	0.03	0.09	0.09	0.02	0.08	0.04
0.04	0.01	0.06	0.04	0.04	0.01	0.05	0.05	0.01	0.05	0.02	0.06	0.02	0.02	0.06	0.02	0.03	0.02	0.03	0.01	0.02	0.06	0.02	0.06
0.04	0.01	0.06	0.04	0.04	0.01	0.05	0.04	0.01	0.05	0.06	0.02	0.02	0.06	0.02	0.02	0.06	0.02	0.02	0.06	0.06	0.02	0.03	0.06
0.04	0.01	0.06	0.04	0.04	0.01	0.05	0.04	0.01	0.05	0.06	0.02	0.02	0.06	0.02	0.02	0.06	0.02	0.02	0.06	0.06	0.02	0.03	0.06
0.01	0.02	0.01	0.04	0.04	0.04	0.03	0.01	0.05	0.03	0.05	0.02	0.01	0.05	0.01	0.05	0.01	0.05	0.01	0.05	0.05	0.02	0.04	0.02
0.03	0.01	0.05	0.03	0.03	0.01	0.04	0.04	0.01	0.04	0.05	0.01	0.01	0.05	0.02	0.02	0.01	0.05	0.01	0.05	0.05	0.02	0.02	0.04
0.03	0.01	0.01	0.03	0.03	0.03	0.02	0.01	0.03	0.02	0.04	0.01	0.01	0.04	0.04	0.01	0.01	0.04	0.04	0.01	0.04	0.04	0.01	0.02	0.03
0.03	0.02	0.01	0.03	0.03	0.03	0.02	0.01	0.03	0.02	0.04	0.01	0.01	0.04	0.01	0.04	0.04	0.01	0.01	0.04	0.04	0.01	0.03	0.02
0.03	0.01	0.01	0.03	0.03	0.03	0.02	0.01	0.03	0.02	0.04	0.01	0.01	0.04	0.04	0.01	0.01	0.04	0.04	0.01	0.04	0.04	0.01	0.03	0.02
0.03	0.01	0.01	0.03	0.03	0.03	0.02	0.01	0.03	0.02	0.04	0.01	0.01	0.04	0.04	0.01	0.01	0.04	0.01	0.04	0.04	0.01	0.03	0.02
0.03	0.01	0.01	0.03	0.03	0.03	0.02	0.01	0.03	0.02	0.04	0.01	0.01	0.04	0.04	0.01	0.01	0.04	0.01	0.04	0.04	0.01	0.02	0.03
0.00	0.01	0.00	0.02	0.02	0.02	0.01	0.00	0.02	0.02	0.03	0.01	0.01	0.03	0.03	0.01	0.01	0.01	0.01	0.03	0.03	0.01	0.01	0.02
0.01	0.00	0.01	0.01	0.01	0.00	0.01	0.01	0.00	0.01	0.01	0.00	0.00	0.01	0.00	0.00	0.01	0.00	0.00	0.00	0.00	0.01	0.00	0.01
0.01	0.00	0.00	0.01	0.01	0.01	0.01	0.00	0.01	0.01	0.00	0.00	0.01	0.00	0.00	0.01	0.00	0.00	0.00	0.01	0.01	0.00	0.01	0.01
0.01	0.00	0.00	0.01	0.01	0.01	0.01	0.00	0.01	0.01	0.01	0.00	0.00	0.01	0.01	0.00	0.00	0.01	0.00	0.01	0.01	0.00	0.01	0.01
0.01	0.00	0.00	0.01	0.01	0.01	0.01	0.00	0.01	0.01	0.01	0.00	0.00	0.01	0.01	0.00	0.00	0.01	0.00	0.01	0.01	0.00	0.01	0.01
0.01	0.01	0.00	0.01	0.01	0.01	0.01	0.00	0.01	0.01	0.01	0.00	0.00	0.01	0.01	0.00	0.00	0.01	0.00	0.01	0.01	0.00	0.01	0.01
0.01	0.00	0.01	0.01	0.01	0.00	0.01	0.01	0.00	0.01	0.01	0.00	0.00	0.01	0.00	0.01	0.01	0.00	0.00	0.00	0.00	0.01	0.00	0.01
0.01	0.00	0.01	0.01	0.01	0.00	0.01	0.01	0.00	0.01	0.01	0.00	0.00	0.01	0.00	0.01	0.01	0.00	0.00	0.00	0.00	0.01	0.00	0.01
0.00	0.00	0.00	0.00	0.00	0.00	0.00	0.00	0.00	0.00	0.00	0.00	0.00	0.00	0.00	0.00	0.00	0.00	0.00	0.00	0.00	0.00	0.00	0.00
0.00	0.00	0.00	0.00	0.00	0.00	0.00	0.00	0.00	0.00	0.00	0.00	0.00	0.00	0.00	0.00	0.00	0.00	0.00	0.00	0.00	0.00	0.00	0.00
0.00	0.00	0.00	0.00	0.00	0.00	0.00	0.00	0.00	0.00	0.00	0.00	0.00	0.00	0.00	0.00	0.00	0.00	0.00	0.00	0.00	0.00	0.00	0.00

Cartesian coordinates for the lowest energy conformers obtained by a multi-step conformation method (see experimental section)

Lowest energy conformer of **4a/4b** (SR/RS):
Standard Nuclear Orientation (Angstroms)

I	Atom	X	Y	Z
1	C	1.900180	1.776441	0.012429
2	C	0.404426	1.785415	0.270323
3	C	-0.342783	0.525443	-0.172133
4	C	-1.811199	0.599260	0.303967
5	C	-2.609839	-0.695017	0.103342
6	C	-3.954355	-0.638983	0.758318
7	C	-5.137235	-0.467420	0.184730
8	C	-6.395640	-0.398179	1.012305
9	C	-5.353279	-0.322984	-1.306240
10	O	2.470374	0.675706	0.699009
11	C	3.839248	0.471682	0.436503
12	C	4.311877	-0.678443	1.312698
13	C	4.850922	-1.736201	0.331789
14	C	4.126351	-1.333658	-0.957073
15	O	4.095987	0.087835	-0.914732
16	H	2.124051	1.692997	-1.053048
17	H	2.351096	2.711913	0.380671
18	H	-0.003748	2.637795	-0.211858
19	H	0.249555	1.923985	1.310942

20	H	-1.834478	0.860673	1.382795
21	H	-2.331617	1.425853	-0.218674
22	H	-2.043329	-1.519729	0.526931
23	H	-2.706778	-0.907004	-0.952020
24	H	-3.931814	-0.718667	1.842518
25	H	-6.205213	-0.511513	2.087324
26	H	-6.909854	0.558506	0.862931
27	H	-7.087861	-1.180720	0.709783
28	H	-5.993940	-1.123242	-1.692691
29	H	-5.870387	0.617320	-1.523060
30	H	-4.433292	-0.336135	-1.888084
31	H	4.374412	1.396682	0.588779
32	H	5.062969	-0.357210	2.023766
33	H	3.415549	-1.043038	1.882922
34	H	4.643670	-2.752583	0.650036
35	H	5.943139	-1.642322	0.197619
36	H	4.644446	-1.622107	-1.870245
37	H	3.100420	-1.714602	-0.995099
38	C	-0.249769	0.298096	-1.687588
39	H	-0.757067	-0.651379	-1.982976
40	H	0.781819	0.222543	-2.023776
41	H	-0.725324	1.131509	-2.251815
42	H	0.139254	-0.320569	0.321884

Lowest energy conformer of 4c/4d (SS/RR):

Standard Nuclear Orientation (Angstroms)

I	Atom	X	Y	Z
1	C	-1.870172	-1.062509	-0.885732
2	C	-0.439810	-0.666472	-1.211667
3	C	0.488120	-0.483261	-0.000017
4	C	0.559279	-1.746720	0.861329
5	C	1.876871	-0.035473	-0.481909
6	C	2.827598	0.431014	0.631959
7	C	4.093289	1.031661	0.083986
8	C	5.311702	0.478235	0.024798
9	C	6.477007	1.224105	-0.572988
10	C	5.651873	-0.899824	0.529673
11	O	-2.429901	-0.094725	-0.013855
12	C	-3.701012	-0.428564	0.480235
13	C	-4.172283	0.699272	1.386018
14	C	-4.776868	1.677670	0.372058
15	C	-5.353279	0.732018	-0.689045
16	O	-4.666681	-0.522552	-0.540733
17	H	-2.464509	-1.123894	-1.805748
18	H	-1.909460	-2.054439	-0.408094
19	H	-0.463867	0.267193	-1.788701
20	H	-0.026043	-1.437484	-1.879580
21	H	0.068357	0.323286	0.615807
22	H	1.239732	-1.620003	1.710261

23	H	-0.419421	-2.005738	1.279366
24	H	0.913401	-2.605890	0.274112
25	H	2.356527	-0.853531	-1.039687
26	H	1.754287	0.788785	-1.198523
27	H	3.053808	-0.399108	1.307560
28	H	2.310931	1.186104	1.240480
29	H	3.975366	2.031422	-0.337235
30	H	7.288841	1.335781	0.159265
31	H	6.898555	0.678309	-1.428273
32	H	6.193670	2.224544	-0.916530
33	H	6.369185	-0.844002	1.360153
34	H	6.136367	-1.487215	-0.261923
35	H	4.783065	-1.466149	0.874305
36	H	-3.655257	-1.416941	0.956583
37	H	-4.939673	0.315401	2.068360
38	H	-3.354822	1.120064	1.975313
39	H	-3.994556	2.312112	-0.054611
40	H	-5.544588	2.324564	0.808204
41	H	-6.422031	0.539862	-0.535941
42	H	-5.209104	1.098267	-1.710405

NMR data calculations obtained using the "Spartan-NMR" calculation method for 4c/4d (SS/RR):

Table S-X. Geminal and vicinal coupling constants obtained using the "Spartan-NMR" calculation method for compounds **4c/4d** (SS/RR):

H\H	1's	1'r	2's	2'r	3'	10'			4'r	4's	5'r	5's	6'	1	2r	2s	3r	3s	4s	4r
1's		-8.7	3.8	13.1																
1'r	-8.7		1.1	6.1																
2's	3.8	1.1		-13.2	11.4															
2'r	13.1	6.1	-13.2		4.1															
3'			11.4	4.1		6.9	6.9	6.9	12.0	4.0										
10'					6.9		-12.8	-12.8												
					6.9	-12.8		-12.8												
					6.9	-12.8	-12.8													
4'r					12.0					-12.9	3.5	4.4								
4's					4.0				-12.9		4.6	13.5								
5'r									3.5	4.6		-14.3	11.6							

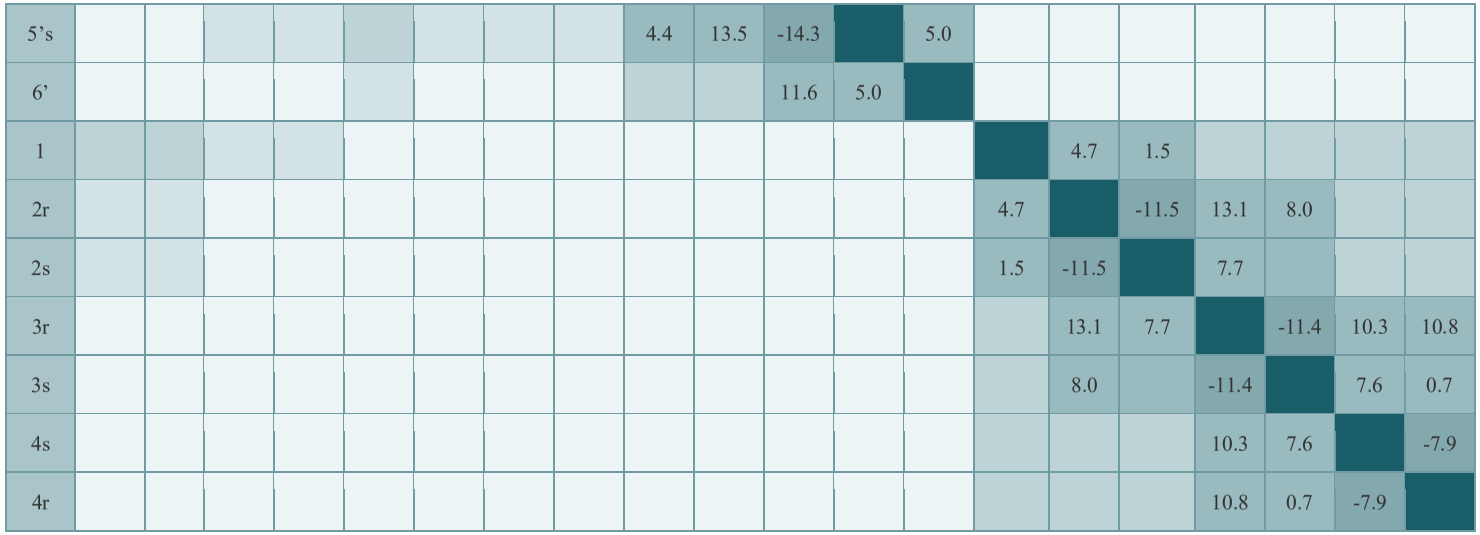

Table S-XI. Chemical shifts, coupling constants, and HMBC interactions obtained using the "Spartan-NMR" calculation method for **4c/4d** (SS/RR):

position	δ_C	mult	δ_H		(J in Hz)	HMBC(H→C)
1'	59.9	CH_2	4.08	m	(13.1,-8.7,3.8)	1, 2, 3, 4, 10, 11
.			3.29	m	(-8.7,6.1,1.1)	1, 2, 3, 11
2'	36.4	CH_2	1.04	m	(-13.2,11.4,3.8,1.1)	2, 3, 4, 10
.			1.94	m	(-13.2,13.1,6.1,4.1)	2, 3, 4, 5, 10
3'	24.2	CH	2.51	m	(12.0,11.4,6.9_{x3},4.1,4.0)	1, 3, 4, 5

10’	19.2	CH_3	1.00	m	(6.9)	1, 2, 4, 5
4’	31.8	CH_2	0.96	m	(-12.9,12.0,4.4,3.5)	1, 2, 3, 5, 6, 8
.			2.09	m	(-12.9,4.6,4.0,1.3)	1, 2, 3, 5, 6, 13
5’	24.7	CH_2	2.32	m	(-14.3,11.6,4.6,3.5)	2, 4, 6, 7, 8
.			2.15	m	(-14.3,13.5,5.0,4.4)	1, 2, 4, 6, 7, 8, 9
6’	126.1	CH	5.91	m	$(11.6,5.0,-2.4_{x3},-1.8_{x3})$	2, 4, 5, 7, 8, 9
7’	130.3	C				...
8’	26.5	CH_3	1.65	ddd	(1.9,-1.8,0.5)	4, 5, 6, 7, 9
9’	17.9	CH_3	1.56	ddd	(-2.4,1.6,0.9)	4, 5, 6, 7, 8, 13
1	102.1	CH	5.06	m	(4.7,1.5)	1, 11, 12, 13
2	33.2	CH_2	1.63	m	(13.1,-11.5,8.0,4.7)	10, 12, 13
.			1.91	m	(-11.5,7.7,1.5)	10, 12, 13
3	24.5	CH_2	2.37	m	(13.1,-11.4,10.8,10.3,7.7)	6, 7, 8, 10, 11, 13
.			1.59	m	(-11.4,8.0,7.6,0.7)	8, 10, 11, 13
4	68.4	CH_2	3.82	m	(10.3,-7.9,7.6)	10, 12
.			4.12	m	(10.8,-7.9,0.7)	4, 6, 7, 9, 10, 11, 12
Label	δ				..	
O	260.1					...
O1	260.4					...

NMR data calculation short output for 4c/4d (SR/RS):

Job type: Geometry optimization.
Method: RHF
Basis set: 3-21G(*)
Number of basis functions: 196
Number of electrons: 126
Parallel Job: 8 threads

SCF model:
A restricted Hartree-Fock SCF calculation will be
performed using Pulay DIIS + Geometric Direct Minimization

Optimization:

Step	Energy	Max Grad.	Max Dist.
1	-691.149054	0.020450	0.091146
2	-691.157759	0.006403	0.116146
3	-691.158450	0.001931	0.027906
4	-691.158524	0.001273	0.065197
5	-691.158586	0.000353	0.018503

Reason for exit: Successful completion
Quantum Calculation CPU Time : 59.77

Quantum Calculation Wall Time: 11.33

SPARTAN'20 Quantum Mechanics Driver: (Win/64b) Release 1.1.4
Job type: Reading previous wavefunction

Job type: Single point.
Method: RWB97X-D
Basis set: 6-31G(D)
Number of basis functions: 292
Number of electrons: 126
Parallel Job: 8 threads

SCF model:
A restricted hybrid HF-DFT SCF calculation will be
performed using Pulay DIIS + Geometric Direct Minimization

SCF total energy: -699.3749650 hartrees

Reason for exit: Successful completion
Quantum Calculation CPU Time : 8:10.89
Quantum Calculation Wall Time: 1:41.83

SPARTAN'20 Quantum Mechanics Driver: (Win/64b) Release 1.1.4
Job type: Geometry optimization.
Method: RWB97X-D
Basis set: 6-31G(D)
Number of basis functions: 292
Number of electrons: 126
Parallel Job: 8 threads

SCF model:
A restricted hybrid HF-DFT SCF calculation will be
performed using Pulay DIIS + Geometric Direct Minimization

Optimization:

Step	Energy	Max Grad.	Max Dist.
1	-699.374965	0.017139	0.070020
2	-699.380637	0.014433	0.146120
3	-699.381405	0.012991	0.104132
4	-699.382234	0.005476	0.081789
5	-699.382901	0.006009	0.104781
6	-699.383352	0.004750	0.094658
7	-699.383672	0.004757	0.104896

8	-699.383559	0.004977	0.058298
9	-699.383858	0.001669	0.043910
10	-699.383829	0.003051	0.030386
11	-699.383889	0.001130	0.024249
12	-699.383886	0.001770	0.009998
13	-699.383893	0.000127	0.002339

Reason for exit: Successful completion
Quantum Calculation CPU Time : 1:37:52.11
Quantum Calculation Wall Time: 19:47.30

SPARTAN'20 Quantum Mechanics Driver: (Win/64b) Release 1.1.4

forcing reuse of RIC despite likely change in input file.

Job type: Geometry optimization.
Method: RWB97X-D
Basis set: 6-31G(D)
Number of basis functions: 292
Number of electrons: 126
Parallel Job: 8 threads

SCF model:

A restricted hybrid HF-DFT SCF calculation will be
performed using Pulay DIIS + Geometric Direct Minimization

2 -699.383893 0.000127 0.000718 Restart with RIC

Reason for exit: Successful completion
Quantum Calculation CPU Time : 3:39.55
Quantum Calculation Wall Time: 37.55

SPARTAN'20 Quantum Mechanics Driver: (Win/64b) Release 1.1.4

Job type: Single point.
Method: RWB97XRV
Basis set: 6-311+G(2DF,2P) [6-311G*]
Number of basis functions: 366 (small basis)
Number of electrons: 126
Parallel Job: 8 threads

SCF model:
A restricted hybrid HF-DFT SCF calculation will be
performed using Pulay DIIS + Geometric Direct Minimization

Number of basis functions: 778 (large basis)

SCF total energy: -699.6155507 hartrees

Reason for exit: Successful completion
Quantum Calculation CPU Time : 29:53.44
Quantum Calculation Wall Time: 4:51.29

SPARTAN'20 Quantum Mechanics Driver: (Win/64b) Release 1.1.4

Job type: Single point.
Method: RWB97X-D
Basis set: 6-31G(D)
Number of basis functions: 292
Number of electrons: 126

SCF model:
A restricted hybrid HF-DFT SCF calculation will be
performed using Pulay DIIS + Geometric Direct Minimization

SCF total energy: -699.3838930 hartrees
NMR shifts (ppm)

Atom		Isotropic	Rel. Shift
1	C	136.9696	

2	C1	158.2735
3	C2	170.0882
4	C3	174.8911
5	C4	162.7652
6	C5	169.5927
7	C6	72.4178
8	C7	68.3592
9	C8	167.8103
10	C9	176.1559
11	O	260.1396
12	C10	96.7206
13	C11	161.3298
14	C12	169.7624
15	C13	129.2388
16	O1	260.4384
17	H-1's	28.3270
18	H-1'r	29.0942
19	H-2's	31.2776
20	H-2'r	30.4056
21	H-3'	29.8903
22	H-10'	30.7571

23	H-10’	31.3329
24	H-10’	31.6444
25	H-4’r	31.3543
26	H-4’s	30.2540
27	H-5’r	30.0305
28	H-5’s	30.1978
29	H-6’	26.4766
30	H-8’	30.6248
31	H-8’	30.5789
32	H-8’	30.6769
33	H-9’	30.1806
34	H-9’	31.0668
35	H-9’	30.8953
36	H-1	27.4167
37	H-2r	30.7050
38	H-2s	30.4343
39	H-3r	29.9799
40	H-3s	30.7428
41	H-4s	28.5762
42	H-4r	28.2813

<step 2>
Job type: NMR coupling constants.

Method: RB3LYP
Basis set: PCJ-0

Reason for exit: Successful completion
Quantum Calculation CPU Time : 3:11:35.02
Quantum Calculation Wall Time: 3:14:23.84

NMR data calculations obtained using the "Spartan-NMR" calculation method for 4a/4b (SR/RS):

Table S-XII. Vicinal coupling constants obtained using the "Spartan-NMR" calculation method for compounds **4a/4b** (SR/RS):

H\H	10'	1	2r	2s	3r	3s	4r	4s	3'	6'	1'r	2'r	4'r	5'r	1's	2's	4's	5's
10'									6.4									
1			5.3	0.7														
2r		5.3			12.6	7.3												
2s		0.7			7.7	0.5												
3r			12.6	7.7			9.4	9.4										
3s			7.3	0.5			1.1	7.8										
4r					9.4	1.1												

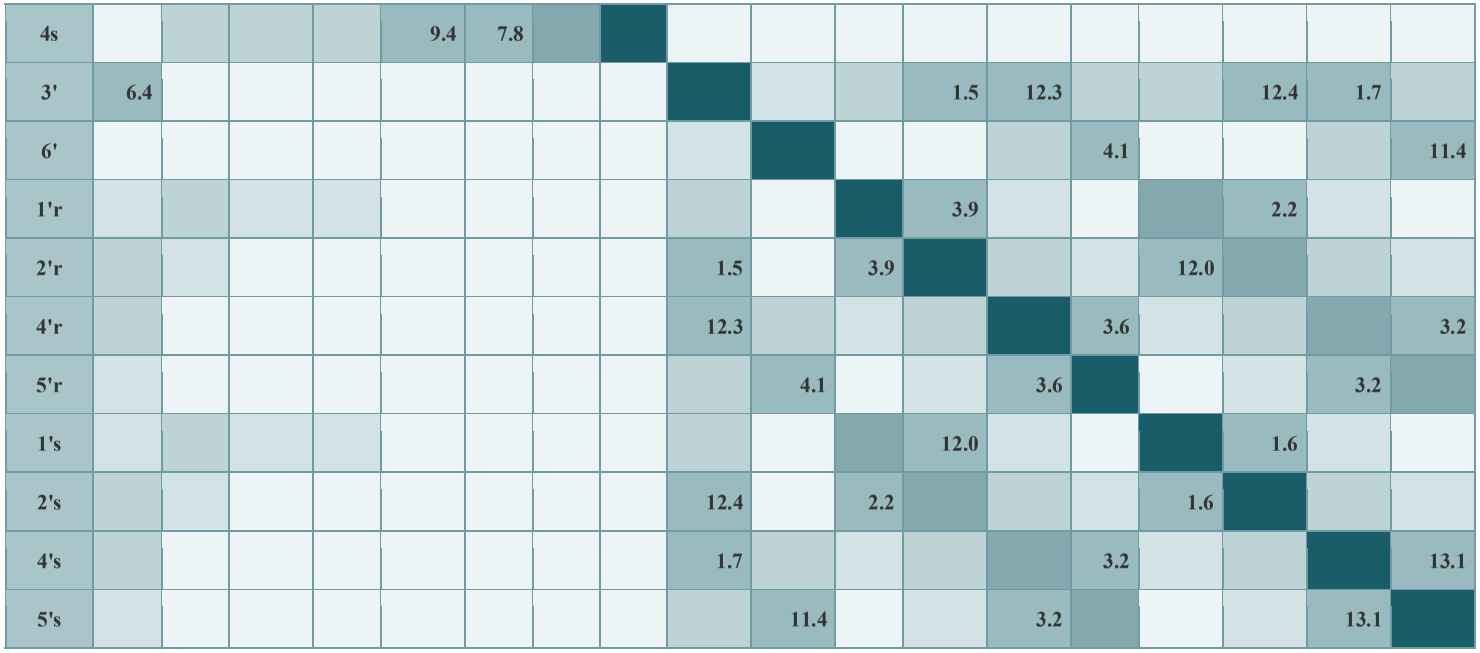

Table S-XIII. Chemical shifts, coupling constants, and HMBC interactions obtained using the "Spartan-NMR" calculation method for **4a/4b** (SR/RS):

position	δ_C	mult	δ_H		(J in Hz)	HMBC(H→C)
-1	98.2	CH	5.1	dd	(5.3,0.7)	-3, -4, -1'
-2	34.0	CH_2	1.74	ddd	(12.6,7.3,5.3)	
.			2.06	ddd	(7.7,0.7,0.5)	-4
-3	25.2	CH_2	2.52	m	(12.6,9.4,9.4,7.7)	
.			1.77	m	(7.8,7.3,1.1,0.5)	-1
-4	65.3	CH_2	4.14	dd	(9.4,1.1)	-1, -2
.			3.93	dd	(9.4,7.8)	-1
-7	129.8	C				...
10'	20.6	CH_3	1.70	d	(6.4)	-2', -4'
-1'	58.5	CH_2	4.05	dd	(3.9,2.2)	-1, -3'
.			3.64	dd	(12.0,1.6)	-1, -3'
-2'	34.0	CH_2	0.86	ddd	(12.0,3.9,1.5)	14, -4'
.			2.37	ddd	(12.4,2.2,1.6)	14, -4'
-3'	24.8	CH	2.32	m	(12.4,12.3,6.4$_{x3}$,1.7,1.5)	-1', -5'
-4'	35.8	CH_2	1.49	ddd	(12.3,3.6,3.2)	14, -2', -6'
.			1.65	ddd	(13.1,3.2,1.7)	14, -2', -6'
-5'	26.4	CH_2	2.04	ddd	(4.1,3.6,3.2)	-7, -3'
.			2.55	ddd	(13.1,11.4,3.2)	-7, -3'
-6'	122.1	CH	5.55	dd	(11.4,4.1)	-4', -8', -9'
-8'	27.6	CH_3	1.88	s		-6', -9'
-9'	19.4	CH_3	1.97	s		-6', -8'

Label	δ	..	
O-C	257.3		...
O-T	256.9		...

NMR data calculation short output for 4a/4b (SR/RS):

Job type: Geometry optimization.
Method: RHF
Basis set: 3-21G(*)
Number of basis functions: 196
Number of electrons: 126
Parallel Job: 8 threads

SCF model:
A restricted Hartree-Fock SCF calculation will be
performed using Pulay DIIS + Geometric Direct Minimization

Optimization:

Step	Energy	Max Grad.	Max Dist.
1	-691.149968	0.018721	0.067863
2	-691.158411	0.009051	0.140266
3	-691.159240	0.005097	0.180275
4	-691.159702	0.004813	0.187081

5	-691.160212	0.006340	0.179353
6	-691.160770	0.005444	0.178209
7	-691.161066	0.003618	0.065290
8	-691.161139	0.006370	0.189339
9	-691.161352	0.003556	0.040822
10	-691.161428	0.002491	0.026574
11	-691.161485	0.000910	0.020079
12	-691.161512	0.000561	0.010548

Reason for exit: Successful completion
Quantum Calculation CPU Time : 2:31.70
Quantum Calculation Wall Time: 22.05

SPARTAN'20 Quantum Mechanics Driver: (Win/64b) Release 1.1.4
Job type: Reading previous wavefunction

Job type: Single point.
Method: RWB97X-D
Basis set: 6-31G(D)
Number of basis functions: 292
Number of electrons: 126
Parallel Job: 8 threads

SCF model:
A restricted hybrid HF-DFT SCF calculation will be
performed using Pulay DIIS + Geometric Direct Minimization

SCF total energy: -699.3766056 hartrees
Reason for exit: Successful completion
Quantum Calculation CPU Time : 8:24.58
Quantum Calculation Wall Time: 1:43.71
SPARTAN'20 Quantum Mechanics Driver: (Win/64b) Release 1.1.4
Job type: Geometry optimization.
Method: RWB97X-D
Basis set: 6-31G(D)
Number of basis functions: 292
Number of electrons: 126
Parallel Job: 8 threads
SCF model:
A restricted hybrid HF-DFT SCF calculation will be
performed using Pulay DIIS + Geometric Direct Minimization

Optimization:

Step	Energy	Max Grad.	Max Dist.
1	-699.376605	0.016169	0.230909
2	-699.372802	0.053463	0.120018

3	-699.377720	0.028155	0.131144
4	-699.378924	0.016620	0.079836
5	-699.378457	0.030392	0.112922
6	-699.381414	0.011629	0.086629
7	-699.379762	0.014341	0.072367
8	-699.382541	0.006247	0.068542
9	-699.381977	0.010908	0.050659
10	-699.383286	0.003823	0.143375
11	-699.383135	0.007341	0.062972
12	-699.383580	0.003543	0.076927
13	-699.383786	0.005418	0.087621
14	-699.384172	0.005457	0.081487
15	-699.384657	0.005887	0.062677
16	-699.385040	0.002453	0.080985
17	-699.385125	0.003419	0.056921
18	-699.385165	0.003178	0.030648
19	-699.385247	0.003205	0.028567
20	-699.385270	0.003504	0.022221
21	-699.385279	0.001668	0.039333
22	-699.385304	0.001997	0.025995
23	-699.385318	0.001070	0.014798
24	-699.385331	0.000494	0.012480

Reason for exit: Successful completion
Quantum Calculation CPU Time : 2:25:36.17
Quantum Calculation Wall Time: 40:38.27

SPARTAN'20 Quantum Mechanics Driver: (Win/64b) Release 1.1.4

forcing reuse of RIC despite likely change in input file.

Job type: Geometry optimization.
Method: RWB97X-D
Basis set: 6-31G(D)
Number of basis functions: 292
Number of electrons: 126
Parallel Job: 8 threads

SCF model:
A restricted hybrid HF-DFT SCF calculation will be
performed using Pulay DIIS + Geometric Direct Minimization

2 -699.385331 0.000493 0.001781 Restart with RIC

Reason for exit: Successful completion
Quantum Calculation CPU Time : 3:29.08

Quantum Calculation Wall Time: 42.45

SPARTAN'20 Quantum Mechanics Driver: (Win/64b) Release 1.1.4

Job type: Single point.
Method: RWB97XRV
Basis set: 6-311+G(2DF,2P) [6-311G*]
Number of basis functions: 366 (small basis)
Number of electrons: 126
Parallel Job: 8 threads

SCF model:
A restricted hybrid HF-DFT SCF calculation will be
performed using Pulay DIIS + Geometric Direct Minimization

Number of basis functions: 778 (large basis)
SCF total energy: -699.6161237 hartrees

Reason for exit: Successful completion
Quantum Calculation CPU Time : 31:47.42
Quantum Calculation Wall Time: 5:43.83

SPARTAN'20 Quantum Mechanics Driver: (Win/64b) Release 1.1.4

Job type: Single point.
Method: RWB97X-D
Basis set: 6-31G(D)
Number of basis functions: 292
Number of electrons: 126

SCF model:
A restricted hybrid HF-DFT SCF calculation will be
performed using Pulay DIIS + Geometric Direct Minimization

SCF total energy: -699.3853308 hartrees

NMR shifts (ppm)

	Atom	Isotropic	Rel. Shift
1	C-1'	136.5505	
2	C-2'	160.9610	
3	C-3'	170.1754	
4	C-4'	159.1862	
5	C-5'	168.5623	
6	C-6'	72.8738	
7	C-7	65.2432	

8	C-8'	167.4099
9	C-9'	175.6451
10	O-C	257.3006
11	C-1	96.7993
12	C-2	161.0552
13	C-3	169.7674
14	C-4	129.7580
15	O-T	256.8932
16	H-1's	28.3934
17	H-1'r	28.7983
18	H-2's	31.5794
19	H-2'r	30.0736
20	H-4'r	30.9513
21	H-4's	30.7931
22	H-5'r	30.4028
23	H-5's	29.8890
24	H-6'	26.8868
25	H-8'a	30.5102
26	H-8'c	30.4960
27	H-8'b	30.6781
28	H-9'b	31.0755
29	H-9'a	29.9914
30	H-9'c	30.3373

31	H-1	27.3399
32	H-2r	30.7011
33	H-2s	30.3806
34	H-3r	29.9200
35	H-3s	30.6741
36	H-4s	28.5102
37	H-4r	28.2994
38	C14	174.4288
39	H-10'a	31.4821
40	H-10'b	30.3953
41	H-10'c	31.6973
42	H-3'	30.1206

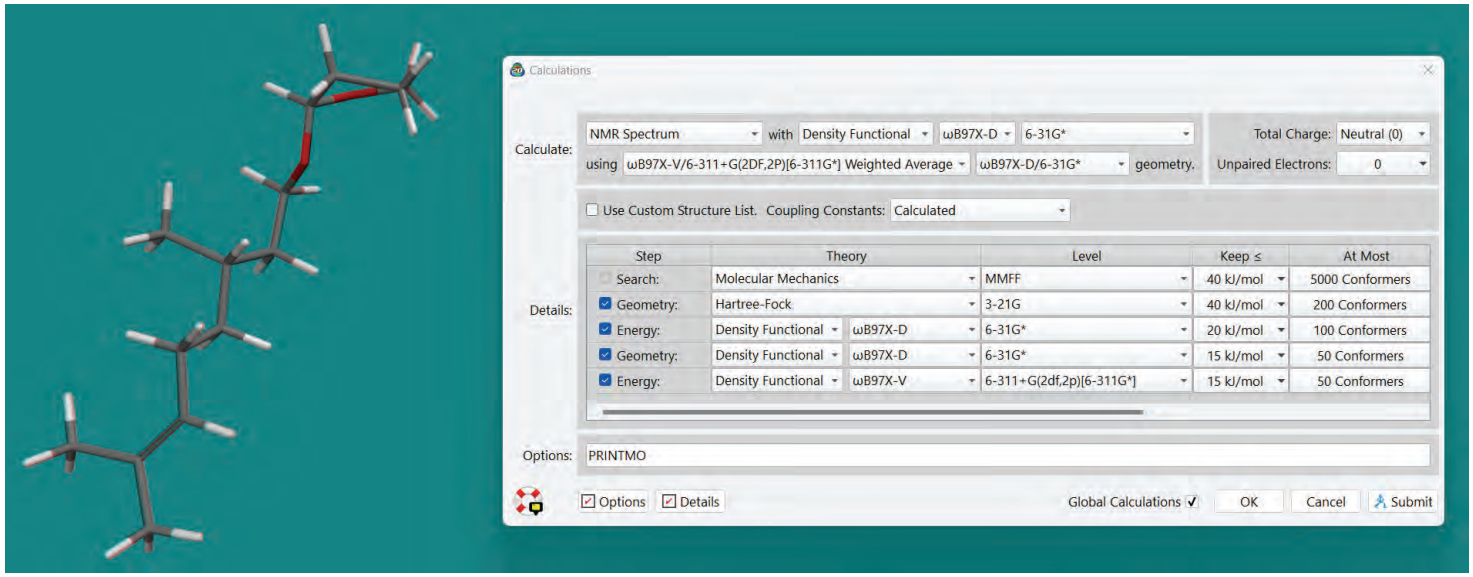

Fig. S-17. NMR data calculation parameters window for “Spartan-NMR” calculation method.

Journal of the Serbian Chemical Society
JSCS-info@shd.org.rs • www.shd.org.rs/JSCS
J. Serb. Chem. Soc. *89* (1) 13–27 (2024)
JSCS–5702
Original scientific paper
Published 12 February 2024

Antioxidant activity according to bioactive compounds content in dried pumpkin waste

SLAĐANA M. STAJČIĆ[1]*, LATO L. PEZO[2], GORDANA S. ĆETKOVIĆ[1], JASNA M. ČANADANOVIĆ-BRUNET[1], ANAMARIJA I. MANDIĆ[3], VESNA T. TUMBAS ŠAPONJAC[1], JELENA J. VULIĆ[1#], VANJA N. TRAVIČIĆ[1] and MIONA M. BELOVIĆ[3#]

[1]*University of Novi Sad, Faculty of Technology, Bulevar Cara Lazara 1, Novi Sad, Serbia,* [2]*Institute of General and Physical Chemistry, Studenski trg 12/V, Belgrade, Serbia and* [3]*University of Novi Sad, Institute for Food Technology in Novi Sad, Bulevar Cara Lazara 1, Novi Sad, Serbia*

(Received 23 May, revised 11 June, accepted 21 July 2023)

Abstract: In this study freeze-drying and oven-drying (at 50 and 65 °C) were applied for the preparation of dried pumpkin waste. The effect of drying methods on physical properties (moisture content, water activity, hygroscopicity, water solubility, bulk and tapped density, flowability and colour), content of bioactive compounds (carotenoids and phenolics) and antioxidant activity were investigated. Also, the influence of one-year storage at –20 °C on the bioactive compounds content and the antioxidant activity of dried pumpkin waste was examined. Results indicated that drying method showed a significant impact on the investigated characteristics. Bioactive compounds content and antioxidant activity by DPPH test of freeze-dried were higher than of oven-dried pumpkin waste, while higher antioxidant activity in reducing power assay was determined by oven-dried pumpkin waste. An artificial neural network model was developed, for the anticipation of antioxidant activity according to bioactive compounds content (phenolics and carotenoids), in oven-dried (at 50 and 65 °C) and in freeze-dried pumpkin waste after one-year storage. These models showed good prediction properties (the r^2 value during training cycle for output variables was 0.999). It was demonstrated that pumpkin waste is potentially an important source of bioactive compounds, which can be used after extraction in suitable forms in the development of functional food products.

Keywords: *Cucurbita moschata*; carotenoids; polyphenols; antioxidants; artificial neural network.

* Corresponding author. E-mail: sladja@uns.ac.rs
# Serbian Chemical Society member.
https://doi.org/10.2298/JSC230517043S

INTRODUCTION

Cucurbita moschata pumpkin is one of the most commonly cultivated pumpkin species.[1,2] It contains numerous bioactive compounds (such as carotenoids, phenolic compounds and vitamins) and possesses a wide range of pharmacological activities.[3] During processing of pumpkin into various products, such as purées, dishes and juices, a large amount of waste (*i.e.*, thick rind, large seeds and pressed residues) is generated.[1,4] Unutilized waste can lead to potential problems for its handling and disposal.[4] Also, these waste materials can be considered as potential source of valuable bioactive compounds.[5,6]

A limiting factor of using wastes as raw materials for the extraction of bioactive compounds may be their deterioration. For the inhibition of microbial growth and facilitating storage of plant materials different drying methods have been employed.[7] The most commonly used drying method includes convection. This method is not expensive, but has the disadvantage of reducing the content of some valuable compounds which often undergo oxidation at higher temperature.[8] Freeze drying, also known as lyophilization, is based on sublimation process where the product is frozen first.[9] In this process, drying is performed at low temperature and pressure, *i.e.*, under conditions that allow removal of water by sublimation, which involves direct phase transition of water from solid to vapor without passing through the liquid phase.[9] Therefore, freeze drying is one of the most useful processes for drying thermosensitive substances.[9,10] Freeze-drying provides excellent quality characteristics such as colour, flavour and chemical composition of the product, but this method includes very high expenses and requires a lot of time.[8] Although, in most cases, freeze dried products exhibit much higher contents of bioactive compounds than hot air dried products, some studies have shown that freeze drying can led to greater loss of bioactive compounds than hot air drying.[7] The effect of a particular drying method on the retention of raw quality is not predictable and depends on the bioactive compounds and the specific plant material involved.[7] Accordingly, the selection of drying treatment as preservation technique of waste materials can have a great influence on the retention of their bioactive constituents and raw quality.

The isolation and utilization of bioactive compounds from waste are of special interest for the food, cosmetic and pharmaceutical industries.[5,6] However, the effectiveness of bioactive ingredients depends on preserving their stability and bioactivity.[11,12] Since the content of bioactive compounds which remains available can be significantly reduced under the adverse conditions during food processing and storage (temperature, oxygen, light), their potential health benefits can be restricted.[11] Therefore, the aim of our study was to determine and compare physical properties, content of bioactive compounds and antioxidant activity of *C. moschata* pumpkin waste subjected to oven and freeze drying. Another objective of this study was to investigate the possibility of predicting the

antioxidant activity of oven-dried (50 and 65 °C) and freeze-dried (–40 °C) pumpkin waste after one-year storage, according to the content of phenols and carotenoids in the samples. These tasks were achieved using artificial neural network model.

EXPERIMENTAL

Chemicals

Folin–Ciocalteau reagent, 2,2-diphenyl-1-picrylhydrazyl radical (DPPH$^{\bullet}$), Trolox and trichloroacetic acid were purchased from Sigma Chemical Co. (St. Louis, MO, USA), ferric chloride was obtained from J.T. Baker (Deventer, Holland). All other chemicals and solvents used were of the highest analytical grade.

Plant material and dried pumpkin waste preparation

Fresh *Cucurbita moschata* pumpkin waste material was obtained after pressing the pulp as by-product from the baby food industry ("Juvitana", Inđija, Serbia) and dried by different methods, in oven (model ST-06, Instrumentaria, Zagreb, Croatia) at 50 °C for 14 h and at 65 °C for 12 h without air flow and in freeze drier (model Christ Alpha 2-4 LSC, Martin Christ, Osterode am Harz, Germany) at –40 °C for 72 h (until moisture content was reduced to 9–11 g/100 g). Dried pumpkin waste was ground, packed in plastic bags, vacuumed and kept at –20 °C until further analysis. Dry matter content was determined by weighing the initial and final weight, and calculated percentage of dried weight.

Physical characterization

Water activity (a_w), moisture content, hygroscopicity, bulk density, tapped density and colour parameters (L^*, a^* and b^*) were determined as reported previously.[13] Colour parameters (C^* and $h°$) and browning index (BI) was calculated as described by Phuon *et al*.[14] The classification of the flowability was made as described by Shishir *et al*.[15] Solubility was determined according to the method of Yamashita *et al*.,[16] with some modifications.

Water activity. a_w was determined by placing approximately 3 g of dried pumpkin waste in the sample holder of a LabSwift-aw metre (Novasina, Switzerland) at 25 °C.

Moisture content. The moisture content of dried pumpkin waste was measured using an air oven method at 105 °C until a constant weight was achieved.

Hygroscopicity. For hygroscopicity 2 g of dried pumpkin waste from the Petri dishes were placed at 25 °C in an airtight plastic container filled with NaCl saturated solution (75.29 % RH). After 1 week, hygroscopic moisture (hygroscopicity) was weighed and expressed as g of moisture per 100 g dry solids.

Solubility. The dried pumpkin waste (0.1 g) was dissolved in 10 mL of distilled water, stirred (Unimax 1010, Heidolph Instruments GmbH, Kelheim, Germany) at 150 rpm and room temperature for 30 min, and then centrifuged (centrifuge Lace 24, Colo Lab Experts, Novo Mesto, Slovenia) at 4000 rpm for 5 min. The supernatant was transferred to a pre-weighed Petri dish and dried at 105 °C until constant weight was achieved. After drying, the dried weight of the soluble solid was measured and used to calculate the percentage solubility.

Bulk and tapped density. For determination of bulk density (Db), the sample (10 g) was poured into a measuring cylinder and the initial volume was noted as the bulk volume (Vb). The Db was calculated according to the formula:

$$D\text{b} = m/V\text{b} \quad (1)$$

where m is the mass of the sample.

For determination of tapped density (*D*t), the sample was tapped 250 times and then the volume was measured. Tapping was continued until the difference between successive volumes was less than 2 % and this value was registered as the tapped volume (*V*t) and *D*t was calculated by the formula:

$$Dt = m/Vt \quad (2)$$

Bulk and tapped density of the samples were expressed in g mL^{-1}.

Flowability. The values of the Carr index and Hausner ratio indicate the quality of the powder in terms of the flow property. Carr index and Hausner ratio were calculated according to the equations:

$$\text{Carr index} = 100((Dt–Db)/Dt) \quad (3)$$

$$\text{Hausner ratio} = Dt/Db \quad (4)$$

Colour. The colour parameters (CIE L^*, a^* and b^*) were determined with a Minolta reflectance colorimeter (Minolta ChromaMeter CR-400, Konica Minolta Inc., Tokyo, Japan) using D65 illumination source at observer angle of 2°. The colour of dried pumpkin waste was measured using attachment for granular materials CR-A50. The liquid extracts were measured in a 10 mm glass cell CM-A98 fixed using specimen holder CM-A96, while standard white calibration plate was fixed behind the cell because of the sample transparency. Chroma (C^*) and hue angle ($h°$) were calculated according to the formulas:

$$C^* = (a^{*2} + b^{*2})^{1/2} \quad (5)$$

$$h° = \arctan(b^*/a^*) \quad (6)$$

Browning index (*BI*) was calculated using the following expression:

$$BI = 100((X – 0.31)/0.17) \quad (7)$$

where

$$X = (a^* + 1.75L^*)/(5.645L^* + a^* − 3.012b^*) \quad (8)$$

Extraction procedure

For the determination of the content of bioactive compounds and antioxidant activity previously described extraction procedure with modification was used.[10] Briefly, dried pumpkin waste was extracted using acetone:ethanol mixture (36:64 volume ratio) in solid to solvent ratio 1:10 using a laboratory shaker (Unimax 1010, Heidolph Instruments GmbH, Kelheim, Germany) at 300 rpm, under light protection, at room temperature. The extraction was performed three times with the same volume of solvents. The obtained three extracts were filtered (Whatman paper No.1), combined, and stored in dark bottles at –20 °C till further analysis.

Determination of β*-carotene and total phenolic content*

The content of *β*-carotene was analysed spectrophotometrically using a Multiskan GO microplate reader (Thermo Fisher Scientific Inc., Waltham, MA, USA) according to the method of Nagata and Yamashita,[17] adapted for 96 well microplate. The *β*-carotene content was expressed as mg of *β*-carotene equivalents per 100 g sample (dry weight, DW). The total content of phenolics was determined spectrophotometrically by Folin–Ciocalteau method,[18] adapted for 96 well microplate. The results of total phenolics content were expressed as gallic acid equivalents (GAE) per 100 g sample (DW).

HPLC analysis

Qualitative and quantitative analysis of flavonoids and phenolic acids was performed by HPLC analysis.[19] Also, analysis of carotenoids was done according to the HPLC method described previously.[13]

Determination of antioxidant activity

Antioxidant activity on DPPH radicals (DPPH assay) was estimated spectrophotometrically using a 96-well microplate reader, following the method described by Girones-Vilaplana *et al*.[20] Reducing power (*RP* assay) was performed with the method of Oyaizu[21] adapted for 96 well microplate. The calibration curves were made with Trolox and results were expressed as mg Trolox equivalents (TE) per 100 g of sample (DW).

Storage stability test

Dried pumpkin waste samples were stored at –20 °C in high-density polyethylene bags for one year. The effect of storage on the stability of bioactive compounds and antioxidant activities were measured using the appropriate methods described above.

ANN modelling

A multi-layer perceptron model (MLP), with three layers was applied for artificial neural network (ANN) modelling, to investigate the antioxidant activity of oven-dried (50 and 65 °C) and freeze-dried (–40 °C) pumpkin waste samples after one-year storage, on the basis of the bioactive compounds content. The experimental database was normalized in order to improve the behaviour of the ANN. Broyden–Fletcher–Goldfarb–Shanno (BFGS) algorithm was employed in solving nonlinear problems during the network modelling.[22] A series of different topologies (more than 100,000) were tested during the modelling, changing the number of neurons in the hidden layer (from 5 to 20), randomly setting initial weights and biases.[23]

The accuracy of the model. The numerical investigation of the developed ANN model's accuracy was performed applying the common used statistical tests, such as coefficient of determination (r^2), reduced chi-square (χ^2), mean bias error (*MBE*), root mean square error (*RMSE*), mean percentage error (*MPE*), average absolute relative deviation (*AARD*) and sum of squared errors (*SSE*).[24]

Global sensitivity analysis

The Yoon's interpretation method was used to determine the relative influence of bioactive compounds content on antioxidant activity of oven-dried and freeze-dried pumpkin waste samples. This method was applied using the weight coefficients of the developed ANN model.[25]

Statistical analysis

All experiments were done in triplicate. The results were expressed as mean value ± standard deviation (±*SD*, $n = 3$). The calculations were performed using StatSoft Statistica 2010 software.

RESULTS AND DISCUSSION

Physical properties of dried pumpkin waste

In recent years, the need for dried products of high quality has been increased. Much attention has been focused to the quality of dried materials.[26] In our study, oven-drying and freeze-drying were applied to obtain dried pumpkin

waste materials. After oven-drying (at 50 and 65 °C) and freeze-drying, dry matter content was determined to be 15.42, 15.40 and 15.37 %, respectively. The influence of drying methods and temperatures on the physical properties of dried pumpkin waste is shown in Table I.

TABLE I. Physical properties of oven-dried (at 50 and 65 °C) and freeze-dried (–40 °C) pumpkin waste; the results are presented as mean ± *SD*; different letters (a–c) in rows indicate that there is significant difference at $p \leq 0.05$, according to Tukey-s HSD test

Physical properties	Oven-dried (50 °C)	Oven-dried (65 °C)	Freeze-dried (–40 °C)
Moisture content, %	10.78±0.33^b	10.18±0.44^b	9.10±0.32^a
Water activity (a_w)	0.274±0.010^c	0.126±0.005^b	0.035±0.001^a
Hygroscopicity, g/100 g	13.29±0.47^a	15.08±0.71^b	15.49±0.48^b
Bulk density, g mL^{-1}	0.40±0.02^c	0.36±0.02^b	0.11±0.00^a
Tapped density, g mL^{-1}	0.58±0.04^c	0.50±0.03^b	0.17±0.01^a
Carr index, %	30.05±1.50^b	27.31±1.24^a	33.35±0.93^c
Hausner ratio	1.43±0.03^b	1.38±0.00^a	1.50±0.02^c
Flowability	Poor	Poor	Very poor
Solubility, %	31.19±1.12^a	33.30±1.47^b	33.76±1.38^b
Colour parameters			
Lightness/darkness (L^*)	49.86±0.01^a	54.11±0.03^b	67.29±0.02^c
Greenness/redness (a^*)	9.45±0.03^c	7.34±0.03^b	5.72±0.01^a
Blueness/yellowness (b^*)	23.05±0.00^a	25.00±0.01^b	29.91±0.01^c
Chroma (C^*)	24.91±0.01^a	26.05±0.01^b	30.45±0.01^c
Hue angle ($h°$)	67.71±0.06^a	73.64±0.06^b	79.17±0.01^c
Browning index (*BI*)	74.49±0.03^c	70.36±0.05^b	63.46±0.01^a

Moisture content, *i.e.*, quantity of water contained in a food system, is an important characteristic of dried powdered products, which is associated with the efficiency of drying process.[27,28] Also, the moisture content of powders has a significant influence on storage stability.[29] Similarly as in our study, the moisture content of oven-drying pumpkin material was higher than that in freeze-dried pumpkin material.[3,30] Aydin and Gocmen[31] reported that moisture contents in hot-air oven-dried and freeze-dried pumpkin flour were 12.64 and 12.56 %, respectively. Probably, the crust formed during hot air drying did not allow removing the moisture from material.[30] Water activity (a_w) represents the availability of free water in a food system which has a crucial role in biochemical reactions.[29] Basically, the most of the adverse changes in food system during storage such as lipid oxidation, enzymatic reactions, non-enzymatic browning, and microbial growth are almost completely obstructed when the water activity value is below 0.4.[32] Therefore, the water activity has been considered as one of the most important quality parameters for long term storage of dried products.[30] In our study, the water activity values of dried pumpkin waste samples provide their good storage stability. Previously, oven-dried pumpkin materials also had higher water activity (0.408) than freeze-dried pumpkin material (0.239).[30] Hygro-

scopicity, *i.e.*, capacity to adsorb ambient moisture, is one of the major factors which affect product stability.[27,33] A prominent property of freeze-dried products is great hygroscopicity.[34] Hygroscopicity is related to the gradient of water concentration between the product and the surrounding environment, which is greater for the less moist powder.[33] Indeed, higher hygroscopicity was determined in freeze-dried pumpkin waste in comparison with oven-dried.

Tapped density represents the real solid density, whereas the bulk density takes into account all the spaces between the particles of powdered products. Lower bulk density implies that more occluded air exists within the powder, thus there is a greater possibility for oxidation and reduced stability of product during storage.[28] The bulk and tapped densities were higher in oven-dried in relation to freeze-dried pumpkin waste, which is in agreement with the study of Que *et al.*[3] According to Carr index and Hausner ratio, oven-dried and freeze-dried pumpkin waste are classified,[15] in terms of flow property as poor and very poor, respectively. Solubility is a property referring to the product behaviour in an aqueous phase and is an indicator for its reconstitution quality. Quick and complete reconstitution of powder is common requirement for its application.[35] The powder structure with more cavities and pores allows easier passage of water, thus facilitates dissolution. Pumpkin waste dried at 65 °C showed higher solubility compared to the waste dried at 50 °C. Solubility can be associated with the amount of starch degradation, since at higher temperature during oven-drying more starch can be decomposed.[3]

Colour is a significant factor for consumers in food choice.[36] It can be used as an indicator of the chemical and quality changes as a consequence of thermal processing.[36] In agreement with our study, oven-drying in comparison to freeze-drying resulted in a darker colour (lower L^* values).[3,30] The lower L^* value and higher a^* value could be indicative of the browning reaction.[31,37] Compared to oven-dried waste samples, freeze-dried waste showed less yellowness and less redness (indicated by lower b^* and a^* values, respectively). Browning is an important colour reaction in food processing such as drying because it affects appearance quality.[36] As an indicator of browning, browning index (*BI*) is often used especially in conventional drying since it represents the purity of brown colour and is considered to be an important parameter associated with browning.[30] In this study, the values of browning index of dried waste samples showed that oven-drying caused more brown compounds. The difference in browning may be related to the removal of water by sublimation and prevention of enzymatic browning reactions during freeze-drying.[38,39] The yellowish colour of dried pumpkin waste powders could be mainly attributed to the presence of carotenoids naturally found in this vegetable. Drying conditions, including high temperature, light and oxygen exposure can cause changes in food surface that lead to colour changes, and also to degradation of carotenoids.[32] The lighter yellowness of

freeze-dried in relation to oven-dried waste is shown by C^* and $h°$ values. Similar colour values as in our study, lightness (L^*), redness (a^*) and yellowness (b^*) of convective dried (55.57, 22.67 and 35.25, respectively) and freeze-dried (77.96, 18.54 and 31.22, respectively) slices *of C. moschata* pumpkin were found.[30] In addition, Que *et al.*[3] reported that the freeze-drying process can significantly decrease the brownish appearance of pumpkin flour and can produce pumpkin powders of high-quality colour.

Bioactive compounds and antioxidant activity of dried pumpkin waste

Effect of drying methods, drying temperatures and storage on the content of bioactive compounds and antioxidant activity of dried pumpkin waste samples is presented in Table II.

TABLE II. The content (mean ± *SD*) of bioactive compounds (phenolics and carotenoids, mg/100 g DW) and antioxidant activity (DPPH and RP assays, mg TE/100 g DW) of oven-dried (at 50 and 65 °C) and freeze-dried (–40 °C) pumpkin waste; different letters (a–c) in rows indicate that there is significant difference at $p \leq 0.05$, according to Tukey's HSD test; * – HPLC analysis was performed after drying of pumpkin waste; n.d. – not detected

Bioactive compounds/antioxidant activity	Oven-dried (50 °C)	Oven-dried (65 °C)	Freeze-dried (–40 °C)
Total phenolics – after drying	201.31±7.27^a	213.61±7.60^b	294.69±14.13^c
Total phenolics – after storage	183.47±7.03^b	180.34±5.39^b	175.60±6.11^a
β-Carotene – after drying	6.51±0.23^b	5.56±0.00^a	14.26±0.27^c
β-Carotene – after storage	2.85±0.12^a	4.57±0.00^b	7.89±0.22^c
Gallic acid*	1.658±0.080^a	1.757±0.078^b	3.802±0.17^c
Protocatechuic acid*	7.644±0.322^b	4.555±0.221^a	9.217±0.43^c
Catechin*	0.490±0.021^a	1.588±0.071^b	1.672±0.067^c
Caffeic acid*	0.128±0.005^c	0.096±0.003^a	0.116±0.003^b
Syringic acid*	0.470±0.021^b	0.288±0.011^a	1.835±0.076^c
Coumaric acid*	0.103±0.004^b	0.097±0.003^a	0.108±0.002^b
Chlorogenic acid*	0.049±0.002^b	0.038±0.001^a	0.224±0.008^c
p-Hydroxybenzoic acid*	2.642±0.131^b	1.726±0.076^a	12.606±0.598^c
Vanillic acid*	0.171±0.006^c	0.117±0.004^a	1.385±0.060^b
Myricetin*	0.010±0.001^b	0.007±0.001^a	1.385±0.056^c
Rutin*	0.127±0.004^b	0.083±0.002^a	0.313±0.011^c
Total phenolics*	13.492	10.352	31.365
Lutein*	0.033±0.001^a	0.037±0.001^b	0.174±0.006^c
Zeaxanthin*	1.598±0.069^b	0.403±0.017^a	1.660±0.081^b
β-Carotene*	4.406±0.187^c	1.303±0.057^a	3.247±0.158^b
β-Cryptoxanthin*	n.d.	n.d.	2.820±0.134
Total carotenoids*	6.037	1.743	7.901
DPPH – after drying	99.27±1.52^b	78.87±0.55^a	131.64±6.40^c
DPPH – after storage	50.56±1.75^b	30.41±0.34^a	65.66±1.55^c
RP – after drying	66.23±1.97^b	140.94±0.77^c	17.39±0.28^a
RP – after storage	60.40±2.68^b	140.20±3.10^c	16.41±0.46^a

The spectrophotometric determinations were done after drying of pumpkin waste and after storage at –20 °C (during one year) of dried pumpkin waste samples. Higher content of total phenolics determined by spectrophotometric and HPLC methods was determined in freeze-dried pumpkin waste in comparison to oven-dried samples. In the study of Aydin and Gocmen,[31] higher level of phenols (236 mg GAE/100 g DW) was found in oven-dried (at 60 °C) pumpkin (*C. moschata* Duch.) flour compared to freeze-dried (226 mg GAE/100 g DW). Also, Que *et al*.[3] reported that content of phenolic compounds (1.64 mg g^{-1}) in hot air--dried (at 70 °C) pumpkin (*C. moschata* Duch.) flour was 4.6 times higher than that in freeze-dried pumpkin (0.39 mg g^{-1}) flour, indicating the formation of phenolics during drying at 70 °C. Higher degree of heating could have a great impact on the increase of total phenolics of pumpkin flour.[3] Beside the difference in sample, extraction processes, drying conditions, cultivar, maturation stage, geography and climate may cause difference in determination of phenolics.[30,40] In the study of Nawirska-Olszanska *et al*.,[41] the content of phenolics in different varieties of *C. moschata* pumpkin was ranged from 141.16 mg/100 g DW to 390.61 mg/100 g DW. Potosi-Calvache *et al*.[42] determined the content of total phenolics (from 27.7 mg GAE/100 g to 79.9 mg GAE/100 g) in samples of *C. moschata* pumpkin dried under different temperature (45-65 °C) and air flow (4––7 m/s). During processing and storage phenolics can be degraded or formed from the availability of their precursors or by non-enzymatic inter conversions between them.[42] In our study, in investigated pumpkin waste powders, *p*-hydroxybenzoic and protocatechuic acid were determined in highest content of all identified phenolic acids, while catechin was determined in highest content of identified flavonoids. Kulczyński and Gramza-Michałowska[1] reported that the profile of bioactive compounds in pumpkin (*C. moschata*) is considerably diversified in its cultivars. In agreement with our study, the content of identified flavonoids were lower than the content of phenolic acids, and high contents of *p*-hydroxybenzoic and protocatechuic acids were also found.[1]

Higher *β*-carotene content, determined spectrophotometrically, was observed in freeze-dried than in oven-dried pumpkin waste samples. Different factors (temperature, oxygen and light) during drying process (*i.e.*, drying conditions) may cause carotenoid degradation.[32,40] In agreement with our study, higher total carotenoid content (between 5 and 160 mg/100 g) was obtained with freeze-drying than by convective drying of 12 pumpkin cultivars.[8,40] Previously, higher drying temperatures also produced greater pigment losses.[32] Colour values, L^*, a^* and b^* of extracts obtained after extraction of oven-dried at 50 °C (59.43, –5.27 and 66.53, respectively), oven-dried at 65 °C (59.27, –5.61, and 67.16, respectively) and freeze dried (56.01, 1.79, and 65.57, respectively) *C. moschata* pumpkin waste, indicated yellow colour that could be attributed to the presence of carotenoids. It is interesting to notice that colour parameter a^* had negative

values in oven-dried samples, indicating the degradation of reddish pigments in comparison to freeze-dried sample, which had positive a^* values. In our study, higher content of total carotenoids determined by HPLC method was found in freeze-dried pumpkin waste in comparison to oven-dried samples. β-Criptoxanthin was not even identified in oven-dried waste. Interestingly, somewhat higher β-carotene content was found in dried pumpkin waste after oven-drying at 50 °C than after freeze-drying. Kulczyński and Gramza-Michałowska[1] reported high variability of carotenoids among pumpkin (*C. moschata*) cultivars, and on average the content of zeaxanthin, lutein and β-carotene of different *C. moschata* cultivars was 2.64, 6.87 and 2.92 mg/100 g DW, respectively.

After storage, the content of phenolics and β-carotene in dried pumpkin waste samples was decreased (Table II). After storage, similar values of phenolics content were found in all dried pumpkin waste samples, while the highest content of β-carotene was determined in freeze dried waste in comparison to oven-dried pumpkin waste samples.

Freeze-dried pumpkin waste exhibited higher antioxidant activity by DPPH test, while higher antioxidant activity in reducing power assay was achieved by oven-dried pumpkin waste (Table II). This can be explained by various mechanisms by which different antioxidants exert their action.[26] Previously, hot-air oven dried (at 60 and 70 °C) pumpkin flours showed higher antioxidant activities by different assays, than freeze-dried samples.[3,31] Phenolics formed from precursors in hot-air drying treatment or generation of Maillard-type antioxidants might be responsible for higher antioxidant activity of hot-air dried pumpkin flour.[3] Samples of dried pumpkin waste in our study showed somewhat lower, but significant antioxidant activity by DPPH test (from 3.15 to 5.26 μmol TE g^{-1}), and by reducing power test (from 0.69 to 5.63 μmol TE g^{-1}) in comparison to the antioxidant activity of dried pumpkin flours (from 5.57 to 7.21 μmol TE g^{-1}) reported by Aydin and Gocmen.[31]

After storage, DPPH antioxidant activity in dried pumpkin waste powders was decreased, while reducing power was almost unchanged in comparison with levels determined before storage (Table II). After storage, the highest reducing power was observed for waste dried at 65 °C, while the highest antioxidant activity by DPPH test was determined for freeze-dried waste.

ANN model

The acquired optimal neural network model could be used to adequately anticipate the antioxidant activity of oven-dried (50 and 65 °C) and freeze-dried (–40 °C) pumpkin waste samples after one year storage, on the basis of phenolics and carotenoids content. The optimal number of neurons was: 9 (network MLP 14-9-4), while the highest r^2 values during the training cycle were 0.999).

The obtained ANN model for the anticipation of output variables was complex (175 weights-biases coefficients) due to the high nonlinearity of the observed system. The goodness of fit between experimental and ANN model calculated values were shown in Table III.

TABLE III. The goodness of fit tests for the developed ANN model

Output variable	χ^2	*RMSE*	*MBE*	*MPE*	*SSE*	*AARD*	r^2
DPPH after drying	1.042	0.589	0.168	0.589	0.957	1.766	1.000
DPPH after storage	0.456	0.390	–0.036	0.718	0.452	1.091	1.000
RP after drying	0.267	0.299	–0.193	0.277	0.156	0.601	1.000
RP after storage	0.690	0.480	–0.349	0.542	0.325	1.046	1.000

The ANN predicted values were very close to the measured values in most cases, in terms of r^2 values.[43,44] The *SSE* values obtained with the ANN model was of the same order of magnitude as experimental errors for output variables reported in the literature.[22,45] The ANN model had an insignificant lack of fit tests, which means the model satisfactorily predicted output variables.

Global sensitivity analysis – Yoon's interpretation method

According to the Fig. 1, gallic acid, syringic acid, chlorogenic acid, *p*-hydroxybenzoic acid, vanillic acid, myrcetin, rutin and lutein content were the most influential parameters with approximately relative importance of 9.222–10.337 % for the prediction of DPPH after drying, while the relative influence of these variables for the prediction of DPPH after storage reached the relative importance of 9.583–10.680 %.The RP assay was mostly influenced by the catechin content, 27.82 % after drying and 28.55 % after the on-year long storage.

CONCLUSION

Different drying methods, including freeze-drying and oven-drying (at 50 °C and 65 °C) caused significant impact on physical properties, bioactive compounds content and antioxidant activity of dried pumpkin waste. In general, carotenoids and phenolics content of the freeze-dried pumpkin waste was higher than of the oven-dried one. The freeze-dried pumpkin waste exhibited higher antioxidant activity by DPPH test, while higher antioxidant activity in reducing power assay was determined for the oven-dried pumpkin waste. After storage at –20 °C during one year, higher content of β-carotene and antioxidant activity by DPPH test, while lower content of phenolics and reducing power were achieved by freeze-dried than by oven-dried pumpkin waste samples.

Also, findings of this study indicate that antioxidant activity of the oven-dried (50 °C and 65 °C) and the freeze-dried (–40 °C) pumpkin waste samples after one year storage could be anticipated, based on the phenolics and carotenoids content. The artificial neural network model showed to be adequate

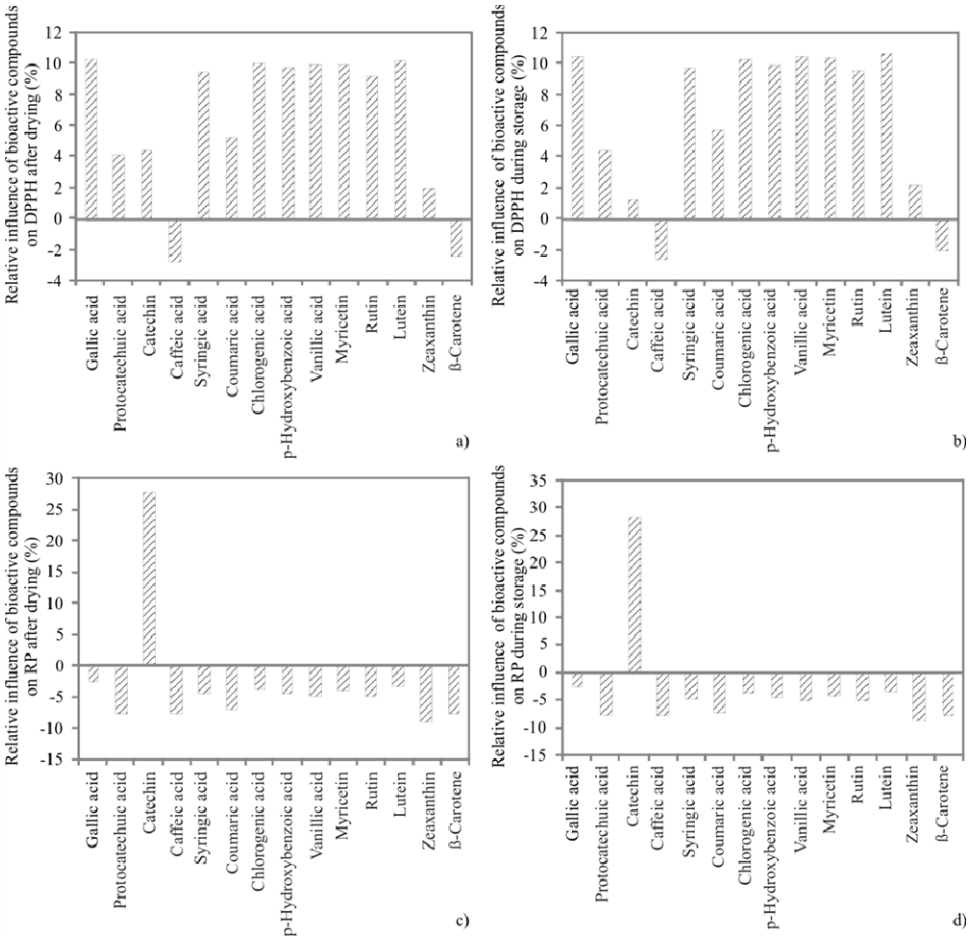

Fig. 1. The relative importance of the bioactive compounds content on antioxidant activity determined by DPPH assay after drying (a) and storage (b), and by RP assay after drying (c) and storage (d) of pumpkin waste samples.

for the prediction of output variables (the r^2 values during training cycle for these variables were: 0.999).

It was demonstrated that pumpkin waste is potentially an important source of bioactive compounds with significant antioxidant properties. In the future, to overcome a main drawback for the application of natural bioactive compounds, namely their instability, different protection systems including encapsulates could be formulated. Therefore, our results support the need for preparation of encapsulates of the bioactive compounds extracted from dried pumpkin waste and evaluation of their physicochemical and stability characteristics, in order of development functional ingredients for value added food products.

Acknowledgement. This work was financially supported by the Ministry of Science, Technological Development and Innovations of the Republic of Serbia (Project No. 451-03-47/ /2023-01/200134, Projects No. 451-03-47/2023-01/200051 and 451-03-47/2023-01/200222).

ИЗВОД

АНТИОКСИДАТИВНА АКТИВНОСТ НА ОСНОВУ САДРЖАЈА БИОАКТИВНИХ ЈЕДИЊЕЊА У СУШЕНОМ ОТПАДУ ТИКВЕ

СЛАЂАНА М. СТАЈЧИЋ[1], ЛАТО Л. ПЕЗО[2], ГОРДАНА С. ЋЕТКОВИЋ[1], ЈАСНА М. ЧАНАДАНОВИЋ-БРУНЕТ[1], АНАМАРИЈА И. МАНДИЋ[3], ВЕСНА Т. ТУМБАС ШАПОЊАЦ[1], ЈЕЛЕНА Ј. ВУЛИЋ[1], ВАЊА Н. ТРАВИЧИЋ[1] и МИОНА М. БЕЛОВИЋ[3]

[1]Универзитет у Новом Саду, Технолошки факултет, Булевар цара Лазара 1, Нови Сад, [2]Институт за општу и физичку хемију, Студентски трг 12/В, Београд и [3]Универзитет у Новом Саду, Научни институт за прехрамбене технологије у Новом Саду, Булевар цара Лазара 1, Нови Сад

У овој студији за припрему сушеног отпада тикве примењено је сушење лиофилизацијом и у сушници (на 50 и 65 °C). Испитан је утицај метода сушења на физичка својства (садржај влаге, активност воде, хигроскопност, растворљивост у води, насипну и тапкану густину, проточност и боју), садржај биоактивних једињења (каротеноида и полифенолних једињења) и антиоксидативну активност. Такође, испитан је утицај складиштења на –20 °C у периоду од годину дана на садржај биоактивних једињења и антиоксидативну активност сушеног отпада тикве. Резултати су показали да метода сушења значајно утиче на испитане карактеристике. Садржај биоактивних једињења и антиоксидативна активност DPPH тестом лиофилизованог отпада били су већи у односу на отпад тикве сушен у сушници, док је већа антиоксидативна активност тестом редукционе способности одређена у отпаду тикве сушеном у сушници. Развијен је модел вештачке неуронске мреже, за предвиђање антиоксидативне активности према садржају биоактивних једињења (полифенолна једињења и каротеноиди), у отпаду тикве сушеном лиофилизацијом и у сушници (на 50 и 65 °C) након годину дана складиштења. Ови модели су показали добра својства предвиђања (вредност r^2 током циклуса тренинга за излазне варијабле била је 0,999). Показано је да је отпад тикве потенцијално важан извор биоактивних једињења, која се након екстракције могу користити у одговарајућим облицима у развоју функционалних прехрамбених производа.

(Примљено 17. маја, ревидирано 11. јуна, прихваћено 21. јула 2023)

REFERENCES

1. B. Kulczyński, A. Gramza-Michałowska, *Molecules* **24** (2019) 2945 (https://doi.org/10.3390/molecules24162945)
2. A. Hussain, T. Kausar, A. Din, A. Murtaza, M. A. Jamil, S. Noreen, H. Rehman, H. Shabbir, M. A. Ramzan, *J. Food Process. Preserv.* **45** (2021) e15542 (https://doi.org/10.1111/jfpp.15542)
3. F. Que, L. Mao, X. Fang, T. Wu, *Int. J. Food Sci. Technol.* **43** (2008) 1195 (https://doi.org/10.1111/j.1365-2621.2007.01590.x)
4. A. A. Shetty, R. Rana, T. Buckseth, S. P. Preetham, *Waste and Biomass Valor.* **3** (2012) 363 (https://doi.org/10.1007/s12649-012-9114-x)
5. A. Hussain, T. Kausar, S. Sehar, A. Sarwar, A. H. Ashraf, M. A. Jamil, S. Noreen, A. Rafique, K. Iftikhar, M. Y. Quddoos, J. Aslam, M. A. Majeed, *Food Chem. Adv.* **1** (2022) 100067 (https://doi.org/10.1016/j.focha.2022.100067)

6. A. Hussain, T. Kausar, S. Sehar, A. Sarwar, A. H. Ashraf, M. A. Jamil, S. Noreen, A. Rafique, K. Iftikhar, J. Aslam, M. Y. Quddoos, M. A. Majeed, M. Zerlasht, *Appl. Food Res.* **2** (2022) 100241 (https://doi.org/10.1016/j.afres.2022.100241)
7. R. Li, H. Shang, H. Wu, M. Wang, M. Duan, J. Yang, *Sci Rep.* **8** (2018) 9529 (https://doi.org/10.1038/s41598-018-27874-4)
8. A. Nawirska, A. Figiel, A. Z. Kucharska, A. Sokoł-Łętowska, A. Biesiada, *J. Food Eng.* **94** (2009) 14 (http://dx.doi.org/10.1016/j.jfoodeng.2009.02.025)
9. M. U. H. Suzihaque, S. A. Hashib, U. K. Ibrahim, *Proc. Soc. Behav. Sci.* **195** (2015) 2829 (https://doi.org/10.1016/j.sbspro.2015.06.401)
10. V. N. Šeregelj, G. S. Ćetković, J. M. Čanadanović-Brunet, V. T. Tumbas Šaponjac, J. J. Vulić, S. M. Stajčić, *Acta Period. Technol.* **48** (2017) 261 (https://doi.org/10.2298/APT1748261S)
11. Z. Fang, B. Bhandari, *Trends Food Sci. Technol.* **21** (2010) 510 (https://doi.org/10.1016/j.tifs.2010.08.003)
12. A. Hussain, T. Kausar, S. Sehar, A. Sarwar, M. Y. Quddoos, J. Aslam, A. Liaqat, T. Siddique, Q. U. An, S. Kauser, A. Rehman, R. Nisar, *Food Prod. Process. Nutr.* **5** (2023) 1 (https://doi.org/10.1186/s43014-023-00138-z)
13. V. Šeregelj, V. Tumbas Šaponjac, S. Lević, A. Kalušević, G. Ćetković, J. Čanadanović-Brunet, V. Nedović, S. Stajčić, J. Vulić, A. Vidaković, *J. Microencapsul.* **36** (2019) 704 (https://doi.org/10.1080/02652048.2019.1668488)
14. V. Phuon, I. N. Ramos, T. R. S. Brandão, C. L. M. Silva, *J. Food Process Eng.* **45** (2021) e13794 (https://doi.org/10.1111/jfpe.13794)
15. M. R. I. Shishir, F. S. Taip, N. A. Aziz, R. A. Talib, *Agric. Sci. Proc.* **2** (2014) 74 (https://doi.org/10.1016/j.aaspro.2014.11.011)
16. C. Yamashita, M. M. Song Chung, C. dos Santos, C. Malacrida, I. C. F. Moraes, I. Branco, *LWT – Food Sci. Technol.* **84** (2017) 256 (https://doi.org/10.1016/j.lwt.2017.05.063)
17. M. Nagata, I. Yamashita, *J. Jpn. Soc. Food Sci. Technol.* **39** (1992) 925 (https://doi.org/10.3136/nskkk1962.39.925)
18. V. L. Singleton, J. A. Rossi, *Am. J. Enol. Vitic.* **16** (1965) 144 (https://doi.org/10.5344/ajev.1965.16.3.144)
19. V. Tumbas Šaponjac, G. Ćetković, J. Čanadanović-Brunet, A. Mandić, V. Šeregelj, J. Vulić, S. Stajčić, *J. Chem.* **2019** (2019) 7184293 (https://doi.org/10.1155/2019/7184293)
20. A. Girones-Vilaplana, P. Mena, D. A. Moreno, C. Garcia-Viguera, *J. Sci. Food Agric.* **94** (2014) 1090 (https://doi.org/10.1002/jsfa.6370)
21. M. Oyaizu, *Jpn. J. Nutr. Diet.* **44** (1986) 307 (https://doi.org/10.5264/eiyogakuzashi.44.307)
22. T. Kollo, D. von Rosen, *Advanced Multivariate Statistics with Matrices*, Springer Dordrecht, 2005 (https://doi.org/10.1007/1-4020-3419-9)
23. C.I. Ochoa-Martínez, A.A. Ayala-Aponte, *LWT – Food Sci. Technol.* **40** (2007) 638 (https://doi.org/10.1016/j.lwt.2006.03.013)
24. M. Aćimović, L. Pezo, V. Tešević, I. Čabarkapa, M. Todosijević, *Ind. Crops Prod.* **154** (2020) 112752 (https://doi.org/10.1016/j.indcrop.2020.112752)
25. Y. Yoon, G. Swales, T. M. Margavio, *J. Oper. Res. Soc.* **44** (2017) 51 (https://doi.org/10.1057/jors.1993.6)
26. S. Roshanak, M. Rahimmalek, S. A. H. Goli, *J. Food Sci. Technol.* **53** (2016) 721 (https://doi.org/10.1007/s13197-015-2030-x)

27. N. M. Nawi, I. I. Muhamad, A. M. Marsin, *Food Sci. Nutr.* **3** (2015) 91 (https://doi.org/10.1002/fsn3.132)
28. S. J. Cynthia, J. D. Bosco, S. Bhol, *Int. J. Food Prop.* **18** (2015) 1793 (https://doi.org/10.1080/10942912.2014.940536)
29. K. Papoutsis, J. B. Golding, Q. Vuong, P. Pristijono, C. E. Stathopoulos, C. J. Scarlett, M. Bowyer, *Foods.* **7** (2018) 115 (https://doi.org/10.3390/foods7070115)
30. G. Caliskan, S. N. Dirim, *Heat Mass Transf.* **53** (2017) 2129 (https://doi.org/10.1007/s00231-017-1967-x)
31. E. Aydin, D. Gocmen, *LWT – Food Sci. Technol.* **60** (2015) 385 (http://dx.doi.org/10.1016/j.lwt.2014.08.025)
32. W. Roongruangsri, J. E. Bronlund, *Int. Food Res. J.* **23** (2016) 962 (http://www.ifrj.upm.edu.my/volume-23-2016.html)
33. R. V. Tonon, S. S. Freitas, M. D. Hubinger, *J. Food Process. Preserv.* **35** (2011) 691 (https://doi.org/10.1111/j.1745-4549.2011.00518.x)
34. A. Nafiunisa, N. Aryanti, D. H. Wardhani, A. C. Kumoro, *J. Phys. Conf. Ser.* **909** (2017) 012084 (https://doi.org/10.1088/1742-6596/909/1/012084)
35. A. R. Oliveira, A. E. C. Ribeiro, É. R. Oliveira, M. C. Garcia, M. S. Soares Júnior, M. Caliari, *Food Sci. Technol.* **40** (2019) 282 (https://doi.org/10.1590/fst.34818)
36. P. B. Pathare, U. L. Opara, F. A. J. Al-Said, *Food Bioprocess Tech.* **6** (2013) 36 (https://doi.org/10.1007/s11947-012-0867-9)
37. N. Bahloul, N. Boudhrioua, M. Kouhila, N. Kechaou, *Int. J. Food Sci. Technol.* **44** (2009) 2561 (https://doi.org/10.1111/j.1365-2621.2009.02084.x)
38. M. Henríquez, S. Almonacid, M. Lutz, R. Simpson, M. Valdenegro, *CyTA – J Food*. **11** (2013) 127 (http://dx.doi.org/10.1080/19476337.2012.703693)
39. D. Mohapatra, Z. M. Bira, J. P. Kerry, J. M. Frías, F. A. Rodrigues, *J. Food Sci.* **75** (2010) 146 (https://doi.org/10.1111/j.1750-3841.2010.01518.x)
40. S. N. Dirim, G. Çalışkan, *Gida J. Food* **37** (2012) 203 (https://dergipark.org.tr/en/pub/gida/issue/6933/92554)
41. A. Nawirska-Olszanska, B. Stępien, A. Biesiada, *LWT – Food Sci. Technol*. **77** (2017) 276 (https://doi.org/10.1016/j.lwt.2016.11.067)
42. D. C. Potosi-Calvache, P. Vanegas-Maheceha, H. A. Martinez-Correa, *DYNA* **84** (2017) 112 (http://dx.doi.org/10.15446/dyna.v84n202.63904)
43. Z. Erbay, F. Icier, *J. Food Eng.* **91** (2009) 533 (https://doi.org/10.1016/j.jfoodeng.2008.10.004)
44. T. Turanyi, A. S. Tomlin, *Analysis of kinetics reaction mechanisms*, Springer, Berlin, 2014 (https://doi.org/10.1007/978-3-662-44562-4)
45. M. Doumpos, C. Zopounidis, *Eur. J. Oper. Res.* **209** (2011) 203 (https://doi.org/10.1016/j.ejor.2010.05.029).

Journal of the Serbian Chemical Society
JSCS-info@shd.org.rs • www.shd.org.rs/JSCS
J. Serb. Chem. Soc. *89* (1) 29–38 (2024)
JSCS–5703
Original scientific paper
Published 12 February 2024

Immobilization of natural betalain pigments in inorganic hosts

LIGIA TODAN[1]*, DANIELA C. CULITA[1], MIRABELA E. SOARE[1], RODICA M. ION[2], RADU C. FIERASCU[2] and MARIA MAGANU[3]

[1]Ilie Murgulescu Institute of Physical Chemistry, Romanian Academy, 202 Splaiul Independentei, 060021 Bucharest, Romania, [2]National Institute for Research & Development in Chemistry and Petrochemistry-ICECHIM, 202 Splaiul Independentei, 060021 Bucharest, Romania and [3]"Costin D. Nenitescu" Institute of Organic and Supramolecular Chemistry, Romanian Academy, 202 B Splaiul Independentei, 060023 Bucharest, Romania

(Received 28 October 2022, revised 21 January, accepted 1 March 2023)

Abstract: In search of new food-grade pH sensitive formulations, red beet extract rich in betacyanin was included in different inorganic matrices based on silica and aluminosilicate to improve the stability of the dye. By the direct method of encapsulation of the pigments in silica support, stabilizing agents such as inclusion complex forming *β*-cyclodextrin and ascorbic acid were added. The post loading system assumes the synthesis of porous silica and aluminosilicate powders and the adsorption of the beet extract by these supports. The unloaded carriers were structurally and texturally characterized (X-ray diffraction, FTIR, N_2-physisorption). The presence of betanin, approved as a red food colorant, was evidenced by UV–Vis spectroscopy in all the hosts. Color properties were investigated as well as the pH generated color variations of the powders exposed to ammonia in the head-space of a sealed vessel. The obtained results could widen the field of applications of beet extract, the prepared ecological formulations could provide added value to edible products packaging.

Keywords: betanin; encapsulation; mesoporous silica; aluminosilicate; color parameters.

INTRODUCTION

Betalains are the major pigments abundantly found in beetroot (*Beta vulgaris)* which are chemically defined as the derivatives of betalamic acid.[1] Betalains can be divided into yellow-orange betaxanthins and red-violet betacyanins. Of the betalains, betanin is approved for use as colorant in food industry (E number E162, CI Natural Red 33) and is considered a better choice than chemically synthesized pigments. It has commercial applications for foodstuff, cosmetics and pharmaceuticals.[2] Betanin is almost totally extracted from beetroot

* Corresponding author. E-mail: l_todan@yahoo.co.uk
https://doi.org/10.2298/JSC221028010T

crops and sold as beetroot extract.[3] All betalains are water soluble. The main factors influencing their stability are light, oxygen concentration, temperature, the presence of water and pH. They retain their tinctorial strength and color shade over a pH range of 3–7.[1,2] The fact that betacyanins show sensitivity to pH makes them suitable for use as colorimetric indicators for detecting changes of the environment especially in case of edible products, thus improving the protection and shelf life of foodstuffs or pharmaceuticals.[4] To preserve the chemical structure of the pigment and to facilitate its use in commercial applications, different ways of stabilization were used. Metal–chelates formation, cyclodextrin complexes, addition of organic acids, inclusion in different matrices should be mentioned.[5,6] It was shown that cyclodextrins are promising stabilizing agents of betalain molecules, *β*-cyclodextrin (*β*-CD) forming an inclusion complex with betanin.[5,6] Copigmentation was used to preserve betalains color intensity and stability. It involves interactions between the dyes and other naturally occurring compounds such as ascorbic or citric acid which can be neutralizing agents for the electrophilic center of betalains.[5,6]

Immobilization of the beet pigments on a solid carrier, organic or inorganic, is a promising approach for improving the properties of the plant derived pigments, thus enabling the inclusion of certain additives that can confer better functionality to encapsulated betalain pigments. A wide range of encapsulation systems have been designed: natural products derived nanocarriers (maltodextrin, caseins), lipid-based nanocarriers, biopolymers based nanocarriers (chitosan, proteins) and inorganic carriers (carbon nanotubes, clay minerals, *γ*-alumina).[6–8] Two approaches for the inclusion of drugs into silica based particles of matrix type have been mentioned, namely direct drug encapsulation when the drug is dissolved in the liquid precursor prior to formation of the matrix and indirect encapsulation or post loading when carrier particles are first synthesized followed by encapsulation of the drug.[9,10]

The purpose of the present work was to obtain formulations betalains–SiO_2 and betalains-aluminosilicate, respectively, and to explore the two above mentioned loading modes of beet pigments into the silica-based carriers. Our results provide novel information about the structure and properties of the final hybrid pigments, especially the color response toward ammonia, a marker of food spoilage, the obtained data contributing to the development of product formulations which can favour the properties of food packaging.

EXPERIMENTAL

Materials

Ludox®SM-30 colloidal silica (30 wt. % suspension in water) and sodium hydroxide were from Sigma Aldrich. *β*-cyclodextrine was purchased from Wacker-Chemie GmbH. Ascorbic acid pharmaceutical grade was purchased from Intra-Laboratories, cetyltrimethylammonium bromide (CTAB) from Carl Roth, aluminium oxide from Merck Millipore, sodium

dodecyl sulfate (SDS) analytical grade from Applichem. The concentrated beetroot juice (100 %, Biotta food grade), produced by extraction of pigments from red beet and its subsequent pasteurization with betanin the major coloring principle, was used as natural dye.

Characterization

X-ray diffraction (XRD) analyses were performed using a 9 kW Rigaku SmartLab diffractometer (Rigaku Corp., Tokyo, Japan, operated at 45 kV and 200 mA, CuKα radiation λ =1.54059 Å), in scanning mode $2\theta/\theta$, between 2 and 90° (2θ) for wide-angle analysis and between 0.05 and 8° (2θ) for small angle analysis, measuring scan step 0.02°, scan speed 8° min^{-1} (wide angle) and 4° min^{-1} (small angle). Components were identified by comparison with ICDD data. FT-IR spectra were recorded on a Brucker Vertex 70 spectrometer with horizontal device for attenuated reflectance and diamond crystal, on a spectral window ranging from 4000 to 400 cm^{-1}, at a spectral resolution of 2 cm^{-1}. Spectra were recorded without any sample preparation and were processed with OPUS 5.5 program (Brucker). Nitrogen adsorption–desorption isotherms at 77 K were recorded on a Micromeritics ASAP 2020 automated gas adsorption system (Norcross, GA, USA). The samples were degassed at 250 °C for 4 h under vacuum before analysis. Specific surface areas (S_{BET}) were calculated according to the Brunauer–Emmett–Teller (BET) equation, using adsorption data in the relative pressure range between 0.05 and 0.30. The total pore volume (V_{total}) was estimated from the amount adsorbed at the relative pressure of 0.99. The pore size distribution curves were obtained from the desorption data using the Barrett–Joyner–Halenda (BJH) model. UV–Vis spectra were recorded using a Jasco V-750 spectrophotometer equipped with an integrating sphere that allows measurements on solid samples. Chromatic parameters were registered with a Konica Minolta CR-410 colorimeter with a white calibration plate (Y = 94.27, x = -1.06, y = 3.45), measurements were done in triplicate and means reported. In the CIE $L^*a^*b^*$ uniform color space the color coordinates are: L^* (brightness), a^* (green-red) chromaticity, b^* (blue–yellow) chromaticity to describe the color of the matrices.[11]

Preparation

The two approaches, mentioned above, were used to include beet extract into the carriers. In the direct encapsulation procedure an aqueous mixture of 5 ml beet juice and 0.1 g β-CD is added, under constant stirring and room temperature, to 20 ml colloidal silica which was previously diluted with 12 ml water and brought to a pH of ~4 with an ascorbic acid solution of 15 %. Then the dye containing composition was introduced in a vacuum rotary evaporator and kept at 30 °C under vacuum until the liquid was evaporated and the precipitate was separated and crushed into powder. It was denoted silica-bet 1.

Two mesoporous supports were prepared for beet juice adsorption. One of them, silica 2, was obtained from colloidal silica and CTAB as template agent, the molar ratio SiO_2/CTAB being equal to $0.12/0.3\times10^{-3}$. The mixture was brought to an acid pH with an acetic acid solution 20 %, under stirring and kept for 5 days at room temperature. The other one, an aluminosilicate carrier (silicaAl 3) was obtained by a hydrothermal process (90 °C, 48 h) in a basic medium from colloidal silica and $Na_2O{\cdot}Al_2O_3$ using SDS as a structure directing surfactant. The molar ratios of the components were SiO_2/Al_2O_3 = 6, SiO_2 /Na_2O = 10/7, SiO_2/SDS = 10/1.4. The silica 2 and silicaAl 3 powders were separated by repeated centrifugation and washing with distilled water and then they were thermally treated at 600 °C, with 5 h plateau and a heating rate of 1 °C min^{-1}. 0.8 g of each host material was mixed with 1.2 ml beet juice, stirred for homogenization and followed by 5 h vacuum drying in dark conditions. A colored powder was obtained.

Equal quantities of the three dye loaded powders were spread on plates and were put in a PET container together with a Petri dish containing ammonium hydroxide solution 25 %. The container was sealed for about 15 min so that the powders should be in contact with the ammonium vapours developed into the headspace. The color changes were determined.

RESULTS AND DISCUSSION

Structural characterization of the unloaded matrices

X-Ray diffraction. The crystallographic structure of the as prepared samples was evaluated by XRD analysis. The diffraction patterns of the powders are presented in Fig. 1. As can be seen in Fig. 1a, the diffraction patterns indicate that the silica carrier is amorphous, marked by the existence of a broad peak at 2θ in

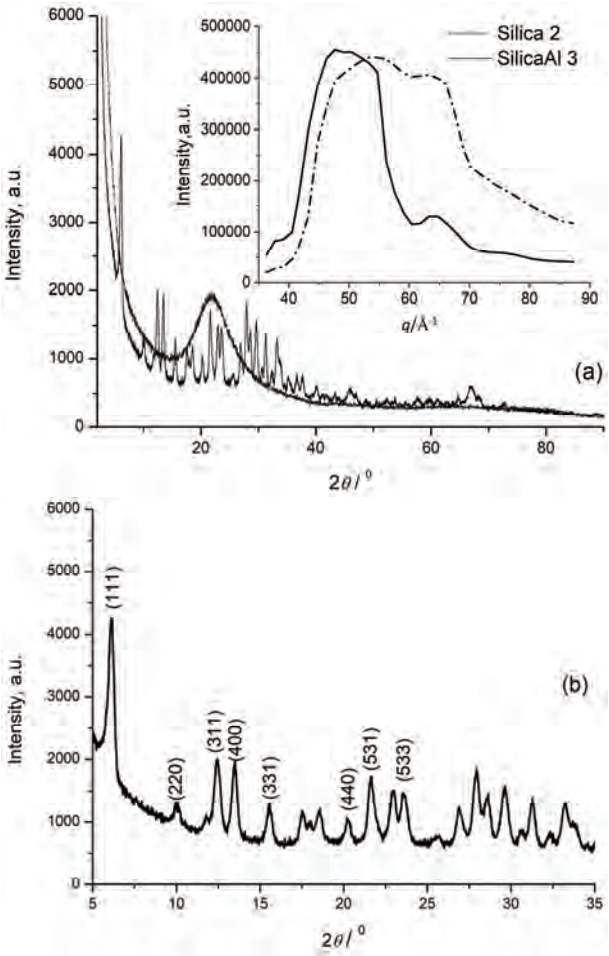

Fig. 1. XRD patterns of Silica 2 and silicaAl 3 (the inset shows SAXS diagram of the same unloaded carriers) (a) and details of crystal structure of silicaAl 3 (b).

the range 20–35° attributed to amorphous silica.[12] The pattern of the aluminosilicate sample in Fig. 1b shows the formation of a crystalline phase of the zeolite Y type (identification was performed using PDXL software from Rigaku connected to ICDD database).

The inset of Fig. 1a shows the SAXS diagram of the two as prepared powders. The variation of the scattering intensities with the scattering vector (q) is due to the electron density difference between the matrices and the empty pores.[13,14] The scattering curves of each of the two samples present a regular structure, confirming the long-range well-ordered mesostructured.[15,16]

N_2 physisorption. In Fig. 2 one can see that both samples show type IV isotherms according to IUPAC classification, typical for mesoporous materials.

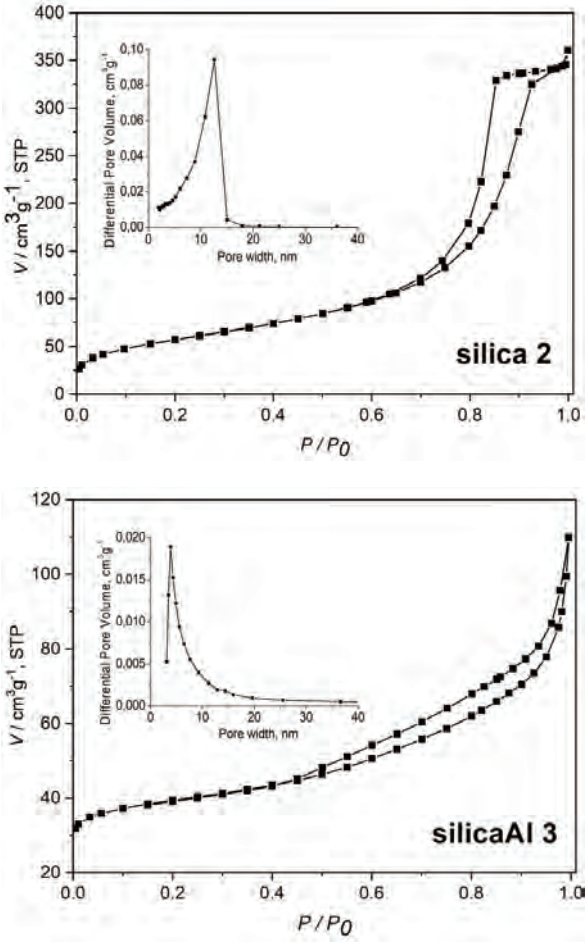

Fig. 2. N_2 adsorption–desorption isotherms and pore size distributions (inset of the figures) of silica 2 and silicaAl 3 supports.

Silica 2 support exhibits a H2 hysteresis loop that indicate the existence of a complex pore structure in which network effects are important. In the case of silicaAl 3 support, the hysteresis loop is of H3 type suggesting an assemblage of slit-shaped pores. The pore size distribution graphs show a unimodal distribution for both types of supports with peak maxima at 12.6 nm for silica and 3.8 nm for aluminosilicate. A *t*-plot analysis indicated the absence of microporosity in the silica support, whereas in aluminosilicate an important fraction of micropores was detected (~70 %). BET surface area, as well as total pore volume are higher for silica type carrier than for zeolite-Y type aluminosilicate (Table I).

TABLE I. Textural parameters of silica 2 and silicaAl 3 supports

Sample	S_{BET} / $m^2\ g^{-1}$	V_{total} / $cm^3\ g^{-1}$
Silica 2	205.3	0.557
silicaAl3	148.5	0.138

Porosity measurements as well as the X-ray analysis prove that the supports are highly ordered materials.

Infrared absorption spectra. Fig. 3 shows the FTIR spectra of the unloaded matrices. The strongest absorption bands of the two samples lie in the wavenumbers range 1200–950 cm^{-1} described as an asymmetric stretching mode O–(Si,Al)–O.[17] Silica 2 sample shows a peak at 1110 cm^{-1}, while silicaAl 3 at 986 cm^{-1}. The presence of Al atoms in the structure generates a shift to lower wavenumbers.[16]

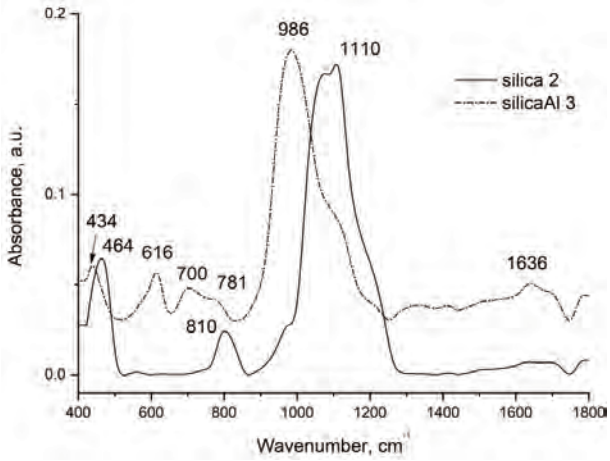

Fig 3. FTIR spectra of silica 2 and silicaAl 3 supports.

In the region 420–500 cm^{-1} the bands are assigned to O–(Si, Al)–O bending mode.[17] A strong sharp band can be seen in the spectrum of silica 2 matrix at 464 cm^{-1}. In the aluminum containing one it is shifted to 434 cm^{-1} and becomes

weaker. Bands corresponding to symmetric stretching modes appear in the range 650–820 cm^{-1}.[17] In the spectrum of the silica 2 sample a single band at 810 cm^{-1} can be attributed to Si–O–Si sym stretching,[18] while the presence of Al in the sample generates a widening and flattening of the bands (781 and 700 cm^{-1}).[18] The absorption bands at 1636 cm^{-1} show the presence of water in the matrices.[12]

FTIR spectra confirm the formation of an aluminosilicate type framework in accordance with XRD results and show that the structure directing agent was removed by thermal treatment.

Characterization of matrices loaded with beet juice pigment

UV–Vis spectroscopy of the dye-carrier formulation. There is an electron resonance system based on the two nitrogen atoms of the betalains molecules which is linked to the colour properties.[19] Bethaxanthins with a more simple structure around nitrogen atom have a typical UV–Vis absorption maximum in the 457–480 nm region and are yellow while the betacyanins with an extended resonance system generate wavelengths in the range 524–542 nm that makes them violet.[19–22]

Fig. 4 presents the UV–Vis spectra of the three prepared samples by inclusion and adsoption. All display the betanin absorption maximum (535–543 nm). Compared to silica-bet 1 spectrum, in which case the pigments can be stabilized by inclusion complex formation with β-CD,[5] the silica 2 and silicaAl 3 samples have different profiles. In case of silica 2, an overlapping of the bands is observed in the 472–535 nm range and silicaAl 3 spectrum shows shifts to lower (415 nm) and higher values (543 nm). Betalains are known as electron donating compounds,[21] and this fact can be due to interactions with the matrices which

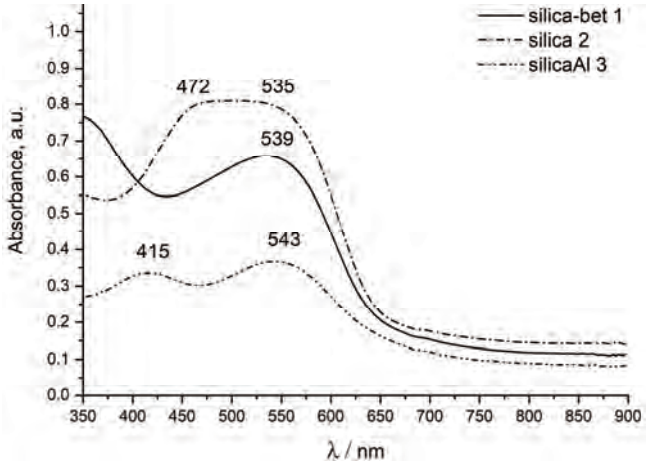

Fig. 4. UV–Vis spectra of the beetroot dye formulations based on silica and aluminosilicate.

become more significant for a high specific surface area and micro/mesoporosity.[23,24] Aluminium coordinative unsaturated sites in the network of silicaAl 3 enhances the interactions with adsorbed betalains.[8,24]

Effect of NH_3 vapors on dye-carrier formulations color change. Mean *L**, *a** and *b** values for the dye loaded powders before and after ammonium exposure are presented in Table II.

TABLE II. Color parameters for beet juice in different matrices before and after exposure to base atmosphere; data are presented as mean ± standard deviation of triplicate analyses

Sample	Color parameters before exposure			Color parameters in NH_3 atmosphere			ΔE
	*L**	*a**	*b**	*L**	*a**	*b**	
Silica 2	84.78±0.43	4.49±0.17	–1.16±0.033	83.13 ±0.29	3.60±0.14	0.70±0.089	1.87
SilicaAl 3	86.21±0.35	3.69±0.38	–1.78±0.014	86.34±0.11	1.99±0.05	0.25±0.080	2.65
Silica-bet1	80.02±0.21	7.68±0.12	–0.24±0.010	85.12±0.47	2.80±0.20	1.72±0.270	7.32

The other parameter in Table II, ΔE, is the color difference between before (L_0, a_0, b_0) and after exposure to NH_3 (L, a, B) and was determined using the following equation:[25]

$$\Delta E = [(L_0 - L^*)^2 + (a_0 - a^*)^2 + (b_0 - b^*)^2]^{1/2} \quad (1)$$

The values of the color parameters presented above, indicate that the as prepared matrices containing beet juice are different: silica-bet 1 and silica 2 are redder, while silicaAl 3 is lighter and yellower. Values ΔE between 1.5–3 (silica 2 and silicaAl 3 sample) indicate distinct and over 6 (silica-bet 1 sample) great differences between the initially prepared samples and the ones exposed to ammonia.[26]

CONCLUSION

Betalains pigments were included in silica and respectively aluminosilicate carriers to stabilize and improve their properties for practical applications. The direct encapsulation approach enabled the incorporation of other natural occurring compounds besides the dye, such as the complex forming β-CD and ascorbic acid, thus upgrading the prepared formulation regarding the color properties and the color variation with pH change. Structure directing agents generated mesoporous silica and zeolite *Y*-type supports with a complex, regular pore layout for the colorant adsorption. Betalains color properties depend on the variation in the physicochemical characteristics of the micro/mesoporous supports.

ИЗВОД

ИМОБИЛИЗАЦИЈА ПРИРОДНИХ БЕТАЛАИНСКИХ ПИГМЕНАТА У НЕОРГАНСКИМ МАТЕРИЈАЛИМА

LIGIA TODAN[1], DANIELA C CULITA[1], MIRABELA E. SOARE[1], RODICA M. ION[2], RADU C. FIERASCU[2] и MARIA MAGANU[3]

[1]Ilie Murgulescu Institute of Physical Chemistry, Romanian Academy, 202 Splaiul Independentei, 060021 Bucharest, Romania, [2]National Institute for Research & Development in Chemistry and Petrochemistry--ICECHIM, 202 Splaiul Independentei, 060021 Bucharest, Romania u [3]"Costin D. Nenitescu" Institute of Organic and Supramolecular Chemistry, Romanian Academy, 202 B Splaiul Independentei, 060023 Bucharest, Romania

У циљу испитивању нових pH осетљивих формулација хране, екстракт црвене цвекле богат бетацијанином, ради побољшања стабилности његове боје, је наношен на различите неорганске подлоге које садрже силицијум-диоксид и алуминосиликате. Директном методом инкапсулације пигмента на неорганску подлогу која садржи силицијум-диоксид и алуминосиликат додат је стабилизатор који представља инклузиони комплекс β-циклодекстрина и аскорбинске киселине. Систем накнадног пуњења укључује синтезу порозног силицијум-диоксид и алуминосиликатног праха и адсорпцију екстракта репе на овим подлогама. Пре наношења екстракта извршена је структурна карактеризација неорганске подлоге (дифракција рендгенских зрака, FTIR и N_2-физисорпција). Присуство бетанина (одобрен као црвена боја за храну) у испитиваним узорцима је одређено применом UV–Vis спектроскопије. Испитиване су промене боје, као и pH генерисане промене боје прахова изложених дејству амонијака при врху капсулираних посуда. Добијени резултати могу допринети већој примени екстракта репе, док предложене еколошке формулације могу бити од значаја код паковања хране.

(Примљено 28. октобра 2022, ревидирано 21. јануара, прихваћено 1. марта 2023)

REFERENCES

1. S. Chethana, C. A. Nayak, K. S. M. S. Raghavarao, *J. Food Eng.* **81** (2007) 679 (https://doi.org/10.1016/j.jfoodeng.2006.12.021)
2. S. Akan, Ö. Horzum, H. C. Akal, *LWT – Food Sci. Technol.* **155** (2022) 112877 (https://doi.org/10.1016/j.lwt.2021.112877)
3. P. S. Grewal, C. Modavi, Z. N. Russ, N. C. Harris, J. E. Dueber, *Metab. Eng.* **45** (2018) 180 (https://doi.org/10.1016/j.ymben.2017.12.008)
4. O. L. Torres Vargas, Y. V. Galeano Loaiza, M. L. González, *J. Mater. Res. Technol.* **13** (2021) 2239 (https://doi.org/10.1016/j.jmrt.2021.05.091)
5. M. I. Khan, *Food Chem.* **197** (2016) 1280 (https://doi.org/10.1016/j.foodchem.2015.11.043)
6. S. J. Calva-Estrada, M. Jiménez-Fernández, E. Lugo-Cervantes, *Food Chem.: Mol. Sci.* **4** (2022) 100089 (https://doi.org/10.1016/j.fochms.2022.100089)
7. S. Li, B. Mu, X. Wang, A. Wang, *Dyes Pigments* **190** (2021) 109322 (https://doi.org/10.1016/j.dyepig.2021.109322)
8. E. Pérez-Ramírez, E. Lima, A. Guzmán, *Dyes Pigments* **120** (2015) 161 (https://doi.org/10.1016/j.dyepig.2015.03.040)
9. E. S. Dolinina, E. Yu. Akimsheva, E. V. Parfenyuk, *J. Mol. Liq.* **287** (2019) 110938 (https://doi.org/10.1016/j.molliq.2019.110938)

10. E. Akbar Hussain, Z. Sadiq, M. Zia-Ul-Haq, *Betalains: Biomolecular Aspects*, Springer International Publishing, Cham, 2018, p. 125 (https://doi.org/10.1007/978-3-319-95624-4)
11. F. Billmeyer, M. Saltzman, *Principles of color technology*, John Wiley & Sons, New York, 2000, p. 1
12. W. Simanjuntak, S. Sembiring, P. Manurung, R. Situmeang, I. M. Low, *Ceram. Int.* **39** (2013) 9369 (https://doi.org/10.1016/j.ceramint.2013.04.112)
13. D. Paudel, R. Atta-Fynn, D. A. Drabold, S. R. Elliott, P. Biswas, *Phys. Rev., B* **97** (2018) 184202. (https://doi.org/10.1103/physrevb.97.184202)
14. D. Orthaber, A. Bergmann, O. Glatter, *J. Appl. Crystallogr.* **33** (2000) 218 (https://doi.org/10.1107/S0021889899015216)
15. C. Boissière, L. Nicole, C. Gervais, F. Babonneau, M. Antonietti, H. Amenitsch, C. Sanchez, D. Grosso, *Chem. Mater.* **18** (2006) 5238 (https://doi.org/10.1021/cm061489j)
16. M. Król, A. Koleżyński, W. Mozgawa, *Molecules* **26** (2021) 342 (https://doi.org/10.3390/molecules26020342)
17. *Molecular Sieve Zeolites-I*, E. M. Flanigen, L. B. Sand, Eds., American Chemical Society, Washington, D.C., 1974, p. 201 (https://doi/10.1021/ba-1971-0101.ch016)
18. J. Yang, Y.-X. Huang, Y. Pan, J.-X. Mi, *Micropor. Mesopor. Mater.* **303** (2020) 110247 (https://doi.org/10.1016/j.micromeso.2020.110247)
19. F. Gandía-Herrero, J. Escribano, F. García-Carmona, *Planta* **232** (2010) 449 (https://doi.org/10.1007/s00425-010-1191-0)
20. F. C. Stintzing, R. Carle, *Trends Food Sci. Technol.* **15** (2004) 19 (https://doi.org/10.1016/j.tifs.2003.07.004)
21. I. Belhadj Slimen, T. Najar, M. Abderrabba, *J. Agric. Food Chem.* **65** (2017) 675 (https://doi.org/10.1021/acs.jafc.6b04208)
22. I. Sadowska-Bartosz, G. Bartosz, *Molecules* **26** (2021) 2520 (https://doi.org/10.3390/molecules26092520)
23. C. Karavasili, E. Kontogiannidou, A.-T. Chatzitaki, P. Barmpalexis, D. G. Fatouros, *Micropor. Mesopor. Mater.* **305** (2020) 110343 (https://doi.org/10.1016/j.micromeso.2020.110343)
24. S. Nastase, L. Bajenaru, C. Matei, R. A. Mitran, D. Berger, *Micropor. Mesopor. Mater.* **182** (2013) 32 (https://doi.org/10.1016/j.micromeso.2013.08.018)
25. N. K. Kortei, G.T. Odamtten, M. Obodai, V. Appiah, P.T. Akonor, *Croat. J. Food Technol. Biotechnol. Nutr.* **10** (2015) 66 (https://hrcak.srce.hr/147825)
26. M. Cruz-Romero, A. L. Kelly, J. P. Kerry, *Innov. Food Sci. Emerg. Technol.* **8** (2007) 30 (https://doi.org/10.1016/j.ifset.2006.05.002).

Journal of the Serbian Chemical Society
JSCS-info@shd.org.rs • www.shd.org.rs/JSCS
J. Serb. Chem. Soc. *89* (1) 39–50 (2024)
JSCS–5704
Original scientific paper
Published 12 February 2024

Study of the metal ion adsorption capacity of palygorskite by computer simulation

CHUAN-WEN LIU[1]*, MIN-HSIEN LIU[2], TO-MAI WANG[3], CHENG-LUNG CHEN[4] and TZU-HAO TING[1]

[1]*Department of Chemistry, R.O.C Military Academy, Kaohsiung City, Taiwan, ROC,* [2]*Department of Chemical and Materials Engineering, Chung-Cheng Institute of Technology, National Defense University, Taoyuan 335, Taiwan, ROC,* [3]*Institute of Nuclear Energy Council, ROC and* [4]*Department of Chemistry, National Sun Yat-sen University, Kahsiung 804, Taiwan, ROC*

(Received 8 July, revised 4 September, accepted 24 October 2023)

Abstract: Palygorskite is a magnesium-rich aluminosilicate clay mineral with a unique chain-layered structure. This structure gives palygorskite a large specific surface area and interesting physical properties. Many researchers have investigated the applications of palygorskite in various fields, including heavy metal adsorption, petroleum and chemical industries, building materials, medicine and agriculture. In this study, molecular dynamics simulations were used to explore the heavy metal adsorption ability of palygorskite. The results showed that polyacrylic acid (PAA) had a heavy metal adsorption ability. In terms of the ability of the substrate to adsorb Pb^{2+}, Ni^{2+} and Cr^{3+}, palygorskite (attapulgite, ATP) was more effective than SiO_2 or clay. Based on this study, the same phenomenon reported in the literature was confirmed, and it was demonstrated that molecular dynamics could properly simulate the filtration of heavy metal ions in water using novel materials. Moreover, H^+ was found to play an essential role in assisting PAA/ATP in capturing heavy metal ions. Using this method, we were able to observe the details of heavy-ion adsorption.

Keywords: palygorskite; molecular dynamics; heavy metal adsorption; polyacrylic acid.

INTRODUCTION

Palygorskite or attapulgite (ATP) is a typical clay soil found throughout the world, with the chemical formula $(Mg,Al)_2Si_4O_{10}(OH)\cdot 4(H_2O)$. Scientists have noted its unique properties and particular chain-layer structure. Numerous res-

* Corresponding author. E-mail: cwl0308@gmail.com
• This work has been published on a prepress server: https://doi.org/10.21203/rs.3.rs-2137418/v1
https://doi.org/10.2298/JSC230708082L

earchers have used ATP in experiments or modified it to improve its properties to expand its application. For example, ATP can be used in heavy metal adsorption, the petroleum and chemical industries, building materials, medicine and agriculture. Rusmin *et al.* developed a simple method for the preparation of a magnetic chitosan-palygorskite nanocomposite that showed excellent effects in terms of removing Pb^{2+} from water; after four adsorption–desorption cycles, it still had an 82% capability.[1] Eleni *et al.* presented a method to remove Ca^{2+} from water using sodium-treated ATP and proposed a kinetic model to explain their experimental results.[2] Wei *et al.* synthesized attapulgite-maintained nanoscale zero-valent iron. Their experimental results confirmed that introducing ATP increased the Cr(VI) removal efficiency.[3] In another study, Ma *et al.* presented a novel method for synthesizing a new material, a polydopamine-modified attapulgite-supported nanosized zero-valent iron composite. The new material reduced the toxicity of Cr (VI) in the solution, and the results showed that ATP played a significant role in this process.[4] Using hydrothermal ATP, Zhang *et al.* demonstrated that benzene, naphthalene and phenanthrene could all be effectively removed after special treatment.[5] Câmara presented the application of ATP in adsorptive desulfurization in petroleum refining, which produced excellent results regarding the adsorption of sulfur compounds in actual diesel fuel.[6] Zhai *et al.* reported that methylene blue-adsorbed palygorskite could effectively degrade bisphenol A over a wide pH range from 3 to 9 through carbonization. Additionally, it can eliminate organic pollutants.[7] Mavrikos *et al.* prepared a novel material with natural ATP and TiO_2, Zn and Cu and demonstrated excellent results for the adsorption of air pollution.[8] Using ATP and wood fiber, Zhou *et al.* prepared an aerogel material with excellent mechanical properties and the ability to self-adjust to humidity.[9] By combining nano clay minerals (ATP) and rigid polyurethane foams, Wang *et al.* created a novel material that enhanced the thermal insulation performance of building materials.[10] Chalvatzi *et al.* found that ATP dietary supplementation could render cecal microbial profiles more homogeneous at the start of lactation and enable more efficient butyrate production.[11] Wang *et al.* presented an embodiment of palygorskite as a medicine carrier and showed that its plasticity and liquidity limits were promising.[12] Yong *et al.* used ATP's ion adsorption properties to capture Cr in alkaline soil with cadmium pollution.[13] Shao *et al.* prepared a new nanoparticle composite in which Pd/Fe was supported on organic ATP to address soil pollution. This composite removed 4,4'-dibrominated diphenyl ether effectively.[14] Zhou *et al.* prepared composite polyacrylic acid (PAA) and ATP (PAA/ATP) to adsorb Pb^{2+}, Ni^{2+} and Cr^{3+} .[15] All these studies showed a different adsorption ability of ATP and its composites. In an earlier simulation in our laboratory, a technical method was used for the liquid chromatographic separation of explosive molecules, and it was a success in that simulation.[16] Prior to this research, we hypothesized that PAA/ATP would adsorb heavy metal ions

but did not know whether PAA or ATP adsorbed more strongly. This was the aim of our study, which we addressed via successful simulation. This study simulated PAA composites of SiO_2 (PAA/Si) and clay (PAA/clay). The adsorption abilities of these composites were compared with those of PAA/ATP described in Zhou's report. Our goal was to demonstrate that simulation, at least qualitatively, predicts complicated composites' adsorption abilities.

THEORY AND METHODS

The Material Studio 6.0 package was used to model these systems in this simulation. In addition, the molecular dynamics (MD) simulation Forcite-calculation module was used to investigate the adsorption of ions by the composites. The adsorption of Pb^{2+}, Ni^{2+} and Cr^{3+} by PAA/ATP was experimentally simulated.[15] A similar simulation method was also used to investigate PAA/SiO_2 and PAA/clay systems.

In this study, molecular dynamics (MD) simulation with the Universal Force Field[17] (UFF) was adopted to carry out the computations.

In UFF, the interaction energy is:

$$E = E_{\mathrm{R}} + E_{\theta} + E_{\varphi} + E_{\mathrm{w}} + E_{\mathrm{vdw}} + E_{\mathrm{el}} \tag{1}$$

where E is the potential energy, E_{R} is the bond stretching energy, E_{θ} and E_{φ} are the angular distortions, E_{w} is the inversion term, E_{vdw} is the nonbonded interaction energy and E_{el} is the electrostatic term. The interaction force and acceleration of each atom are:

$$\vec{F}_i = m_i \vec{a}_i \tag{2}$$

$$\vec{a}_i = -\nabla_i E \tag{3}$$

The atomic position and velocity were obtained by numerically solving the Newtonian equation by the Verlet method:

$$\vec{v}\left(t + \frac{1}{2}\delta t\right) = \vec{v}\left(t - \frac{1}{2}\delta t\right) + \vec{a}(t)\delta t \tag{4}$$

$$\vec{r}_i(t + \delta t) = \vec{r}_i(t) + \vec{v}\left(t + \frac{1}{2}\delta t\right)\delta t \tag{5}$$

In our simulation, the conventional MD method was adopted, and the system was simulated to reach thermal equilibrium:

$$K.E \sim \frac{3}{2} NkT \tag{6}$$

After the system was well equilibrated, further simulations were carried out to collect trajectories for subsequent analysis.

Different radial distribution functions (RDFs) can be calculated using Eq. (7) to analyze the simulation results:

$$g(r) = \frac{\mathrm{d}n_r}{\rho 4\pi r^2 \mathrm{d}r} \tag{7}$$

where $\mathrm{d}n_r$ is the number of atoms distributed in $r \rightarrow r + dr$, and ρ is the bulk density. RDF, $g(r)$, is the probability of an atom being at a distance r from another tagged atom. It shows a

significant probability of probable distance ranges. RDF analyzes atom distributions in the solid, liquid and gas phases.

This research examined four different systems: PAA/ATPno, with the ATP surface treated with the PAA functional group in a neutral solution; PAA/ATPH, with the ATP surface treated with the PAA functional group in an acidic solution; PAA/Sino, with the SiO_2 surface treated with the PAA functional group in neutral solution; and PAA/Clayno, with the clay surface treated with the PAA functional group in neutral solution. All four systems contained the same ratios of heavy metal ions Pb^{2+}, Ni^{2+} and Cr^{3+}. Table I displays the components for each of the four systems.

TABLE I. Composition of modeled systems

Property	PAA/ATPno	PAA/ATPH	PAA/Sino	PAA/Clayno
Pb^{2+}	30	50	30	30
Ni^{2+}	30	50	30	30
Cr^{3+}	30	50	30	30
Cl^-	90	150	90	90
NO_3^-	120	200	120	120
H_2O	3300	3300	3300	3300
H^+	–	300	–	–
Substrate	ATP (palygorskite, attapulgite)		SiO_2 (quartz)	Clay (kaolinite)
Density of solution, g/cm^3	1.0	1.0	1.0	1.0
Box size, Å^3	52×51×90	52×51×100	50×51×87	51×45×90

In this simulation, SiO_2 and clay were also selected as substrates through the same Si atom in their structures. The three-dimensional structure of ATP was adopted from the Inorganic Crystal Structure Database (ICSD) No. 185485[18] and the literature.[19] The 3D structures of SiO_2 and clay were also obtained from the ICSD. The structures are shown in Fig. 1 (a, b and c).

The surfaces of the substrates were covered with polyacrylic acid ($(C_3H_4O_2)_n$, $n = 5$). In this simulation, PAA was synthesized from polyacrylic acid and modified ATP. In the first step, modified ATP was formed by putting ATP into 3-mercapto-1-propane sulfonic acid sodium ($C_3H_7O_3S_2Na$, MPS). In the second step, polyacrylic acid was added to the modified ATP, and the polymerization process was conducted. PAA was therefore obtained via two steps in this experiment; the final 3D structure of PAA is shown in Fig. 1d.[15]

To build the PAA/ATP, PAA/SiO_2, and PAA/Clay systems, 10 PAA molecules were evenly distributed on the surface of the clay, ATP and SiO_2. Solutions of PAA/ATPno, PAA/ATPH, PAA/SiO_2 and PAA/clay were mixed in the amorphous cell module at a density of 0.3 g/cm^3. Next, the systems were simulated to their thermal equilibrium states, after which they were compressed slightly (3 %), and an MD simulation was carried out until a new thermal equilibrium was reached. The above steps were repeated until the system density was 1.0 g/cm^3. After this stage, an MD simulation of 10,000 fs was performed to ensure that the solutions were well mixed. Then, these solutions were placed on top of the substrates, and an MD simulation of 1,000,000 fs in each system was performed to stabilize the systems. Snapshots of the system are shown in Fig. 2.

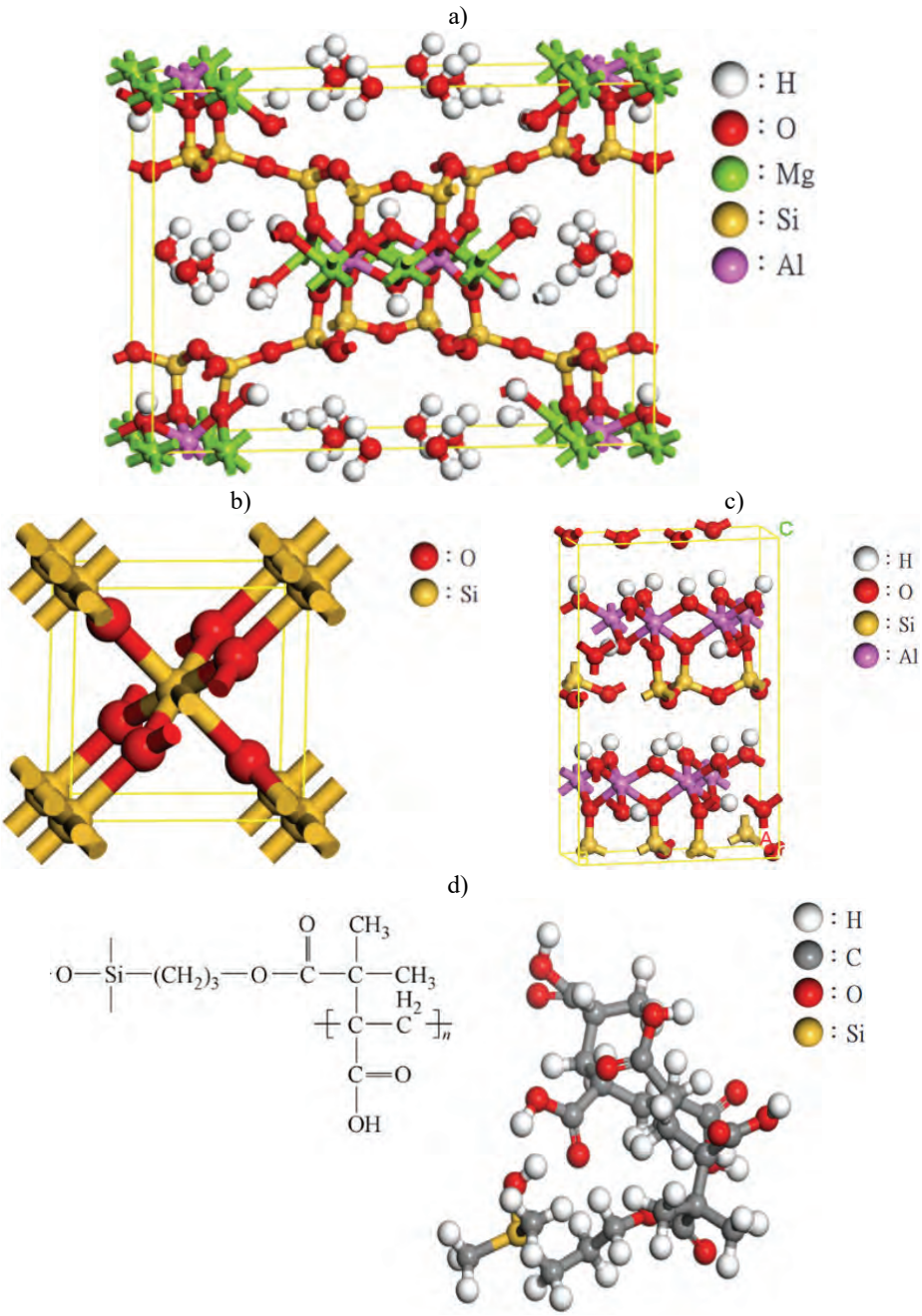

Fig. 1. 3D structure of: a) ATP, b) SiO_2, c) clay and d) PAA.

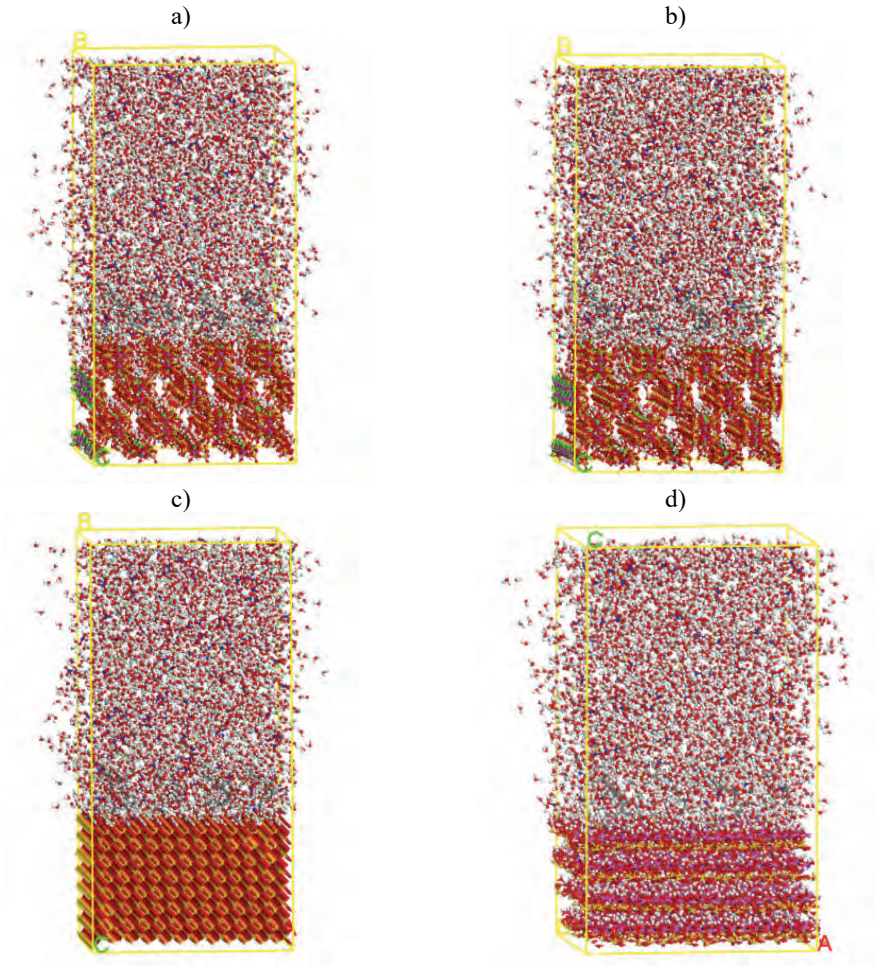

Fig. 2. Simulation model of the: a) PAA/ATPno, b) PAA/ATPH, c) PAA/Sino and d) PAA/Clayno systems.

RESULTS AND DISCUSSION

The results from the literature showed the adsorption ability of the PAA/ /ATP substrate in an acidic solution to be Pb^{2+} (35 mg g^{-1}) > Cr^{3+} (16 mg g^{-1}) > Ni^{2+} (2 mg g^{-1}).[15] Fig. 3 shows the calculated RDFs of O in the PAA molecule to ions in the PAA/ATPH system. Fig. 3 shows that the corresponding peak intensities were 7.2 for Pb^{2+} at 2.7 Å, 5.8 for Cr^{3+} at 2.3 Å and 4.4 for Ni^{2+} at 2.3 Å. These peaks indicate that the simulated amounts of adsorption ions were in the same order as reported in the literature. Therefore, the correct results obtained using our simulation showed that the modeling method is appropriate for these composite systems.

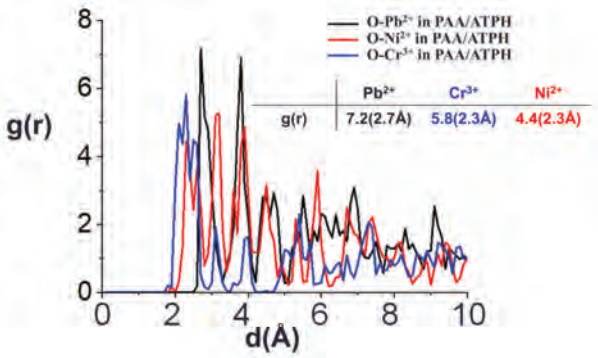

Fig. 3. RDF of O(PAA)–M^+ in the PAA/ATPH system.

Similar analyses were carried out for the other composite systems. The simulated RDFs are shown in Table II. The adsorption abilities were Ni^{2+} (10.1) > Pb^{2+} (6.2) > Cr^{3+} (4.6) for the PAA/ATPno system, Cr^{3+} (15.3) > Pb^{2+} (11.9) > Ni^{2+} (2.5) for the PAA/Sino system, and Cr^{3+} (52.3) > Pb^{2+} (5.5) > Ni^{2+} (5.1) for the PAA/Clayno system. In the PAA/Sino system, the adsorption capacities for Cr^{3+} (15.3) and Pb^{2+} (11.9) were more significant than those for Ni^{2+} (2.5). In the PAA/Clayno system, the adsorption capacity for Cr^{3+} (52.5) was more significant than that for Pb^{2+} (5.1) and Ni^{2+} (5.5).

TABLE II. RDF analyses of O (PAA) to M^+ and O (water) to M^+ in the four systems

System	O(PAA)···M^+			O(water)···M^+		
	Pb^{2+}	Cr^{3+}	Ni^{2+}	Pb^{2+}	Cr^{3+}	Ni^{2+}
PAA/ATPH	7.2 (2.7Å)	5.8 (2.3Å)	4.4 (2.2Å)	1.8 (3.0Å)	2.9 (2.2Å)	2.4 (1.9Å)
PAA/ATPno	6.2 (2.7Å)	4.6 (2.0Å)	10.1 (2.0Å)	2.3 (2.9Å)	4.7 (2.0Å)	2.3 (2.9Å)
PAA/Sino	11.9 (2.9Å)	15.3 (1.8Å)	2.5 (1.8Å)	1.9 (3.0Å)	4.0 (2.0Å)	3.1 (2.0Å)
PAA/Clayno	5.1 (2.7Å)	52.3 (1.8Å)	5.5 (2.0Å)	2.1 (3.1Å)	3.1 (2.2Å)	4.6 (2.0Å)

As presented in Table II, the RDF of the M^+ to O (water) in the liquid system shows that the order of adsorption capacity was the same for all four systems: Cr^{3+} > Ni^{2+} > Pb^{2+}. As Cr^{3+} is the most significant positively charged ion, it attracts more O (water) than the other two ions. According to the literature, the hydrated radius of Ni^{2+} is 0.69 Å[20] and that of Pb^{2+} is 1.19 Å.[21] Therefore, O (water) is closer to Ni^{2+} than Pb^{2+}, and the number of neighboring water molecules around Ni^{2+} was more significant than that around Pb^{2+}.

In Table II, the RDF of O(PAA)–M^+ in the PAA/ATPno, PAA/ATPH, PAA/Sino and PAA/Clayno systems showed that the adsorption capacity for the Pb^{2+} by the PAA polymer was of the order: PAA/Sino > PAA/ATPH > PAA/ATPno > PAA/Clayno. The order for Ni^{2+} was: PAA/ATPno > PAA/Clayno > PAA/ATPH > PAA/Sino. The order for Cr^{3+} was: PAA/Clayno > PAA/Sino > PAA/

/ATPH > PAA/ATPno. These results showed that the most significant adsorption number of O(PAA)–Pb^{2+} was observed in the PAA/Sino system, the most significant adsorption number of O(PAA)–Ni^{2+} was in PAA/ATPno, and the most significant adsorption number of O(PAA)–Cr^{3+} was in PAA/Clayno.

Fig. 4 shows the RDF of O (PAA) in the four systems. In the dynamic snapshot, the peak at 0.61–0.69 Å represented =O and –O in the COOH functional group. It has been shown that the distance between the O atoms in the –COOH group decreased in the PAA/ATPH, PAA/Sino and PAA/Clayno systems. It was also observed that M^+ had a greater possibility of moving close to the –COOH group, causing the phenomenon that =O and –O became closer to each other in the RDF analysis. In addition, the M^+ in the PAA/ATP system did not show this phenomenon. The peak at 2.27–2.29 Å was the normal RDF of O atoms in the –COOH functional group in the four systems. However, the PAA/ATPH system had two peaks of low intensity of 2.81 and 4.65 Å, which showed that the PAA molecules in the PAA/ATPH system had the possibility of getting closer to each other. This phenomenon was most evident in the PAA/ATPH system of the four systems.

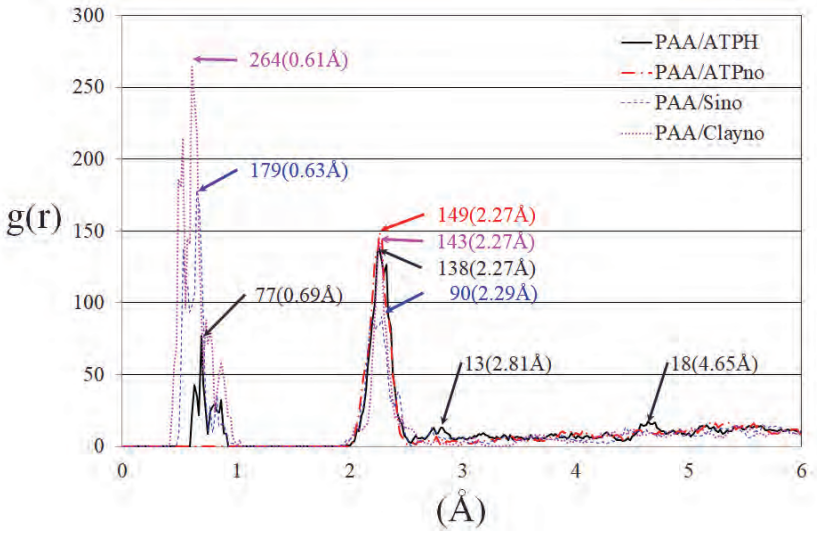

Fig. 4. RDF analysis of O (PAA) in the four systems.

The above analysis showed the adsorption of metal ions by PAA. In addition, we were also interested in the adsorption site of the polymer. By analyzing 101 frames of trajectories in 10 ps, Pb^{2+}, Ni^{2+} and Cr^{3+} near the surface of the substrates within 10 Å were counted, as shown in Fig. 5. This shows the number of heavy metal ions trapped by PAA/substrate. The count of heavy metal ions

inside the PAA molecule differed from the results of the RDF analysis of heavy metal ions and the O atom of the PAA molecule.

On the other hand, the PAA/ATPH system had the most of Pb^{2+} inside the PAA molecule. The PAA/ATPno system was the best for Cr^{3+}, and the PAA/ /ATPH system still proved the most effective in terms of capturing Ni^{2+} in comparison with the other systems. The PAA/Clayno system could have shown better results regarding the numbers inside the PAA molecule for heavy metal ions. However, the RDF results showed that the PAA/Clayno system had excellent adsorption of Cr^{3+}. One possible reason for this result was that the heavy metal ions were adsorbed by the –COOH group on the PAA molecule, showing that this –COOH group played an essential role in the adsorption of heavy metal ions. The clay substrate had little effect on the adsorption of heavy metal ions.

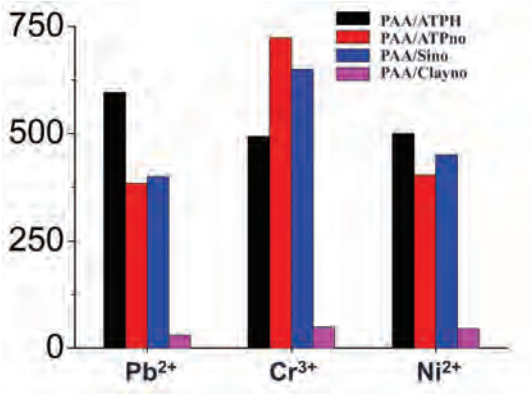

Fig. 5. Analysis of ions inside the PAA molecular chain in the PAA/ATPH, PAA/ATPno, PAA/Sino and PAA/ /Clayno systems.

According to the PAA/Clayno system data in Fig. 5, the trajectory of the Cr^{3+} near the clay was analyzed, as shown in Fig. 6. The resulting analysis showed that the PAA/Clayno dynamic simulation trajectory in 5 ps included 5000 steps and 51 frames. In the Cr^{3+} trajectory, it was almost wandering in a cube with a side length of 0.6 Å. Therefore, Fig. 6 might provide strong evidence to support the conclusion, shown in Fig. 5, that Cr^{3+} near the surface of the clay substrate within 10 Å were almost captured by the –COOH group and occupied the site of the –COOH group's activity. As a result, the low number of ions present in the PAA molecular chain of the PAA/Clayno system, depicted in Fig. 5, caused a significant difference in the RDF of O (PAA)–Cr^{3+}, as shown in Table II. This may be a type of fouling of the PAA molecules in the PAA/Clayno system.

CONCLUSION

ATP is a clay mineral with expanding applications owing to the development of technology. In this research, a 3D model of ATP was built to simulate its beh-

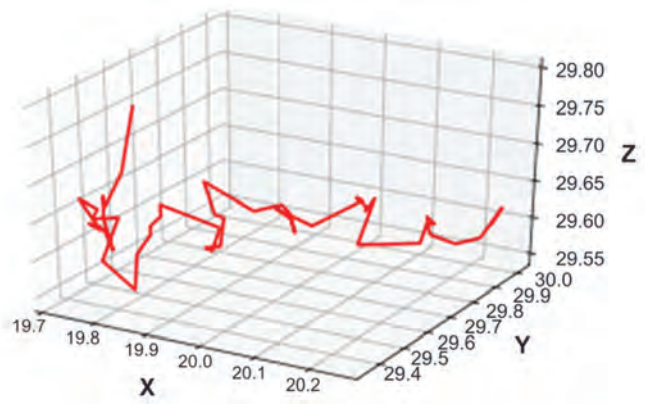

Fig. 6. Trajectory of Cr^{3+} near the surface of the clay substrate within 10 Å.

avior. Modeling research would assist in follow-up ATP research. According to the results, PAA molecules have excellent adsorption ability. The ability of the systems with PAA added to the substrate to adsorb Pb^{2+}, Ni^{2+} and Cr^{3+} was in the order ATP > SiO_2 > clay. In comparing the four systems, PAA/ATPno proved the most effective in adsorbing the Ni^{2+}, while for adsorbing Pb^{2+}, PAA/Sino was the best among the four systems. On the other hand, PAA/Clayno was the most effective at adsorbing the Cr^{3+}. For both Pb^{2+} and Cr^{3+}, the PAA/Sino system is the most efficient of the four systems. Furthermore, the H^+ evenly disperses the PAA molecules to improve the ability of the PAA/ATP system to adsorb heavy metal ions such as Pb^{2+}, Ni^{2+} and Cr^{3+}. According to the results of this simulation, the PAA/ATPH system has an excellent ability to adsorb heavy metal ions. This simulation could help advance research in nanotechnology and its application in ATP.

Acknowledgment. Ministry of Science and Technology Projects (number: MOST 1110036232).

ИЗВОД

ПРОУЧАВАЊЕ АДСОРПЦИОНОГ КАПАЦИТЕТА ПАЛИГОРСКИТА ПРЕМА МЕТАЛНИМ ЈОНИМА РАЧУНАРСКОМ СИМУЛАЦИЈОМ

CHUAN-WEN LIU[1], MIN-HSIEN LIU[2], TO-MAI WANG[3], CHENG-LUNG CHEN[4] и TZU-HAO TING[1]

[1]Department of Chemistry, R.O.C Military Academy, Kaohsiung City, Taiwan, ROC, [2]Department of Chemical and Materials Engineering, Chung-Cheng Institute of Technology, National Defense University, Taoyuan 335, Taiwan, ROC, [3]Institute of Nuclear Energy Council, ROC и [4]Department of Chemistry, National Sun Yat-sen University, Kahsiung 804, Taiwan, ROC

Палигорскит је минерал алуминосиликатне глине богат магнезијумом са јединственом ланчаном слојевитом структуром. Ова структура даје палигорскиту велику специфичну површину и занимљива физичка својства. Многи истраживачи су истраживали примену палигорскита у различитим областима, укључујући адсорпцију тешких метала, индустрију нафте, хемијску индустрију, грађевинске материјале, медицину и пољоприв-

реду. У овој студији, коришћене су симулације молекулске динамике за истраживање способности палигорскита за адсорпцију тешких метала. Резултати су показали да полиакрилна киселина (PAA) има способност адсорпције тешких метала. Као супстрат за адсорбовање Pb^{2+}, Ni^{2+} и Cr^{3+}, палигорскит (атапулгит, ATP) је био ефикаснији од SiO_2 или глине. На основу ове студије потврђен је исти феномен описан у литератури и показано је да молекулска динамика може правилно симулирати филтрацију јона тешких метала у води користећи нове материјале. Штавише, откривено је да H^+ игра кључну улогу у помагању PAA/ATP у хватању јона тешких метала. Користећи ову методу, могли смо да посматрамо детаље адсорпције тешких јона.

(Примљено 8. јула, ревидирано 4. септембра, прихваћено 24. октобра 2023)

REFERENCES

1. R. Rusmin, B. Sarkar, R. Mukhopadhyay, T. Tsuzuki, Y. Liu, R. Naidu, *J. Colloid Interface Sci.* **608** (2022) 575 (https://doi.org/10.1016/j.jcis.2021.09.109)
2. G. Eleni, P. Georgios, K. Konstantina, B. Alexandros, *Water Supply* **22** (2022) 156 (https://doi.org/10.2166/ws.2021.283)
3. Y. Wei, M. Usman, M. Faroop, M. Adeel, F. U. Haider, Z. Pan, W. Chen, H. Liu, L. Cai, *Water, Air, Soil Poll.* 233 (2022) 48 (https://doi.org/10.1007/s11270-022-05513-z)
4. B. Ma, J. Yao, Z. Chen, B. Liu, J. Kim, C. Zhao, X. Zhu, V. G. Mihucz, T. Minkina, T. S. Knudsen, *Chemosphere* **287** (2022) 131970 (https://doi.org/10.1016/j.chemosphere.2021.131970)
5. S. Y. Zhang, Y. L. Zhang, X. S. Su, Y. Zhang, *Chem. Res. Chin. Univ.* **29** (2013) 37 (https://doi.org/10.1007/s40242-013- 2303-8)
6. A. B. F. Câmara, R. V. Sales, L. C. Bertolino, R. P. P. Furlanetto, E. Rodriguez-Castellón, L. S. de Carvalho, *Adsorption* **26** (2020) 267 (https://doi.org/10.1007/s10450-019-00144-z)
7. P. Zhai, H. Liu, F. Sun, T. Chen, X. Zou, H. Wang, Z. Chu, C. Wang, M. Liu, D. Chen, *Appl. Clay Sci.* **216** (2022) 106327 (https://doi.org/10.1016/j.clay.2021.106327)
8. A. Mavrikos, D. Papoulis, N. Todorova, I. Papailias, C. Trapalis, D. Panagiotaras, D. A. Chalkias, E. Stathatos, E. Gianni, K. Somalakidi, D. Sygkridou, S. Komarneni, *J. Photochem. Photobiol., A* **423** (2022) 113568 (https://doi.org/10.1016/j.jphotochem.2021.113568)
9. X. Zhou, H. Jin, A. Gu, X. Li, L. Sun, P. Mao, Y. Yang, S. Ding, J. Chen, S. Yun, *J. Clean. Prod.* **335** (2022) 130367 (https://doi.org/10.1016/j.jclepro.2022.130367)
10. Y. Wang, K. Cui, B. Fang, F. Wang, *Nanomaterials* **12** (2022) 609 (https://doi.org/10.3390/nano12040609)
11. S. Chalvatzi, M. S. Kalamaki, K. Arsenos, P. Fortomaris, *J. Appl. Microbiol.* **120** (2022) 1033 (https://doi.org/10.1111/jam.13041)
12. J. Wu, S. Ding, J. Chen, S. Zhou, H. Ding, *Int. J. Biol. Macromol.* **68** (2014) 107 (https://doi.org/10.1016/j.ijbiomac.2014.04.030)
13. Y. Yong, Y. Xu, Q. Huang, Y. Sun, L. Wang, X. Liang, X. Qin, L. Zhao, *Sci. Total Environ.* **813** (2022) 152636 (https://doi.org/10.1016/j.scitotenv.2021.152636)
14. J. Shao, Y. Zhang, Z. Liu, Z. Fei, Y. Sun, Z. Chen, X. Wen, W. Shi, D. Wang, C. Gu, *Environ. Sci. Pollut. Res.* **29** (2 022) 4461 (https://doi.org/10.1007/s11356-021-15997-7)
15. S. Zhou, A. Xue, Y. Zhang, Q. Wang, M. Li, X. Chu, Y. Zhao, W. Xing, *J. Ind. Eng. Chem. (China)* **66** (2015) 618 (https://doi.org/10.11949/j.issn.0438-1157.20141244)

16. C. W. Liu, B. C. Kuo, M. H. Liu,Y. R. Huang, C. C. Chen, *J. Mol. Graph. Model.* **85** (2018) 331 (https://doi.org/10.1016/j.jmgm.2018.09.009)
17. A. K. Rappe, C. J. Casewit, K. S. Colwell, W. A. Goddard III, W. M. Skiff., *J. Am. Chem. Soc.* **114** (1992) 10024 (https://doi.org/10.1021/ja00051a040)
18. R. Giustetto, R. Compagnoni, *Clay Miner.* **46** (2011) 371 (https://doi.org/10.1180/claymin.2011.046.3.371)
19. L. Boudriche, R. Calvet, B. Hamdi, H. Balard, *Colloids Surfaces, A* **392** (2011) 45 (https://doi.org/10.1016/j.colsurfa.2011. 09.031)
20. I. Mobasherpour, E. Salahi, M. Pazouki, *Arabian J. Chem.* **5** (2012) 439 (https://doi.org/10.1016/j.arabjc.2010.12.022)
21. I. Persson, *Pure Appl. Chem.* **82** (2010) 901 (https://doi.org/10.1351/PAC-CON- 09-10-22).

Journal of the Serbian Chemical Society
JSCS-info@shd.org.rs • www.shd.org.rs/JSCS
J. Serb. Chem. Soc. *89* (1) 51–61 (2024)
JSCS–5705
Original scientific paper
Published 12 February 2024

Synthesis, characterization, and catalytic properties of $GdCoO_3$ for dry reforming of methane

REGINA K. ALLABERGENOVA[1]*, DARIA A. BOBKOVA[1], ELIZAVETA M. BORODINA[1], TATIANA A. KRYUCHKOVA[1,2]*, EKATERINA B. MARKOVA[1], TATIANA F. SHESHKO[1], NIKOLAI N. LOBANOV[3] and ALEXANDER G. CHEREDNICHENKO[1]

[1]*Physical and Colloidal Chemistry Department, Faculty of Science, RUDN University, 6 Miklukho-Maklaya St, Moscow, 117198, Russian Federation,* [2]*Moscow Pedagogical State University, MPGU, 1/1 Malaya Pirogovskaya Str., Moscow, 119991, Russian Federation and* [3]*Inorganic Chemistry Department, Faculty of Science, RUDN University, 6 Miklukho-Maklaya St, Moscow, 117198, Russian Federation*

(Received 17 May, revised 8 August, accepted 12 December 2023)

Abstract: Perovskite oxides (ABO_3) due to their high thermal stability and the ability to control the physico-chemical properties are considered as an alternative to traditional catalysts containing noble and transition metals. Herein, the recent research breakthroughs of $GdCoO_3$ catalysts in experimental studies are summarized in detail. First, the perovskite-type $GdCoO_3$ complex oxides were obtained by co-precipitation method with the various precipitators and were characterized by X-ray diffraction (XRD), low temperature nitrogen adsorption and IR spectroscopy. Physical and chemical analysis showed that the choice of precipitant doesn't significantly affect the phase composition of the perovskites. The catalytic performance of gadolinium cobaltites was discussed. It was found that the use of cobaltites obtained by co-precipitation leads to the inhibition of the side reaction of the reverse steam reforming of carbon monoxide. Finally, the investigation of the used catalysts demonstrated the formation of $Gd_2O_2CO_3$ and metallic cobalt, which indicates the nature of active centres: gadolinium is the centre of CO adsorption, while hydrogen chemisorption occurs on cobalt-sites.

Keywords: synthesis gas; catalysis; perovskites; cobalt; conversion.

INTRODUCTION

As of this date, oil remains the main source of raw materials to produce motor fuel and products of the main organic synthesis. Demand for oil largely depends on the current economic situation and prices for oil products. However,

* Corresponding author. E-mail: r.allabergenova.25@gmail.com, kryuchkova-ta@rudn.ru
https://doi.org/10.2298/JSC230517096A

the volume of natural oil production is growing every year, and these volumes barely have time to cover the existing needs. According to the forecasts of the International Energy Agency, the onset of "peak oil" (maximum world oil production) should be expected in 2030, after which there will be a decline in production volumes around the world. For this reason, today much attention is paid to the development of GTL (gas-to-liquids) technology. GTL is the production of petroleum products from natural gas or associated petroleum gas, about 30 % of which in Russia is simply burned by flares after production. At the same time, efforts worldwide to reduce CO_2 emissions are driving growing research interest in finding effective ways to chemically activate this inert molecule. Catalytic processes are of utmost importance in this area, while renewable energy sources are the most suitable to provide these high-energy transformations.[1]

In this context, carbon dioxide conversion of methane (dry reforming of methane, DRM), as the first stage of GTL technology, is an attractive way for the transition from the use of fossil resources to the effective conversion of CO_2 and CH_4 into synthetic fuel, because the resulting synthesis gas can subsequently be converted by the Fischer-Tropsch synthesis into various hydrocarbon fractions.[1]

Moreover, the reaction is environmentally beneficial, because two greenhouse gases are used in it:[2]

$$CH_4 + CO_2 \rightarrow 2CO + 2H_2, \quad \Delta H = 247 \text{ kJ/mol} \tag{1}$$

DRM is an endothermic process, and it is carried out at operating temperatures above 1000 K, and this requires heat-resistant catalysts with high productivity. Most often, supported catalysts based on noble metals such as Rh, Ru or Ir are used for this process.[3] Transition metals such as Ni, Co, Fe can also be effectively used as an alternative and cost-effective active phase.[3]

In most cases, the most common metallic, bimetallic and oxide catalysts have low selectivity and are rapidly deactivated by sintering and carburizing the surface, which reduces their efficiency in the DRM. Therefore, the search for the most suitable catalyst for this process is an urgent task for many scientists. In this regard, the properties of complex oxides with the structure of perovskite are being studied. These compounds are stable at high temperatures, easy to prepare and have a lower cost than noble metal catalysts. Another interesting feature of perovskites is the ability to regulate catalytic characteristics by varying their chemical composition at the A- and B-positions.[4–8] For example, in previous work[9] on the study of $LnFeO_3$ under DRM conditions, it was shown that the maximum catalytic activity was observed on samples containing gadolinium in the A-position, which contributed to the further study of gadolinium-containing complex oxides. And the study of $GdMeO_3$ (Me = Fe, Co, Mn) obtained by solid phase[10] synthesis revealed the influence of the nature of the B-element on the efficiency of the catalyst. Moreover, in addition to varying the chemical compo-

sition, the characteristics of active centres of systems can be influenced by the synthesis method,[11] which leads to a change in its catalytic properties, and this has also been confirmed in our previous works.[9,10]

The purpose of this work was to study the catalytic properties of complex oxides with the perovskite structure of the $GdCoO_3$ composition under conditions of carbon dioxide conversion of methane, as well as to identify the correlation "synthesis conditions – physicochemical properties – catalytic characteristics".

EXPERIMENTAL

The synthesis of complex oxides $GdCoO_3$ was carried out by the co-precipitation method using solutions of sodium hydroxide and ammonium carbonate as precipitators.[12,13] The synthesized $GdCoO_3$ oxides are respectively named as $GCO_{precipitator}$.

GCO_{NaOH}. For the synthesis of GCO_{NaOH} 3 mol $Gd(NO_3)_3 \cdot 6H_2O$ and 4 mol $Co(NO_3)_2 \cdot 6H_2O$ were dissolved in 40 mL of water. 0.027 mol of anhydrous glucose, 0.08 mol ethylene glycol and 60 mL of 4M NaOH solution was added to the resulting solution. The pH of the solution was adjusted to 10 by dropwise addition of 15 mL of 5.4 M HNO_3. A suspension was obtained and held for 24 h in a drying oven at 100 °C. The brown precipitate was filtered and washed with more water, then annealed in a muffle oven for 3 h at 300 °C and 4 h at 700 °C.

$GCO_{(NH4)2CO3}$. For the synthesis of $GCO_{(NH_4)_2CO_3}$ stoichiometric proportions of $Gd(NO_3)_3 \cdot 6H_2O$ and $Co(NO_3)_2 \cdot 6H_2O$ were dissolved in a small amount of distilled water and stirred for 2 h at 80 °C. Next, the calculated amount of $(NH_4)_2CO_3$ was also dissolved in distilled water and then slowly added to the first solution. The resulting suspension was stirred for 3 h at 80 °C. The precipitate was filtered on a Buchner funnel and washed with distilled water to give a colourless filtrate. The precipitate was then transferred to porcelain crucibles, dried for 12 h at 120 °C, and calcined for 10 h at 850 °C.

Physical and chemical methods of catalysts research

X-ray phase analysis was carried out on the device Rigaku MiniFlex II X-ray diffractometer with Cu anode (Kα radiation =1.5418 Å).

IR spectra of the samples were obtained on a Nicolet 6700 spectrophotometer. The samples were prepared in powder form for all catalysts. Sample preparation was performed by impaired total internal reflection (ATR). Equipped with polycrystalline diamond prefix was used. Spectra were obtained in the mid and far IR regions (4000–400 cm^{-1}).

The parameters of the porous structure of the samples were determined from isotherms of nitrogen vapour adsorption at 77 K temperature measured at the ASAP 2020-MR Micromerics automatic high-vacuum unit (USA) in the range of relative vapour pressures from 0.001 to 0.98. Previously, the samples were evacuated to a residual vacuum of less than 10^{-7} mm Hg without heating.

Catalytic tests

The reaction of dry reforming of methane over synthesized catalysts was carried out in a flow-through mode in the temperature range of 773–1223 K at atmospheric pressure and the reaction mixture flow of 0.9–1.0 L/h. The ratio of the reactants was CO_2:CH_4 1:1, the catalyst weight in all experiments was 0.1 g. The catalyst was mixed with quartz in a ratio of 1:1 in order to avoid the formation of hot spots in the catalytic bed alongside with increasing the

volume. Analysis of the composition of the reaction mixture was carried out on a Crystal 2000 M chromatograph (carrier gas – argon, column length – 2 m, diameter – 3 mm, sorbent – Porapak Q) using a flame ionization detector and a heat conductivity detector connected in a series. Catalytic characteristics such as methane and carbon dioxide (X) conversions, selectivity (S) of reaction products were determined and calculated.

Conversion of CH_4 and CO_2 reactants were calculated using the formula:

$$X_i = 100(n_0 - n)/n_0 \quad (2)$$

where n – the amount of CH_4 or CO_2 in exhaust gas, mol; n_0 – initial amount of product in the reaction mixture, mol.

Hydrogen selectivity was calculated as the ratio of hydrogen generated to the total amount of methane reacted:

$$S_{H_2} = 100n(H_2)/2n(CH_4)_{reacted} \quad (3)$$

Carbon monoxide selectivity was calculated as the ratio of CO generated to total CH_4 and CO_2, reacted:

$$S_{CO} = 100n(CO)/(n(CH_4)_{reacted} + n(CO_2)_{reacted} \quad (4)$$

Carbon balance was calculated as:

$$\text{Carbon balance} = 100\frac{n_{ur}(CH_4) + n_{ur}(CO_2) + n(CO)}{n_0(CH_4) + n_0(CO_2)} \quad (5)$$

where $n_{ur}(CH_4)$ and $n_{ur}(CO_2)$ – unreacted amount of CH_4 and CO_2, mol; $n_0(CH_4)$ and $n_0(CO_2)$ – initial amount of CH_4 and CO_2, mol; $n(CO)$ – amount of CO in reaction mixture, mol.

The quantification error of each component included a measurement error of the temperature and feed rate of the reaction mixture and did not exceed 5 %.

RESULTS AND DISCUSSION

The reaction of DRM over GCO oxides obtained by co-precipitation method showed their high catalytic activity in comparison with the previously studied oxides.[9,10] At temperatures above 950 K, there was a sharp rise in CH_4 and CO_2 conversions to 80–90 %. Almost complete transformations of the reactants were achieved at 1100 K and these indicators did not decrease with a further rise in temperature (Fig. 1). It is worth noting that on the sample obtained with NaOH as the precipitant, significant CH_4 conversions were observed about 50 K lower than on the sample obtained with $(NH_4)_2CO_3$. Moreover, the choice of precipitator was somewhat affected by the selectivity of the reaction products when the highest values were achieved on the sample obtained in the presence of ammonium carbonate as the precipitator (Table I).

It was found that the hydrogen selectivity values on the test samples were significantly higher than the carbon monoxide selectivity values, which in turn leads to high ratio values H_2:CO of 1.5–2. High “non-stoichiometric” values of the synthesis gas ratio for the classical process may indicate the possibility of side reactions involving methane. Indeed, in parallel with the decrease in carbon monoxide selectivity, a sharp increase in the degree of carbonization of the cat-

alysts surface was observed in the temperature range 1073–1223 K. The carbon balance value did not exceed 65 %.

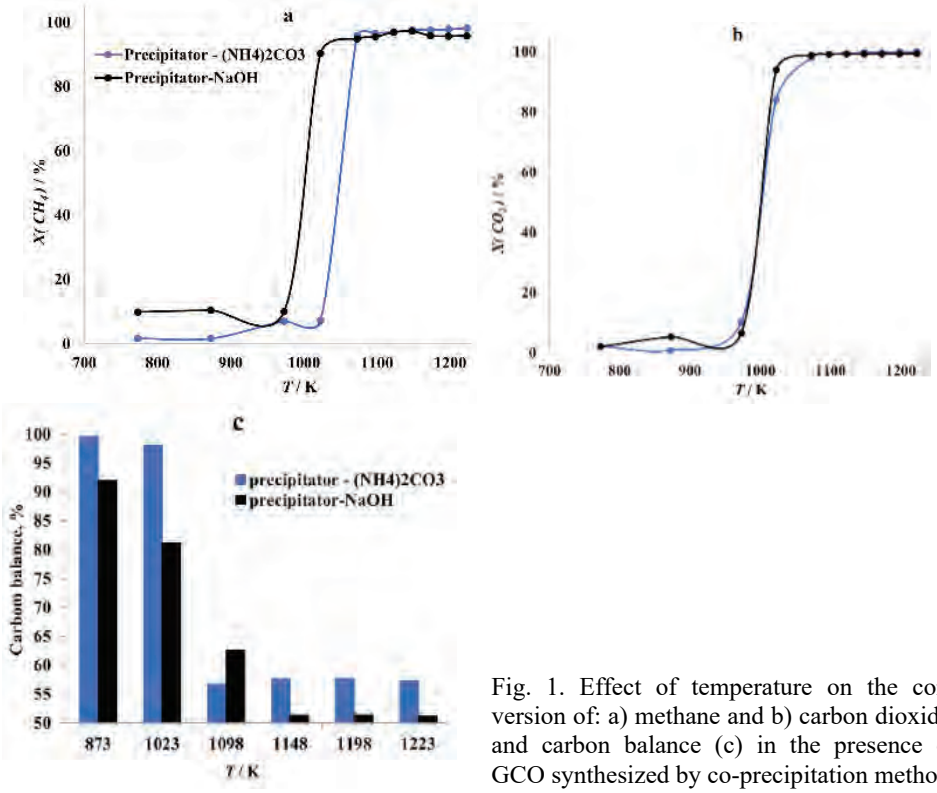

Fig. 1. Effect of temperature on the conversion of: a) methane and b) carbon dioxide, and carbon balance (c) in the presence of GCO synthesized by co-precipitation method.

TABLE I. Catalytic perfomance of GCO catalysts in the temperature range 1123–1223 K

Parameter	$GCO_{(NH_4)_2CO_3}$			GCO_{NaOH}		
	T / K					
	1123	1173	1223	1123	1173	1223
$S(H_2)$ / %	99	99	99	89	81	76
$S(CO)$ / %	57	56	56	48	45	57
$n(H_2)/n(CO)$	1.82	1.90	1.99	1.96	1.90	1.41
$X(CH_4)/X(CO_2)$	0.98	0.98	0.98	0.98	0.97	0.96

According to the literature data,[14] the increase in hydrogen selectivity, the ratio of synthesis gas components and a noticeable decrease in carbon balance indicate the occurrence of various side processes along with the DRM reaction, among which the methane decomposition reaction carried out in two directions (Eqs. (6) and (8)), as well as the reverse steam conversion of CO (Eq. (8)) prevail under these conditions:

$$CH_4 \rightarrow C + 2H_2, \quad \Delta H = 74.8 \text{ kJ/mol} \tag{6}$$

$$CH_4 \rightarrow CH_x + (4 - x)H \tag{7}$$

$$CO + H_2O \rightarrow CO_2 + H_2, \quad \Delta H = -41 \text{ kJ/mol} \tag{8}$$

Confirmation of the reaction (8) can be the formation of water in the reaction products, as well as the ratio $X(CH_4)/X(CO_2) < 1$.[15] Analysis of the obtained results and comparison with previously studied systems[9,10] suggests that the use of GCO obtained by co-precipitation method as a catalyst leads to suppression of the reverse steam conversion reaction of CO. Indeed, we see that the ratio $X(CH_4)/X(CO_2) \approx 1$ and water in reaction products for the considered interval of temperatures is registered only in insignificant quantity. At the same time, the formation of carbon deposits on the catalyst surface and the practical absence of hydrocarbons in the products indicate a more intensive side reaction of decomposition (Eq. (7)). Samples of GCO oxides were characterized by a set of methods of physicochemical analysis. Fig. 2 demonstrates results of X-ray phase analysis of the GCO complex oxide before (a) and after (b) catalysis. Sample diffractograms turned out to be similar to those described in the literature for gadolinium cobaltites.[16]

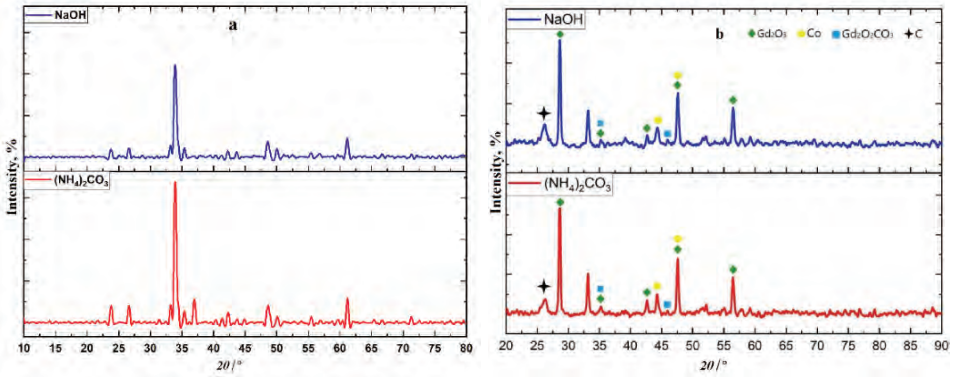

Fig. 2. XRD patterns of the GCO complex oxide before (a) and after (b) catalysis.

Testing the catalysts stability was carried out in a periodic mode (heating the catalyst to the experimental temperature (T = 1173 K), keeping it in isothermal conditions for 9–10 h, cooling in the reaction medium to room temperature and repeating all stages of the experiment, number of cycles – 3). Table II demonstrates results of the catalytic experiment. It was shown that the samples, regardless of the preparation method and high surface carbonization, do not lose their activity in the DRM reaction: the catalytic characteristics remained practically unchanged for more than 30 h of operation under reaction conditions (the total residence time of the catalyst under DRM conditions without considering the

period of its heating in the methane–carbon dioxide mixture to operating temperature).

TABLE II. GCO stability in dry reforming of methane (T = 1173K)

Sample	Time, h					
	10		20		30	
	$X(CH_4)$ / %	$X(CO_2)$ / %	$X(CH_4)$ / %	$X(CO_2)$ / %	$X(CH_4)$ / %	$X(CO_2)$ / %
$GCO_{(NH_4)_2CO_3}$	97	99	98	99	97	99
GCO_{NaOH}	96	99	97	99	96	98

The presence of a distinctive 100 % high intensity peak at 2θ 33.90° indicates the production of samples with a perovskite phase It is worth noting that the use of different precipitators in the synthesis does not affect the width of the peaks and their position on diffractograms, which indicates similar values of crystallite sizes GCO and is confirmed by calculating the average particle diameter using the Scherrer formula (Table III).

TABLE III. S_{BET}, average particle diameter and space group of GCO catalysts

Sample	S_{BET} / m^2 g^{-1}	r_{XRD} / nm	Space group
$GCO_{(NH_4)_2CO_3}$	6.9	25	Pbnm
GCO_{NaOH}	6.6	25	Pbnm

The calculation of unit cell parameters (Table IV) confirmed that the samples have an orthorhombic crystal lattice ($a \neq b \neq c$) and belong to the space group Pbnm. The calculated parameters of the elementary cells slightly differ from the literature, which indicates some distortion of the crystal lattice; however, the nature of the distortion of the lattice geometry can be associated with the presence of impurity phases, despite their absence in the X-ray spectra, due to the possible low concentration and detection limits of X-ray diffraction analysis.

TABLE IV. Lattice parameters (in nm) of GCO

Sample	a	b	c
$GCO_{(NH_4)_2CO_3}$	5.161	5.459	7.512
GCO_{NaOH}	5.320	5.419	7.227
Literature (PDF # 00-047-0579)	5.218	5.390	7.445

In such a way, similar conversion and selectivity values may be due to similar structural and texture characteristics of the oxides.

Fig 2b shows diffractograms of samples of GCO_{NaOH} and $GCO_{(NH4)2CO3}$ after catalysis. Under the reaction medium influence, the perovskite phase partially disappears and three additional phases of Gd_2O_3, $Gd_2O_2CO_3$ and Co are formed. Analysis of literature data[17] suggests that the presence of a carbonate

complex in diffractograms after catalysis of the $Gd_2O_2CO_3$ indicates that the adsorption and the further conversions of carbon dioxide takes place at A-type (Gd) centers. And the appearance of cobalt in a metal state on diffractograms suggests its reduction "from the perovskite structure" with atomic hydrogen formed during the chemisorption of methane in reactions (6) and (7). Fig. 3 demonstrates the chemical property of the DRM process on perovskite-type catalysts.

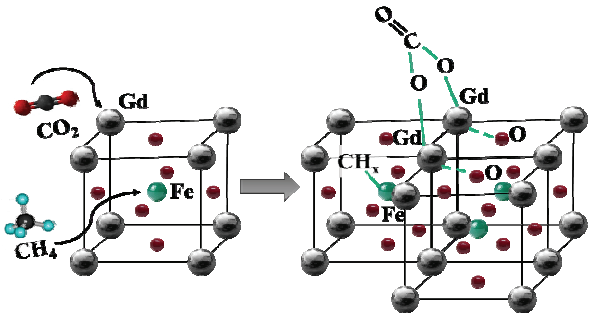

Fig. 3. Illustration of dry reforming of methane reaction.

Analysis of the X-ray diffractograms also showed the presence of carbon on the surface of the test samples, which correlates with the calculation of the carbon balance and indicates the occurrence of side reactions: the methane decomposition (Eq. (7)) and Boudoir reaction:

$$CO \rightarrow C + CO_2, \quad \Delta H = -72.5 \text{ kJ/mol} \tag{9}$$

In addition to the X-ray analysis, the resulting complex oxides were studied by IR spectroscopy.

Fig. 4 shows the IR spectra for the GCO_{NaOH}. The absorption bands corresponding to valence vibrations of Gd–O and Co–O can be observed on the spectrum before catalytic transformations in the region of 500–700 cm^{-1} and no reliable signals are observed in the region of 900–4000 cm^{-1}. On the IR spectrum of the "used-on" surface, the absorption bands were identified in the region of 2800–3000 cm^{-1}, corresponding to valence vibration of the C–H bond, which are most likely associated with the processes of methane chemisorption on the perovskite surface. The bands at 1900–2400 cm^{-1} belong to the Me–CO_2 vibrations and indicate the carbon dioxide adsorption both from the environment and after DRM on the catalyst surface, which is confirmed by XRD data. A wide high intensity band with $\bar{\nu}$ = 1078 cm^{-1} is also observed, which corresponds to the valence vibrations of the Si–O bond and is explained by the presence of quartz in the samples used as a substrate. The appearance of bands 3600–3800 cm^{-1}, corresponding to the valence vibrations of the OH group is due to the presence of adsorbed water, with the intensity of these bands exceeding the values of the

"clean surface" spectrum. Therefore, it can be said that the water is reactive and confirms the progress of the by-process - the reverse water-gas shift reaction.

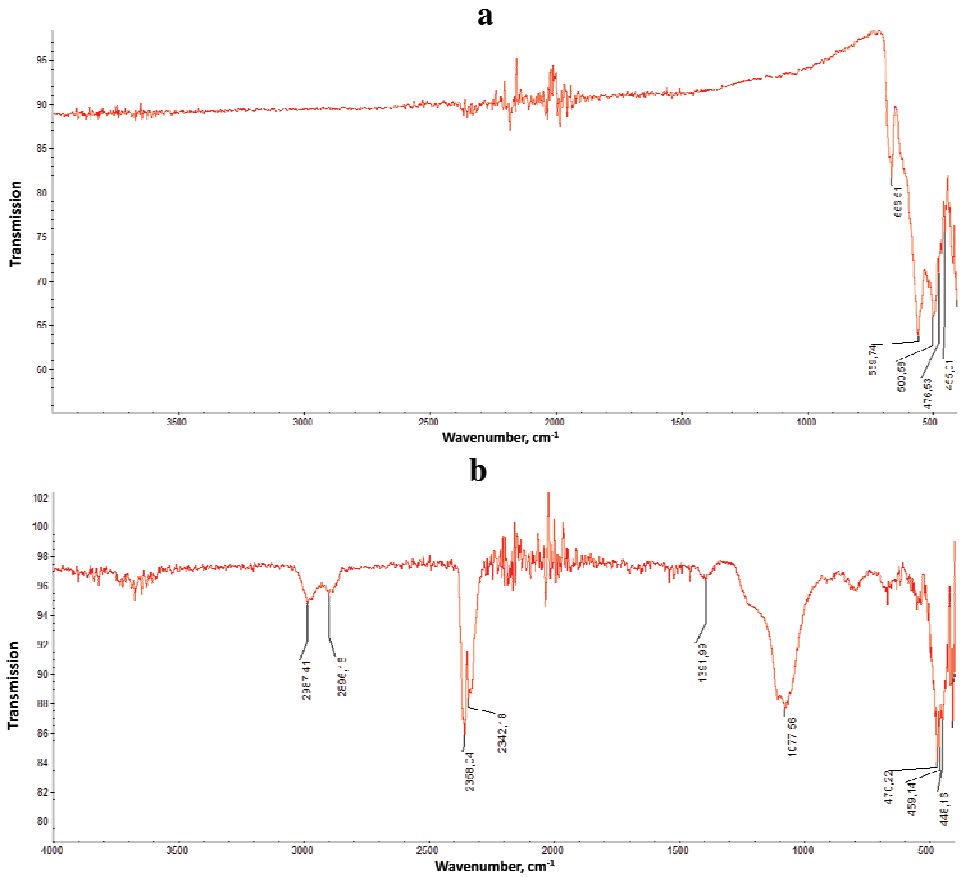

Fig. 4. IR spectra of the GCO_{NaOH} sample before (a) and after (b) catalysis.

CONCLUSION

It was found that the $GdCoO_3$ catalyst obtained by the co-precipitation method showed high catalytic activity and stability, regardless of the preparation method. Physical and chemical analysis showed that the choice of precipitant doesn't significantly affect the phase composition of the perovskites and as a consequence on the catalytic performance. The use of gadolinium cobaltites has been shown to inhibit the side reaction of reverse vapour conversion of carbon monoxide. The complex of physicochemical methods of the study revealed that under the reaction medium influence there is a change in the phase composition

of the catalyst sample associated with the appearance of oxycarbonate complexes of gadolinium and the metal phase of cobalt.

Acknowledgments. The work was carried out within the framework of the project of the Ministry of Education of the Russian Federation “Research on the problems of recycling waste of natural origin for the practical use of the products obtained” (122122600056-9).

ИЗВОД

СИНТЕЗА, КАРАКТЕРИЗАЦИЈА И КАТАЛИТИЧКЕ ОСОБИНЕ $GdCoO_3$ ЗА СУВО РЕФОРМИСАЊЕ МЕТАНА

REGINA K. ALLABERGENOVA[1], DARIA A. BOBKOVA[1], ELIZAVETA M. BORODINA[1], TATIANA A. KRYUCHKOVA[1,2], EKATERINA B. MARKOVA[1], TATIANA F. SHESHKO[1], NIKOLAI N. LOBANOV[3] и ALEXANDER G. CHEREDNICHENKO[1]

[1]Physical and Colloidal Chemistry Department, Faculty of Science, RUDN University, 6 Miklukho-Maklaya St, Moscow, 117198, Russian Federation, [2]Moscow Pedagogical State University, MPGU, 1/1 Malaya Pirogovskaya Str., Moscow, 119991, Russian Federation и [3]Inorganic Chemistry Department, Faculty of Science, RUDN University, 6 Miklukho-Maklaya St, Moscow, 117198, Russian Federation

Перовскитни оксиди (ABO_3) захваљујући високој термичкој стабилности и могућности контроле физичко–хемијских својстава представљају алтернативу традиционалним катализаторима који садрже племените и прелазне метале. У овом раду су представљени резултати експерименталних истраживања $GdCoO_3$ катализатора. Комплексни оксиди $GdCoO_3$ перовскитног типа добијени методом копреципитације са различитим таложним агенсима карактерисани су применом дифракције X-зрачења (XRD), ниско температурске адрсорпције/десорпције азота и IC спектроскопије. Физичка и хемијска анализа је показала да избор таложног агенса не утиче значајно на фазни састав перовскита. Такође су испитивана каталитичка својства гадолинијум-кобалтита. Показано је да примена кобалтита добијених копреципитацијом доводи до инхибиције споредне реакције реверзибилног реформинга угљен-моноксида. Коначно, испитивањем коришћених катализатора утврђено је да долази до формирања $Gd_2O_2CO_3$ и металног кобалта, што указује на природу активних центара: гадолинијум је центар за CO адсорпцију док се хемисорпција водоника одвија на кобалтним центрима.

(Примљено 17. маја, ревидирано 8. августа, прихваћено 12. децембра 2023)

REFERENCES

1. S. V. Razmanova, I. A. Machula, *Oil Gas Geol. Theory Practice* **10** (2015) 37 (https://doi.org/10.17353/2070-5379/38_2015)
2. G. R. S. Santos, O. M. Basha, R. Wang, H. Ashkanani, B. Morsi, *Catal. Today* **371** (2021) 93 (http://dx.doi.org/10.1016/j.cattod.2020.07.012)
3. M. M. Nair, S. Kaliaguine, *New J. Chem.* **40** (2016) 4049 (http://dx.doi.org/10.1039/C5NJ03268G)
4. W. Y. Kim, J. S. Jang, E. C. Ra, K. Y. Kim, E. H. Kim, J. S. Lee, *Appl. Catal., A* **575** (2019) 198 (https://doi.org/10.1016/j.apcata.2019.02.029)
5. K. Sutthiumporn, T. Maneerung, Y. Kathiraser, S. Kawi, *Int. J. Hydrogen Energy* **37** (2012) 11195 (https://doi.org/10.1016/j.ijhydene.2012.04.059)
6. E. le Saché, L. Pastor-Pérez, V. Garcilaso, D. J. Watson, M. A. Centeno, J. A. Odriozola, T. R. Reina, *Catal. Today* **357** (2020) 583 (https://doi.org/10.1016/j.cattod.2019.05.039)

7. R. Pereniguez, V. M. Gonzalez-delaCruz, A. Caballero, J. P. Holgado, *Appl Catal., B* **123**–**124** (2012) 346 (https://doi.org/10.1016/j.apcatb.2012.04.044)
8. S. Bhattar, M. A. Abedin, S. Kanitkar, J. J. Spivey, *Catal. Today* **365** (2021) 2 (https://doi.org/10.1016/j.cattod.2020.10.041)
9. V. V. Kost, T. A. Kryuchkova, V. D. Zimina, T. F. Sheshko, A. G. Cherednichenko, V. V. Kurilkin, M. G. Safronenko, L. V. Yafarova, *Bulg. Chem. Commun*. **51** (2019) 138 (http://www.bcc.bas.bg/BCC_Volumes/Volume_51_Special_D_2019/BCC-51-D-2019-138-142-Kost-29.pdf)
10. T. A.Kryuchkova, T. F.Sheshko, V. D. Zimina, V. V. Kurilkin, Y. M.Serov, I. A. Zvereva, L. V. Yafarova, in *Proceedings of 9th International Conference on Nanomaterials - Research & Application* (2018). TANGER Ltd.. Ostrava, Czech Republic, p. 327
11. C. Shi, S. Wang, X. Ge, S. Deng, B. Chen, J. Shen, *J. CO_2 Util.* **46** (2021) 101462 (https://doi.org/10.1016/j.jcou.2021.101462)
12. E. V. Dokuchits, A. N. Tafilevich, N. V. Shtertser, T. P.Minyukova, *J. Sib. Fed. Univ.: Chem.* **12** (2019) 177 (http://dx.doi.org/10.17516/1998-2836-0117)
13. M. Mousavi and A. N. Pour, *New J. Chem.* **43** (2019) 10763 http://dx.doi.org/10.1039/C9NJ01805K
14. J. M. Lavoie. *Front. Chem.* **2** (2014) 1 (http://dx.doi.org/10.3389/fchem.2014.00081)
15. M. K. Nikoo, N. A. S. Amin, *Fuel Process. Technol.* **92** (2011) 678 (http://dx.doi.org/10.1016/j.fuproc.2010.11.027)
16. S. V. Kurgan, G. S. Petrov, L. A. Bashkirov, A. I. Klyndyuk, *Inorg. Mater*. **40** (2004) 1224 (http://dx.doi.org/10.1023/B:INMA.0000048227.83354.3c)
17. M. R. Goldwasser, M. E. Rivas, M. L. Lugo, E. Pietri, J. Pérez-Zurita, M. L. Cubeiro, A. Griboval-Constant, G. Leclercq, *Catal. Today* **107**–**108** (2005) 106 (http://dx.doi.org/10.1016/j.cattod.2005.07.073).

Journal of the Serbian Chemical Society
JSCS-info@shd.org.rs • www.shd.org.rs/JSCS
J. Serb. Chem. Soc. *89* (1) 63–77 (2024)
JSCS–5706
Original scientific paper
Published 12 February 2024

[BMIm][PF6]/silicon oil/multi-walled carbon nanotubes paste electrode: Electrochemical properties and application for lead and cadmium ion determinations

HAI D. TRAN[1], UYEN P. N. TRAN[2] and DINH QUAN NGUYEN[3,4]*

[1]Faculty of Environment, Ho Chi Minh University of Natural Resources and Environment, Ho Chi Minh City, Vietnam, [2]Faculty of Engineering and Technology, Van Hien University, Ho Chi Minh City, Vietnam, [3]Laboratory of Biofuel and Biomass Research, Faculty of Chemical Engineering, Ho Chi Minh City University of Technology (HCMUT), 268 Ly Thuong Kiet, District 10, Ho Chi Minh City, Vietnam and [4]Vietnam National University Ho Chi Minh City, Linh Trung Ward, Thu Duc District, Ho Chi Minh City, Vietnam

(Received 22 June, revised 21 July, accepted 11 December 2023)

Abstract: The electroanalytical methods have been developed for wide application, especially for trace metal ions. In this study, the applicability of 1-butyl--3-methylimidazolium hexafluorophosphate ([BMIm][PF6]) ionic liquid as a pasting binder to fabricate a multi-walled carbon nanotube paste electrode (MWCNT PE) for detecting Pb^{2+} and Cd^{2+} was evaluated. The electrochemical properties of electrodes were explored by cyclic voltammetry, electrochemical impedance spectroscopy and linear sweep anodic stripping voltammetry. The use of [BMIm][PF6] alone as a conductive binder resulted in an electrode that was unsatisfactory for electrochemical analysis. However, the MWCNT PE with the pasting mixture of silicon oil and [BMIm][PF6] displayed excellent sensitivity for the Pb^{2+} and Cd^{2+} determinations, with limits of detection of 2.25 and 1.59 μg L^{-1}, respectively. The proposed electrode was demonstrated to be a reliable sensor for accurately quantifying trace amounts of Pb^{2+} and Cd^{2+}, exhibiting good repeatability, reproducibility and stability.

Keywords: capacitive current; heavy metal; electrochemical analysis; cyclic voltammetry; anodic stripping voltammetry.

INTRODUCTION

Heavy metals are essential micronutrients for living organisms in small amounts. However, they become toxic when their concentrations exceed certain thresholds.[1–3] The common heavy metals in water are arsenic, cadmium, chromium, lead, copper, nickel and zinc. These metals can damage the brain, lungs, kidneys, liver, blood composition and other organs.[1] In the long term, heavy

* Corresponding author. E-mail: ndquan@hcmut.edu.vn
https://doi.org/10.2298/JSC230622095G

metals can also damage DNA repair pathways and protein function, which can have a negative impact on the genetic basis of organisms.[4] Therefore, analytical techniques have been developed for monitoring trace heavy metal ions in water.

Electrochemical analysis is a powerful technique for the trace determination of analytes, especially heavy metals.[5–7] Electrical signals generated from redox reactions on the working electrode surface are transferred to an electronic device that records the variability of electrical parameters.[8,9] Therefore, the electrochemical properties of the working electrode play an important role in the sensitivity and selectivity of electroanalysis.

Among popular electrode types, carbon paste electrodes (CPEs) are widely applicable because of their low background current, ease of preparation, simple renewal, cost-effectiveness and high feasibility.[10,11] Graphite,[12] glassy carbon,[13] diamond,[14] carbon nanofiber[15] and multi-walled carbon nanotubes (MWCNTs)[16] have been applied for constructing a CPE. MWCNTs have been shown to have interesting electrochemical properties, such as large electroactive sites, chemical inertness, a fast electron transfer rate and functional flexibility.[17,18] These properties demonstrate that MWCNTs are a promising material for CPEs. However, the sensitivity of CPEs is often limited by the presence of a non-electrical conductive binder in the paste composite.[19] Gou *et al.* fabricated a MWCNT tower electrode using a polystyrene binder and found a limit of detection (*LOD*) of 2.48 and 2.8 μg L^{-1} for Pb^{2+} and Cd^{2+}, respectively.[20] In a study by Tarley *et al.*,[21] a MWCNT PE with mineral oil binder was constructed, achieving an *LOD* of 6.6 μg L^{-1} for Pb^{2+} and 8.4 μg L^{-1} for Cd^{2+}. The higher *LOD*s of 1.31 mg L^{-1} for Pb^{2+} and 47 μg L^{-1} for Cd^{2+} at the MWCNT PE using paraffin oil binder were reported.[22]

Ionic liquids (ILs) have recently been proposed as an effective pasting binder for CPEs due to their high chemical and thermal stability, negligible vapour pressure and high conductivity.[19,23] IL-CPEs exhibit enhanced electrochemical responses for analytical applications.[23] Ping *et al.* reported that the bismuth film-modified graphite PE using *n*-octylpyridinium hexafluorophosphate binder achieved an *LOD* of 0.12 μg L^{-1} for Pb^{2+} and 0.1 μg L^{-} for Cd^{2+}.[24] In a careful procedure, a pasting mixture of acid-treated MWCNTs, graphite and triphenylphosphine was used to fabricate PE, which can detect Pb^{2+} and Cd^{2+} at low *LOD*s of 0.012 μg L^{-1} for Pb^{2+} and 0.008 μg L^{-1} for Cd^{2+}.[25] Yang *et al.* used a suspension of NH_2-functionalized SnO_2 nanowire and $[C_4dmim][NTf_2]$ to modify the surface of a glassy carbon electrode for Cd^{2+} determinations with an *LOD* of 0.6 μg L^{-1}.[26] More recently, bismuth nanoparticle-modified PE based on carbon nanofibers/$[EMIm][NTf_2]$/paraffin oil/graphite composite was shown to be effective for Pb^{2+} and Cd^{2+} detections, achieving *LOD*s of 0.12 and 0.25 μg L^{-1}, respectively.[27]

This study presented a simple protocol to prepare a PE using pristine MWCNTs and a mixture of [BMIm][PF6] and silicon oil as a pasting binder for individual determinations of Pb^{2+} and Cd^{2+}. The effects of [BMIm][PF6] on the electrochemical behaviour of the fabricated PE were explored. The proposed electrode was applied for detecting Pb^{2+} and Cd^{2+} in simulated solutions and tap water using linear sweep anodic stripping voltammetry (LSASV). The reliability, repeatability and reproducibility of the proposed electrode were also evaluated.

EXPERIMENTAL

Reagents and materials

MWCNTs were synthesized by the chemical vapor deposition technique and supplied by Vinanotech (Vietnam). Silicon oil, *n*-hexane, and potassium chloride (KCl) were obtained from Merck. Potassium hexacyanoferrate ($K_3Fe(CN)_6$), lead, and cadmium nitrate salts were purchased from Sigma. All of the chemicals used in this study were in analytical grade. Double-distilled water was used for the preparation of all solutions. [BMIm][PF6] was supplied by Himedia Laboratories Pvt. Ltd., India.

Apparatus

All electrochemical experiments were performed using MPG2 Biologic system (Biologic Sci. Ins., India) controlled by ECLab® software. A three-electrode cell was assembled with the fabricated electrode as the working electrode, a platinum plate as the counter electrode, and an Ag/AgCl reference electrode. All experiments were conducted at room temperature (27 °C). A 7800 ICP-MS system was operated according to the EPA 200.8 method.

Preparation of paste electrodes

Raw MWCNTs were heated at 350 °C for 6 h in nitrogen effluent to remove moisture and then used for electrode fabrication.

i) Preparation of [BMIm][PF6]/MWCNT electrodes. 0.5 g of MWCNTs was dispersed into *n*-hexane solvent in a covered beaker under ultrasonication for 5 min. Different amounts of [BMIm][PF6] were then added to this suspension, and the beaker was opened. The weight ratios of the [BMIm][PF6]:MWCNT were studied at 15:85, 20:80, 25:75 and 30:70. The mixture was continuously ultrasonicated until a paste form was formed. The fresh paste composite was carefully packed onto a 10 mm-deep perforated polytetrafluoroethylene rod with a 3 mm inner diameter. A copper wire was inserted into the capillary tube and served as the electrical contact component.

ii) Preparation of silicon/[BMIm][PF6]/MWCNT electrodes. The same procedure was performed, but silicon oil was added to the mixture along with [BMIm][PF6]. The desired weight ratios of silicon:[BMIm][PF6]:MWCNT were 20:0:80, 19:1:80, 15:5:80, 17:3:80 and 10:10:80. The obtained electrodes were labelled S-20/B-0, S-19/B-1, S-17/B-3, S-15/B-5 and S-10/B-10, respectively.

The electrode surface was renewed for each electrochemical performance by polishing on abrasive paper.

Electrochemical measurements

i) Cycle voltammetry (CV) measurements were performed in a 50 ml solution containing 0.1 M KCl and 50 mM $K_3Fe(CN)_6$. Linear weep voltammograms were recorded in a potential range from –0.2 to 1.0 V, with scan rates ranging from 10 to 200 mV s^{-1}. A nitrogen flow was

bubbled into the analytical solution to remove dissolved oxygen before starting a potential sweep.

ii) Electrochemical impedance spectroscopy (EIS) was recorded in the frequency range of 0.01−10 kHz using a single sinusoidal excitation with an amplitude of 10 mV. EIS measurements were performed in the electrolyte containing 0.1 M KCl and 50 mM $K_3Fe(CN)_6$.

iii) The linear sweep anodic stripping voltammetry (LSASV) method was applied to detect Pb^{2+} and Cd^{2+} in solutions with the following steps: Firstly, the metal ion was accumulated on the working electrode surface for deposition time at a deposition potential while the solution was stirred at 150 rpm. Next, the stirrer was stopped until the solution reached a resting state. After that, the potential was linearly swept from deposition potential to 0 V with a scan rate of 50 mV s^{-1}. The current was recorded during the scan, releasing an anodic stripping voltammogram. The LSASV measurements were performed for individual solutions of Pb^{2+} (1, 1.5, 4.5, 9, 18, 27 and 36 μg L^{-1}) and Cd^{2+} (0.5, 1.5, 3.5, 7, 10, 15 and 20 μg L^{-1}). The deposition time and the deposition potential for the LSASV performances were optimized in this study.

Determinations of Pb^{2+} and Cd^{2+} in real sample

Tap water was collected for determining Pb^{2+} and Cd^{2+} concentrations using the LSASV and ICP-MS methods. According to the standard addition method, 10 mL of Cd^{2+} solution (1.0 mg/L), 10 mL of Pb^{2+} solution (1.0 mg/L) and 7.45 g of KCl were transferred to a 1000 ml-volumetric flask and then adjusted to 1000 mL using a tap water sample. This solution was next adjusted to pH 4 using HNO_3 0.1 M solution. The obtained analytical solution was extracted three repeated times of Pb^{2+} and Cd^{2+} determinations.

RESULTS AND DISCUSSION

Electrochemical behavior of [BMIm][PF6]/MWCNT electrodes

Fig. 1 shows the CVs of the [BMIm][PF6]/MWCNT electrodes in 50 mM of $Fe(CN)_6]^{3-/4-}$ solution. The background responses of the electrodes were large due to the contribution of capacitive current generated by both the [BMIm][PF6] and MWCNTs at the electrode surface.[23,28] This behaviour is inconvenient in analytical applications because the large capacitive currents can obscure the electroanalytical signals (faradaic currents), especially at low analytic concentrations.[29–31] The redox peaks appeared most obviously at the electrode containing 20 % weight of [BMIm][PF6], with peak-to-peak separation (ΔE_p) of 455 mV. This is larger than the theoretical value of 59 mV, indicating that a multi-electron transfer process occurs at the [BMIm][PF6]/MWCNT electrode surface.[32,33] This is likely due to the trapping of ions and/or charges in the [BMIm][PF6] layer rather than their transfer to the solution.[34,35] This experimental result demonstrates that using [BMIm][PF6] alone as a conductive binder is insufficient to enhance the electrochemical signal. Further improvements are necessary to reduce the background capacitive current.

Electrochemical behavior of silicon/[BMIm][PF6]/MWCNT electrodes

As discussed above, the [BMIm][PF6]/MWCNT electrode turned out not to be satisfactory for electroanalytical applications. To mitigate the background

current, silicon oil was used along with [BMIm][PF6] as a pasting binder to fabricate electrodes. CV analyses were conducted to assess the enhancement of the electrochemical characteristics of the silicon/[BMIm][PF6]/MWCNT electrode.

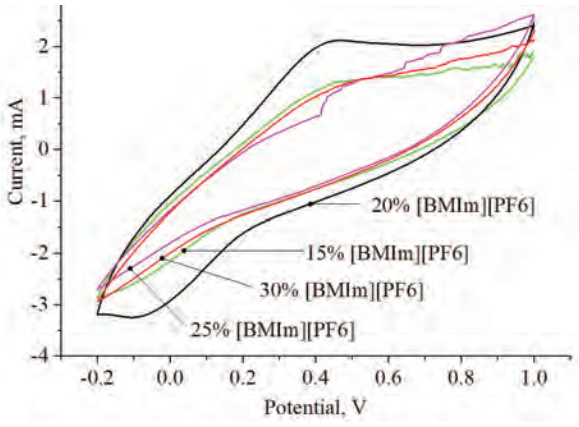

Fig. 1. Cyclic voltammograms of the [BM Im][PF6]/MWCNT electrodes (solution containing 0.1 M KCl and 50 mM $K_3[Fe(CN_6)]$, pH 4, scan rate: 20 mV s^{-1}).

It is known that [BMIm][PF6] molecules can cover and interact with the outside surface of MWCNTs *via* π-π interactions,[36] causing a thick interface layer between the electrode surface and electrolyte. As a result, the cyclic voltammograms obtained in the absence and presence of $Fe(CN)_6]^{3-/4-}$ (Fig. 2a and b, respectively) show that the non-faradaic current increased with the amounts of [BMIm][PF6] applied. As depicted in Fig. 2a, the S-20/B-0 electrode exhibits a significantly low background response, contrasting with the S10/B-10 electrode. However, the high charge conductivity nature of [BMIm][PF6] contributed to the enhancement of the signal response rate of the silicon/[BMIm][PF6]/MWCNT electrodes. As a result, the peak currents of the $Fe(CN)_6]^{3-/4-}$ redox couple were improved, as shown in Fig. 2b and Table I. The oxidation peaks occurred at 0.28 V and were unchanged at different electrodes. However, the reduction peaks were slightly shifted to the left with the increasing [BMIm][PF6] content, resulting in a larger ΔE_p. This trend is consistent with the previous reports for $[C_4mpyrr][NTf_2]$/bamboo-like MWCNT[31] and [BMIm][PF6]/graphite.[37]

The results in Table I show that increasing the amount of [BMIm][PF6] in the paste composite increases the i_{pa} and i_{pc} values, indicating a positive effect of [BMIm][PF6] on the electrochemical performance of the electrodes. The i_{pa}/i_{pc} ratios at the S-20/B-0, S-19/B-1, S-17/B-3, and S-15/B-5 electrodes are close to unity (1.034, 0.979, 1.022 and 0.945, respectively), while this ratio at the S-10/B--10 electrode is 0.826. The ΔE_p values for all five electrodes are in the range of 114–162 mV. These results suggest that the electron transfer processes at the

S-10/B-10 electrode are irreversible, while the processes at the other electrodes are quasi-reversible.[32,38] This finding indicates that the use of a mixture of silicon oil and [BMIm][PF6] as a paste binder can enhance the electrochemical properties of the electrode, compared to the use of silicon oil or [BMIm][PF6] alone.

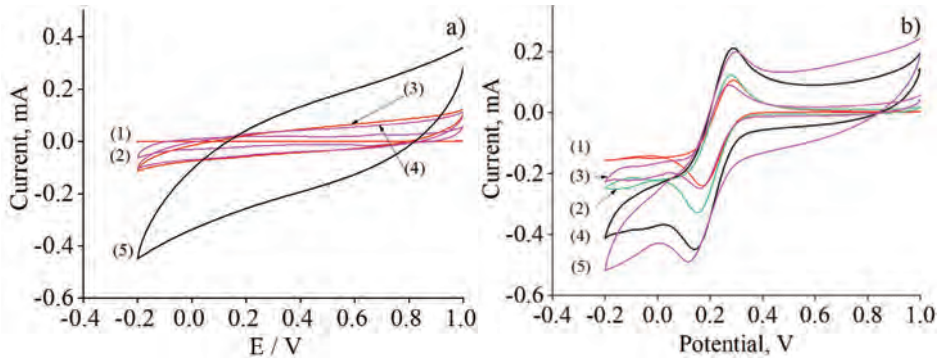

Fig. 2. CVs in solution of: a) 0.1 M KCl and b) 0.1 M KCl and 50 mM $K_3Fe(CN)_6$ at (1): S-20/B-0, (2): S-19/B-1, (3): S-17/B-3, (4): S-15/B-5 and (5) S-10/B-10 electrodes (pH 4, scan rate: 10 mV s^{-1}).

TABLE I. Results from CV measurements in solution of 0.1 M KCl and 50 mM $K_3Fe(CN)_6$ at silicon/[BMIm][PF6]/MWCNT electrodes (pH 4, scan rate of 10 mV s^{-1}); i_{pa} and i_{pc} are the oxidation and reduction peak currents

Parameter	Electrode				
	S-20/B-0	S-19/B-1	S-17/B-3	S-15/B-5	S-10/B-10
i_{pa} / μA	245	320	368	324	251
i_{pc} / μA	237	327	360	343	304
i_{pa}/i_{pc} ratio	1.034	0.979	1.022	0.945	0.826
ΔE_p / mV	114	130	152	155	162

The current response of the $Fe(CN_6)^{3-/4-}$ redox couple at the S-17/B-3 electrode was obviously higher than that of the other electrodes. As a result, the S-17/B-3 electrode was selected for the following electrochemical studies.

The S-17/B-3 electrode

i) Study on cyclic voltammetry. The electrochemical properties of the S-17/B-3 electrode were investigated using CV in $Fe(CN_6)^{3-/4-}$ solution at different potential sweep rates (v:10, 20, 30, 40, 50, 70, 100, 150 and 200 mV s^{-1}). The inset in Fig. 3a shows the recorded CVs, which reveals that the ΔE_p increases with v. This suggests that equilibrium at the electrolyte-electrode interface has not been reached.[39]

Fig. 3a shows linear relationships with a non-zero intercept between peak currents ($|i_p|$) and $v^{0.5}$, which is consistent with previous studies.[23,40] This

behaviour indicates that the electrochemical process at the S-17/B-3 electrode was a diffusion-controlled mechanism.[23,38] Additionally, the non-zero intercept of $|i_p| \sim v^{0.5}$ lines demonstrated the existence of spherical diffusion[41] and/or non-faradaic components[42] in the electrode processes. This is attributed to the nature of a non-planar electrode surface or the capacitive characteristics of the interfacial layer.[42–44] Furthermore, the $i_{pa} \sim v^{0.5}$ line was slightly steeper than the $-i_{pc} \sim v^{0.5}$ line, indicating that the quasi-reversible redox reactions of $Fe(CN_6)^{3-/4-}$ occurred at the electrode surface with a faster charge transfer rate in the oxidation process, compared to the reduction process.[45]

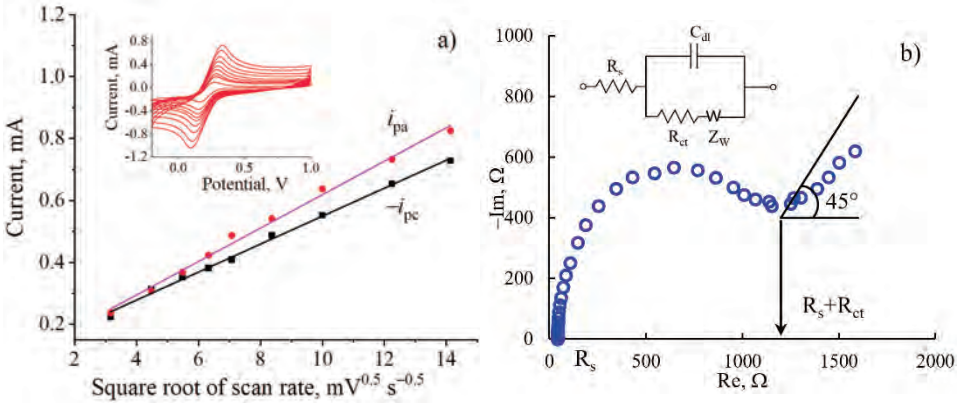

Fig. 3. a) Plots of peak currents against squared root of scan rate (the inset: cyclic voltammograms) and b) Nyquist plot (inset: equivalent circuit model). Electrolyte: 0.1 M KCl, 50 mM $K_3Fe(CN)_6$, pH 4.

ii) Study on electrochemical impedance spectroscopy. The characteristics of the electrode/electrolyte interface, including electron transfer resistance (R_{ct}), double layer capacitance (C_{dl}) and molecules/species diffusion (Z_W) were explored by EIS analysis.[46] As illustrated in Fig. 3b for the Nyquist plot, the EIS represents a semicircle in the mid-frequency range and a tail in the low-frequency range. The intercept between the semicircle and the real axis corresponds to the solution's electric resistance (R_s).[46] The Randles circuit (the inset in Fig. 3b) was preferred to fit the experimental impendence data, revealing R_s = 43.3 Ω, C_{dl} = = 0.46 mF, R_{ct} = 1004 Ω. A similar result was reported in the previous report.[47] The slope of the tail in the Nyquist plot is gentler than 45°, indicating the diffusion processes at a non-planar electrode surface.[48]

iii) Optimization of the LSASV conditions. The influence of solution pH on the Pb^{2+} and Cd^{2+} determinations was investigated. At low pH, the competition between H^+ and metal ions for the active sites at the electrode surface was more intense. Oppositely, it shifts to the hydrolysis of Pb^{2+} and Cd^{2+} at high pH, which results in the peak currents of Pb^{2+} and Cd^{2+} first increasing and then dec-

reasing with pH rising from 2 to 6, as presented in Fig. 4a. The highest peak current is achieved at pH 3 for Pb^{2+} and pH 5 for Cd^{2+}. Additionally, the stripping current of Pb^{2+} and Cd^{2+} at pH 4 deviated by 3.1 and 1.8 %, compared to the highest current, respectively. Therefore, pH 4 was considered for the following analysis.

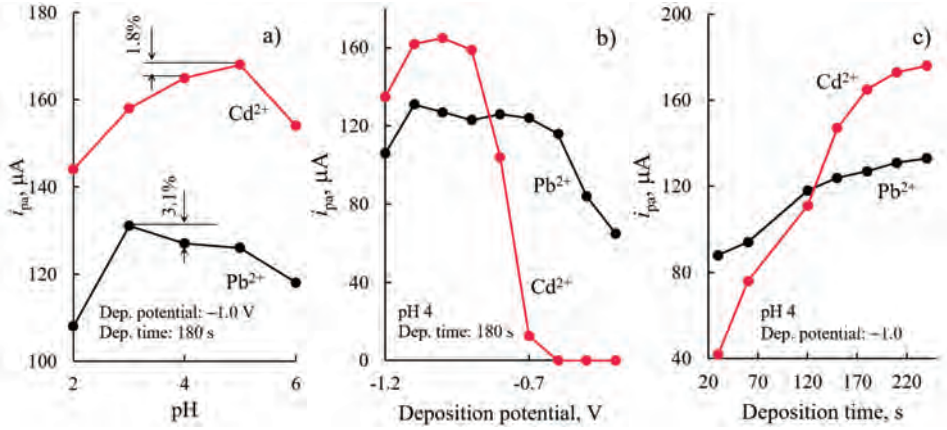

Fig. 4. Dependence of stripping peak current on: a) solution pH, b) deposition potential, c) deposition time (electrolyte: 0.1 M KCl, Pb^{2+}, 10 μg L^{-1}, Cd^{2+}, 10 μg L^{-1})

The dependence of the Pb^{2+} and Cd^{2+} stripping peak currents on the deposition potential ranging from −0.4 to −1.2 V was found and shown in Fig. 4b. The negative shift of the deposition potential from −0.4 to −1.0 V can improve the reduction of Pb^{2+} and Cd^{2+} on the electrode surface, resulting in an increase in the stripping peak current. However, water in acidic conditions can be electrolyzed at a potential less than −1.0 V, forming hydrogen atoms, which are firmly active intermediates. This led to the formation of metal hydrides, which then released cathode surface.[49] As a result, the deposited metal layer was corroded, interfering with signal response. Therefore, −1.0 V exhibits a suitable deposition potential for subsequent experiments.

As shown in Fig. 4c, the stripping peak currents of Pb^{2+} and Cd^{2+} noticeably increased with the deposition time up to 180 s. When the deposition time was prolonged, the deposition processes on the electrode surface tended to the equilibrium. Therefore, with 240 s of deposition time, the stripping peak currents of both Pb^{2+} and Cd^{2+} were only 1.07-fold higher compared with 180 s of deposition time. For balancing the signal intensity and the analysis time, 180 s was considered the deposition time for the electrochemical analysis of Pb^{2+} and Cd^{2+}.

As discussed above, the appropriate parameters of LSASV performance using the S-17/B-3 electrode for Pb^{2+} and Cd^{2+} determinations were found, parti-

cularly pH 4, deposition potential at −1.0 V and deposition time for 180 s. These conditions were applied for all following ASV experiments.

iv) Application for individual Pb^{2+} and Cd^{2+} determinations. In this study, the LSASV method was applied to determine the Pb^{2+} and Cd^{2+} concentrations in the ranges of 1–36 μg L^{-1} and 0.5–20 μg L^{-1}, respectively. Fig. 5 shows the LSASV voltammograms for different ion concentrations at a scan rate of 50 mV s^{-1}. The higher metal ion concentration resulted in a broader peak and a higher peak current. The stripping peak positions for Pb^{2+} and Cd^{2+} were well-defined at −0.36 and −0.64 V, respectively, and were unchanged with increasing ion concentration. These peaks appeared at more positive potentials than in previous studies.[21,50] This may be because Cd^{2+} and Pb^{2+} were chelated with $BMIIM^{+}$, resulting in a change in their redox status.[51–53]

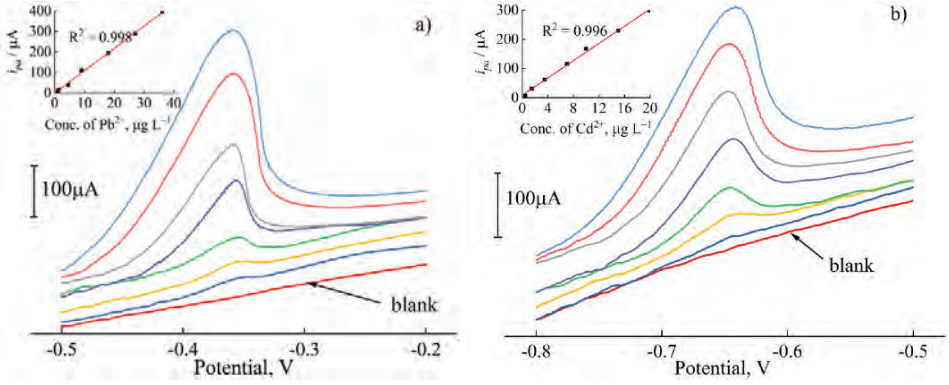

Fig. 5. The LSASV voltammograms for different concentrations of: a) Pb^{2+} and b) Cd^{2+} (scan rate: 50 mV s^{-1}, pH 4, deposition potential: −1.0 V, deposition time: 180 s). Insets: respective calibration plots for Pb^{2+} and Cd^{2+}.

For evaluating the applicability of the S-17/B-3 electrode for metal ions determination, linear regressions were performed between peak currents and ion concentrations. The insets in Fig. 5a and b show the calibration curves for Pb^{2+} and Cd^{2+}, respectively, which correspond to the following linear equations with R2 of 0.998 and 0.996, respectively.

The S-17/B-3 electrode exhibited a higher sensitivity to Cd^{2+} (14.7 μA $μg^{-1}$ L) than Pb^{2+} (10.9 μA $μg^{-1}$ L). The *LOD*s were found to be 2.25 μg L^{-1} for Pb^{2+} and 1.59 μg L^{-1} for Cd^{2+}, according to the 3σ criterion (n = 7). These *LOD*s are lower than the acceptable limits for Pb^{2+} (10 μg L^{-1}) and Cd^{2+} (3 μg L^{-1}) in drinking water, according to the WHO guidelines. Therefore, the proposed electrode suits Pb^{2+} and Cd^{2+} determinations in real applications.

The accuracy of the electrode was verified by comparing the analytical results from LSASV with those from ICP-MS for individual solutions of Pb^{2+} or

Cd^{2+}. Three simulated solutions of Pb^{2+} (10 μg L^{-1}) and Cd^{2+} (10 μg L^{-1}) in 0.1 M KCl solution (pH 4) were tested, illustrating results in Table II.

TABLE II. Concentrations of Pb^{2+} and Cd^{2+} in simulated solutions by the LSASV and ICP-MS methods

Method	Simulated sample			Mean	*RSD* / %
	#1	#2	#3		
	For Pb^{2+} determination				
LSASV	10.12	9.74	9.53	10.17	5.68
ICP-MS	9.86	9.93	9.90	9.90	0.35
	For Cd^{2+} determination				
LSASV	9.64	9.84	9.58	9.69	1.41
ICP-MS	9.78	9.82	9.86	9.82	0.41

The mean concentrations of Pb^{2+} and Cd^{2+} in simulated solutions were determined to be 10.17 and 9.69 μg L^{-1} with the LSASV method, and 9.90 and 9.82 μg L^{-1} with the ICP-MS method, respectively. In small values of the relative standard deviations (*RSD*s), the ICP-MS method exhibits a high-reliability method for Pb^{2+} and Cd^{2+} determinations and was used as the standard method in this study. The difference between the results from LSASV and ICP-MS was –4.3 % for Pb^{2+} and –6.0 % for Cd^{2+}, indicating the considerable applicability of S-17/B-3 electrode for monitoring Pb^{2+} and Cd^{2+}.

v) Repeatability, reproducibility and stability. Six individual solutions of Pb^{2+} and Cd^{2+} (10 μg L^{-1}) in 0.1 M KCl (pH 4) were prepared for the repetitive measurements using the LSASV method with the S-17/B-3 working electrode. The peak currents for Pb^{2+} (108, 104, 98, 106, 110 and 105 μA) and Cd^{2+} (157, 146, 161, 155, 148 and 152 μA) were recorded, revealing RSDs of 3.9 % for Pb^{2+} and 3.7 % for Cd^{2+}. Four different S-17/B-3 electrodes were fabricated following the identified procedure to assess the reproducibility. These electrodes were applied to determine the concentrations of Pb^{2+} and Cd^{2+} solutions at 10 μg L^{-1}. The *RSD*s were found to be 4.8 % for Pb^{2+} and 2.5% for Cd^{2+}. The S-17/B-3 electrode was also stored at room temperature (25–35 °C), at 60–80 % relative humidity, and without exposure to sunlight. Compared to the new electrode, the stripping peak currents at the electrode stored for 25 and 28 days declined by 3.4 and 7.6 % for Pb^{2+} and 2.1 and 3.2 % for Cd^{2+}, respectively. These results indicate that the S-17/B-3 electrode can be used to determine trace concentrations of Pb^{2+} and Cd^{2+} in aqueous solutions.

vi) Interference study. Common ions in tap water, such as Na^+, NH_4^+, Cu^{2+}, Ca^{2+}, Cl^-, F^-, NO_3^-, HCO_3^-, were added into the electrolyte containing 10 μg L^{-1} of Cd^{2+} or Pb^{2+} for the interference investigations. With ±5 % tolerable error, the maximum concentrations of the interfering salts were determined, as shown in Table III. The presence of Cl^-, F^- is not suitable for Pb^{2+} determination

due to the formation of weak dissociative $PbCl_2$ and PbF_2 forms. The Cd^{2+} determination has been interfered with in a wide range of interfering concentrations.

TABLE III. Effect of interferences on the individual determinations of Pb^{2+} (10 μg L^{-1}) and Cd^{2+} (10 μg L^{-1})

Interference (concentration range)	Highest concentration of interference with ±5 % tolerable error	
	For Pb^{2+} determination	For Cd^{2+} determination
NaCl (25–2000 mg/L)	Not suitable	500
$NaNO_3$ (25–2000 mg/L)	1000	1000
NaF (1–20 mg/L)	Not suitable	1
$NaHCO_3$ (50–500 μg/L)	200	100
NH_4Cl (100–500 μg/L)	Not suitable	500
$Pb(NO_3)_2$ (100–500 μg/L)	Non test	200
$Cd(NO_3)_2$ (100–500 μg/L)	300	Non test
$Cu(NO_3)_2$ (50–500 μg/L)	500	500
$Ca(NO_3)_2$ (5–500 mg/L)	500	500

vii) Application for real sample. The collected sample was used to prepare electrolytes containing 0.1 M KCl, 10 μg L^{-1} of Pb^{2+} and 10 μg L^{-1} of Cd^{2+} (pH 4) for LSASV and ICP-MS analyses. As presented in Table IV, the difference of the found Pb^{2+} and Cd^{2+} concentrations by LSASV and ICP-MS was less than 5 %. This result indicates that the S-17/B-3 electrode can provide good accuracy and reliability for the Pb^{2+} and Cd^{2+} determinations using the LSASV method.

TABLE IV. Concentrations of Pb^{2+} and Cd^{2+} in working solutions prepared from tap water medium

Method	Added, μg L^{-1}	Found, μg L^{-1}			Mean
		#1	#2	#3	
		For Pb^{2+}			
LSASV	10	13.05	12.86	12.92	12.94
ICP-MS	10	12.42	13.55	13.21	13.06
		For Cd^{2+}			
LSASV	10	10.12	10.37	10.03	10.17
ICP-MS	10	10.42	10.55	10.61	10.53

CONCLUSION

The MWCNT PEs were fabricated in the presence of [BMIm][PF6]. The [BMIm][PF6]/MWCNT PE exhibited high non-faradaic components, making it unacceptable for analytical applications. However, the electrochemical behaviour of the electrode was improved using the pasting mixture of silicon oil and [BMIm][PF6]. Increasing the amount of [BMIm][PF6] increased both the charge transfer rate and background response. At a mass ratio of silicon oil to [BMIm][PF6] of 17:3, the corresponding S-17/B-3 electrode was the most suitable for determining Pb^{2+} and Cd^{2+} concentrations, using LSASV method. The

influence of solution pH, deposition potential, and deposition time were studied. Under optimal conditions, the linear relationships between the analytical responses and concentrations of Pb^{2+} (1–36 μg L^{-1}) or Cd^{2+} (0.5–20 μg L^{-1}) were expressed. The low detection limits, good accuracy, high repeatability, reproducibility, and stability of the proposed electrode demonstrated its applicability to determining Pb^{2+} and Cd^{2+} traces in solutions. However, the results from interference studies showed that the signal response for Pb^{2+} was significantly interfered with by Cl^- and F^-. The concentrations of Pb^{2+} and Cd^{2+} in tap water were successfully determined at the S-17/B-3 electrode with high consistency to results from ICP-MS method.

Acknowledgement. We acknowledge Ho Chi Minh City University of Technology (HCMUT), VNU-HCM for supporting this study.

ИЗВОД

ЕЛЕКТРОДА ОД УГЉЕНИЧНЕ ПАСТЕ ТИПА [BMIM][PF6]/СИЛИКОНСКО УЉЕ/ВИШЕСЛОЈНЕ УГЉЕНИЧНЕ НАНОЦЕВИ: ЕЛЕКТРОХЕМИЈСКА СВОЈСТВА И ПРИМЕНА ЗА ОДРЕЂИВАЊЕ ЈОНА ОЛОВА И КАДМИЈУМА

HAI D. TRAN[1], UYEN P. N. TRAN[2] и DINH QUAN NGUYEN[3,4]

[1]Faculty of Environment, Ho Chi Minh University of Natural Resources and Environment, Ho Chi Minh city, Vietnam, [2]Faculty of Engineering and Technology, Van Hien University, Ho Chi Minh City, Vietnam, [3]Laboratory of Biofuel and Biomass Research, Faculty of Chemical Engineering, Ho Chi Minh City University of Technology (HCMUT), 268 Ly Thuong Kiet, District 10, Ho Chi Minh City, Vietnam и [4]Vietnam National University Ho Chi Minh City, Linh Trung Ward, Thu Duc District, Ho Chi Minh City, Vietnam

Електроаналитичке методе су развијене за широку област примена, а посебно за детекцију трагова метала. У овом раду је испитана могућност примене јонске течности 1-бутил-3-метилимидазолијум хексафлурофосфата ([BMIm][PF6]) као везива у електроди од пасте вишеслојних угљеничних наноцеви за детекцију Pb^{2+} и Cd^{2+}. Електрохемијска својства електрода су испитана методама цикличне волтаметрије, спектроскопије електрохемијске импеданције и анодне линеарне волтаметрије. Коришћењем самог [BMIm][PF6] као везива није добијена електрода задовољавајућих карактеристика за електрохемијску анализу. Међутим, паста од угљеничних наноцеви за силиконским уљем и [BMIm][PF6] је показала одличну осетљивост за одређивање Pb^{2+} и Cd^{2+}, са границама детекције од 2,25 и 1,59 μg L^{-1}, редом. Предложена електрода се показала као поуздан сензор за тачно квантитативно одређивање јона Pb^{2+} и Cd^{2+} у траговима, испољавајући добру поновљивост, репродуктивност и стабилност.

(Примљено 22. јуна, ревидирано 21. јула, прихваћено 11. децембра 2023)

REFERENCES

1. M. Jaishankar, T. Tseten, N. Anbalagan, B. B. Mathew, *Interdiscip. Toxicol.* **7** (2014) 60-72 (https://doi.org/10.2478/intox-2014-0009)
2. M. Balali-Mood, K. Naseri, Z. Tahergorabi, M. R. Khazdair, M. Sadeghi, *Front. Pharmacol.* **12** (2021) 227 (https://doi.org/10.3389/fphar.2021.643972)
3. X. Yang, J. Yan, F. Wang, J. Xu, X. Liu, K. Ma, X. Hu, J. Ye, *J. Serb. Chem. Soc.* **81** (2016) 697 (https://doi.org/10.2298/10.2298/JSC151124011Y)

4. M. E. Morales, R. S. Derbes, C. M. Ade, J. C. Ortego, J. Stark, P. L. Deininger, A. M. Roy-Engel, *PloS One* **11** (2016) e0151367 (https://doi.org/10.1371/journal.pone.0151367)
5. B. K. Bansod, T. Kumar, R. Thakur, S. Rana, I. Singh, *Biosens. Bioelectron.* **94** (2017) 443 (https://doi.org/10.1016/j.bios.2017.03.031)
6. E. C. Okpara, O. E. Fayemi, O. B. Wojuola, D. C. Onwudiwe, E. E. Ebenso, *RSC Adv.* **12** (40) (2022) 26319 (https://doi.org/10.1039/D2RA02733J)
7. J. Lv, Y. Tang, L. Teng, D. Tang, J. Zhang, *J. Serb. Chem. Soc.* **82** (2017) 73 (https://doi.org/10.2298/JSC160419090L)
8. O. A. Farghaly, R. A. Hameed, A.-A. H. Abu-Nawwas, *Int. J. Electrochem. Sci.* **9** (2014) 3287 (http://www.electrochemsci.org/papers/vol9/90603287.pdf).
9. J. M. Díaz-Cruz, N. Serrano, C. Pérez-Ràfols, C. Ariño, M. Esteban, *J. Solid State Electrochem.* **24** (2020) 2653 (http://doi.org/10.1007/s10008-020-04733-9)
10. C. Apetrei, I. M. Apetrei, J. A. D. Saja, M. L. Rodriguez-Mendez, *Sensors* **11** (2) (2011) 1328 (https://doi.org/10.3390/s110201328)
11. R. Rejithamol, S. Beena, *Front. Sens.* **3** (2022) 901628 (https://doi.org/10.3389/fsens.2022.901628)
12. A. J. Slate, D. A. Brownson, A. S. A. Dena, G. C. Smith, K. A. Whitehead, C. E. Banks, *Phys. Chem. Chem. Phys.* **20** (2018) 20010 (https://doi.org/10.1039/C8CP02196A)
13. J. Wang, Ü. A. Kirgöz, J.-W. Mo, J. Lu, A. N. Kawde, A. Muck, *Electrochem. Commun.* **3** (2001) 203 (https://doi.org/10.1016/S1388-2481(01)00142-4)
14. R.-l. Stefan, S. G. Bairu, *Talanta* **63** (2004) 605 (https://doi.org/10.1016/j.talanta.2003.12.023)
15. S. Motoc, F. Manea, C. Orha, A. Pop, *Sensors* **19** (6) (2019) 1332 (https://doi.org/10.3390/s19061332)
16. M. D. Rubianes, G. A. Rivas, *Electrochem. Commun.* **5** (2003) 689 (https://doi.org/10.1016/S1388-2481(03)00168-1)
17. K. Gong, Y. Yan, M. Zhang, L. Su, S. Xiong, L. Mao, *Anal. Sci.* **21** (2005) 1383 (http://doi.org/10.2116/analsci.21.1383)
18. C. L. Brito, E. I. Ferreira, M. A. La-Scalea, *Electrochi. Acta* **459** (2023) 142486 (https://doi.org/10.1016/j.electacta.2023.142486)
19. K. Fan, J. Wu, *Anal. Methods* **5** (2013) 5146 (https://doi.org/10.1039/C3AY40997J)
20. X. Guo, Y. Yun, V. N. Shanov, H. B. Halsall, W. R. Heineman, *Electroanalysis* **23** (2011) 1252 (https://doi.org/10.1002/elan.201000674)
21. C. R. T. Tarley, V. S. Santos, B. E. L. Baêta, A. C. Pereira, L. T. Kubota, *J Hazard. Mater.* **169** (2009) 256 (https://doi.org/10.1016/j.jhazmat.2009.03.077).
22. T.L. Hai, T.D. Hai, in *Proceedings of the 3rd International Conference on Chemical Engineering, Food and Biotechnology*, AIP Conference Proceedings **1878** (2017) 020023 (https://doi.org/10.1063/1.5000191)
23. H. Liu, P. He, Z. Li, C. Sun, L. Shi, Y. Liu, G. Zhu, J. Li, *Electrochem. Commun.* **7** (2005) 1357 (https://doi.org/10.1016/j.elecom.2005.09.018).
24. J. Ping, J. Wu, Y. Ying, M. Wang, G. Liu, M. Zhang, *J. Agric. Food Chem.* **59** (2011) 4418 (https://doi.org/10.1021/jf200288e).
25. H. Bagheri, A. Afkhami, H. Khoshsafar, M. Rezaei, A. Shirzadmehr, *Sens. Actuators, B* **186** (2013) 451 (https://doi.org/10.1016/j.snb.2013.06.051)

26. M. Yang, T.-J. Jiang, Z. Guo, J.-H. Liu, Y.-F. Sun, X. Chen, X.-J. Huang, *Sens. Actuators, B* **240** (2017) 887 (https://doi.org/10.1016/j.snb.2016.09.060).
27. L. Oularbi, M. Turmine, F. E. Salih, M. E. Rhazi, *J. Environ. Chem. Eng.* **8** (2020) 103774 (https://doi.org/10.1016/j.jece.2020.103774)
28. J. N. Barisci, G. G. Wallace, R. H. Baughman, *J. Electroanal. Chem.* **488** (2000) 92 (https://doi.org/10.1016/S0022-0728(00)00179-0).
29. C. Sandford, M. A. Edwards, K. J. Klunder, D. P. Hickey, M. Li, K. Barman, M. S. Sigman, H. S. White, S. D. Minteer, *Chem. Sci.* **10** (2019) 6404 (https://doi.org/10.1039/C9SC01545K)
30. S. G. Hernández-Vargas, C. A. Cevallos-Morillo, J. C. Aguilar-Cordero, *Electroanalysis* **32** (2020) 1938 (https://doi.org/10.1002/elan.201900701)
31. R. T. Kachoosangi, G. G. Wildgoose, R. G. Compton, *Electroanalysis* **19** (2007) 1483 (https://doi.org/10.1002/elan.200703883).
32. N. Elgrishi, K. J. Rountree, B. D. McCarthy, E. S. Rountree, T. T. Eisenhart, J. L. Dempsey, *J. Chem. Educ.* **95** (2018) 197 (https://doi.org/10.1021/acs.jchemed.7b00361)
33. M. Sýs, E. Khaled, R. Metelka, K. Vytřas, *J. Serb. Chem. Soc.* **82** (2017) 865 (https://doi.org/10.2298/JSC170207048S)
34. G. Shul, J. Sirieix-Plenet, L. Gaillon, M. Opallo, *Electrochem. Commun.* **8** (2006) 1111 (https://doi.org/10.1016/j.elecom.2006.05.002)
35. K. Kirchner, T. Kirchner, V. Ivaništšev, M. V. Fedorov, *Electrochim. Acta* **110** (2013) 762 (https://doi.org/10.1016/j.electacta.2013.05.049)
36. N. Maleki, A. Safavi, F. Tajabadi, *Anal. Chem.* **78** (2006) 3820 (https://doi.org/10.1021/ac060070+)
37. M. Musameh, J. Wang, *Anal. Chim. Acta* **606** (2008) 45 (https://doi.org/10.1016/j.aca.2007.11.012)
38. Y. Zhang, J. B. Zheng, *Electrochim. Acta* **52** (2007) 7210 (https://doi.org/10.1016/j.electacta.2007.05.039)
39. J.-Y. Lu, Y.-S. Yu, T.-B. Chen, C.-F. Chang, S. Tamulevičius, D. Erts, K. C.-W. Wu, Y. Gu, *Polymers* **13** (2021) 343 (https://doi.org/10.3390/polym13030343)
40. M. B. Gholivand, A. Azadbakht, *Electrochim. Acta* **56** (2011) 10044 (https://doi.org/10.1016/j.electacta.2011.08.098)
41. O. A. González-Meza, E. R. Larios-Durán, A. Gutiérrez-Becerra, N. Casillas, J. I. Escalante, M. Bárcena-Soto, *J. Solid State Electrochem.* **23** (2019) 3123 (http://doi.org/10.1007/s10008-019-04410-6)
42. P. Monk, in *Fundamentals of Electro-Analytical Chemistry*, P. Monk, Ed., John Wiley & Sons Ltd., Chichester, 2001, p 131 (https://doi.org/10.1002/9780470511329.ch6)
43. T. Tichter, J. Schneider, C. Roth, *Front. Energy Res.* **8** (2020) 155 (https://doi.org/10.3389/fenrg.2020.00155)
44. J. S. Čović, A. R. Zarubica, A. L. Bojić, T. M. Troter, M. S. Ranđelović, *J. Serb. Chem. Soc.* **85** (2020) 1185 (https://doi.org/10.2298/JSC200221043C)
45. C. O. Laoire, E. Plichta, M. Hendrickson, S. Mukerjee, K. M. Abraham, *Electrochim. Acta* **54** (26) (2009) 6560 (https://doi.org/10.1016/j.electacta.2009.06.041)
46. H. S. Magar, R. Y. Hassan, A. Mulchandani, *Sensors* **21** (19) (2021) 6578 (https://doi.org/10.3390/s21196578)
47. M. S. Ahmad, I. M. Isa, N. Hashim, S. M. Si, M. I. Saidin, *J. Solid State Electrochem.* **22** (2018) 2691 (http://doi.org/10.1007/s10008-018-3979-y)

48. A. C. Lazanas, M. I. Prodromidis, *ACS Meas. Sci. Au* **3** (3) (2023) 162 (https://doi.org/10.1021/acsmeasuresciau.2c00070)
49. T. Wirtanen, T. Prenzel, J.-P. Tessonnier, S. R. Waldvogel, *Chem. Rev.* **121** (2021) 10241 (https://doi.org/10.1021/acs.chemrev.1c00148)
50. D. Zhao, X. Guo, T. Wang, N. Alvarez, V. N. Shanov, W. R. Heineman, *Electroanalysis* **26** (2014) 488 (https://doi.org/10.1002/elan.201300511)
51. M. Tian, L. Fang, X. Yan, W. Xiao, K. H. Row, *J. Anal. Methods Chem.* **2019** (2019) 1948965 (https://doi.org/10.1155/2019/1948965)
52. C. M. Simonescu, V. Lavric, A. Musina, O. M. Antonescu, D. C. Culita, V. Marinescu, C. Tardei, O. Oprea, A. M. Pandele, *J. Mol. Liq.* **307** (2020) 112973 (https://doi.org/10.1016/j.molliq.2020.112973)
53. R. Nazar, N. Iqbal, A. Masood, M. I. R. Khan, S. Syeed, N. A. Khan, *Am. J. Plant Sci.* **3** (2012) 1476 (http://doi.org/10.4236/ajps.2012.310178).

Journal of the Serbian Chemical Society
JSCS-info@shd.org.rs • www.shd.org.rs/JSCS
J. Serb. Chem. Soc. *89* (1) 79–90 (2024)
JSCS–5707
Original scientific paper
Published 12 February 2024

Structure and thermal stability of phosphochlorinated polybutadiene/carbon black composite synthesized *via* oxidative chlorophosphorylation reaction

NADA M. EDRES[1,2], IRADA A. BUNIYAT-ZADEH[2], SOLMAZ B. ALIYEVA[3], SINAN M. TURP[4] and RASIM M. ALOSMANOV[2]*

[1]*Faculty of Education/Department of Chemistry, Khartoum University, 406, Khartoum, Sudan,* [2]*Faculty of Chemistry, Baku State University, AZ1148, Baku, Z. Khalilov, Azerbaijan,* [3]*Women Researchers Council, Azerbaijan State University of Economics (UNEC), Istiglaliyyat 6, AZ1001 Baku, Azerbaijan and* [4]*Faculty of Engineering, Bitlis Eren University, Bitlis, Turkiye*

(Received 31 July, revised 14 September, accepted 21 October 2023)

Abstract: The aim of the presented work was to obtain a new type of homogeneous composite based on an industrial polymer (polybutadiene, PB) and a well-known inexpensive filler (carbon black P-234, CB). For this purpose, the reaction of oxidative chlorophosphorylation (OxCh) was used. This makes it possible to introduce CB into the cross-linked structure of the modified polymer and ensure optimal distribution of the filler in it. The structure and thermal stability of the composite synthesized by the OxCh reaction were studied. Analysis of the composite by Fourier-transform infrared spectroscopy indicates a uniform distribution of carbon black in the network structure of the matrix and the physical interaction of the phases of the composite. Ultraviolet-visible spectrum data confirmed the improvement in light absorption in a wide range of the electromagnetic spectrum and the decrease in the optical band gap energy of the phosphochlorinated PB (PhPB) matrix with the addition of CB (E_g of PhPB = 3.25 eV; E_g of PhPB/CB composite = 2.28 eV). The influence of CB on the thermal stability of the PhPB matrix was studied using thermogravimetric and differential thermogravimetric analysis. After thermal analysis, the char yield for PhPB was 41 wt. %, and for PhPB/CB composite was 35.2 wt. %. Compared to PhPB, the increase in char yield, the decrease in maximum thermal decomposition temperature, and the high-integrated thermal decomposition temperature for the PhPB/CB composite show the improvement in the thermal stability of PhPB due to CB.

Keywords: rubber; filler; spectroscopy; chemical modification; matrix; infrared spectroscopy.

* Corresponding author. E-mail: r_alosmanov@rambler.ru
https://doi.org/10.2298/JSC230731080E

INTRODUCTION

Polymer/carbon black (CB) composites are unusual materials that find versatile applications in a variety of industrial, electronic, and biotechnological devices. For example, they are used as temperature sensors in many systems,[1,2] including sensors for volatile organic compounds with a wide range of applications such as toluene, acetone, cyclohexane and carbon tetrachloride.[3,4] The authors of the studies[5,6] discussed the improvement of wear resistance, erosion resistance of protective coatings, and electromagnetic shielding through the use of polymer/CB composites. Nakashima *et al.*[7] and Inan *et al.*[8] presented feasible membrane fuel cells operating over a wide range of temperatures and humidity levels in their studies. Nonwoven materials with modified CB nanoparticles in a Nylon-6 matrix polymer have been obtained and proposed as an adsorbent material (hemodialysis membrane).[9] A new structure of carbon nanofibers is discussed, which will be potentially useful for energy and water purification.[10] Harraz and colleagues[11] successfully created a new gold nanoparticle-decorated polypyrrole–CB/SnO_2 photocatalyst that was used to remove the insecticide imidacloprid and methylene blue under visible light illumination. A new scheme for harvesting solar energy was also demonstrated, based on the pyroelectric effect using absorbers from nanocomposite polymers of graphene and CB.[12]

Improving the performance of polymer/CB composites in all areas of application mainly depends on improving their mechanical, electrical and thermal properties, which are greatly influenced by CB.[13–15]

CB has the appropriate physical and chemical properties and is used in industry as a reinforcing rubber filler, UV stabilizer, sorbent and pigment.[16–18] CB is an amorphous particle with pores, it consists of more than 97 % carbon with a very low content of oxygen, hydrogen, sulfur, and organic compounds. CB has an interesting surface with various functional groups such as quinine, hydroxyl and carboxyl groups, which are necessary to create a cross-linked structure to improve the mechanical properties of polymers, especially rubbers. CB particles oriented in various morphologies by van der Waals forces exhibit structures with medium and high aggregates, as well as graphite-like structures.[19,20] Various CB structures are important for the thermal and electrical properties of polymer composites.[14,21,22]

Analysis of literature data shows that the properties of polymer composites using CB are determined not only by the nature of the polymer matrix, but also by the degree of uniform distribution of the filler in the matrix. In addition, structural studies of polymer/CB composites show that for designing such materials with the improved performance, it is necessary to achieve a higher degree of distribution of CB aggregates in the polymer. And the above mentioned, in turn, is established by the method of preparing composites.[22–25]

In this paper, we continue our previous studies of phosphochlorinated polybutadiene (PhPB) and its composites with various fillers, using the oxidative chlorophosphorylation reaction[26–28] as a tool. Using this reaction, we are for the first time conducting a study of the structure and thermal stability of the PhPB composite with the expedient commercially available CB P-234, with the assumption of further use. The results on the structure and thermal stability of the composite can be taken into account when using it as adsorbents.

EXPERIMENTAL

Materials

PB was purchased from Voronezh Synthetic Rubber Plant (Russia). CB P-234 was purchased from ABA Providing (Russia). PCl_3 and CCl_4 were supplied by Gorex-Analyt GmbH and used without further purification. Oxygen was supplied to the reaction medium by purging through the concentrated H_2SO_4.

Preparation of PhPB/CB composite

The construction of the cross-linked structure of PB and the preparation of its composite with a CB filler was carried out by the OxCh reaction. Initially, a 6 % solution of PB in CCl_4 was prepared in a flat-bottomed three-necked flask. The flask was then equipped with a reflux condenser, a thermometer, and a bubbler to supply oxygen gas to the reaction medium. Then, CB was added to the PB in a ratio of 1:10 (PB to CB) and the mixing of the mixture was started. Oxygen was supplied to the reaction medium at a rate of 7 L h^{-1}. The reaction was started with the gradual dropwise addition of 10 ml of PCl_3. An increase in temperature to 56°C indicated the exothermic nature of the reaction. A black solid was formed in the reaction medium and the temperature dropped back to room temperature. After completion of the reaction, the liquid phase containing PCl_3, CCl_4, and intermediate product $POCl_3$ was separated from the solid by distillation using a water jet pump. The resulting product contains functional groups $–P(O)(Cl)_2$ and $–OP(O)(Cl)_2$ and was therefore subjected to hydrolysis at 50 °C for 2 h. Hydrolysis product, *i.e.*, the PhPB/CB composite was washed with deionized water until neutral pH and finally dried first in air and then in a vacuum drying oven. The synthesis mechanism of PhPB/CB composite is given in Scheme 1.

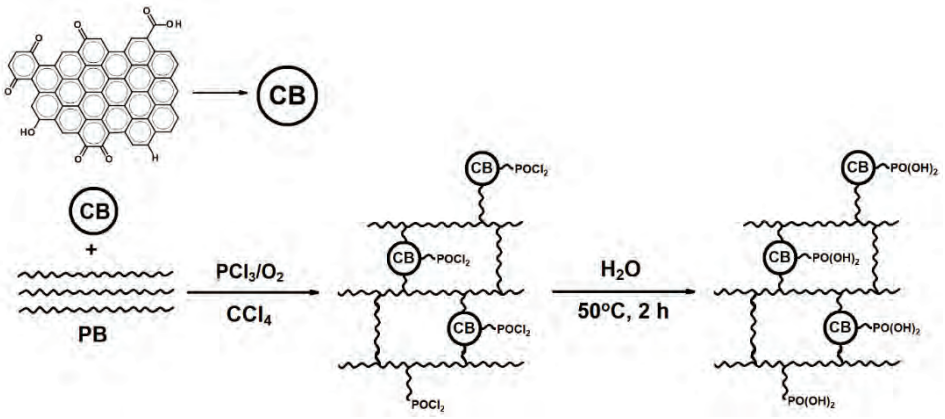

Scheme 1. Synthesis mechanism of PhPB/CB composite.

Preparation of PhPB

To compare the results obtained for the PhPB/CB composite, PhPB with a cross-linked structure was synthesized by the OxCh reaction of PB without CB filler.[29]

Characterization of CB, PhPB and PhPB/CB composite

The Fourier-transform infrared (FTIR) spectra of all samples were measured on a Perkin Elmer Spectrum 100 FTIR spectrophotometer in the range from 650 to 4000 cm^{-1}. UV–Vis spectroscopic studies of the samples were carried out on a Specord 210 Plus spectrophotometer (Analytik Jena, Germany) in the wavelength range from 200 to 700 nm. Absorption spectra obtained using UV–Vis spectroscopy were also used to estimate the optical band gap energies for the samples using Tauc's plot.[30] TG and DTG analysis of all samples was carried out on a Terra-ZA thermogravimetric analyzer in the temperature range from 26 to 750 °C (heating rate 10 °C min^{-1}) on a ceramic crucible in a nitrogen atmosphere. Approximately 4––4.5 mg of each sample was used.

RESULTS AND DISCUSSION

Characterization of CB, PhPB and CB/PhPB composite

A comparative analysis of the FTIR spectra of CB, PhPB, and the PhPB/CB composite was carried out firstly, to characterize the functional groups on the CB secondly, to study the modification of PB by the OxCh reaction and finally, to study the possibility of interaction between the CB filler and the modified PhPB.

The FTIR spectra of CB, PhPB and PhPB/CB composite are shown in Fig. 1. In the spectrum of CB the broad band at 3467 cm^{-1} (Fig. 1c) refers to the stretching of the –OH hydroxyl groups. The smaller absorption bands at 1239 and 1787 cm^{-1} are associated with the elongation of the carboxyl group C–O and C=O, respectively. The slightly intense band at 2328 cm^{-1} is usually associated with the C=O force, also the band at 980 cm^{-1}, indicates C=C–H bending vibrations. The bands at 2106 and 2660 cm^{-1} were attributed to the $–CH_2$ tension. These results of the analysis confirmed the presence of hydroxyl (–OH) and carboxyl (–COOH) groups on the CB surface. The presence of these functional groups plays a significant role in the interaction of CB with the modified PB during the construction of the composite structure.[31,32]

In the spectrum of PhPB obtained by the OxCh reaction (Fig. 1a), peaks were found at 3384, 2931, 2868, 2280 and 2099 cm^{-1}, corresponding to the –OH vibration of $–P(O)(OH)_2$ functional groups. The associated P=O stretching vibrations and P–OH stretching vibrations appear at 1174 and 739 cm^{-1}, respectively. An intense peak at 983 cm^{-1} corresponds to C–O–P, which indicates the addition of the $–PO(OH)_2$ group to the rubber matrix chain through oxygen. The adsorption peak at 1446 cm^{-1} is attributed to $–CH_2$ groups.[33]

After the interaction of the filler with the polymer matrix by the OxCh reaction, the FTIR spectrum of the obtained PhPB/CB composite (Fig. 1b) shows a slight increase in the C–O–R intensity (broad band at 982 cm^{-1}), which is associated with the physical interaction of the PhPB with CB functional groups. As a

rule, the absence of a significant effect on the FTIR spectra of PhPB after the addition of CB indicates a uniform distribution of CB particles throughout the polymer matrix. A similar result was observed in the FTIR spectra of HDPE, PP, PET and nylon/carbon black composites.[1,34]

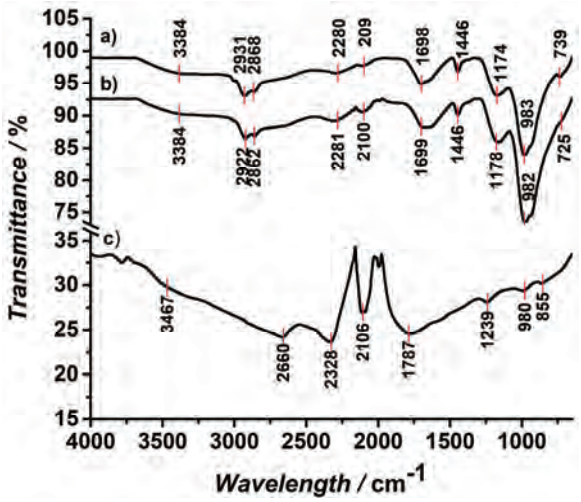

Fig. 1. FTIR spectra of PhPB (a), PhPB/CB composite (b) and CB (c).

UV–Vis analysis

UV–Vis measurements were carried out to study the effect of CB particles on the optical properties of the PhPB matrix. UV–Vis spectra of the PhPB matrix observe absorption at a wide range of 256 to 390 nm due to π–π* absorption of

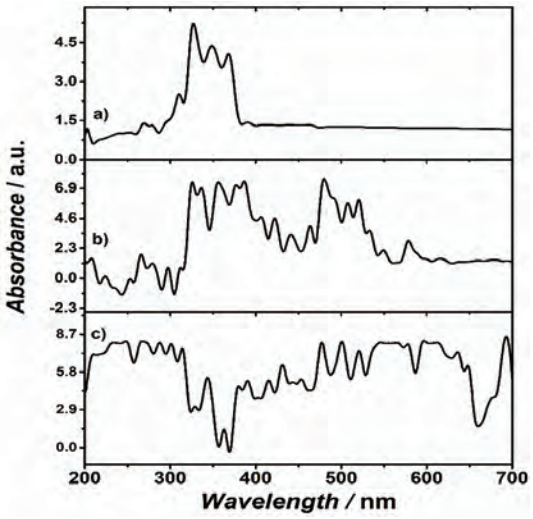

Fig 2. UV–Vis spectra of samples PhPB (a), PhPB/CB composite (b) and CB (c).

the conjugate system in the polybutadiene as shown in Fig. 2c.[35] This peak shifted to a wide range at the visible region in case of PhPB/CB composite as seen in Fig. 2b.

Direct allowed band gap of CB, PhPB and PhPB/CB composite was analyzed by Tauc's equation.[30] As can be seen in Fig. 3, the optical band gaps of PhPB (Fig. 3a) and PhPB/CB composite (Fig. 3c) are 3.25 and 2.28 eV, respectively. The smaller optical band gap of the PhPB/CB composite was attributed to disorder in the polymer matrix by the incorporation of CB particles, and thus the adsorption shift of the composite (Fig. 2b) into the visible region in the electromagnetic spectrum, due to the nature of the CB, that CB has black color and absorbs UV–Vis light as in Fig. 2a.[30] In addition, the decrease in the optical band gap of the polymer matrix is a good indicator of the increase in conductivity, which adapts the contribution of CB particles to the composite structure. Similar optical properties were observed in the polyethylene oxide/carbon black composite.[36]

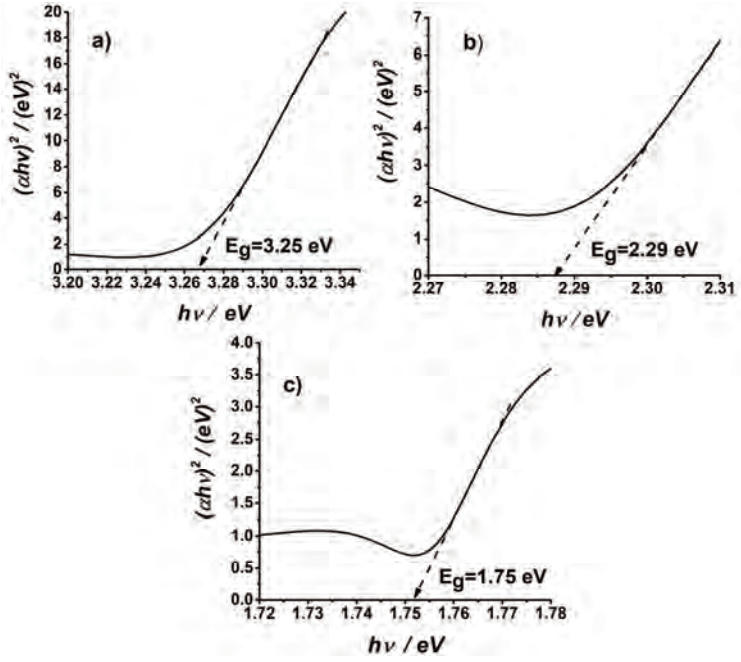

Fig. 3. The optical band gap energies of PhPB (a), PhPB/CB composite (b),and CB (c).

TG/DTG analysis

Based on the thermogravimetric analysis of CB (P-234), the TG curve in Fig. 4 shows two decomposition stages. The first stage below 120 °C is associated with the evaporation of adsorbed water from the sample. The second stage

on the curve in the range of 120–750 °C is associated with the release of volatile oxygen-containing fragments of functional groups onto the surface of the CB.[32] The DTG curve clearly shows maxima (exo-peaks) characteristic of volatile fragments, which are associated with the release of CO_2 during the decomposition of carboxyl groups in the range of 120–470 °C, and a large amount of CO from all oxygen-containing functional groups, reaching a maximum at 700 °C.[37] A less intense peak in the region of lower temperatures may be associated with the release of residual water, which is physically associated with the CB.[36]

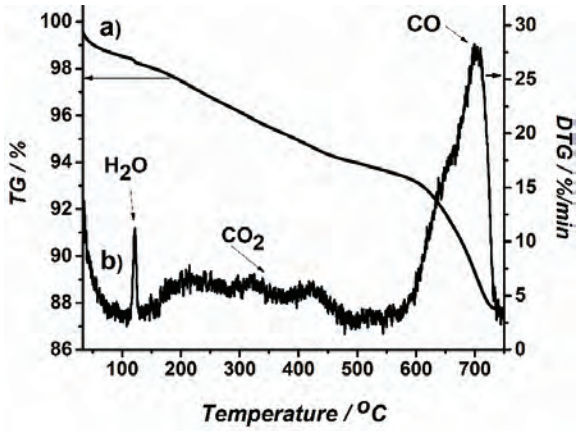

Fig. 4. TG (a) and DTG (b) thermogram CB (P-234).

To assess the effect of CB on the thermal stability of the polymer matrix, TG/DTG analyses of the PhPB matrix and the PhPB/CB composite were carried out. The results are presented in Fig. 5. The TG/DTG curves show three stages of thermal degradation for both PhPB and the PhPB/CB composite, indicating a similar degradation mechanism. A significant weight loss was observed in the range of 125–500 °C (second and third stages), weight loss below 125 °C (first stage) is due to the evaporation of physically bound water molecules, while the decomposition of functional groups and the polymer chain occurs in the second and third stages, respectively. The maximum decomposition temperatures and weight loss obtained for PhPB and the PhPB/CB composite are listed in Table I. The higher weight loss of PhPB compared to the PhPB/CB composite was observed in the second and third stages, and the apparent weight loss of the polymer matrix is due to the high amount of volatile components formed in the process of destruction. The composition exhibits greater thermal stability with less weight loss. This may be due to the presence of the CB filler, which has a shielding effect on the composite and slows down the thermal decomposition process. Accordingly, a comparison of the DTG curves of the polymer matrix and the composite showed a decrease in t_{max} in the second and third stages due to the

addition of CB to the matrix, as indicated in Table I. This is due to the dispersion of the CB of the filler in the PhPB matrix, due to the effect on the matrix cross--link density, as well as by increase of t_{max} at the first stage due to a larger amount of evaporated water adsorbed on the CB filler. The split peak in the third stage of decomposition in the polymer matrix and composite results from parallel multiple decomposition reactions at higher decomposition temperatures. A large amount of residue is also obtained in composites with styrene-butadiene or natural rubber, including CB as a filler.[38,39]

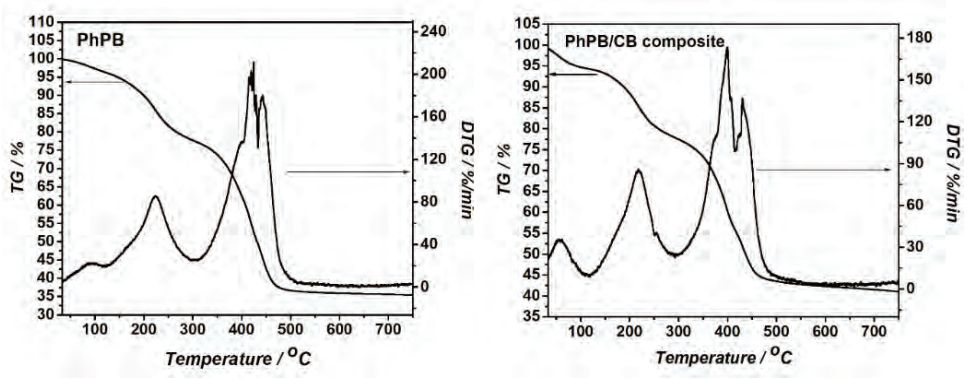

Fig. 5. TG/DTG Thermograms of PhBB and PhPB/CB composite.

TABLE I. Parameter obtained from TG and DTG thermograms

Sample	TG					DTG	
	Step	Temp. range °C	Mass loss wt. %	Yield at 750 °C wt. %	IPDT °C	T_{max} °C	DTG_{max} % min^{-1}
PhPB	1st	25–125	3.8			98	0.31
	2nd	125–303	18.9	35.2	1064	223.4	1.61
	3rd	303–750	42			424.3	4.16
PhPB/CB	1st	26–114	5.6			55.7	0.84
composite	2nd	114–290	16.5	41	1316	218.3	2.01
	3rd	290–750	36.9			400	4.06

Moreover, the PhPB/CB composite exhibits a higher resistance to thermal degradation according to integral decomposition temperature (IPDT) values calculated from the TG curve (Fig. 6) using the Doyle equation:[40]

$$IPDT = A^* K^* (T_f - T_i) + T_i \quad (1)$$

where A^* is $[(A_1+A_2)/(A_1+A_2+A_3)]$, K^* is a coefficient $[(A_1+A_2)/A_1]$, and T_i and T_f are initial temperatures and final temperature, respectively. A_1, A_2 and A_3 are area ratios in TG thermogram as shown in Fig. 4.

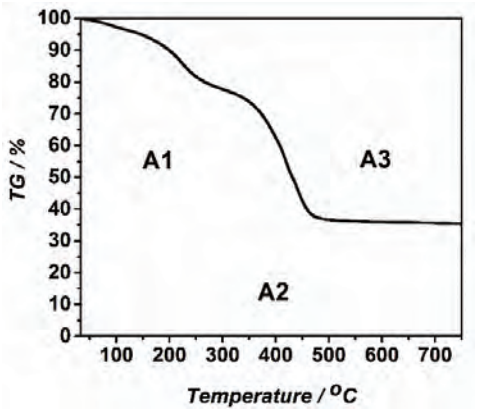

Fig. 6. Schematic representation of TGA area for calculation of IPDT values.

Probable structure of the produced polymer/CB composite

According to the results of analysis for the polymer/CB composite using IR, UV spectroscopy and TG/DTG, its structure has the following features:

– There is a chemical bond between the chains of macromolecules and CB in the composite;

– CB is evenly distributed in the polymer matrix.

The probable polymer/CB structure is shown in Fig. 7.

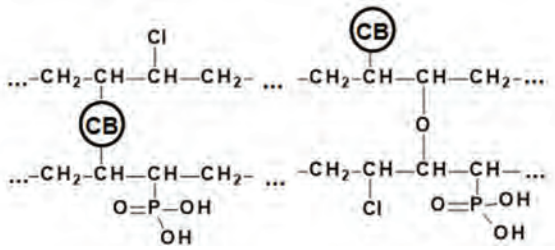

Fig. 7. Probable chemical structure of PhPB/CB composite.

CONCLUSION

PhPB/CB composite was synthesized by OxCh reaction. PhPB/CB composite and its constituent components, *i.e.*, CB and PhPB, were studied by FTIR, UV–Vis and TG/DTG analysis methods. According to the results of FTIR spectroscopy, we have found that the proposed OxCh reaction succeeded in modifying and constructing the cross-linked structure of PB obtaining well dispersed CB P-234 filler into a modified PB structure. The result of UV–Vis studies showed that due to the nature of the added CB, the PhPB/CB composite absorbs UV–Vis lights in a wider wavelength range than the PhPB matrix. The fact that the optical band gap width of the PhPB/CB composite is less than that of PhPB was attributed to the fact that CB imparts electrical conductivity to the polymer matrix.

According to the results obtained from the study of the thermal properties of the samples, PhPB/CB composite exhibits a higher resistance to thermal degradation.

Based on the overall results, it can be said that by using the OxCh reaction and CB as a filler, it is possible to improve the thermal, electrical, and optical properties of PB, as well as to synthesize a composite material with a cross--linked structure.

ИЗВОД

СТРУКТУРА И ТОПЛОТНА СТАБИЛНОСТ ФОСФОХЛОРИСАНОГ ПОЛИБУТАДИЕН-ЧАЂ КОМПОЗИТА СИНТЕТИСАНОГ ПУТЕМ ОКСИДАТИВНЕ ХЛОРОФОСФОРИЛАЦИЈЕ

NADA M. EDRES[1, 2], IRADA A. BUNIYAT-ZADEH[2], SOLMAZ B. ALIYEVA[3], SINAN M. TURP[4] и RASIM M. ALOSMANOV[2]

[1]Faculty of Education/Department of Chemistry, Khartoum University, 406, Khartoum, Sudan, [2]Faculty of Chemistry, Baku State University, AZ1148, Baku, Z. Khalilov, Azerbaijan, [3]Women Researchers Council, Azerbaijan State University of Economics (UNEC), Istiglaliyyat 6, AZ1001 Baku, Azerbaijan и [4]Faculty of Engineering, Bitlis Eren University, Bitlis, Turkiye

Циљ представљеног рада био је да се добије нови тип хомогеног композита заснованог на индустријском полимеру (полибутадиен, PB) и добро познатом јефтином пуниоцу (чађ P-234, CB). У ту сврху коришћена је реакција оксидативне хлорофосфорилације (OxCh). То омогућава увођење CB у умрежену структуру модификованог полимера и обезбеђивање оптималне расподеле пуниоца у њему. Проучавана је структура и топлотна стабилност композита синтетисаног OxCh реакцијом. Анализа композита FTIR методом указује на уједначену расподелу пуниоца у умреженој структури матрице и физичку интеракцију фаза композита. Подаци ултраљубичастог видљивог спектра потврдили су побољшање апсорпције светлости у широком спектру електромагнетног спектра и смањење оптичког енергетског јаза фосфохлорне PB (PhPB) матрице са додатком CB (E_g 3,25 eV; E_g PhPB/CB композита 2,28 eV). Утицај CB на топлотну стабилност PhPB матрице проучаван је коришћењем термогравиметријске и диференцијалне термогравиметријске анализе. Након термалне анализе, остатак за PHPB је био 41 мас. %, а за PhPB/CB композит 35,2 мас. %. У поређењу са PHPB, повећање остатка, смањење максималне температуре топлотног распадања и висока температура термалне декомпозиције за PhPB/CB композит показују побољшање топлотне стабилности PHPB због CB.

(Примљено 31. јула, ревидирано 14. септембра, прихваћено 21. октобра 2023)

REFERENCES

1. A. K. Sahu, K. Sudhakar, R. M. Sarviya, *Case Stud. Therm. Eng.* **15** (2019) 100534 (https://doi.org/10.1016/j.csite.2019.100534)
2. J. G. Jeon, G.-W. Hong, H.-G. Park, S. K. Lee, J.-H. Kim, T. J. Kang, *Sensors* **21** (2021) (https://doi.org/10.3390/s21051560)
3. B. Matthews, J. Li, S. Sunshine, L. Lerner, J. W. Judy, *IEEE Sens. J.* **2** (2002) 160 (https://doi.org/10.1109/JSEN.2002.800284)
4. A. N. Mallya, R. Kottokkaran, P. C. Ramamurthy, *Sensors Actuators, B* **201** (2014) 308 (https://doi.org/10.1016/j.snb.2014.04.056)

5. M. Dong, Q. Li, H. Liu, C. Liu, E. K. Wujcik, Q. Shao, T. Ding, X. Mai, C. Shen, Z. Guo, *Polymer* **158** (2018) 381 (https://doi.org/10.1016/j.polymer.2018.11.003)
6. V. Khomenko, O. Butenko, O. Chernysh, V. Barsukov, M. P. Suchea, E. Koudoumas, *Coatings* **12** (2022) 665 (https://doi.org/10.3390/coatings12050665)
7. M. R. Berber, T. Fujigaya, N. Nakashima, *Mater. Today Energy* **10** (2018) 161 (https://doi.org/10.1016/j.mtener.2018.08.016)
8. H. Doğan, E. Yıldız, M. Kaya, T. Y. Inan, *Bull. Mater. Sci.* **36** (2013) 563 (https://doi.org/10.1007/s12034-013-0512-x)
9. M. Andrade-Guel, P. Y. Reyes-Rodríguez, C. J. Cabello-Alvarado, G. Cadenas-Pliego, C. A. Ávila-Orta, *Nanomaterials* **12** (2022) (https://doi.org/10.3390/nano12234247)
10. H. Gaminian, M. Montazer, *Cellulose* **25** (2018) 5227 (https://doi.org/10.1007/s10570-018-1929-6)
11. M. Faisal, J. Ahmed, J. S.Algethami, M. Jalalah, S. A. Alsareii, M. Alsaiari, F. A. Harraz, *J. Ind. Eng. Chem.* **121** (2023) 287 (https://doi.org/10.1016/j.jiec.2023.01.032)
12. L. Battista, L. Mecozzi, S. Coppola, V. Vespini, S. Grilli, P. Ferraro, *Appl. Energy* **136** (2014) 357 (https://doi.org/10.1016/j.apenergy.2014.09.035)
13. A. Verma, K. Baurai, M. R. Sanjay, S. Siengchin, *Polym. Compos.* **41** (2020) 338 (https://doi.org/10.1002/pc.25373)
14. V. Mishra, *IOP Conf. Ser. Mater. Sci. Eng.* **1116** (2021) 12004 (https://doi.org/10.1088/1757-899X/1116/1/012004)
15. F. Avilés, A. I. Oliva-Avilés, M. Cen-Puc, *Adv. Eng. Mater.* **20** (2018) 1701159 (https://doi.org/10.1002/adem.201701159)
16. *Carbon Black Science and Technology*, 2nd ед., J.-B. Donnet, ed., Second Edi Routledge, New York, 1993
17. O. Kochkodan, V. Maksin, *J. Serb. Chem. Soc.* **85** (2019) 112 (https://doi.org/10.2298/JSC190416112K)
18. V. Panić, A. Dekanski, B. Nikolic, *J. Serbian Chem. Soc.* **78** (2013) 2141 (https://doi.org/10.2298/JSC131031128P)
19. A. Y. Watson, P. A. Valberg, *AIHAJ J. Sci. Occup. Environ. Heal. Saf.* **62** (2001) 218 (https://doi.org/10.1080/15298660108984625)
20. C. M. Long, M. A. Nascarella, P. A. Valberg, *Environ. Pollut.* **181** (2013) 271 (https://doi.org/10.1016/j.envpol.2013.06.009)
21. J. Song, K. Tian, L. Ma, W. Li, S. Yao, *Int. J. Heat Mass Transf.* **137** (2019) 184 (https://doi.org/10.1016/j.ijheatmasstransfer.2019.03.078)
22. J. Guo, C.-H. Tsou, Y. Yu, C.-S. Wu, X. Zhang, Z. Chen, T. Yang, F. Ge, P. Liu, M. R. De Guzman, *Iran. Polym. J.* **30** (2021) 1251 (https://doi.org/10.1007/s13726-021-00973-2)
23. R. Hong, Z. Zhao, J. Leng, J. Wu, J. Zhang, *Compos., B* **176** (2019) 107214 (https://doi.org/10.1016/j.compositesb.2019.107214)
24. Q. Zhang, J. Wang, B.-Y. Zhang, B.-H. Guo, J. Yu, Z.-X. Guo, *Compos. Sci. Technol.* **179** (2019) 106 (https://doi.org/10.1016/j.compscitech.2019.05.008)
25. S. Fang, S. Wu, J. Huang, D. Wang, Z. Tang, B. Guo, L. Zhang, *Ind. Eng. Chem. Res.* **59** (2020) 21047 (https://doi.org/10.1021/acs.iecr.0c04242)
26. S. Aliyeva, R. Alosmanov, I. Buniyatzadeh, G. Eyvazova, A. Azizov, A. Maharramov, *Colloid Polym. Sci.* **297** (2019) 1529 (https://doi.org/10.1007/s00396-019-04565-8)
27. S. Aliyeva, A. Maharramov, A. Azizov, R. Alosmanov, I. Buniyatzadeh, G. Eyvazova, *Anal. Lett.* **49** (2016) 2347 (https://doi.org/10.1080/00032719.2016.1139586)

28. R. Alosmanov, J. Imanova, K. Wolski, R. Ziemmermann, S. Fiejdasz, J. Przewoźnik, K. Goc, C. Kapusta, S. Zapotoczny, M. Szuwarzyński, *Materials (Basel)* **11** (2018) (https://doi.org/10.3390/ma11122595)
29. R. Alosmanov, *J. Serbian Chem. Soc.* **81** (2016) 42 (https://doi.org/10.2298/JSC151008042A)
30. A. P. S. Chauhan, K. Chawla, *J. Mol. Liq.* **221** (2016) 292 (https://doi.org/10.1016/j.molliq.2016.05.043)
31. P. Dong, T. Maneerung, W. C. Ng, X. Zhen, Y. Dai, Y. W. Tong, Y.-P. Ting, S. N. Koh, C.-H. Wang, K. G. Neoh, *J. Hazard. Mater.* **321** (2017) 62 (https://doi.org/10.1016/j.jhazmat.2016.08.065)
32. S. Yu, Z. Tang, S. Fang, S. Wu, B. Guo, *Compos., A* **149** (2021) 106589 (https://doi.org/10.1016/j.compositesa.2021.106589)
33. R. Alosmanov, K. Wolski, G. Matuschek, A. Magerramov, A. Azizov, R. Zimmermann, E. Aliyev, S. Zapotoczny, *J. Therm. Anal. Calorim.* **130** (2017) 799 (https://doi.org/10.1007/s10973-017-6464-4)
34. H.-J. Choi, M. S. Kim, D. Ahn, S. Y. Yeo, S. Lee, *Sci. Rep.* **9** (2019) 6338 (https://doi.org/10.1038/s41598-019-42495-1)
35. R. M. Sankar, T. K. Roy, T. Jana, *Bull. Mater. Sci.* **34** (2011) 745 (https://doi.org/10.1007/s12034-011-0190-5)
36. H. Miqdad, *Int. J. Appl. Eng. Res.* **13** (2018) 5411 (https://www.ripublication.com/ijaer18/ijaerv13n7_116.pdf)
37. E. Jakab, M. Omastová, *J. Anal. Appl. Pyrolysis* **74** (2005) 204 (https://doi.org/10.1016/j.jaap.2005.02.001)
38. N. Jetro Nkengafac, A. Alegria, S. Arrese-Igor, A. Edgengele, E. Eugene, *J. Mat. Sci. Res. Rev.* **3** (2020) 237 (https://journaljmsrr.com/index.php/JMSRR/article/view/121/241)
39. G. T. Mohanraj, T. Vikram, A. M. Shanmugharaj, D. Khastgir, T. K. Chaki, *J. Mater. Sci.* **41** (2006) 4777 (https://doi.org/10.1007/s10853-006-0065-0)
40. C. D. Doyle, *Anal. Chem.* **33** (1961) 77 (https://doi.org/10.1021/ac60169a022).

Journal of the Serbian Chemical Society
JSCS-info@shd.org.rs • www.shd.org.rs/JSCS
J. Serb. Chem. Soc. *89* (1) 91–106 (2024)
JSCS–5708
Original scientific paper
Published 12 February 2024

Preparation and *in-vitro* evaluation of single and bi-layered beeswax-based microparticles for colon-specific delivery of mesalamine

RYM BRAHMI[1], KHEIRA DIAF[1], ZINEB ELBAHRI[2]* and MILAD BAITICHE[3]

[1]*Laboratory of Macromolecular and Physical Organic Chemistry, Faculty of Exact Sciences, Djillali Liabes University of Sidi Bel Abbes, 22000, Algeria,* [2]*Laboratory of Materials and Catalysis, Faculty of Exact Sciences, Djillali Liabes University of Sidi Bel Abbes, Algeria and* [3]*Laboratory of Preparation, Modification and Applications of Multiphase Polymeric Materials, Department of Process Engineering, The Faculty of Technology of Ferhat Abbas University of Setif, Algeria*

(Received 1 May, revised 17 July, accepted 20 November 2023)

Abstract: Beeswax is selected as a natural coating material for the development of new colon specific drug delivery systems charged by mesalamine. In a first step, beeswax microparticles are prepared using hot-melt process of micro-encapsulation where drug:beeswax ratio, stirring speed, emulsifier concentration and pH of external phase are varied for the optimization of the drug entrapment and microparticles' morphology. The effect of the nature of the emulsifier is also discussed by studying the hydrophilic–lipophilic balance (HLB) value. In a second step, to obtain delayed delivery systems, bi-layered microspheres are elaborated by the process of emulsion–solvent evaporation using ethylcellulose or cellulose acetate butyrate as outer enteric coating layer. All formulations are characterized by infrared spectroscopy, X-ray diffraction, scanning electron microscopy and optical microscopy. The drug release is established in simulated gastric, small bowel and colon liquids and the release mechanism is discussed by applying the Korsmeyer–Peppas model.

Keywords: beeswax; mesalamine; colon-specific delivery; double walled microspheres.

INTRODUCTION

Mesalamine or 5-aminosalicylic acid (5-ASA) is an active substance that has been used as a potent non-steroidal anti-inflammatory drug, its efficacy is proved against gastrointestinal tract diseases and especially that of colon part, such as ulcerative colitis and Crohn's desease.[1,2] Obviously, the oral administration of the drug remains a painless and favourite method for patients but it can reduce

* Corresponding author. E-mail: elbahrizineb@yahoo.fr
https://doi.org/10.2298/JSC230501088B

the drug bioavailability and therefore its therapeutic efficacy. In fact, mesalamine is absorbed into the proximal small intestine and metabolized without reaching the therapeutic levels in inflamed sites.[3] So, multiple kinds of colonic drug delivery systems such as gastroretentive dosage forms, pH-dependent dosage forms, or mucoadhesive dosage forms are developed to improve the effectiveness of inflammatory bowel diseases treatments.[3–5] In these systems, the active therapeutic substance is usually coated in a shell that controls the drug release through three parameters often operating in a combined way; the first one is related to the pH values of the gastrointestinal tract, this formula generally showed neglected release in a strongly acidic environment.[5,6] The second parameter is based on the transit time of the gastrointestinal tract;[5,7] for example, as reported by Souza *et al.*,[8] the delayed drug delivery is acquired by the relaxation behaviour of Xylan chains in the first 4 h; in this study, the microspheres were able to reach the large intestine with about 40 % of initial drug load, which could be sufficient for the local treatment of inflammation according to the researchers.[8] Finally, the presence of colonic flora ensures a specific release of the drug, this type of microscopic vector is generally based on polysaccharides since they are indigestible in the small intestine. However, they undergo complete or partial degradation by carbohydrate-active enzymes (CAZymes) in the colon.[9–11] For example, pH––enzyme double-dependent mesalamine colon-specific delivery system were developed by Jin *et al.*;[12] the authors succeeded in developing a dual pH-dependent and enzymatic degradation systems based on chitosan and eudragit S100 for the specific release of mesalamine in the colon.[12]

Thus, in the present investigation, an attempt is made to prepare colon drug delivery microspheres using mesalamine as active ingredient and beeswax as natural coat. Beeswax is a complex mixture composed of hydrocarbons, free fatty acids, esters of fatty acids and fatty alcohol, diesters and exogenous substances.[13] This coat material is chosen, in one hand, for its edible properties and long resistance to external environmental factors (oxygen, humidity, digestive properties).[13,14] In the other hand, it is confirmed by several studies that the drug encapsulation using this lipid material is effective in protecting and improving the release properties of compounds, especially in the medical field, as it allows a prolonged release of the drugs using simple methods with low production costs.[15–19] Beeswax is mostly used as gastro-resistant coat for anti-inflammatory drugs.[15,18,19] and it has been also tested to obtain delayed formulations for an anti-cancer drug.[17] So, the objective of the present work is to develop new reservoir devices by a combination of beeswax, as primary coat and cellulose derivative polymers as second layer, for a colon specific drug delivery. For the research purpose the optimized beeswax microspheres are firstly prepared by emulsion–melt solidification technique and by varying some process parameters, *i.e.*, drug:polymer ratio, stirring speed, emulsifier nature and concentration and the

pH of external phase. Secondly, double walled microspheres are formed using emulsion–solvent evaporation technique where ethylcellulose and cellulose acetate butyrate are chosen and tested as second coat to obtain colon-specific drug delivery systems.

EXPERIMENTAL

Materials

Mesalamine is obtained from SALEM laboratory (Algeria), beeswax is obtained from beekeeping farm (west of Algeria), ethyl cellulose (EC, 22 mPa s) and cellulose acetate butyrate (CAB, M = 70000) are purchased from Sigma–Aldrich. Polyvinyl alcohol (PVA, 98––99 % hydrolysed, polymerisation degree:1700–1800, viscosity: 25–32 cP) is from Biochem Chermopharma, Tween 80 origin is Sigma–Aldrich, Span 80 is from Biochem Chermopharma and dichloromethane (DCM) is from Sigma–Aldrich.

Preparation of microspheres and double coated microspheres

Mesalamine microspheres based on beeswax are prepared by using hot-melt technique of micronecapsulation; 2g of beeswax is melted in a water bath at 90 °C, then 0.25 g of mesalamine is added under magnetic stirring. The mixture is then emulsified in 100 mL of hot (85––90 °C) aqueous solution (distilled water with pH 6.1±0.1 or acetate buffer solution at pH 4±0.1), containing 1.5 % of emulsifier and stirred mechanically at 800 rpm using DLS stirrer. After 3 min of emulsion, the system is cooled using an ice bath until 10° C under continuous stirring. After 20 min, solidified microspheres are collected by filtration and washed with distilled water and finally dried at room temperature for 48 h.

To obtain double walled microparticles, solvent evaporation method is used; so selected beeswax microspheres are dispersed in 25mL of DCM coating solution containing 0.4 g of EC or CAB as matrix, the polymer:microspheres ratio is maintained at 1:1. This organic phase is then poured into 100 mL of 1 % of PVA aqueous acetate buffer solution (pH 4) under stirring (800 rpm) for 3 h until the complete solvent evaporation. After filtration, the obtained double walled microspheres are washed with distilled water and dried at room temperature for 48 h.

Microparticles' characterization

For microparticles' characterization, FTIR spectra of drug, beeswax and formulations are registered using a Bruker Alpha FTIR spectrometer in the absorbance range of 4000–400 cm^{-1}. Powder X-Ray diffractogramms of mesalamine, beeswax and D_{11} batch of microspheres are recorded using Rigaku diffractometer type Ultima IV. The samples are scanned in the range of 2θ from 0 to 80° using an incident beam the Kα1 line of copper. Shape and surface morphology of microspheres are examined using Hitachi TM-1000 scanning electron microscope (SEM). The particles are observed using the optical microscopy type Optika stereomicroscope of the series SZM 1 and equipped with a camera and software, in order to identify the size and morphology of microparticles. The mean diameter, d_{10}, is calculated using the following equation and by counting and measuring more than 500 microparticles of each batch:

$$d_{10} = \frac{\sum n_i d_i}{\sum n_i} \quad (1)$$

where d_i is the droplet diameter, n_i is the number of droplets with diameter d_i; d_{10} is the average number diameter.

Determination of the drug content and encapsulation efficiency

5 mg of microspheres are dispersed in 10 mL of a suitable solvent (0.5 M HCl solution) under stirring for 15 min at 90 °C for the complete removal of mesalamine. After cooling at room temperature, the obtained mixture is filtered and analysed by UV–Vis spectrophotometry using Shimadzu 240 1PC spectrophotometer at λ_{max} = 305.8 nm, the drug extraction is carried out in triplicate and the results are expressed by the mean ± *SD*.

The entrapment efficiency and drug content are calculated using the following formulas:

$$\text{Efficiency} = 100\frac{m_{\text{drug extract}}}{m_{\text{initial drug}}} \quad (2)$$

$$\text{Drug loading} = 100\frac{m_{\text{drug extract}}}{m_{\text{microsphers}}} \quad (3)$$

In-vitro *drug release studies*

The drug release is monitored using a Shimadzu 240 1PC dual beam UV–Vis spectrophotometer. 200 mg of microspheres are dispersed in 900 mL of dissolution medium at 37±0.4 °C under magnetic stirring of 100 rpm. At selected time intervals, 3 mL of sample is withdrawn and analysed and quickly reintroduced into the release reactor. The drug release is carried out in simulated gastric medium of pH 1.2 for a period of 2 h, in simulated small bowel liquid (pH 8) for 6 h and in colon simulated liquid at pH 6.5 for 5 days. These mean values of periods are selected based on the available studies on patients with active ulcerative colitis and Crohn disease.[20-23]

Kinetic treatment of mesalamine release data

The release data are mathematically fitted according to Korsmeyer–Peppas kinetic model:

$$\frac{m_t}{m_i} = K_K t^n \quad (4)$$

where m_t is the amount of drug release in time t, m_i is the initial amount of drug in the microsphere and m_t/m_i fractional mass of drug released at time t. K_K is the rate constant of Korsmeyer–Peppas model and n is the diffusion exponent according to Korsmeyer–Peppas, this model is verified for 60 % of the drug released.[24-27] The selected model is applied for each step of drug release in selected time intervals corresponding to the pH medium (from 0–120 min for pH 1.2, from 120–360 min for pH 8 and from 1440–7200 min for pH 6.5).

RESULTS AND DISCUSSION

Optimization of beeswax microspheres

In order to obtain the ideal combination of morphology, encapsulation efficiency and yield, some process parameters, *i.e.*, drug:beeswax ratio, stirring speed (*N*, rpm) and external phase pH was studied, and in these experiments PVA is used as surfactant and its concentration was also varied. As shown in Table I, using a drug:beeswax ratio of 1:4 (D_0 formulation), the droplets clung together and formed aggregates. Consequently, to obtain individualized formulations, the drug concentration is reduced to 1:8 (drug:beeswax) and the effects of both the emulsifier concentration and the stirring speed on the drug entrapment

were studied in two external phases of pH 6.1 and 4. The results showed that using pH 6.1 of the external phase, the obtained microparticles are spherical but the drug entrapment efficiency didn't exceed 42 %; it increased when the PVA concentration was risen to 1.5 % and it decreased when the stirring speed of emulsion is increased. For these formulations (D_1–D_5), the microspheres' size (d_{10}) varied from 94 to 133 μm and is largely affected by the stirring speed. In fact, the particle size decreased when the stirring speed of emulsion increased and the results is in agreement with the inertial break-up theory.[28]

TABLE 1. Composition and physicochemical properties of bee wax microspheres

Code	Drug:pol. ratio	N rpm	PVA %	pH of external phase	Particles' shape	Drug loading %±*SD*	Entrapment efficiency %±*SD*	d_{10} μm
D_0	1:4	800	1	6.1±0.1	Aggregate	6.5±0.6	32.5±2.9	122.2
D_1	1:8	800	0.5	6.1±0.1	Spherical	2.3±0.4	20.9±4.1	100.8
D_2	1:8	800	1	6.1±0.1	Spherical	4.1±1.1	37.2±10.3	133.0
D_3	1:8	800	1.5	6.1±0.1	Spherical	4.6±0.5	41.7±4.6	124.0
D_4	1:8	800	2	6.1±0.1	Spherical	3.4±0.4	30.7±4.1	131.9
D_5	1:8	1000	1	6.1±0.1	Spherical	2.4±0.2	21.5±2.2	94.1
D_6	1:8	800	0.5	4.0±0.1	Spherical	2.6±0.2	23.1±2.3	106.2
D_7	1:8	800	1	4.0±0.1	Spherical	5.2±0.1	.471±0.9	139.0
D_8	1:8	800	1.5	4.0±0.1	Spherical	5.2±0.5	47.3±4.7	129.8
D_9	1:8	800	2	4.0±0.1	Spherical	3.6±0.6	32.7±5.7	133.7

In order to improve the drug encapsulation, the beeswax solution was emulsified in an external phase with a lower pH (pH 4) where mesalamine was less soluble.[29] Indeed, the spherical microparticles were obtained and a highest encapsulation efficiency of 47.3 % was obtained for D_8 formulation. On the basis of these experimental results, D_8 experimental conditions were subsequently maintained for the preparation of another formulations where the emulsifier nature was varied as following.

HLB value effect on loaded beeswax microspheres properties

An attention was drawn on the surfactant effect, in fact, it had been proved that the surfactant nature can affect the drug transfer in the external phase and so the drug entrapment.[30] Really, surfactants are agents that reduce the surface tension or interfacial tension, and these excipients can be added in drug formulation especially to improve the drug solubility.[31,32] It was reported that surfactants having HLB (hydrophilic–lipophilic balance) values higher than 15 were best solubilising agents.[33] So, Span 80 was selected and used to reduce the HLB value and consequently to reduce the drug solubility in the aqueous phase.

For the purpose, new formulations (D_{10} and D_{11}) were prepared using Tween 80 (HLB_A = 15) as hydrophilic surfactant and a mixture of Tween 80

(HLB_A = 15) and Span 80 (HLB_B = 4.3) as lipophilic surfactant (Table II). The *HLB* value of the surfactant mixture was set to 9; this value of *HLB* is required for the lipid phase such as beeswax to form stable emulsions.[34] The surfactant ratio is determined according to the following theoretical calculation:[35]

$$A = \frac{100(9 - HLB_B)}{HLB_A - HLB_B} \quad (5)$$

The results as shown in Table II are promising, in other words the drug entrapment efficiency was successfully increased using the surfactant mixture; indeed, the drug entrapment efficiency in formulation D_{11} reached 86 %, in this case the HLB value is lower and the lipophilic character of emulsifier mixture may prevent the drug loss. However, the use of Tween 80 alone has led to the decrease of drug entrapment.

TABLE II. Effect of surfactant on bee wax microspheres properties

Code	Emulsifier nature	*HLB* value	Drug loading %±*SD*	Entrapment efficiency %±*SD*	d_{10} / µm
D_8	PVA	18	5.2±0.5	47.3±4.7	129.8
D_{10}	Tween 80	15	4.7±0.8	42.3±7.5	70.2
D_{11}	(Span 80 +Tween 80)	9	9.6±0.9	86.2±8.1	91.6

Regarding the particles' size, using Tween 80, the microsphere size clearly decreased compared to PVA. In fact, the *HLB* value has a significant effect on the droplet size,[36] the same results are obtained by Kim and Cho[36] where small droplets are obtained at *HLB* value between 13.5 and 14.5. While the microparticles' size increased when the mixture Tween 80:Span 80 is used as remarked by Kim and Cho,[36] the size droplet increased when *HLB* value was lower than 13.

Double-walled microspheres' characteristics

The experimental conditions of batch D_{11} gave the most desired results with the highest encapsulation efficiency of 86.2 % and the suitable spherical particles, so they are chosen for the second coating process. Ethylcellulose (EC) and cellulose acetate butyrate (CAB) are selected for covering the beeswax microspheres of the D_{11} batch, as described in the Experimental. The results are displayed in Table III.

TABLE III. Double walled microspheres' characteristics

Code	Polymer matrix	Particles morphology	Drug loading %±*SD*	Entrapment efficiency % ±*SD*	d_{10} / µm
F1	EC	Spherical	8.6±0.4	77.9±3.5	144.7
F2	CAB	Spherical aggregates	7.8±0.1	70.6±0.1	131.6

Through this study, actually, the particles' size increased due to the presence of the second wall but a difference is noticed between the two polymeric coats. The microspheres coated by EC are more spherical and larger than those obtained by CAB. The double coating process induced a loss of drug entrapment of 1 and 1.8 % for EC and CAB, respectively. The lower loss can be related to the higher viscosity of EC organic phase which can limit the drug migration to the external phase.[37,38] We concluded that the EC–beeswax formulations called F1 gave the best results, *i.e.*, the spherical microparticles with the uppermost drug entrapment.

Microparticles' characterization

Infrared spectroscopy analysis is performed to identify the interaction between mesalamine and coating polymers. So, FT-IR spectra of the individual constituents and microparticles are acquired as shown in Fig. 1. The infrared spectrum of pure mesalamine displayed characteristic bands[39,40] like C–N stretching vibration at 1262 cm^{-1}, the bending vibration of N–H at 1616 cm^{-1}, C=O of acrylic acid stretching vibration at 1645 cm^{-1} and a large band between 2500–3300 cm^{-1} which corresponds to the stretching vibration of O–H of acid bond and NH_2 group, and C–H bond of the aromatic group at 807–833 cm^{-1}.

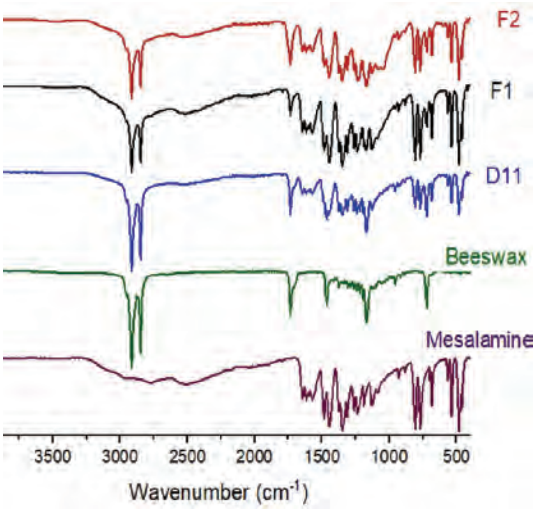

Fig. 1. Infrared spectra of mesalamine, beeswax and formulations (F1, F2 and D_{11}).

The beeswax spectrum showed alkanes adsorption bands assigned to C–H stretching at 2954 and 2848 cm^{-1}, C–H bend or scissoring at 1472 cm^{-1}; and CH_2 rocking seen in long-chain alkanes (718 cm^{-1}). The sharp band observed at 1736 cm^{-1} is attributed to the carbonyls in the ester linkages between the fatty acids and glycerol backbone.[41]

All absorption bands of mesalamine and beeswax are observed in the infrared spectrum of microparticles as shown for D_{11} in Fig. 1, which confirms

the actual mesalamine loading and also the absence of chemical interactions between the components during the formulation process.

In addition to the bands already distinguished in D_{11} spectrum, the FT-IR spectra of double walled formulation, *i.e.*, F1 and F2 showed a small absorption at 1056 cm^{-1}, which can correspond to the glycosidic C–O–C vibration band of cellulose.

Beeswax X-ray diffractogram (Fig. 2) displayed sharp and intense peaks at 2θ 22.1 and 24.51° in addition to weaker peaks at 2θ 19.98 and 36.7°. The mesalamine pattern showed a range of intense peaks at 2θ 8, 15.6 and 17.1° and other weak peaks between 23.1 and 48.9° confirming crystalline forms of beeswax and mesalamine. An important diminution of the mesalamine peak intensity is observed in the XRD pattern of microparticles, indicating a reduced drug crystallinity after the process formulation. Beeswax XRD peaks remained virtually unchanged. It has been also seen that mesalamine loses its crystallinity when it is loaded in PLGA nanoparticles.[42]

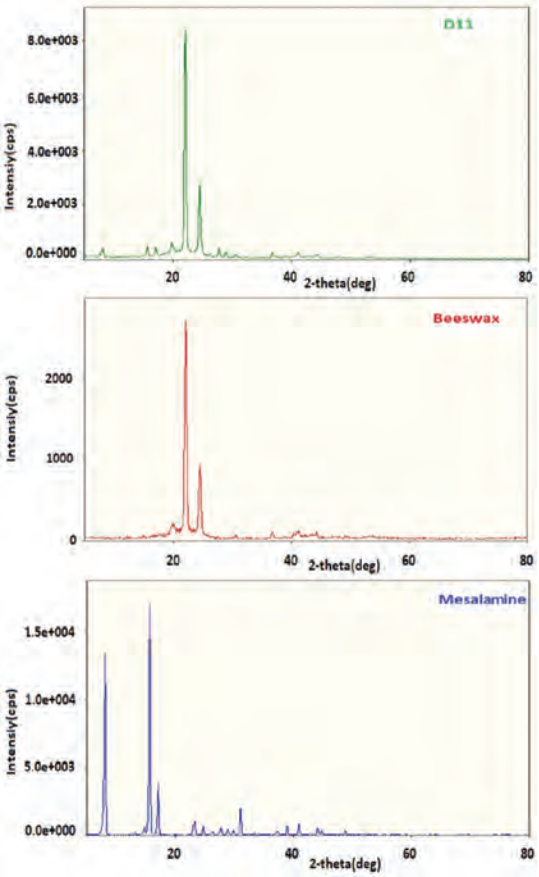

Fig 2. X-ray diffractograms of beeswax, mesalamine and microparticles of D_{11}.

Microscopic observation of the lots D_8, D_{10}, D_{11} and F1, as shown in Fig. 3, revealed spherical shape of microparticles. The surface of beeswax microspheres and the double walled microspheres appeared in SEM micrographs (Fig. 4) with rough and spotted state. The surface of the double walled microparticles is different from that simple beeswax microspheres; EC gave rise to an uniform external layer, as remarked in the case of F_1batch.

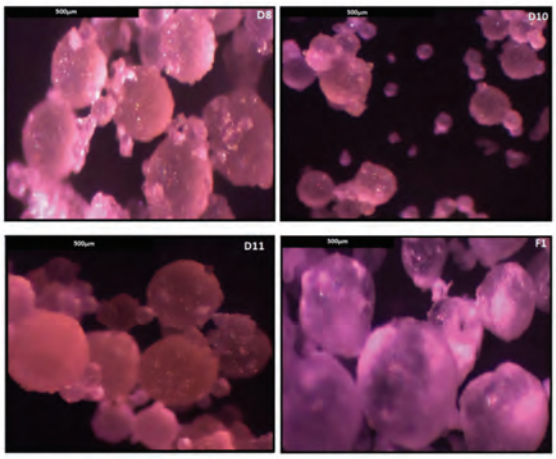

Fig. 3. Optical microscopy images of microparticles of lots D_8, D_{10}, D_{11} and F1.

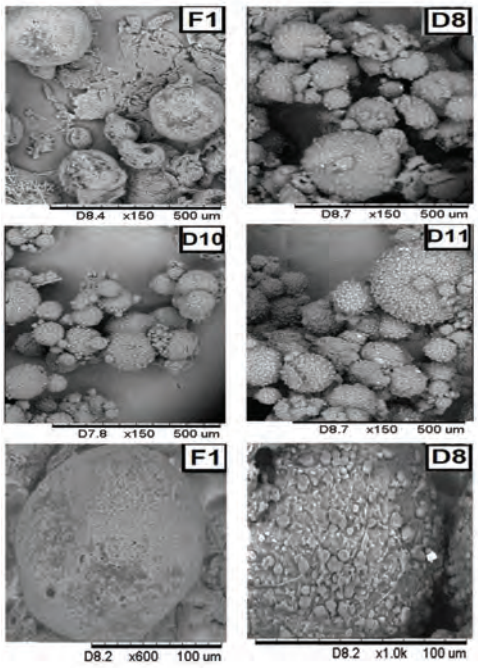

Fig. 4. SEM micrographs of microparticles of lots D_8, D_{10}, D_{11} and F1.

In-vitro *drug release studies*

The drug release is carried out in three selected simulated digestive liquids with pH 1.2, 6.5 and 8. The mesalamine release profiles of D_8, D_{10}, D_{11} beeswax lots and F1 and F2 double walled beeswax microspheres are given in Fig. 5. It is well distinguished that in the acidic medium (pH 1.2), the drug is discharged from simple beeswax formulations (D_8, D_{10}, D_{11}) and is not discharged by double walled microspheres F1and F2. In pH 8, the drug release began slightly in F1 and F2 formulations and increased in pH 6.5.

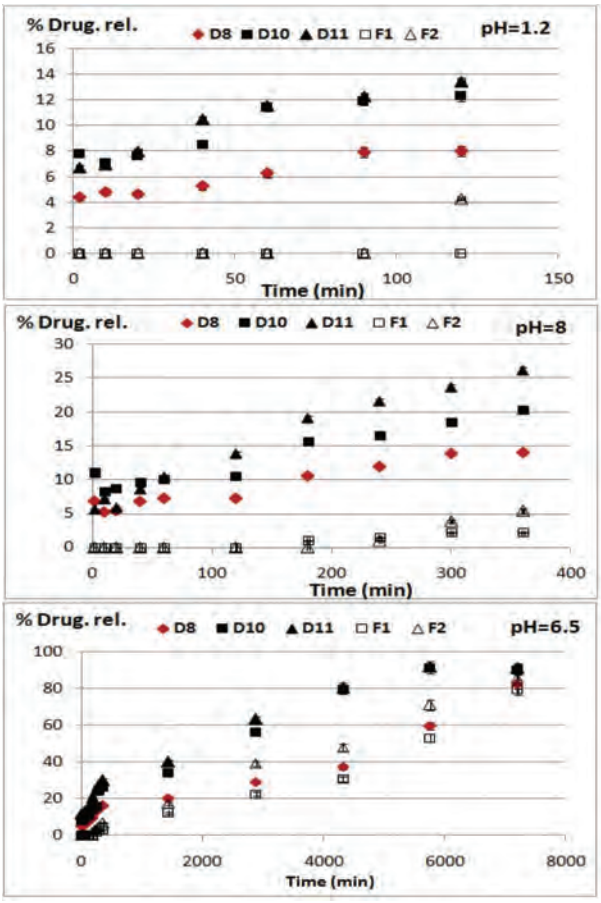

Fig. 5. Drug release profiles of mesalamine from single beeswax and double walled beeswax microparticles in simulated liquids (pH 1.2, 8 and 6.5).

The release data are summarized in Table IV. The percentage of mesalamine released from the formulations D_8, D_{10} and D_{11} and detected in the acidic medium (pH 1.2) after 120 min of release time varied from 8 to 13.5 %. How-

ever, for the double walled microparticles of F1, the drug release didn't occur during 120 min of contact time. In the simulated small bowel liquid (pH 8) and after 6 h of contact time, the drug release varied from 14 to 26 % and from 2.1 to 5.4 % for simple beeswax formulations (D_8, D_{10}, D_{11}) and double coated formulations (F1 and F2), respectively. Finally, in the colon simulated liquid where pH 6.5 and after 96 h (4 days) of contact time, the % of drug release for D_8 and F1 didn't exceed 60 % and for D_{10} and D_{11} reached 91 % and remained at 70 % for F2 microspheres.

TABLE IV. Mesalamine release data in simulated gastric (pH 1.2), small bowel (pH 8) and colon (pH 6.5) liquids

Formulation	pH	Drug rel., %	Korsmeyer–Pepas model			
			Time interval, min	K	n	R^2
D8	1.2	7.9	0–120	0.024	0. 23	0.843
	8	14.0	120–360	0.004	0.61	0.950
	6.5	59.3	1440–7200	0.001	0.73	0.932
D10	1.2	12.3	0–120	0.037	0.25	0.918
	8	20.2	120–360	0.008	0.55	0.932
	6.5	90.6	1440–7200	0.003	0.64	0.964
D11	1.2	13.4	0–120	0.052	0.18	0,879
	8	26.1	120–360	0.010	0.55	0.977
	6.5	91.6	1440–7200	0.008	0.54	0.963
F1	1.2	0	0–120	–	–	–
	8	2.1	120–360	–	–	–
	6.5	52.9	1440–7200	$3\ 10^{-5}$	1.12	0.959
F2	1.2	4.2	0–120	–	–	–
	8	5.4	120–360	–	–	–
	6.5	70.7	1440–7200	1510^{-5}	0.97	0.987

In summary, the mesalamine is slowly discharged from D_8 microparticles which are prepared using PVA as emulsifier, in contrary to D_{10} and D_{11} beeswax microspheres, that are prepared using Tween 80 and a mixture of Tween 80 and Span 80. So, D_8 beeswax microparticles can be used for sustained and prolonged drug release. The results can be related to the microparticles' size, since it is known that the smaller particle size results in an increase of dissolution because the contact surface area is increased;[43] in fact, the D8 microparticles' size is higher than those of D_{10} and D_{11} and then it causes a slowly drug dissolving and release.

Regarding the bi-layered beeswax microparticles F1 and F2, these devices exhibited a delayed release effect in simulated gastric media due to the acid resistance of the outer enteric coating layer,[5,44] so they can be considered as colon-specific delivery systems. In fact, the coating using pH-sensitive polymers or

biodegradables matrices, such as polysaccharides, provides delayed release and protects the active drug from gastric fluid.[45].

In addition, the results showed that the percentages of drug released in the first eight hours, *i.e.*, before reaching the simulated colon region are 22, 33 and 50 % for D_8, D_{10} and D_{11} formulations, respectively. It didn't exceed 10 % for the F2 double coated microparticles and is lower than 3% for F1 microparticles.

Release data analysis

In order to identify the drug dissolution mechanism through beeswax and double coated beeswax microparticles in each release medium, the Korsmeyers––Peppas model was tested. This model is developed to analyse both Fickian and non-Fickian release of drug from swelling or non-swelling polymeric delivery systems. As reported in Table IV, the release data are fitted according to the selected model in the appropriate time intervals which are specified in Table IV. In the semi-empirical model of Korsmeyer–Peppas (Eq. (4)), the exponent of time (n) is related to the drug release mechanism. So, n-values are indicative for diffusion or relaxation/erosion-controlled drug release. In one hand, the limit values of n depend on the dosage form geometry; it is equal to 0.50, 0.45 and 0.43 for slabs, cylinders and spheres, respectively. In the other hand, this limit is also dependent on the width of spherical polymeric particles' size distribution.[46] If we consider the spherical geometry, when $n = 0.43$, the release mechanism is controlled by Fick's diffusion. When $0.43 < n < 0.85$, the drug release mechanism is related to non-Fick's diffusion or anomalous transport. When $n = 0.85$, the drug release mechanism is governed by Case-II transport.[47] It is also reported that when $n > 0.85$, the release mechanism belongs in matrix erosion or relaxation and generally when the exponent $n < 0.5$, the drug release mechanism is related to the quasi-Fickian diffusion model, and the value of $n = 1$ indicates zero order release.[48–50]

So, regarding the mesalamine release from D_8, D_{10} and D_{11} formulations, and for the first two hours corresponding to the retention time in the stomach, the coefficient of regression R^2 of Korsmeyer–Peppas model varied between 0.843––0.918 (Table IV). On the basis of n-values of Korsmeyer–Pepas equation which are lower than 0.43, the release mechanism can be assumed to be the quasi-Fickian diffusion model, it assumed to non-swellable matrix diffusion.[49] In this step of drug release (pH 1.2), the formulations F1 and F2 didn't discharge the drug.

In the simulated small bowel medium (pH 8), the model is fitted from 120 to 360 min so during the next four hours, and the results showed that R^2 varied from 0.932–0.977 for D_8, D_{10} and D_{11} formulations. However, the value of the Korsmeyer–Pepas exponent, n, is close to 0.55, which belongs to $0.43 < n < 0.85$ demonstrating that the release mechanism corresponds to a non-Fickian or anomalous transport, so that the release mechanism is governed by simultaneously

various phenomena such as diffusion and relaxation.[46,49] Concerning the double coated microparticles of F1 and F2, the experimental data are not sufficient to apply the mathematical model.

Finally, in the colon simulated medium (pH 6.5), the model is fitted from the first to fifth day of drug release. The results showed that the mesalamine is discharged in this medium from all formulations. For the beeswax microparticles, the coefficient R^2 of Korsmeyer–Pepas model varied from 0.932–0.964 and the n exponent varied from 0.54 to 0.73, indicating that the drug release is also anomalous and is governed by a non-Fick's transport. About the double walled formulations (F1 and F2), the release data are well fitted according to the Korsmeyer–Pepas model (R^2 0.959–0.987) and the values of the exponent n are 1.12 and 0.97 for F1 and F2, respectively, so they can be considered as close to unit, in this case, the release mechanism is controlled by Case II transport or zero order release. The obtained release profiles obviously indicate that the drug release is actually delayed using these new formulations.

CONCLUSION

The objective of this work is to develop colon specific drug delivery systems that use natural materials and should be capable to deliver the most drug quantity in colon region. Really, beeswax is chosen as matrix for mesalamine drug formulation and successful results are being recorded. The optimization of the microencapsulation process by varying some parameters such as drug:beeswax ratio, emulsifier concentration and nature, and the stirring speed of emulsion permitted to allow spherical microparticles, with a drug entrapment efficiency varying from 42 to 86 %. The D_8 bath of microparticles offered a slow and prolonged drug release which became faster in simulated colon liquid. In addition, bi-layered microparticles which are prepared using cellulose derivatives, *i.e.*, ethylcellulose and cellulose acetate butyrate are promising, in fact, the drug release didn't occur in acidic medium from these new devices. The drug release mechanism is related to the quasi-Fickian diffusion model in acidic medium (pH 1.2), to a non-Fick's transport in the simulated small bowel medium (pH 8) and in the colon simulated medium (pH 6.5), it is assumed to a non-Fick's transport for beeswax formulations and controlled by Case II transport or zero order release for the double coated microparticles. In conclusion, this bi-layer coating methodology can successfully be applied to produce delayed and especially colon specific drug release formulations.

Acknowledgements. The authors thank the following institutions: "Ministère de l'enseignement supérieur et de la recherche scientifique" and "Direction Générale de la Recherche Scientifique et du Développement Technologique" of Algeria for supporting the doctorate project and for SNDL documentation database.

ИЗВОД

ПРИПРЕМА И *IN VITRO* ЕВАЛУАЦИЈА ЈЕДНОСЛОЈНИХ И ДВОСЛОЈНИХ МИКРОЧЕСТИЦА НА БАЗИ ПЧЕЛИЊЕГ ВОСКА ЗА КОЛОН-СПЕЦИФИЧНУ ДОСТАВУ МЕСАЛАМИНА

RYM BRAHMI[1], KHEIRA DIAF[1], ZINEB ELBAHRI[2] и MILAD BAITICHE[3]

[1]Laboratory of Macromolecular and Physical Organic Chemistry, Faculty of Exact Sciences, Djillali Liabes University of Sidi Bel Abbes, 22000 Algeria, [2]Laboratory of Materials and Catalysis, Faculty of Exact Sciences, Djillali Liabes University of Sidi Bel Abbes, Algeria и [3]Laboratory of Preparation, Modification and Applications of Multiphase Polymeric Materials, Department of Process Engineering, The Faculty of Technology of Ferhat Abbas University of Setif, Algeria

Пчелињи восак је одабран као природни материјал за облагање ради у циљу нових система за доставу и контролисано отпуштање лекова специфичних за колон, уз додатак месаламина. У првом кораку, припремљене су микрочестице пчелињег воска коришћењем поступка микроинкапсулације топљењем, где је вариран однос лек:пчелињи восак, брзина мешања, концентрација емулгатора и pH спољне фазе ради оптимизације задржавања лека и морфологије микрочестица. Такође је разматран утицај природе емулгатора праћењем вредности хидрофилно–липофилног баланса (*HLB*). У другом кораку, како би се добили системи за одложено отпуштање лека, израђене су двослојне микросфере поступком испаравања растварача уз употребу етилцелулозе и ацетилбутирата целулозе као спољног слоја за облагање. Све формулације су окарактерисане инфрацрвеном спектроскопијом, рендгенском дифракционом анализом, скенирајућом електронском микроскопијом и оптичком микроскопијом. Ослобађање лека је испитивано у симулираним течностима желуца, танког црева и дебелог црева, а механизам ослобађања је разматран применом Korsmeyer–Peppas модела.

(Примљено 1. маја, ревидирано 17. јула, прихваћено 20. новембра 2023)

REFERENCES

1. A.K. Dash, Mesalamine, in *Analytical Profiles of Drug Substances and Excipients*, Brittain Harry G, Ed., Academic Press, Cambridge, MA, 1998, pp. 209–242 (https://www.elsevier.com/books/analytical-profiles-of-drug-substances-and-excipients/brittain/978-0-12-260825-4)
2. M. Ham, A. C. Moss, *Expert Rev. Clin. Pharmacol*. **5** (2012) 113 (https://doi.org/10.1586/ecp.12.2)
3. A. H. Teruel, I. G. Alvarez, M. Bermejo, V. Merino, M. D. Marcos, F. Sancenon, M. Alvarez, R. M. Mañez, *Int. J. Mol. Sci.* **21** (2020) 6502 (https://doi.org/10.3390/ijms21186502)
4. S. Hua, *Front. Pharmacol.* **11** (2020) 524 (https://doi.org/10.3389/fphar.2020.00524)
5. A. K. Philip, B.Philip, *Oman Med. J.* **25** (2010) 79 (https://doi.org/10.5001/omj.2010.24)
6. R. Katta, D. Raja, S. Bharath, B. B.V. Raj, *Int. J. App. Pharm.* **9** (2017) 1 (https://doi.org/10.22159/ijap.2017v9i4.17326)
7. I. R. Wilding, S. S. Davis, M. Bakhshaee, H. N. Stevens, R. A. Sparrow, J. Brennan, *J. Pharm. Res.* **9** (1992) 654 (https://doi.org/10.1023/a:1015806211556)
8. B. S. Souza, H. R. Marcelino, F. Alexandrino, S. C. C. Urtiga, K. C. H. Silva, D. C. F. Soares, E. S. T. Egito, *Appl. Sci.* **9** *(*2019) 3519 (https://doi.org/10.3390/app9173519)
9. A. El Kaoutari, F. Armougom, D. Raoult, B. Henrissat, *Med. Sci. (Paris)* **30** (2014) 259 (https://doi.org/10.1051/medsci/20143003013)

10. S. L. Kosaraju, *Crit. Rev. Food. Sci. Nutr.* **45** (2005) 251 (https://doi.org/10.1080/10408690490478091)
11. Y. Karrout, C. Neut, D. Wils, F. Siepmann, L. Deremaux, M.-P. Flament, L. Dubreuil, P. Desreumaux, J. Siepmann, *Eur. J. Pharm. Sci.* **37** (2009) 427 (https://doi.org/10.1016/j.ejps.2009.03.014)
12. L. Jin, Y-C. Ding, Y. Zhang, X-Q. Xu, Q. Cao, *Drug Des. Devel. Ther.* **10** (2016) 2021 (https://doi.org/10.2147/DDDT.S107283)
13. A. P. Tulloch, *Bee World* **61** (1980) 47 (https://doi.org/10.1080/0005772x.1980.11097776)
14. F. Fratini, G. Cilia, A. Turchi, A. Felicioli, *Asian Pac. J. Trop. Med.* **9** (2016) 839 (https://doi.org/10.1016/j.apjtm.2016.07.003)
15. M. Ranjha, H. Khan, S. Naseem, *J. Mater. Sci.: Mater. Med.* **21** (2010) 1621 (https://doi.org/10.1007/s10856-010-4034-4)
16. D.V. Gowda, M. Manjunatha, V. Balmurlidhara, S. Mohammed Khan, *Pharm. Lettre* **2** (2010) 232 (https://www.scholarsresearchlibrary.com/articles/study-on-encapsulation-of-ranolazine-in-bees-wax-microspherespreparation-characterization-and-release-kinetics-ofmicrosp.pdf)
17. V. Subha, W. Arulsha, S. Kirubanandan, S. Renganathan. *MOJ Drug. Des. Develop. Ther.* **2** (2018) 156 (https://doi.org/10.15406/mojddt.2018.02.00042)
18. N. A. Elechi, H. C. Mital, *Int. J. Pharm. Sci. Res.* **3** (2012) 1632 (http://dx.doi.org/10.13040/IJPSR.0975-8232.3(6).1632-36)
19. C. O. Nnadi, A. A. Attama, L. O. Ugwu, *Int. J. Res. Med. Health Sci.* **1** (2013) 31 (https://www.ijsk.org/uploads/3/1/1/7/3117743/3_design_and_evaluation_of_sustained_release_potential_of_diclofenac_potassium_contained_in_beeswax_matrix.pdf)
20. A. G. Press, I. A. Hauptmann, L. Hauptmann, B. Fuchs, M. Fuchs, K. Ewe, G. Ramadori, *Aliment. Pharmacol. Ther.* **12** (1998) 673. (http://dx.doi.org/10.1046/j.1365-2036.1998.00358.x)
21. S. Nugent, D. Kumar, D. Rampton, D. Evans, *Gut* **48** (2001) 571 (http://dx.doi.org/10.1136/gut.48.4.571)
22. A. Newton, N. Kumar, *Interdiscip. J. Microinflammation* **1** (2014) 1 (https://www.omicsonline.org/open-access-pdfs/ibd-impact-of-colonic-ph-onset-of-action-and-other-factors-in-modern-therapeutic-approach-ijm.1000116.pdf)
23. J. Fallingborg, P. Pedersen, B.A. Jacobsen, *Dig. Dis. Sci.* **43** (1998) 702 (http://dx.doi.org/10.1023/a:1018893409596)
24. A. Gokhale, *Pharm. Technol. Eur.* **26** (2014) 38 (https://www.researchgate.net/publication/285996771_Achieving_zero-order_release_kinetics_using_multi-step_diffusion-based_drug_delivery)
25. S. Dash, P. N. Murthy, L. Nath, P. Chowdhury, *Acta Pol. Pharm.* **67** (2010) 217 (https://www.ptfarm.pl/pub/File/Acta_Poloniae/2010/3/217.pdf)
26. M. Paarakh, P. Ani Jose, C. M. Setty, G. V. Peter, *I. J. P. R. T.* **8** (2018) 12 (https://www.ijprt.org/index.php/pub/article/view/85/82)
27. R. Gouda, H. Baishya, Q. Zhao, *J. Develop. Drugs* **6** (2017) 1 (http://dx.doi.org/10.4172/2329-6631.1000171)
28. J. O. Hinze, *AIChE J.* **1** (1955) 289 (http://dx.doi.org/10.1002/AIC.690010303)
29. D. L. French, J.W. Mauger *Pharm. Res.* **10** (1993) 1285 (https://doi.org/10.1023/A:1018909527659)
30. R. Dinarvand, S. H. Moghadam, A. Sheikhi, F. Atyabi, *J. Microencapsul.* **22** (2005) 139 (https://doi.org/10.1080/02652040400026392)

31. A. Müllertz, A. Ogbonna, S. Ren, T. Rades, *J. Pharm. Pharmacol.* **62** (2010) 1622 (http://dx.doi.org/10.1111/j.2042-7158.2010.01107.x.)
32. A. Hassan Al-Hmoud, E. Ibrahim Nasser, E. I. El-Hallous, *Afr. J. Pharm. Pharmacol.* **8** (2014) 364 (https://academicjournals.org/journal/AJPP/article-full-text-pdf/725A2B243946)
33. R. B. Pedada, E. Vanka, A.M.S. Sudhakar Babu, PK. Desu, PR. Bharathi, PV. Rao, *PharmaTutor* **1** (2013) 60 (https://www.pharmatutor.org/pdf_download/pdf/1(2)-enhancement-of-solubility-an-over-view.pdf)
34. A. K. Hassan *J. Pharm. Sci*. **80** (2018) 334 (http://dx.doi.org/10.4172/pharmaceutical-sciences.1000362)
35. *The HLB System: A Time-Saving Guide To Emulsifier Selection*, rev. ed., ICI Americas,Wilmington, DE, 1984, pp.5–6 (http://www.scientificspectator.com/documents/personal%20care%20spectator/The%20HLB%20Book%20ICI.pdf)
36. E. Kim, W. G. Cho, *J. Korean Appl. Sci. Technol.* **31** (2014) 203 (http://dx.doi.org/10.12925/jkocs.2014.31.2.203)
37. S. A. Nour, N. S. Abdelmalak, M. J. Naguib, *Drug Deliv.* **22** (2015) 286 (https://doi.org/10.3109/10717544.2014.889779)
38. W. M. Obeidat, J. C. Price, *J. Microencapsul.* **20** (2003) 57 (https://doi.org/10.1080/0265204021000022716)
39. D. Kaushik, K. Sharma, S. Sardana, *Indian J. Pharm. Educ. Res.* **50** (2016) S106 (https://www.ijper.org/article/420)
40. W. Banabid, F. Djerboua, A. Maiza, Z. ElBahri, M. Baitiche, *Indian J. Pharm. Educ.* **51** (2017) S46 (http://dx.doi.org/10.5530/ijper.51.2s.49)
41. A. Bucio, R. Moreno-Tovar, L. Bucio, J. Espinosa-Dávila, F. Anguebes-Franceschi, *Coatings* **11** (2021) 261 (https://doi.org/10.3390/coatings11030261)
42. N. M. Mahajan, DR. D. M. Sakarkar, A. S. Manmode, *Int. J. Pharm. Pharmacol. Sci.* **3** (2011) 208 (https://innovareacademics.in/journal/ijpps/Vol3Issue4/2581.pdf)
43. A M. Hillery, A.W. Lloyd, J. Swarbrick, *Drug Delivery and Targeting for Pharmacists and Pharmaceutical Scientists*, ISBN 0-203-34655-6 (Adobe eReader Format), Taylor & Francis e-Library, 2005 (https://doi.org/10.1201/b12801)
44. A. Gazzaniga, P. Iamartino, G. Maffione, M. E. Sangalli, *Int. J. Pharmaceutics* **108** (1994) 77 (https://doi.org/10.1016/0378-5173(94)90418-9)
45. M. K. Chourasia, S. K. Jain, *J. Pharm. Pharmaceut. Sci.* **6** (2003) 33 (https://sites.ualberta.ca/~csps/JPPS6(1)/S.Chourasia/colon.pdf)
46. P. L. Ritger, N. A. Peppas, *J. Controlled Rel.* **5** (1987) 23 (https://doi.org/10.1016/0168-3659(87)90034-4)
47. J. Siepmann, N A. Peppas, *Int. J. Pharm.* **418** (2011) 6 (https://doi.org/10.1016/j.ijpharm.2011.03.051)
48. M. Thakare, B. Israel, S. T. Garner, H. Ahmed, P. Garner, D. Elder, J. C. Price, and A. C. Capomacchia, *Pharm. Dev. Technol.* **18** (2013) 1213 (https://doi.org/10.3109/10837450.2011.620969)
49. A. G. Prasanth, A. S. Kumar, B. S. Shruthi, S. Subramanian, *Mater. Res. Express* **6** (2019) 125427 (https://doi.org/10.1088/2053-1591/ab5811)
50. M. Padmaa Paarakh, P. A. Jose, C. M. Setty, G. V. Peter Christopher, *Int. J. Pharm. Res. Technol. (IJPRT)* **8** (2018) 12 (https://ijprt.org/index.php/pub/article/view/85/82).

Journal of the Serbian Chemical Society
JSCS@tmf.bg.ac.rs • www.shd.org.rs/JSCS

J. Serb. Chem. Soc. *89* (1) 107–121 (2024)
JSCS–5709

Original scientific paper
Published 12 February 2023

Deep eutectic solvents formed by pharmaceutical ingredients and their potential influences on solid preparations

SARA TOUFOUKI[1], AHMAD ALI[1], YOUMO WANG[1], RUI LI[1], YU CAO[2]* and SHUN YAO[1]**

[1]*School of Chemical Engineering, Sichuan University, Chengdu, 610065, China and* [2]*College of Life Science & Biotechnology, Mianyang Normal University, Mianyang. 621000, China*

(Received 25 August, revised 22 September, accepted 20 December 2023)

Abstract: Some active pharmaceutical ingredients (APIs) and excipients can form deep eutectic solvents (DESs), which will lead to severe defects in solid preparations. This work first prepared related typical DESs by mixing APIs and excipients from marketable drugs. Then two different types of the binary eutectic mixtures were investigated, which were composed of menthol (HBD) and citric acid (HBA), ME/CA, as well as phenyl salicylate (HBA) and benzoic acid (HBD), Salol/BA. These binary mixtures were applied to investigate their possible effects on capsules and tablets, which could be liquefaction or the stickiness of the solid formulations. The comprehensive characterizations and studies on phase behaviours of the binary mixtures were carried out, and the spectral analysis confirmed the formation of the eutectic liquids from individual components. Furthermore, the binary mixtures have increased the tablet strength when increasing the compression force, leading to the stickiness of powders during pressing. Moreover, the capsules were softened by the existence of DESs. After morphological observation and quantitative analysis, the corresponding suggestions and countermeasures were provided in the conclusions.

Keywords: excipients; marketable drugs; binary mixtures; phase behaviours.

INTRODUCTION

Deep eutectic refers to the phenomenon of wetting or liquefaction after mixing two or more substances. Sometimes it can be used, but occasionally it adversely affects the products.[1] The resulting deep eutectic solvents (DES) or deep eutectic liquids (DEL) have attracted considerable attention recently, which correspond to a broad class of low melting temperature liquids that are composed of at least two substances with H-bonds, mainly a hydrogen bond acceptor (HBA) and a hydrogen bond donor (HBD).[2] These eutectic liquids are generally featured

*,** Corresponding authors. E-mail: (*)cusack@scu.edu.cn, (**)agnes_cy2004@163.com
https://doi.org/10.2298/JSC230825099T

by strong solubility, biodegradability, a wide range of polarity, high thermochemical stability, water compatibility and a negligible toxicity profile.[3] Moreover, H-bonds play an essential role in their properties (*e.g.*, melting point, density, viscosity, *etc*.), which can be revealed by infrared and nuclear magnetic resonance spectroscopy.[4] Besides that, some possible reactions occurring between two kinds of solids also attract attention from researchers and some key mechanisms are being continuously explored.[5,6]

The breakthroughs achieved in green solvents promote the emergence of therapeutic deep eutectic solvents (THEDES) or active pharmaceutical ingredient–deep eutectic solvents (API–DESs), and many APIs are HBD for containing amines, carboxylic acids or hydroxyl groups. The most commonly used is menthol, which can be combined with coenzyme Q10, borneol, paeonol, ibuprofen, aspirin and other APIs to form DESs.[7–9] Moreover, three kinds of arginine-based THEDES were designed as drug solubilization vehicles for lidocaine;[10] Shekaari *et al.*[11] have successfully prepared a stable ion-gel system containing an anti-cancer drug, 5-fluorouracil, and a choline chloride-ascorbic acid DES. A recent study[12] showed that DESs could play the multiple roles of the solvent, reactant and shape control agent simultaneously. With the increasing application of DES in the pharmaceutical field, many problems that have not been paid attention to before need to be studied; one of them is the effect of DES formation on various solid preparations.

Despite all the promising features of DESs in the pharmaceutical field, there are some potential problems that are related to the formation of eutectic mixtures between APIs or between APIs and excipients upon the manufacturing processes, resulting in incompatibilities and instability of the final pharmaceutical products. For the solid preparations, the granules can be liquefied, the tablets can be adhered, or the capsules can become soft or leak resulting from deep eutectic phenomena. Sticking on the formed punch is a severe issue in the tablets production process; when it occurs, the tablet machine must be repaired, which is a costly process.[13] In fact, it is known that applying the compression forces causes damage and changes in terms of the drug properties. Moreover, the contact between the APIs and the excipients upon compression facilitates the formation of the eutectic mixtures. Ibuprofen is one of the APIs that is commonly used in tablet preparation. However, when mixed with other drugs or excipients, this component forms a eutectic mixture. Setyawan *et al.*[14] studied the sticking phenomena of ibuprofen–stearic acid due to the formation of the eutectic liquid by the compression forces. This eutectic formation was further confirmed by FTIR, X-ray powder diffraction, scanning electron microscopy and hot-stage microscopy studies. To the best of our knowledge, there are no studies focused on the effect of deep eutectic solvents on solid pharmaceutical preparations. After searching and summarizing for marketable medicines, it has been found that the

mixtures of some ingredients show deep eutectic behaviours and can affect related solid preparations (see Fig. S-1 of the Supplementary material to this paper); however, a part of the DELs was unstable (*e.g.*, the acetaminophen, ibuprofen and salicylic acid series). Racemic menthol, citric acid, phenyl salicylate and benzoic acid are four common components in these medicines (the former two as ingredients in Orofar capsules, Pharma Express, France; the latter two as ingredients in Hyophen tablets, BioComp Pharma, Inc., USA), and there is a chance of using them together. Meanwhile their mixtures can become stable DESs.

EXPERIMENTAL

Chemical reagents and materials

Menthol (99.0 %), citric acid (98.5 %), phenyl salicylate (98 %) and Sudan red were from Aladdin Company (Shanghai, China). Benzoic acid (95.5 %) was obtained from the Fangzheng reagent factory (Tianjin, China). Ethanol (99.5 %), glycerin (99 %), methanol (99 %), choline chloride (99.0 %) and urea (99.5 %) were bought from Kelong Chemicals Inc. (Chengdu, China). Acetone (99.5 %) was purchased from Changlian Chemicals Inc. (Chengdu, China). Deionized water was obtained by a UPH-1-10T water purification system (Chengdu, China). Empty gelatin capsules, glutinous rice capsules, and enteric capsules were obtained from a local drug store.

Formation of DESs

According to the DESs in Fig. S-1, menthol was mixed with citric acid at 150 °C under constant stirring for 2 to 4 h until a homogeneous liquid formed. The mole ratios of the eutectic compositions were found to be 3:1, 4:1, 5: and 6:1 (marked as DES 1–4) for menthol and citric acid. The prepared mixtures were dried under vacuum at 50 °C for 24 h before characterization.

The second kind of DES was prepared by mixing phenyl salicylate and benzoic acid in different molar ratios at 80 °C for 3 h until transparent liquids were obtained. The unsuccessful preparations were also eliminated for further characterization; only the products with mole ratios of 12:1 and 9:1 were liquids at room temperature.

Characterization of DESs

Attenuated total reflection-Fourier transformed infrared spectroscopy (ATR-FTIR) analysis. ATR-FTIR analysis of DESs and their individual components was performed by using a Spectrum Two FTIR spectrometer equipped with ATR (PerkinElmer, Waltham, USA) for liquid samples. For each sample, 32 scans were taken from 4000 to 400 cm^{-1}. Spectra were analyzed using Excel Ms. The results are shown in Fig. S-2 of the Supplementary material. It can be found that the FTIR spectrum of menthol exhibits a series of typical IR absorbance peaks, as illustrated in Fig. S-2A, which includes the stretching modes of the OH at 3255 cm^{-1}, and the C–H at 2959 and 2868 cm^{-1}. The FTIR spectrum of citric acid showed absorption bands at around 3491 cm^{-1} for the free hydroxyl group (–OH) in the molecule, C=O stretching at 1728.30 cm^{-1}, a peak at approximately 1133 cm^{-1} corresponding to the C–OH band, and 786 cm^{-1} attributed to CH_2 stretching. The menthol–citric acid binary mixtures spectrum displays O–H, C–H, C=O, and C–O stretching modes, appearing at around 3600–3230 cm^{-1}, 2958–2846 cm^{-1} and 1711 and 1019 cm^{-1}, respectively. Both representative groups of components were identified, and the O-H stretching band was shifted in the spectra of the prepared binary mixture, which confirms the formation of the eutectic liquid.

Similarly, Fig. S-2B shows the FTIR spectra of the pure components and their binary mixtures of different mole ratios (12:1 and 9:1), the spectrum of benzoic acid exhibits strong broad band around 3300–2500 cm^{-1}, which can be assigned to O–H stretching; the featured band at 1670 cm^{-1} corresponds to carbonyl (C=O) stretching vibration, and the C–O stretching of benzoic acid exists at 1287 cm^{-1}. Salol exhibited O–H bonding at 3400–2900 cm^{-1} and a C=O carbonyl stretching vibration peak at 1687 cm^{-1}. There are also several peaks due to C–O stretching vibrations around 1335–1127 cm^{-1}. The FTIR results of the DESs prepared by salol-benzoic acid further confirm the formation of eutectic solvents. The vibration bands at nearly 3300 to 3000 cm^{-1} refer to the hydroxyl group. The peaks at 1679 cm^{-1} refer to the presence of the C=O carbonyl stretching vibration peak. The peaks at 1330–1125 cm^{-1} are due to C–O stretching vibrations. The FTIR spectra of binary mixtures displayed the main vibration frequencies corresponding to pure components with slight shifts, which supports the formation of a eutectic system. Furthermore, FTIR validated the formation of H bonds between choline chloride and various HBDs by shape changes and shifts in the characteristic absorbance of the specified chemical compounds.

Proton nuclear magnetic resonance analysis. Proton NMR spectra were recorded with an AV II-400 MHz spectrometer (Bruker, Billerica, MA, USA), and the chemical shift data were processed using MestReNova software. The ^{1}H-NMR spectra of menthol, citric acid and the DESs are shown in Fig. S-3A–F of the Supplementary material. All the normal peaks of both pure components appeared in the spectra of the prepared DES with a slight shift, this suggests the formation of the hydrogen bonds between the menthol and citric acid again. The proton NMR analysis of the phenyl salicylate–benzoic acid and its pure components are shown in Fig. S-4A–D of the Supplementary material. The ^{1}H-NMR spectra of the mixtures are almost identical to those of the pure components. Moreover, the chemical shift of the –OH group of phenyl salicylate was slightly shifted from 10.52 to 10.54 ppm; this slight shift of hydrogens of the neat components toward the downfield of the spectra is the evidence of hydrogen bonds forming between phenyl salicylate and benzoic acid.

Phase diagrams. The melting points of the DESs were measured using the generally acknowledged thermometer method. A small amount of each mixture was put in a sample tube attaching to a WRS-1A thermometer (Jiahangbochang Sci. & Tel. Inc., Beijing, China) placed in a heating bath (±0.1 °C), and the temperatures at which the mixtures started to melt and the temperatures at which the mixtures melted completely were recorded. All the experiments were performed in triplicate.

Viscosity. The viscosity of DESs was determined using the NDJ-5S/8S type digital rotary viscosity rotational viscometer (Meiyu Instrumental Inc., Shanghai, China) equipped with a water circulator (±0.1 °C). The heating profile was set at a temperature range from 5 to 35 °C for the menthol–citric acid DESs and 35 to 55 °C for the phenyl salicylate–benzoic acid DESs. All the experiments were performed in triplicate. The viscosity–temperature dependence of the tested DESs can be described in this work using the VTF equation:

$$\eta = A\mathrm{e}^{(B/(T-T_0)} \quad (1)$$

where η is the dynamic viscosity, mPa s; T is the temperature in K; A, B and T_0 are VTF fitting parameters. The fitting parameters of A (mPa s), B (K) and T_0 (K) are tabulated in Table S-I of the Supplementary material along with the fitting coefficient R^2 values. The predicted viscosity values are depicted in Fig. S-5 of the Supplementary material.

Density. The density of the newly synthesized DESs was determined using the pycnometer method. Firstly, the dry flask and stopper were weighed on the analytical balance; sec-

ondly, the pycnometer filled with UP water was also measured using the analytical balance; finally, the pycnometers filled with the prepared eutectic mixtures were measured on the precise analytical balance (±0.0001 g). After determining the weight of each sample, the density was calculated using the following formula:

$$\rho_M = \rho_w \frac{m_M - m_p}{m_w - m_p} \quad (2)$$

where ρ_M is the density of the DESs, g/cm^3; ρ_w is the density of water, g/cm^3; m_M is the mass of the dry pycnometer full of DESs, g; m_p the mass of the dry pycnometer, g; m_w is the mass of the dry pycnometer full of water, g. Each measurement was repeated in triplicate, and the average value was adopted. All the measurements were carried out in a temperature range of 5 to 35 °C for menthol–citric acid DESs and 35 to 55°C for the phenyl salicylate–benzoic acid DESs.

The excess molar volume was determined using the following equation:

$$V_E = V - x_1V_1 - x_2V_2 \quad (3)$$

where V represents the molar volume of the mixture, cm^3/mol; x_1 and x_2 are the mole fraction of component 1 and 2, respectively, and V_1 and V_2 are the molar volume of component 1 and component 2 of the system, respectively, cm^3/mol.

Determination of DESs solubility in different solvents

The saturated solubility of DESs in various solvents, including water, glycerin, ethanol, methanol and acetone, was determined at room temperature according to the appendix of China Pharmacopoeia (2020 edition). The results are provided in Table S-IV of the Supplementary material.

Study of eutectic liquids formed by APIs on capsules

Dissolving test. Three different types of capsules were chosen for the study of the eutectic phenomenon in capsules, including enteric, glutinous rice and gelatin capsules; each type of capsule shell was cut into small pieces, then placed in sample vials that contained 5 ml of the prepared eutectic mixtures based on menthol and citric acid (DES 1–4). Each vial was placed into a temperature-controlled bath at different temperatures (±0.1 °C) with constant stirring (300 rpm). The dissolving process was observed during different periods, namely after 12 and 24 h.

Corrosion test. The eutectic liquids in different molar ratios were mixed with the pigment of Sudan red, which was used to make the corrosion in the capsules easier to notice. Then, each capsule type was loaded with the mixture of the tested eutectic liquid and this red pigment. The filling was in the body part of every capsule, which was closed by putting the top half of the capsule over the bottom and pressing down. Then, the loaded capsules were placed on filter papers in a vertical position in the incubator at 25, 30 and 40 °C for observing the change.

Soften test. Each type of capsule was cut into strips of several mm in length and placed in vials containing DESs of different molar ratios. The capsule shell fragments were kept in the DESs for one day. The tension measurements were carried out by using a ZP-5 type digital force gauge test machine (<0.5 kg, ±0.001 kg, Fuma Electrical Instrument Inc., Dongguan, China). Soften coefficient of the different types of capsules incubated in DESs of different mole ratios, which was calculated using the following equation:

$$\text{Soften coefficient} = 100\frac{\text{Soften data after soften by DES}}{\text{Soften data after soften by DES}} \quad (4)$$

Study of eutectic liquids formed by APIs on tablets

Tablet pressing. For clear observation, the tablets were made of pure components of phenyl salicylate and benzoic acid without any pharmaceutical excipients, as well as the binary mixtures of phenyl salicylate–benzoic acid in the previously known ratios, forming DES mainly in the 12:1 and 9:1 ratios. The powders were mixed in a mortar to homogenize the mixture and then compressed using the HY-12 type tablet pressing machine (Tianguang Optical Instrument Co., Ltd., Tianjin, China) in various compression forces (5, 10, 15, 20 and 25 MPa) and held for 3 min.

Tablet tensile strength. The previously prepared tablets were compressed with different forces and used to measure the tablet tensile strength. Each tablet was measured in thickness and diameter using a digital caliper (±0.01 cm). The hardness of the tablets was measured using the YPD-300d tablet hardness tester (Huanghai Drug Testing Instruments Co., Ltd., Shanghai, China). Tensile strength was determined using the following equation:

$$\sigma = 2F/\pi Dt \quad (5)$$

where σ is tensile strength, N/cm^2; F is tablet hardness, N; D is tablet diameter, cm; T is thickness of the tablet, cm.

Fourier-transform infrared spectroscopy

The powders were mixed with KBr and compressed at 15 MPa using a hydraulic press until a transparent disc was formed. The FTIR spectra were obtained using the spectrophotometer (PerkinElmer, Fermont, USA) in the range of 450–4000 cm^{-1}.

Scanning electron microscopy

The morphology of compressed pure components and binary mixture tablets was observed using JSM-7500F scanning electron microscopy (SEM, 25–800,000×, JEOL, Tokyo, Japan).

RESULTS AND DISCUSSION

In the following study, two different types of deep eutectic systems were investigated, including the binary mixtures of menthol (HBD) and citric acid (HBA), ME/CA, as well as phenyl salicylate (HBA) and benzoic acid (HBD), Salol/BA. Firstly, the formed DESs were identified according to the spectral analysis shown in Figs. S-2–S-4 of the Supplementary material. As we know, to determine the system composition and melting temperature at the eutectic point as well as melting temperature of the system at any specific composition, phase diagram of the eutectic systems, should be known. Thus, a binary phase diagram obtained by measuring the melting points of individual component, *i.e.*, menthol (ME) and citric acid (CA) as well as their binary mixtures, is shown in Fig. 1A. As depicted, the melting temperatures of the system at any examined composition of ME/CA mixture are lower than those of the individual components, forming a single eutectic point at mixture composition of 80 mol % ME and 20 mol % CA. This system is a simple eutectic, with a eutectic temperature of 37.0 °C. In the case of Salol/BA (Fig. 1B) a depression of the melting temperature, similar

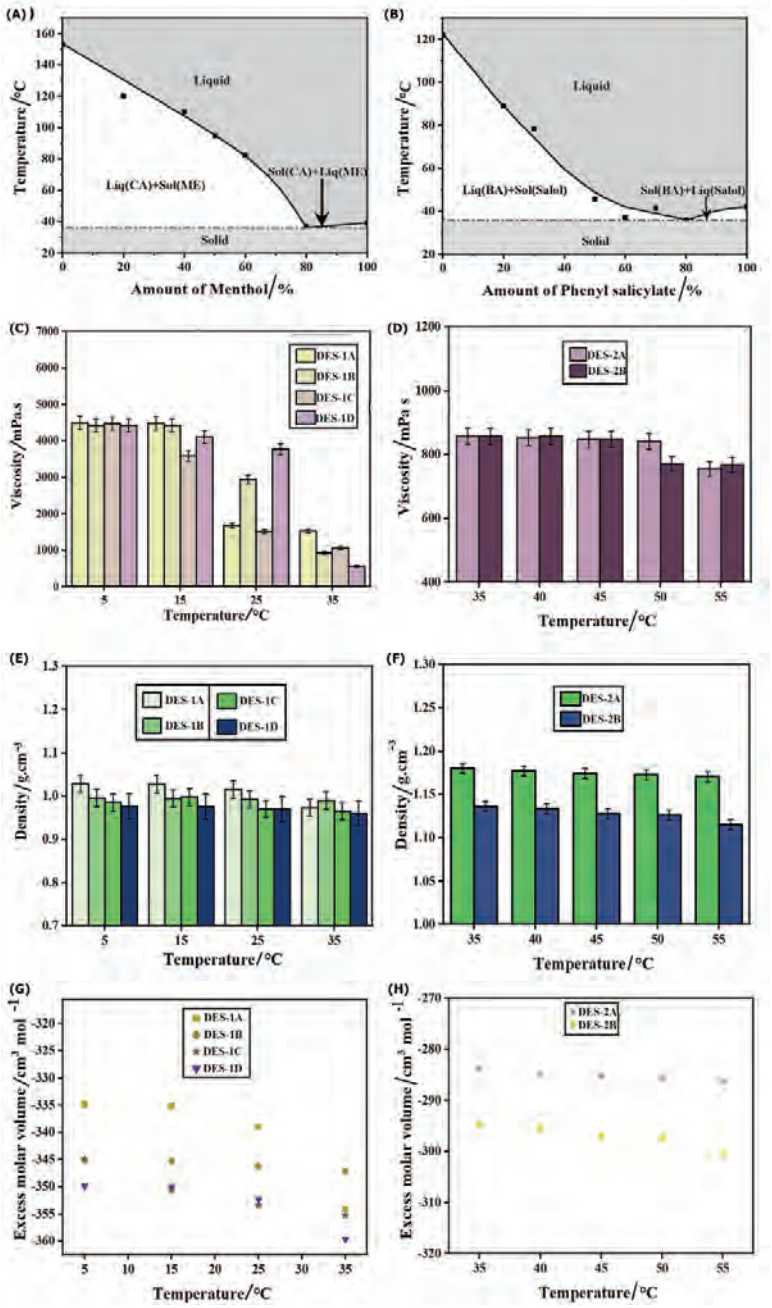

Fig. 1. Phase diagrams of binary mixture: A) menthol/citric acid (ME/CA) and B) phenyl salicylate/benzoic acid (Salol/BA); temperature dependence of: viscosity of: C) DES-1 and D) DES-2, density of: E) DES-1 and F) DES-2, and excess of molar volume of: G) DES-1 and H) DES-2; DES-1 and DES-2 denotes eutectic systems ME/CA and Salol/BA, respectively.

to the first examined system (ME/CA), occurs for 80 mol % Salol and 20 mol % BA (eutectic composition), and melting temperature/point of mixture at eutectic composition is 36.5 °C. This result was consistent with prior investigations[15] that found DESs to have a lower melting temperature than their individual components. The results indicate that they can remain liquid under normal drug production, storage and transportation temperatures (0.0–50.0 °C) once the DESs are formed, thus having a significant impact on the appearance and quality of solid preparations.

Generally, DESs have a higher viscosity than organic solvents, which will make the solid preparations sticky. The viscosity of the DES-1 with different composition of single compounds, *i.e.*, ME/CA mole ratio: 3:1 (DES-1A), 4:1 (DES-1B), 5:1 (DES-1C) and 6:1 (DES-1D) when temperature varied in the range 5.0–35.0 °C, was examined. For the second examined system (DES-2), viscosity was determined for two different composition of single compounds, *i.e.*, Salol/BA mole ratio 12:1 (DES-2A) as well as 9:1 (DES-2B) when temperature varied in the range 35.0–55.0 °C. As shown in Fig. 1C and D, the temperature significantly affects the viscosity of both chemical types of DESs (DES-1 and DES-2) at all DESs eutectic compositions (DES-1A-D and DES-2A-B).The order of decreasing the DESs viscosity was DES-1A > DES-1C > DES-1B > DES-1D. Furthermore, the viscosity of the mixture increases (at a given temperature) as the CA proportion in examined mixtures increases. This was confirmed by Shafie *et al.*, who noticed that increasing the concentration of citric acid in the mixtures led to a high viscosity value.[16]

Density is widely used to evaluate the fluidity and compressibility of particles, which has a significant impact on all aspects of pharmaceutical production. It also helps researchers to understand the liquid behaviours. Likewise, the temperature and liquid composition effects on density. At room temperature, most of the previously studied DESs have densities in the range of 1.0–1.35 g cm^{-3},[17] and are generally higher than those of water.[18] With the temperature increased from 5.0 to 35.0 °C, the density values decreased for DES-1A from 1.028 to 0.9730 g cm^{-3}, DES-1B from 0.9950 to 0.9894 g cm^{-3}, DES-1C from 0.9850 to 0.9651 g cm^{-3}, and for DES-1D from 0.9767 to 0.9600 g cm^{-3} (see Fig. 1E). As is expected, the increase in the citric acid molar ratio in the mixture results in a high density of DESs, which explains why DES-1A has a higher density than the other binary mixtures. This finding is in accordance with Shafie's study, which found that increasing the concentration of citric acid leads to a higher density.[16] As shown in Fig. 1F, the densities of phenyl salicylate–benzoic acid mixtures decreased as the temperature increased from 35.0 to 55.0 °C; it can be clearly noticed that the density of the mixtures increased when the molar ratio of phenyl salicylate to benzoic acid increased from 9:1 to 12:1. Therefore, the temperatures as well as composition of examined DESs are affect its measured density. Fur-

thermore, it was found that as the amount of Salol increases in the mole ratio, the density of DES-Bs decreases. At 25.0 °C, choline chloride–urea DES (as control) has been reported to have densities ranging from 1.0921 to 1.4851 g cm^{-3}, which is higher than the densities of the menthol–citric acid DESs studied here. This is due to the larger molecular size and the polar nature of the choline chloride-based DESs compared to the formed DESs in this study.[18] Overall, at 35.0 °C, the highest density was obtained for molar ratio of Salol to BA of 12:1 (DES-2A), while the lowest density was observed for molar ratio of ME to CA of 6:1 (DES-1D). Commonly, the thermal motion of ions and the increase in free volume increase the coefficient of isobaric expansion as the temperature increases, meanwhile the density becomes lower. Here isobaric thermal expansion coefficients at 35.0 °C for Salol to BA of 12:1 and ME to CA of 6:1 were also investigated and compared here. As the result, 4.91±0.05 K^{-1} (for the former) and 2.78 ± 0.07 K^{-1} (for the latter) were obtained, respectively. It indicates the thermal motion within molecules in DES-1D system was more sensitive to temperature change than in DES-2A.

The excess molar volumes (V_E) of DESs for different molar ratios of single component at different temperatures can be used to understand more about the behaviour of eutectic mixtures; moreover, it can provide information on a solution's non-idealities and the intermolecular interactions. According to the results in Tables S-2 and S3 and Fig. 1G–H, the V_E values were negative for all the DESs-1A–1D. The negative V_E of menthol and citric acid DESs are attributed to their strong interactions, unlike molecular interactions through hydrogen bonding.[19] Therefore, a more efficient packing interaction occurred when the two components were mixed. Furthermore, the V_E values decreased when the concentration of menthol in the mixture increased, which indicates that the mole ratios have an effect on the excess molar volume and that the concentration of menthol in the mixtures has a more significant effect on the volume of the mixture compared to the concentration of citric acid in the mixtures. Moreover, the higher the temperature, the lower is V_E. This result indicate that the mixture exhibits a lower volume than the sum of the pure menthol and pure citric acid volumes in DES--1A–1D and pure phenyl salicylate–benzoic acid in the DES 12:1 and 9:1 It is a characteristic of eutectic mixtures and reflects the strong intermolecular interactions and the formation of a single solid phase at the eutectic point. Other studies on binary mixtures also have negative values of V_E.[19,20] Finally, according to the results in Table S-IV, all the tested DESs are obviously hydrophobic.

In the following investigation, three kinds of most popular capsules were firstly chosen, including gelatine, glutinous and enteric capsules (containing cellulose acetate phthalate), which are all mainly based on hydrophilic materials. It can be found that the tested DESs will not dissolve their small pieces under general storage temperature within 24 h (see Fig.S-6 of the Supplementary material); however, they will make them softer. The soften coefficients of the different

types of capsules incubated in DES- different molar ratios of ME:CA, are shown in Fig. 2A.

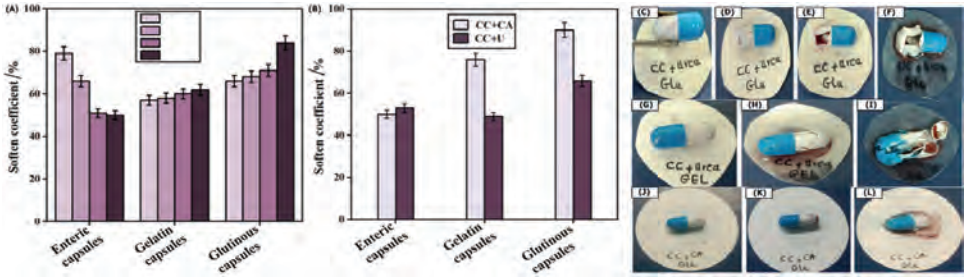

Fig. 2. Soften coefficient of enteric, gelatin and glutinous capsules incubated in: A) DES-1A–1D and B) choline chloride–citric acid (CC+CA) as well as choline chloride–urea (CC+U) DESs; photographs of different kind of capsules (glutinous and gelatinous) filled with CC and U based DESs after different time: 10 (C), 20 (D), 30 min (E) and 1 day (F) (glutinous capsules) and 10 (G), 15 min (H) and 1 day (I) (gelatinous capsules), as well as photographs of glutinous capsules filled with CC and CA based DESs after different time: 10 (J), 15 min (K) and 1 h (L). All measurements were performed at room temperature.

The enteric capsules exhibit a high soften coefficient (79 %) at the DES (menthol–citric acid) with mole ratio of 3:1, while the lowest soften coefficient was observed at the mole ratio of 6:1. The second type of capsules (gelatin capsules) show similar results, with the soften coefficient varying from 57 to 62 %. As for glutinous capsule, it had the highest soften coefficient among all the other types of capsules in menthol–citric acid with mole ratio of 6:1, whereas the soften coefficient lowered to 66 % for the ratio of 3:1. Clearly, the results above suggest that the DESs have a mollification effect on the tested capsules, making them more brittle. This change cannot be detected visually or by other methods; only the tests in this section can perform quantitative analysis for it. These findings suggest that the molar ratio of the eutectic solvent components can play a significant role when the degree of softening of the capsules shell is involved. In order to explore the possible difference, two choline chloride-based DESs were compared with DES-1A–1D for it is the most widely used HBA (Fig. 2B). As the result, for all DESs, the highest soften extent occurred in the DES formed by choline chloride–citric acid (1:1) and glutinous capsules (nearly 90 %); the second soften extent occurred in the DES formed by menthol–citric acid (6:1) and the corresponding capsules. Predominately, the enteric capsules exhibited the strongest resistance to DESs. The overall trend reflects not only the influence of different HBD and HBA types, but also the impact of the varied molar ratio of the two components. Finally, the results of the soften extent corrosion test further prove the DESs with the HBA of choline chloride have obvious effect on all the three kinds of capsules (Fig. 2C). As the fastest case, the leakage and crack were

noticeable from the fifth minute onward for the glutinous capsule filled with choline chloride–urea. Secondly, the gelatinous capsules started to break 10 min after loaded with the same DES. The glutinous capsules filled with the choline chloride–citric acid started to break after 1 h. Differently, the hydrophobic DES--1A–1D did not corrode all the capsules under the same conditions within 24 h (Fig. S-7 of the Supplementary material). Therefore, special attention should be paid to the choline chloride-involved mixture.

As for the tablet pressing, the tablets based on the binary mixture of the ratio 12:1 at 25 N broke when it was tried to remove from the mould (Fig. 3A). The eutectic liquid was formed during the compression up to 15 N for all the binary mixtures. Fig. 3B shows a graphical presentation for the tablet tensile strength versus the compression forces of the tablet made of phenyl salicylate, benzoic acid and their eutectic formation ratios 12:1 and 9:1. These two ratios demonstrated the tensile strength of 265.2 and 172 N cm^{-2} at 15 N, respectively. The tensile strength of both ratios increased with the compression forces. However, the ratio of 12:1 showed higher tensile strength values over the ratio 9:1. Moreover, both ratios showed higher tensile strength from 10 to 25 N. Similar trend was observed in the previous studies on binary mixture of ibuprofen–stearic acid[14] and acetaminophen–caffeine anhydrous and acetaminophen–prophylphenazone at certain pressure.[21] One possible explanation for this increase of tensile strength values is the formation of eutectic solvents when mixing the two components at certain ratio and applying certain pressure. The eutectic formation between the components may have influenced the crystal structure and the alignment of the material, leading to weaker intermolecular forces and lower tensile strength values. By examining the obtained tensile strength values, it was determined that the most appropriate sample was the binary mixture with a ratio of 12:1 and its compressed tablet under a force of 15 N. Finally, the changing trend of the tablet weight and tensile strength in stability test is shown in Fig. S-8 of the Supplementary material. It can be found the influence of DES on the tensile strength is more significant than that on the tablet weight in one week. Moreover, the rate of strength decline is accelerating, and the formation of DES is obviously disadvantageous for the tablet stability during its storage.

FTIR spectra (KBr) of phenyl salicylate, benzoic acid and their binary mixture ratio 12:1 compressed at 15 N is shown in Fig. 3C, the FTIR spectrum of phenyl salicylate shows a typical absorbance band O–H at wavenumber ranges of 3982–2835 cm^{-1} and 3733–3596 cm^{-1}, the peaks in 2421–2227 cm^{-1}, 2226––2014 cm^{-1} and 2017–1857 cm^{-1} are due to the asymmetric and symmetric stretching vibrations of the C=O group. The spectrum of benzoic acid compressed in 15 N shows peaks at 3770–3609 cm^{-1} is due to the stretching vibration of the –OH group. The peaks at 651 and 510 cm^{-1} refer to out-of-plane bending vibration of the C–H bond in the aromatic ring. The changes including the

changes in position of peaks, the changes in the intensity of peaks noticed in FTIR spectrum of the binary mixture ratio 12:1 are indicative of the formation of eutectic mixtures. Moreover, the FTIR spectrum of a binary mixture of ibuprofen and stearic acid[14] was studied after being compressed at a pressure of 19.9 kN. The study revealed changes in the spectrum of the binary mixture, suggesting some form of interaction between the compounds.

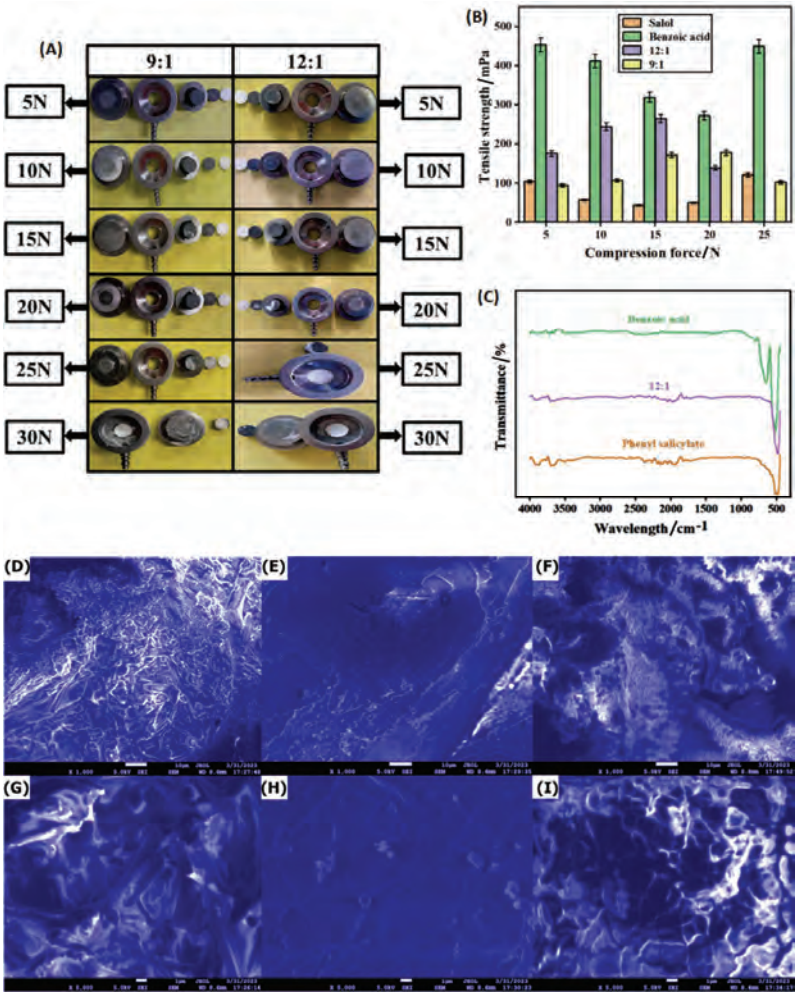

Fig. 3. A) Adhesion phenomena of phenyl salicylate-benzoic acid at different ratios (9:1, 12:1) and compression forces (5–30 N); B) tensile strength of pure components and its binary mixtures at different compression force (5–25 N); C) FTIR spectra of phenyl salicylate, benzoic acid and their binary mixture ratio 12:1 compressed at 15 N; SEM images: D) compressed phenyl salicylate at 15 N, 1000×; E) compressed benzoic acid at 15 N, 1000×; F) compressed binary mixture of phenyl salicylate–benzoic acid at 15 N, 1000×;

G) compressed phenyl salicylate at 15 N, 5000×; H) compressed benzoic acid at 15 N, 5000×; I) compressed binary mixture of phenyl salicylate–benzoic acid at 15 N, 5000×.

In order to study the morphology, SEM analysis was performed for phenyl salicylate, benzoic acid and its binary mixture 12:1 compressed on 15 N. The obtained photographs are shown in Fig. 3D. The loss of boundaries was observed in the three kinds of tablet resulting in a smooth surface. This phenomenon observed in the tablets is called sintering of the tablets. The same phenomenon occurred in the stearic acid and the ibuprofen-stearic acid the compressed tablets prepared by Setyawan *et al.*[14] The sintering phenomenon occurs when the temperature rises upon compression which forms the eutectic liquid, the presence of which affects the morphology and the structure of the pure components, allowing the particles to be rearranged and the filling of voids between the particles.[14]

CONCLUSION

In summary, the resulting DESs have lower melting points than their pure components and form simple eutectic point systems. The nature of the DESs has a different impact on capsules; menthol–citric acid DESs exhibit hydrophobic characteristics that result in a comparatively weaker effect on capsules than choline chloride-based DESs, which possess hydrophilic characteristics. DESs that have hydrophilic nature alter more the capsules in a short time. The tablets contain a mixture of phenyl salicylate and benzoic acid, confirming that the applications of the pressure to the APIs results in the formation of eutectic liquids; the applied force directly correlates with the degree of stickiness observed. Considering the deep eutectic is a common problem in the pharmaceutical field, and it can be prevented by several approaches. During the compression of the powders, the temperature tends to rise, leading to the formation of deep eutectic solvents. Thus, changing the temperature and the compaction forces can be an effective approach to avoid or reduce this phenomenon. The on-line monitoring of temperature can be of help to avoid reaching the eutectic point and maintain the APIs in a solid state. One another effective approach is to use the encapsulation technology. For instance, using the lyophilization method can transform the liquid form of nanoparticles into dry powders; this process ensures the stabilization and prevents the degradation of the product to be used in the creation of solid preparations. In addition, the solid dispersion is a useful way to prevent the formation of DESs during the manufacturing process and maintain the stability during the storage and the transportation by the dispersion of drugs in a stable matrix resistant to high temperatures. At last, the prevention of direct contact between the DES-forming APIs can be realized by changing the order of mixing the components, allowing the dissolution of each component separately. Alternatively, the multilayered tablets or capsules can also divide the ingredients into different layers, allowing APIs with low melting points to be positioned in the centre layer

and surrounded by stable excipients at high temperatures. Finally, nano-coating the APIs with a thin layer of polymers or surfactants is ideal to prevent the deep eutectic by creating a physical barrier between the APIs and excipients.[22,23]

SUPPLEMENTARY MATERIAL

Additional data and information are available electronically at the pages of journal website: https://www.shd-pub.org.rs/index.php/JSCS/article/view/12564, or from the corresponding author on request.

Acknowledgements. It was supported by Natural Science Foundation of Sichuan Province (2022NSFSC1604), Chengdu Key R & D Supporting Project (2022-YF05-00910--SN), Sichuan University-Luzhou Science and Technology Innovation Platform Construction Project (2022CDLZ-20) and National Natural Science Foundation of China (82273814). Special thanks to the Engineering Experimental Teaching Center in School of Chemical Engineering of SCU for FTIR and NMR, etc.

ИЗВОД

ЕУТЕКТИЧКИ РАСТВАРАЧИ ДОБИЈЕНИ ОД ФАРМАЦЕУТСКИХ САСТОЈАКА И ЊИХОВИ ПОНТЕЦИЈАЛНИ УТИЦАЈИ НА ПРИПРЕМУ ЧВРСТИХ ФОРМУЛАЦИЈА

SARA TOUFOUKI[1], AHMAD ALI[1], YOUMO WANG[1], RUI LI[1], YU CAO[2] и SHUN YAO[1]

[1]School of Chemical Engineering, Sichuan University, Chengdu, 610065, China и [2]College of Life Science & Biotechnology, Mianyang Normal University, Mianyang. 621000, China

Одређени активни фармацеутски састојци (APIs) и ексципијенси могу формирати еутектичке растваче (DESs), који доводе до стварања дефеката у припреми чврстих формулација. У овом раду су припремљени типични DESs мешањем APIs и ексципијенаса присутних у регистрованим лековима. Затим су испитивана два различита типа бинарних еутектичких смеша, које су се састојале од ментола и лимунске киселине као и фенил салицилата и бензојеве киселине. Испитиван је потенцијални утицај ових бинарних смеша на капсуле и таблете, који може довсети до ликвефације или лепљивости чврстих формулација. Извршена је детаљна карактеризација и испитивање фазног понашања бинарних смеша, и спектрална анализа је потврдила формирање еутектичких течности из индивидуалних компоненти. Такође, бинарне смеше су повећале чврстину таблете при повећању силе компресије, што резултује лепљивошћу прашкова при примени притиска. Додатно, капсуле су омекшале у присуству DESs. Након морфолошких испитивања и квантитативне анализе, одговарајуће сугестије и првентивне мере су дате у закључцима.

(Примљено 25. августа, ревидирано 22. септембра, прихваћено 20. децембра 2023)

REFERENCES

1. A. R. C. Duarte, A. S. D. Ferreira, S. Barreiros, E. Cabrita, R. L. Reis, A. Paiva, *Eur. J. Pharm. Biopharm.***114** (2017) 296 (https://doi.org/10.1016/j.ejpb.2017.02.003)
2. B. S. Đorđević, D. Z. Troter, V. B. Veljković, M. L. J. Kijevčanin, I. R. Radović, Z. B. Todorović, *J. Serb. Chem. Soc.* **85** (2020) 1303 (https://doi.org/10.2298/JSC200425050D)
3. F. Al-Akayleh, R. M. Khalid, D. Hawash, E. Al-Kaissi, I. S. Al-Adham, N. Al-Muhtaseb, M. Jaber, M. Al-Remawi, P. J. Collier, *Lett. Appl. Microbiol.* **75** (2022) 607 (https://doi.org/10.1111/lam.13699)

4. M. Patrycja, P. Andrzej, B. Grzegorz, *J. Chromatogr., A* **1570** (2018) 28 (https://doi.org/10.1016/j.chroma.2018.07.070)
5. G. Q. Zhong, R. R. Jia, Y. Q. Jia, *Adv. Mater. Res.* **549** (2012) 292 (https://doi.org/10.4028/www.scientific.net/AMR.549.292)
6. M. Phutke, A. R. Raichur, A. K. Suresh, *Ind. Eng. Chem. Res.* **61** (2022) 11636 (https://doi.org/10.1021/acs.iecr.2c00513)
7. M. M. Santos, L. C. Branco, *Pharmaceut.* **12** (2020) 909 (https://doi.org/10.3390/pharmaceutics12100909)
8. Y. Liu, Y. Wu, J. Liu, W. Wang, Q. Yang, G. Yang, *Int. J. Pharmaceut.* **622** (2022) 121811 (https://doi.org/10.1016/j.ijpharm.2022.121811)
9. M. H. Zainal-Abidin, M. Hayyan, G. C. Ngoh, W. F. Wong, C. Y. Looi, *J. Control. Rel.* **316** (2019) 168 (https://doi.org/10.1016/j.jconrel.2019.09.019)
10. A. Gutiérrez, S. Aparicio, M. Atilhan, *Phys. Chem.* **21** (2019) 10621 (https://doi.org/10.1039/C9CP01408J)
11. H. Shekaari, M. T. Zafarani-Moattar, M. Mokhtarpour, *J. Iran. Chem. Soc.* **19** (2022) 4275 (https://doi.org/10.1007/s13738-022-02602-y)
12. Y. Liu, X. Wei, J. Chen, Y. L. Yu, J. H. Wang, H. Qiu, *Anal. Chem.* **94** (2022) 5970 (https://doi.org/10.1021/acs.analchem.2c00428)
13. S. Chattoraj, P. Daugherity, T. McDermott, A. Olsofsky, W. J. Roth, M. Tobyn, *J. Pharm. Sci.* **107** (2018) 2267 (https://doi.org/10.1016/j.xphs.2018.04.029)
14. D. Setyawan, D. Isadiartuti, S. D. Betari, D. P. Paramita, *Indones. J. Pharm.***27** (2016) 28 (https://doi.org/10.14499/indonesianjpharm27iss1pp28)
15. M. Zdanowicz, K. Wilpiszewska, T. Spychaj, *Carbohyd. Polym.* **200** (2018) 361 (https://doi.org/10.1016/j.carbpol.2018.07.078)
16. M.H.Shafie, R.Yusof, C.Y.Gan, *J. Mol. Liq.* **288** (2019) 111081 (https://doi.org/10.1016/j.molliq.2019.111081)
17. Q. Zhang, K. D. O. Vigier, S. Royer, F. Jérôme, *Chem. Soc. Rev.* **41** (2012) 7108 (https://doi.org/10.1039/C2CS35178A)
18. K. A. Omar, R. Sadeghi, *J. Mol. Liq.* **360** (2022) 119524 (https://doi.org/10.1016/j.molliq.2022.119524)
19. U. R. Kapadi, D. G. Hundiwale, N. B. Patil, M. K. Lande, P. R. Patil, *Fluid Phase Equilib.* **192** (2001) 63 (https://doi.org/10.1016/S0378-3812(01)00621-5)
20. H. Shekaari, M. T. Zafarani-Moattar, M. Mokhtarpour, S. Faraji, *J. Mol. Liq.* **289** (2019) 111077 (https://doi.org/10.1016/j.molliq.2019.111077)
21. M. Bi, S. J. Hwang, K. R. Morris, *Thermochim. Acta* **404** (2003) 213 (https://doi.org/10.1016/S0040-6031(03)00185-0)
22. S. Swaminathan, B. Ganapathy, M. Wang, F. Wang, J. Wooding, J. Frankel, S. Chiruvolu, S. Rengarajan, P. Narwankar, *Powder Technol.* **425** (2023) 118525 (https://doi.org/10.1016/j.powtec.2023.118525)
23. R. N. Dave, L. Beach, M. P.Mullarney, C. Ghoroi, in *Proceedings of AIChE Annual Meeting* (2010), *2010 Annual Meeting*, Food, Pharmaceutical & Bioengineering Division, New York (https://www.aiche.org/conferences/aiche-annual-meeting/2010/proceeding/paper/444f-novel-continuous-device-surface-modification-cohesive-pharmaceutical-powders-dry-coating-nano).

Journal of the Serbian Chemical Society
JSCS@tmf.bg.ac.rs • www.shd.org.rs/JSCS
J. Serb. Chem. Soc. 89 (1) S52–S58 (2024) *Supplementary material*

SUPPLEMENTARY MATERIAL TO

Deep eutectic solvents formed by pharmaceutical ingredients and their potential influences on solid preparations

SARA TOUFOUKI[1], AHMAD ALI[1], YOUMO WANG[1], RUI LI[1], YU CAO[2]* and SHUN YAO[1]**

[1]*School of Chemical Engineering, Sichuan University, Chengdu, 610065, China and* [2]*College of Life Science & Biotechnology, Mianyang Normal University, Mianyang. 621000, China*

J. Serb. Chem. Soc. 89 (1) (2024) 107–121

Table S-I. VTF equation parameters of viscosity for the DESs.

DESs	A	B	T_0	R^2
DES 1	3029.339	0	0.003595	1.0000
DES 2	3181.367	0	0.003595	0.9995
DES 3	2651.201	0	0.003595	0.9999
DES 4	3215.718	0	0.003595	0.9996

Table S-II. Excess molar volume of the menthol-citric acid DESs (5-35 °C).

Temperature	Excess molar volume			
	DES 1	DES 2	DES 3	DES 4
5 °C	-334.788	-345.165	-344.859	-349.867
15 °C	-335.122	-345.343	-350.652	-350.007
25 °C	-339.043	-346.275	-353.392	-352.382
35 °C	-354.165	-347.174	-355.207	-359.605

Table S-3. Excess molar volume of the phenyl salicylate-benzoic acid DESs (35-55 °C).

Temperature	Excess molar volume	
	DES 12:1	DES 9:1
35°C	-283.749	-294.745
40°C	-284.868	-295.417
45°C	-285.253	-296.970
50°C	-285.567	-297.425
55°C	-286.202	-300.302

*,** Corresponding authors. E-mail: (*)cusack@scu.edu.cn, (**)agnes_cy2004@163.com

Table S-IV. Solubilities of the DESs in different solvents at room temperature*

DESs		Solubility of DESs				
		Water	Glycerin	Ethanol	Methanol	Acetone
menthol-citric acid	DES 1	PS	I	ES	ES	I
	DES 2	I	I	ES	ES	I
	DES 3	I	I	ES	ES	I
	DES 4	I	I	ES	ES	I
phenyl salicylate-benzoic acid	DES 12:1	I	I	ES	ES	I
	DES 9:1	I	I	ES	ES	I

*S: ES: easily soluble, I: insoluble and PS: poorly soluble

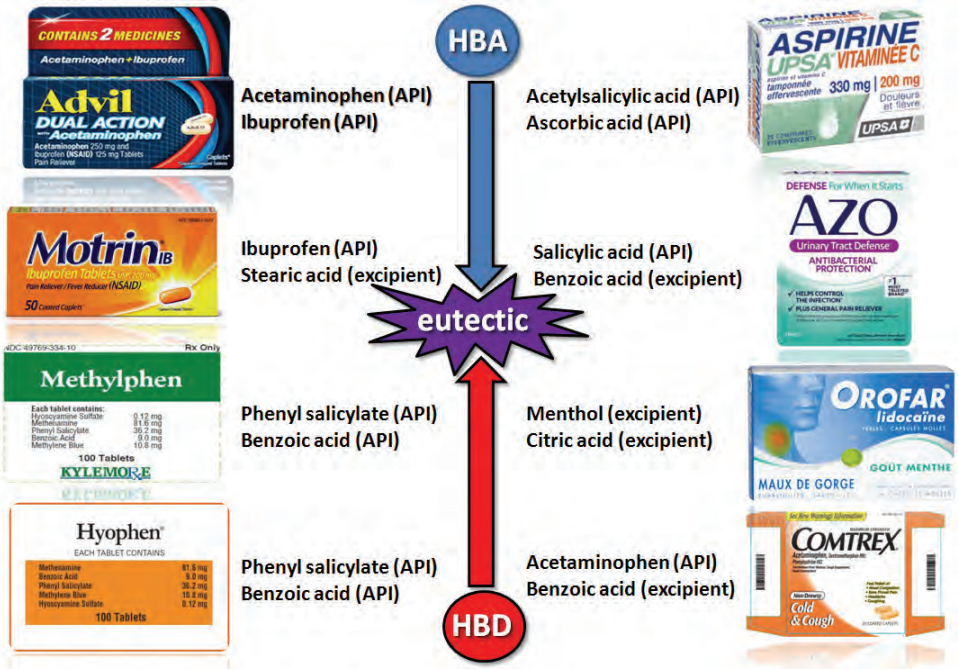

Fig. S-1. Common drug ingredients forming deep eutectic liquids.

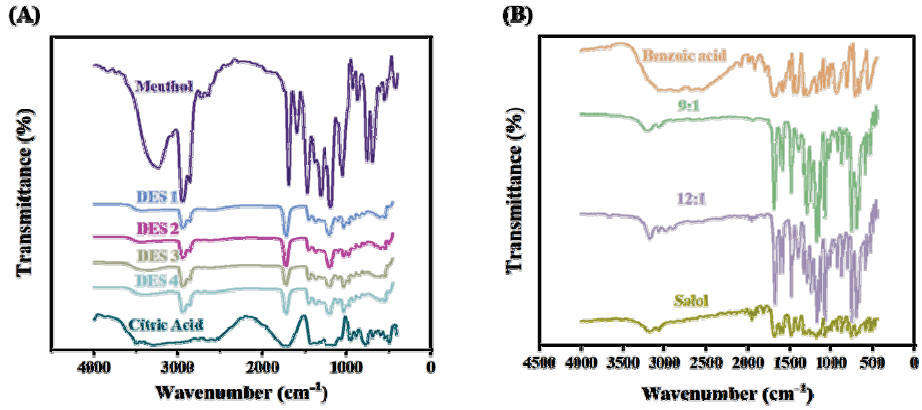

Fig. S-2. FTIR spectra of DESs composed of menthol and citric acid in various molar ratios (A); phenyl salicylate-benzoic acid DESs (B) and related pure components.

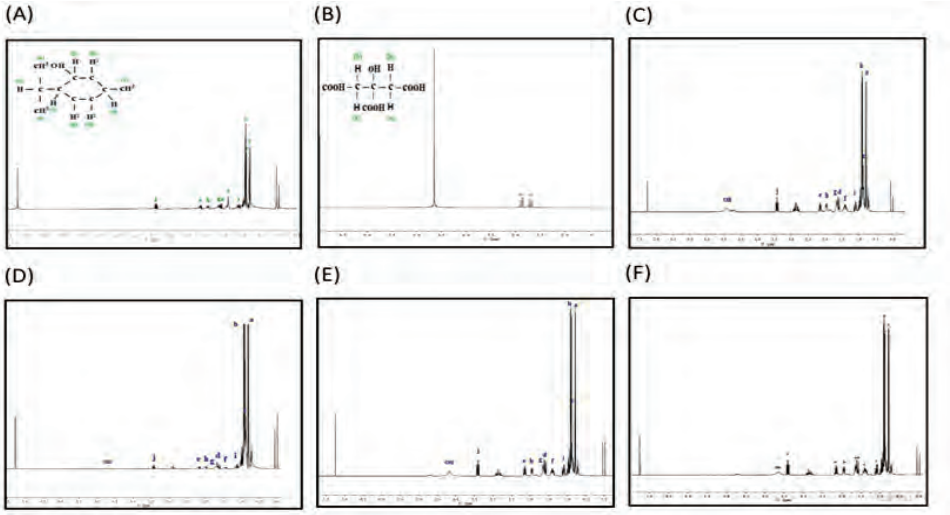

Fig. S-3. ^{1}H-NMR spectra (400 MHz, $CDCl_3$ for citric acid, DES 1-4 and D_2O for menthol) of (A) menthol, (B) citric Acid, (C) DES 1,(D) DES 2, (E) DES 3, and (F) DES 4.

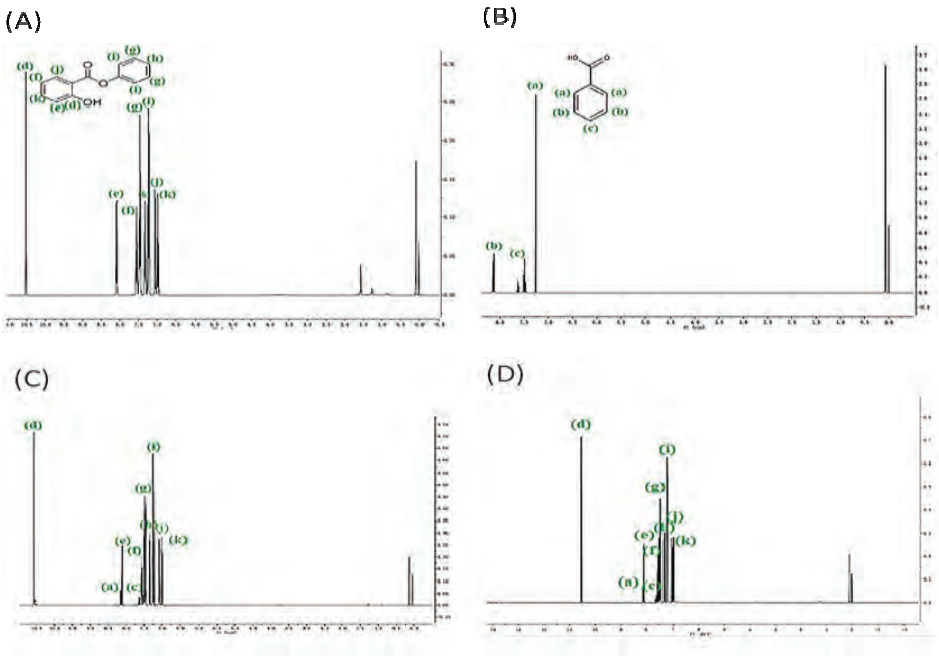

Fig. S-4. ^{1}H-NMR spectra (400 MHz, $CDCl_3$) of (A) phenyl salicylate, (B) benzoic acid, (C) their binary mixtures of 12:1 molar ratio, (D) binary mixtures of 9:1 molar ratio.

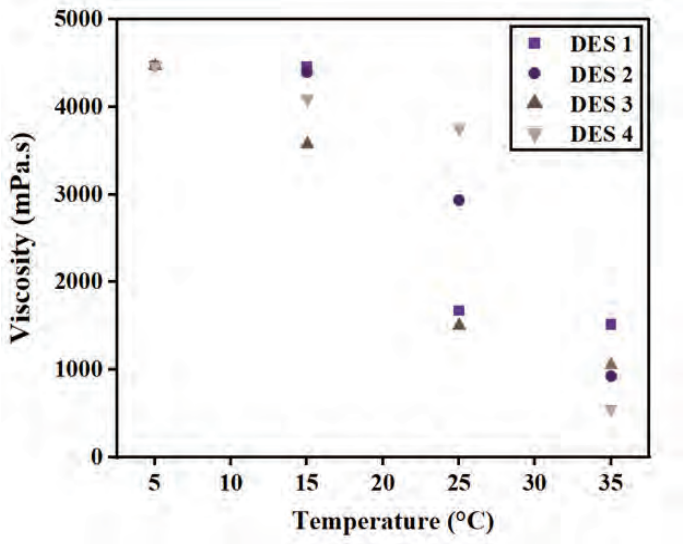

Fig. S-5. Plot of the predicted viscosity values of menthol-citric acid DESs.

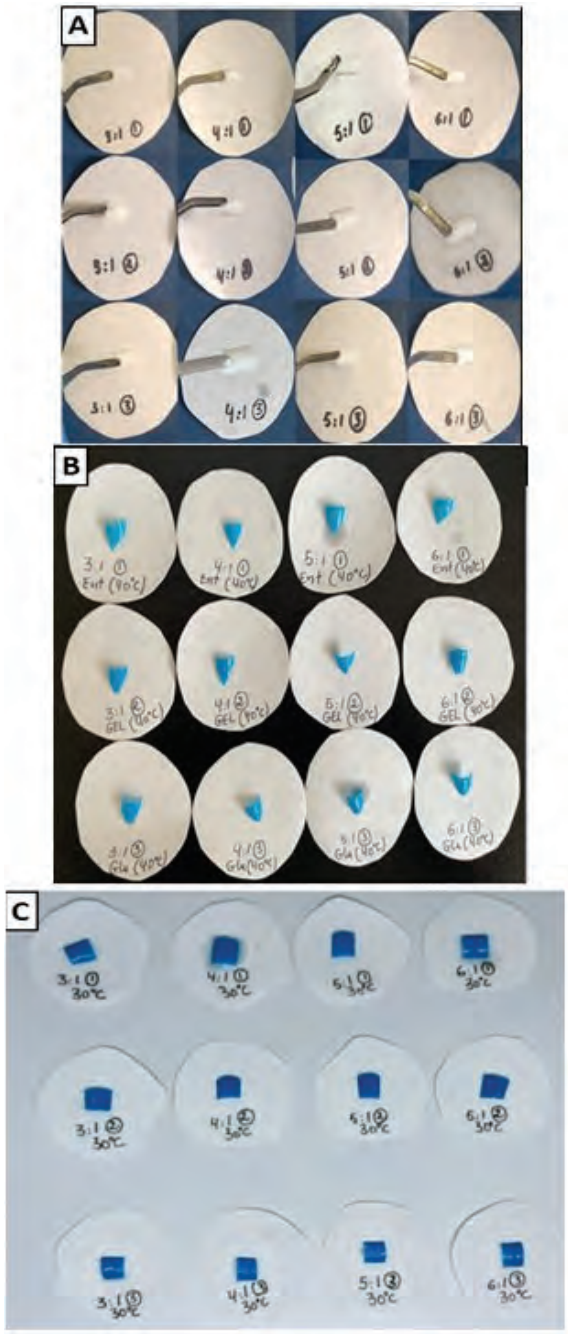

Fig.S-6. Photographs of the shells of enteric (1), gelatin (2) and glutinous (3) capsules taken after (A) 24 hours dissolved at 25°C;(B) 24 hours dissolved at 30°C; and (C) 24 hours dissolved at 40°C.

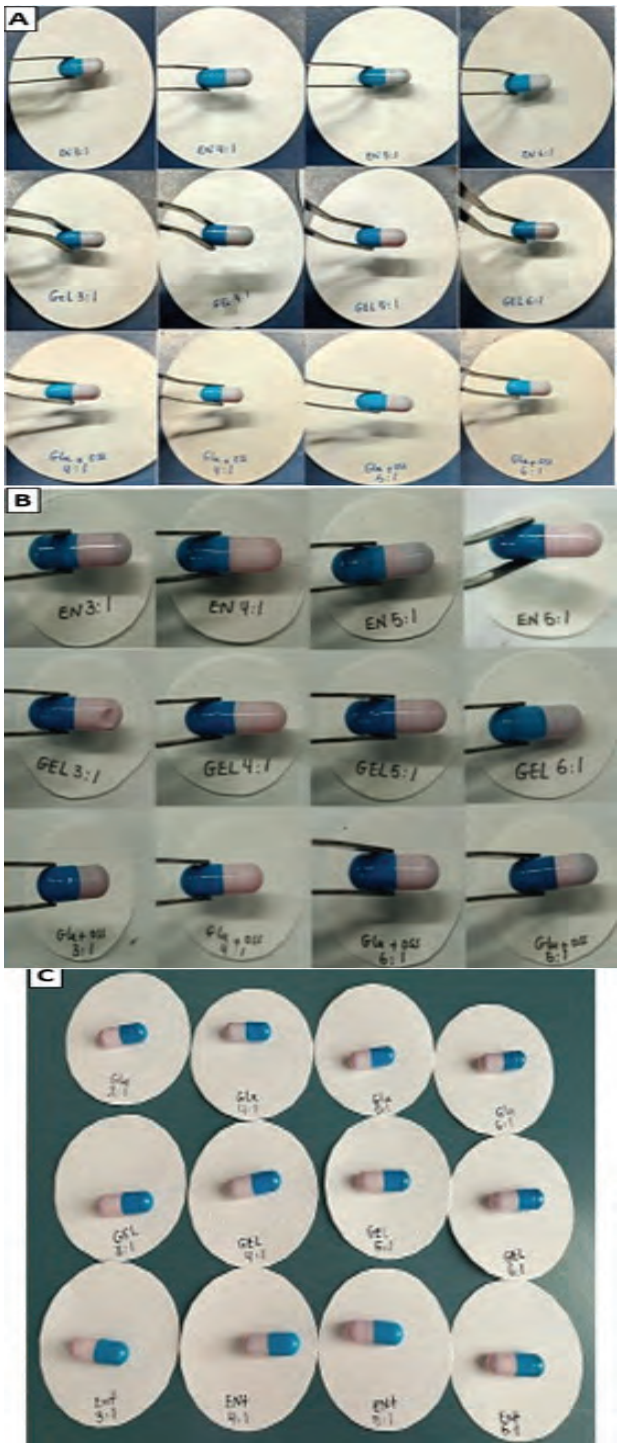

Fig. S-7. Photographs of enteric (Ent), gelatin (Gel) and glutinous capsules taken after 24 h filled with the tested DESs of different molar ratios at (A) 25 °C, (B) 30 °C, and (C) 40 °C.

REFERENCES

1. T. Zhang, J. Hu, S. Tang, *Chin. J. Chem. Eng.* **26** (2018) 1513 (https://doi.org/10.1016/j.cjche.2018.02.001)
2. D. Setyawan, D. Isadiartuti, S. D. Betari, D. P. Paramita, *Indones. J. Pharm.* **27** (2016) 28 (https://10.14499/indonesianjpharm27iss1pp28)
3. C. Coquelet, E. Auger, A. Valtz, *J. Solution Chem.* **48** (2019) 455 (https://10.1007/s10953-019-00870-6).

Journal of the Serbian Chemical Society
JSCS-info@shd.org.rs • www.shd.org.rs/JSCS
J. Serb. Chem. Soc. *89* (1) 123–140 (2024)
JSCS–5710
Original scientific paper
Published 14 February 2024

Facile chemical activation process of kapok husk as a low-cost biosorbent for removal methylene blue dye in aqueous solution

RAHMIANA ZEIN[1]*, HAMDHAN FATHONY[1], PUTRI RAMADHANI[2] and DESWATI DESWATI[3]

[1]Laboratory of Environmental Analytical Chemistry, Department of Chemistry, Andalas University, Padang 25163, Indonesia, [2]Research Center for Chemistry, National Research and Innovation Agency of Indonesia, Jakarta 10340, Indonesia and [3]Laboratory of Applied Analytical Chemistry, Department of Chemistry, Andalas University, Padang 25163, Indonesia

(Received 3 March, revised 19 May, accepted 29 October 2023)

Abstract: This study discusses kapok husk (KH) activated by HNO_3 as a biosorbent for methylene blue dye and analyses its adsorption ability. The adsorption capacity of KH is 330.161 mg g^{-1} with optimum conditions at pH 9, concentration 5500 mg L^{-1}, contact time 15 min, and biosorbent temperature 25 °C. The isotherm study followed the Langmuir isotherm model, as seen from the R^2 value of 0.9993 and maximum adsorption capacity of 312.5 mg g^{-1}, which indicated a monolayer in the adsorption process. The kinetic data show that KH followed the pseudo-second-order model. The results of the TGA analysis show that thermal stability affects the performance of biosorbents in the adsorption process. FTIR and SEM-EDS characterisation results showed that electrostatic interactions, cation exchange, and pore filling regulate the methylene blue dye adsorption mechanism on the surface of the KH. The reusability of KH through adsorption–desorption cycle analysis was achieved five times. This indicates that the biosorbent can be economically feasible for real wastewater treatment based on its good reusability and simple preparation and activation.

Keywords: adsorption; isotherm; kinetics; kapok husk; methylene blue.

INTRODUCTION

The textile industry has grown rapidly, accounting for two-thirds of the total dyestuff market. About 5–15 % of the dye is released into the wastewater during the dyeing process.[1,2] Water availability for various needs tends to decrease quantitatively and qualitatively. On the other hand, water demand tends to increase, so water resource management problems always arise. If the liquid waste is discharged into water bodies, it can harm human health.[3,4] The growth of toxic

* Corresponding author. E-mail: rzein@sci.unand.ac.id
https://doi.org/10.2298/JSC230303084Z

waste metal contamination in the environment was caused by increasing industrial activities and human lifestyle.[5] Synthetic dyes often used in industry were derivatives of indigo, anthraquinone, sulfur, triphenylmethyl (trityl) and azo. However, most synthetic dyes currently used in the industry were azo derivatives.[1] Methylene blue (MB) is one of the dyes used in the industry. MB can cause eye burns that result in permanent eye injury in humans and aquatic animals. MB can also cause gastrointestinal irritation with nausea, vomiting, diarrhoea, and skin irritation symptoms.[6]

One alternative that researchers widely use for dye wastewater treatment is the adsorption method. Nowadays, the researcher is concerned with producing low-cost adsorbents as an alternative material, such as using organic solid waste from agricultural and fishery by-products.[4] Several adsorbents have been reported for MB dye removals, such as bivalve shells (1 mg g^{-1})[7], lala clam shells (9.615 mg g^{-1})[8], catappa shells (88.620 mg g^{-1}) [9], lemongrass leaves (43.160 mg g^{-1}) [10] and activated carbon from starch (38.314 mg g^{-1}).[11] The modification and carbonization process which requires high costs but has a lower adsorption capacity, is a consideration for researchers, so it is necessary to find an efficient, low-cost, abundant and environmentally friendly adsorbent. This research used chemically activated kapok waste to remove methylene blue dye.

Kapok (*Ceiba pentandra* L.) is a plant found in tropical forests in Indonesia. This plant is cultivated to use fibres as a filling material for pillows, mattresses, cushions, *etc*. Using kapok produces waste or by-products in the form of husk, which is usually thrown into the environment or burned, harming the environment. This kapok husk contains carbohydrates, and lignin has an active side that can absorb cationic pollutants.[12]

Previous research has been reported on using kapok husk to remove Pb(II) and Cd(II) ions with adsorption capacity of 223.72 and 88.70 mg g^{-1}, respectively. [13] Meanwhile, the adsorption of dyes using kapok peel has never been done before, so kapok husk was investigated as an MB adsorbent with the batch method by taking into account the parameters of pH, concentration, contact time and heating temperature of the biosorbent. The isotherm analysis, kinetic analysis, and characterization of biosorbent were studied in order to determine the adsorption mechanism of MB dye on kapok husk.

EXPERIMENTAL

Materials and methods

Kapok husk (*Ceiba pentandra* L.) samples were collected from the Ombilin kapok plantation in West Sumatera, Indonesia. Methylene blue, HNO_3, NaOH, buffer solution and acetic acid were purchased from Merck. Methylene blue dye was diluted with double-distilled water to make a stock solution. The pH of the solution was adjusted using NaOH (0.01 M) and HNO_3 (0.01 M). The initial and final concentration of the solution was measured using a UV–Vis spectrophotometer (Genesys 20 Thermo Scientific).

Preparation and activation of Kapok husk biosorbent

The kapok husk was cleaned and dried, cut into small pieces, and ground using a grinder. Then, the size was uniformed using a 400 mesh sieve (≤36 μm) to form a powder.[13] The kapok husk powder was soaked for 3 h in 0.01 M HNO_3 with a ratio of powder to HNO_3 of 1:3.[14] After that, it was washed with distilled water until the pH was neutral, filtered and air-dried.[13,15] pH_{pzc} was determined by adding 0.1 g of kapok peel powder into 25 mL of 0.1 M KCl solution at pH 2–9, then stirring for 24 h. Then, the initial pH versus ΔpH (final pH–initial pH) was plotted and the point of intersection at $y = 0$ was obtained.[9,13]

Biosorbent characterization

The biosorbents were characterized by Fourier transform infra-red spectroscopy (FTIR), scanning electron microscope with energy dispersive spectroscopy (SEM-EDS), X-ray fluorescence (XRF) and thermogravimetric analysis (TGA). FTIR (IRTracer-100-Shimadzu) analysed the kapok husk's functional groups before and after dye adsorption. SEM-EDS (Inspect F50) was used to analyse the surface morphology of kapok husk before and after dye adsorption. XRF (PANanalytical Epsilon 3) was used to determine the chemical composition of kapok husk before and after dye adsorption. TGA (Shimadzu DTG-60) was used to observe changes in mass with a function of time and temperature.

Biosorption studies

Using a batch system, the adsorption process was investigated. Batch studies were carried out at various pH (5–10), initial MB dye concentration (300–6000 mg L^{-1}), contact time (5–60 min) and biosorbent temperature (25, 50, 75 and 100 °C), with 10 ml of dye solution, biosorbent mass 0.1 g, and stirring speed 150 rpm. The mixture was filtered and analysed by UV–Vis spectrophotometer at 664 nm. The amount of MB dye adsorbed into the adsorbent was calculated by the following equation:

$$q_e = \frac{V(C_0 - C_e)}{m} \quad (1)$$

where C_0: initial dye concentration (mg L^{-1}); C_e: concentration of dye at equilibrium (mg L^{-1}); V : volume of solution (L); m: amount of biomass (g).[16]

RESULTS AND DISCUSSION

Biosorbent characterization

Characterization of biosorbent using FTIR. Functional groups on the kapok husk surface (KH) were identified by FTIR spectral analysis. The FTIR spectrum of the KH before and after MB dye adsorption is shown in Fig. 1. FTIR analysis was carried out from wave numbers 400–4000 cm^{-1}, which can be seen in Fig. 1.

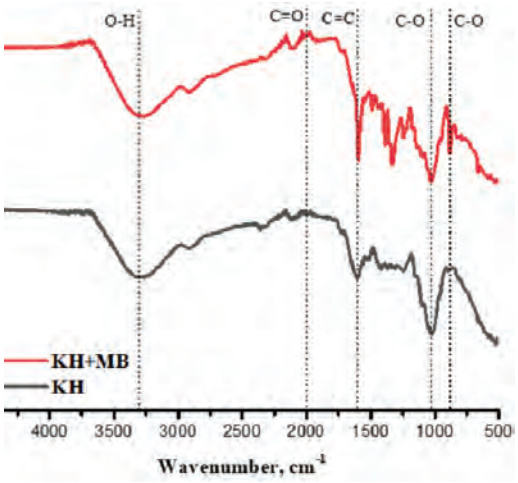

Fig. 1. FTIR spectrum of KH before and after MB dye adsorption.

Fig. 1 shows a peak at wave number 3294.49 cm^{-1} before adsorption, indicating the presence of O–H stretching alcohol or intermolecular hydrogen bonds of carbohydrates in organic compounds (such as cellulose, hemicellulose and lignin). This wave figure shifted to 3284.77 cm^{-1} after KH adsorbed MB. This shift suggested the formation of bonds between the MB dye and the hydroxyl group (–OH) of the biosorbent.[14] The peak at 896.86 cm^{-1} was shifted to 883.40 cm^{-1}, indicating that the C–O bending group (alkene) contributed to the adsorption process. The wave number shift also occurred in the functional groups O–H alcohol (1369.96 cm^{-1}) and O–H carboxylic acids (1417.68 cm^{-1}). Oxygen-containing functional groups such as alcohols and carboxylic acids could bind to methylene blue molecules.[17] The shift in the wave number to either a larger or a smaller number indicates a change in the vibrational energy and a change in the inter and intra-molecular bonds in the biosorbent structure, as well as an interaction between the biosorbent functional group and MB dye in the form of electrostatic interactions.[18] The presence of MB molecules on the surface of the biosorbent was proved by the shift of the C–N group of aromatic amines from 1244.09 to 1246.02 cm^{-1}. A heterocyclic amine and an amine group linked to an aromatic ring make up the dye MB.[10]

Characterization of biosorbent using SEM-EDS. SEM-EDS analysis provides information on the surface morphology and chemical composition of the biosorbent. The electrons from the high-energy beam used during SEM analysis interact with the atoms of the material's surface matrix, producing various types of signals containing information about the sample's surface morphology and the results are obtained in photographs.[19] SEM testing can also provide qualitative

information regarding the distribution pattern of methylene blue dye on the surface of the biosorbent.[20] The sample testing results using SEM can be seen in Fig. 2.

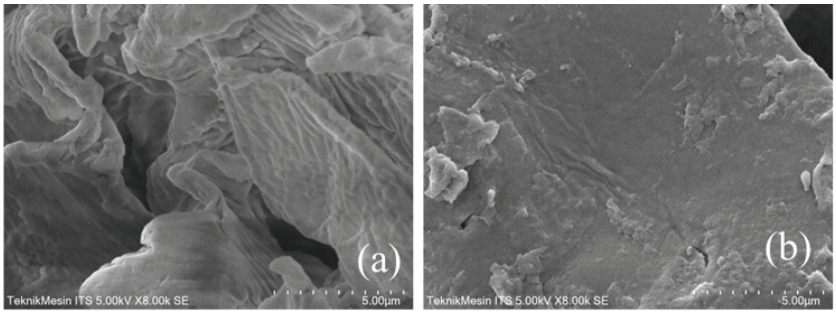

Fig. 2. SEM photos of kapok husk (a) before and (b) after adsorption.

Fig. 2 (a and b) shows the surface of the biosorbent before and after the adsorption of methylene blue at a magnification of 8000 times. In Fig. 2a, it can be seen that the surface of the biosorbent before the adsorption of the dye has a rough surface and has large cavities and pores. Based on the size of the hole and pores, it can be assumed that the holes and pores in the biosorbent most likely play a role in the adsorption of methylene blue dye. Fig 2b confirms that cavities and pores play a role in the adsorption of methylene blue dye, where the surface of the biosorbent, after adsorption MB, becomes smoother due to the trapping of methylene blue dye molecules and covers the cavities and pores of the biosorbent. This indicates that the process of adsorbing methylene blue dyes, apart from occurring chemically due to the abundance of functional groups on the surface, also occurs physically through the pores on the surface of the biosorbent.[21] The same result was reported by Mosoarca *et al*.[22]

In addition to qualitatively analysing the surface morphology of the biosorbent, SEM-EDS can also explore the abundance of elements present on the surface of the biosorbent and prove the adsorption of methylene blue dye on the surface of the biosorbent and confirmed by the results of the EDS analysis. Table I displays the EDS analysis outcomes of biosorbents before and after adsorption.

TABLE I. The relative abundance of elements (%) on the surface of the biosorbent (KH) before and after MB adsorption

Element	Before adsorption	After adsorption
C	27.78	35.55
O	61.96	51.69
Si	0.90	0.68
S	3.28	9.42
Ca	6.08	2.67

Based on Table I, elements O and C were more dominant than other elements. The biosorbent was an organic compound rich in C and O atoms. The biosorbent's increase in the percentage of C and S elements demonstrates that it successfully adsorbed the methylene blue dye.[23] Due to the presence of these elements throughout the adsorption process, the percentage of O, Si and Ca elements decreased following the adsorption of the methylene blue dye. The same result has been reported by Zein *et al.*,[10] where lemongrass leaves biowaste in the EDS analysis for elements C and S showed an increase in the percentage of elements, while elements O, Si, and Ca showed a decrease in the percentage of elements due to the formation of various interactions between dyes and biosorbents during adsorption process.

Characterization of biosorbent using XRF. XRF analysis provides information on the chemical composition of kapok husk before and after dye adsorption.[24] XRF analysis was also associated with EDS analysis. XRF analysis can be seen in Table II.

TABLE II. Chemical composition (%) of kapok husk before and after MB dye adsorption

Element/Oxide	KH	KH + MB
K	11.026	0.24
K_2O	9.652	0.117
S	3.452	62.932
SO_3	7.035	76.525
Si	1.222	0.534
SiO_2	2.038	1.15

Table II shows that the dominant KH contains K and K_2O, where the percentage of K and K_2O was above 9 %. It can be seen that the adsorption of methylene blue on the KH biosorbent significantly reduces of the K element. The K element decreased from 11.026 to 0.24 %, indicating that the site occupied by both K elements was replaced by methylene blue during the adsorption process, indicating the occurrence of cation exchange.[24,25] Element S in KH biosorbent increased significantly from 3.452 to 63.932 %, indicating that both biosorbents have adsorbed methylene blue.[9]

Characterization of biosorbent using TGA. TGA analysis aims to determine the mass fraction and stability of the biosorbent against high-temperature treatment. [10,21] The biosorbent thermogram can be seen in Fig. 3.

The results of TGA analysis on kapok husk showed a degradation step, as shown in Fig. 3. The first stage at a temperature of 25 to 100 °C decreased the initial mass due to the loss of water molecules and volatile compounds on the surface of the biosorbent, so that the pores of the biosorbent were wide open.[18] In the second stage, at a temperature of 100–350 °C, the biosorbent decomposes at temperatures above 200 °C for the structural units of cellulose, hemicellulose and

lignin, which form CO_2 gas and water.[26,27] At this stage, the destruction of all functional groups causes the adsorption capacity to be lower. In the third stage (>350 °C), the decomposition of biosorbent solid residues forms ash.[10]

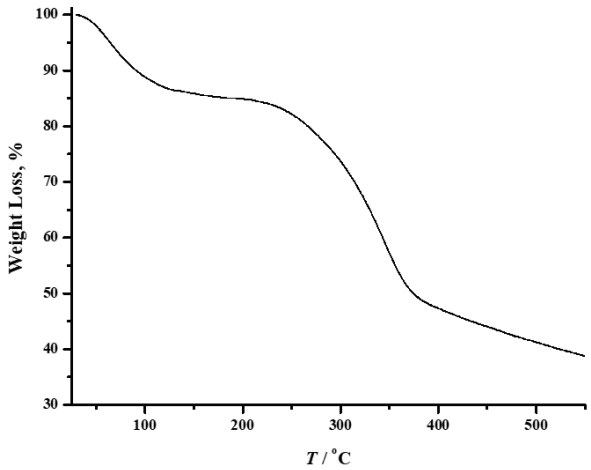

Fig. 3. Thermogram of kapok husk.

Analysis of pH_{pzc}

pH_{pzc} was a pH value indicating that a solid's surface has a zero charge. pH_{pzc} was used to measure or determine the electrokinetic properties of a surface.[28] The pH value describes the point of zero charges only for systems where H^+/OH^- was the potential determining ion. Due to the presence of functional groups such as OH^- groups, the adsorption of cationic dyes was favoured at pH > pH_{pzc}.[29] In contrast, adsorption of anionic dyes was favoured at pH < pH_{pzc}, where the surface becomes positively charged.[30]

In this study, pH_{pzc} was used to detect the zero charge of kapok husk. Fig. 4 shows that the pH_{pzc} of kapok husk was 7.3. This proves that the zero charge on the kapok husk was at pH 7.3. The removal process of cationic dyes in aqueous solutions using kapok husk at a pH above 7.3. Meanwhile, a pH value lower than 7.3 was not favourable for the adsorption of cationic dyes.

Effect of pH

Changes in pH solution have a strong influence on the adsorption process. The adsorption capacity of methylene blue dye by the kapok husk biosorbent increased until it reached the optimum solution pH at pH 9. The effect of this pH could be explained by the pH_{pzc} of the kapok husk, which was 7.3. At values higher than pH_{pzc}, the kapok husk particles acquire a negative surface charge, which leads to a stronger electrostatic attraction, making them suitable for adsorption of the cationic dye methylene blue.[31] Zein *et al*. also reported that the

optimum pH for MB adsorption using lemongrass leaves biowaste was pH 9.[10] The effect of pH on the adsorption capacity was shown in Fig 5.

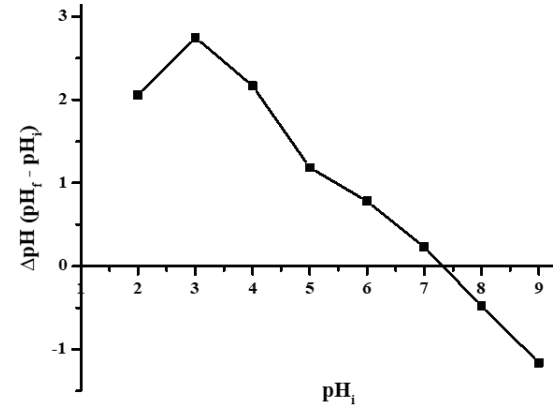

Fig. 4. pH_{pzc} for kapok husk.

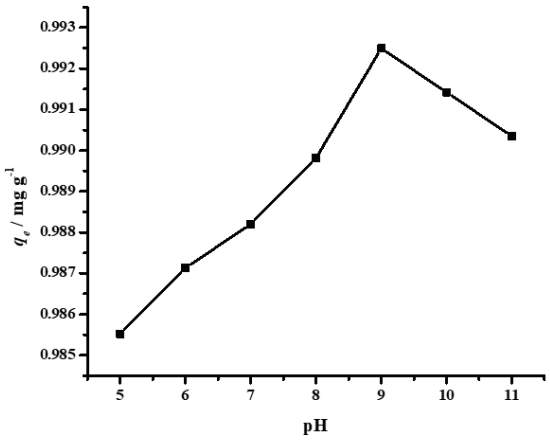

Fig. 5. Effect of the pH on methylene blue dye adsorption capacity. Experimental conditions: C_0: 10 mg L^{-1}; biosorbent mass: 0.1 g; stirring speed: 150 rpm; contact time: 60 min; particle size : ≤36 μm; MB volume: 10 mL.

Effect of initial concentration

The initial concentration of the dye affects the adsorption capacity value and shows the mechanism that occurs during the adsorption process. The MB dye concentration used to study KH adsorption capacity was 300–6000 mg L^{-1} with an optimum pH of 9. Fig. 6 shows the adsorption capacity value increased from 300 mg L^{-1} to a concentration of 5500 mg L^{-1} with a capacity of adsorption of 314.08 mg g^{-1}. Meanwhile, at a concentration higher than 5500 mg L^{-1}, the adsorption capacity value decreased to 306.70 mg g^{-1} at 6000 mg L^{-1}. It can be assumed that the optimal adsorption capacity of KH was 314.08 mg g^{-1} at a concentration of 5500 mg L^{-1}.

The driving force or mobility of the dye molecules to diffuse will rise with an increase in the initial concentration of MB. As a result, mass was transferred

from the liquid phase (the dye solution) to the solid phase (the biosorbent), increasing the adsorption capacity. If it is supposed the MB concentration increases higher than the optimal adsorption capacity, [10] it will interfere with the interaction between KH and MB during the adsorption process so that the adsorption capacity decreases.[9]

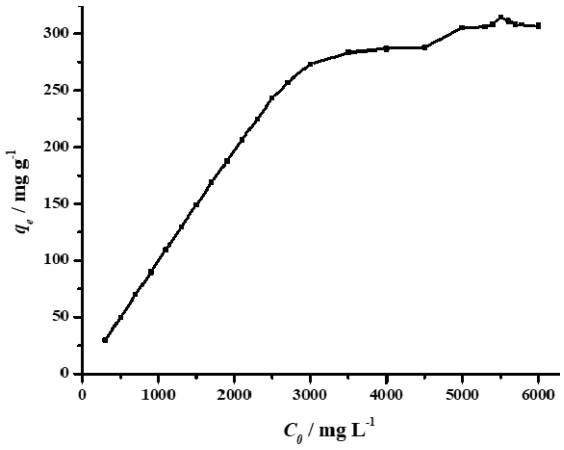

Fig. 6. Effect of the initial concentration on methylene blue dye adsorption capacity. Experimental conditions: pH: 9; biosorbent mass: 0.1 g; stirring speed: 150 rpm; contact time: 60 min; particle size: ≤36 μm; MB volume: 10 mL.

Effect of contact time

The influence of contact time on the biosorption process was conducted within 5, 15, 30, 45 and 60 min. The effect of contact time on the value of the adsorption capacity of KH can be seen in Fig 7. Fig 7 shows the adsorption capacity increased with the contact time from 5 to 15 min with an adsorption capacity value of 330.16 mg g^{-1}. However, after 15 min, the adsorption capacity decreased. In this study, it was assumed that the optimum contact time and equilibrium were reached within 15 min with the optimum adsorption capacity of 330.16 mg g^{-1}. Numerous positively charged adsorbent surfaces were readily available, which speeds up the adsorption process on KH. The adsorption process moves slowly because the active site of KH has been saturated after 15 min, and there was a repulsive interaction between MB and KH molecules.[32] The similar contact time results on cationic dye adsorption were observed using Terminalia catappa[9] and Lemongrass leaves biowaste.[10]

Effect of biosorbent temperature

The study of the temperature dependence of the sorption reaction provides valuable information about the enthalpy changes during adsorption. In addition, temperature changes will make the equilibrium capacity of the adsorbent different for a particular adsorbate.[33] Because many wastes containing different dyes were produced and disposed of at relatively high temperatures.[34] Therefore, to

determine the effect of heating temperature, the adsorption experiments were carried out at 25, 50, 75, and 100 °C, respectively, as shown in Fig. 8.

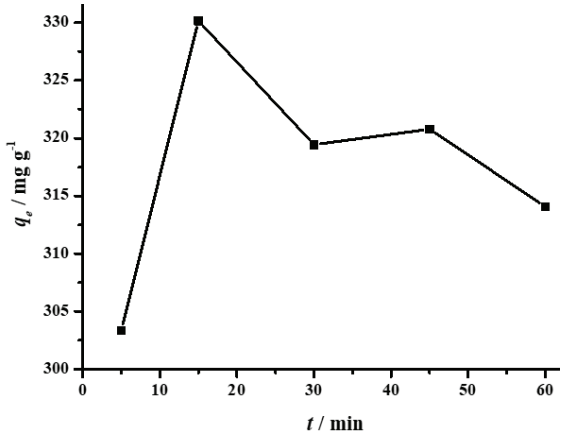

Fig. 7. Effect of the contact time on methylene blue dye adsorption capacity. Experimental conditions: pH: 9; C_0: 5500 mg L^{-1}; biosorbent mass: 0.1 g; stirring speed: 150 rpm; particle size: ≤36 μm; MB volume: 10 mL.

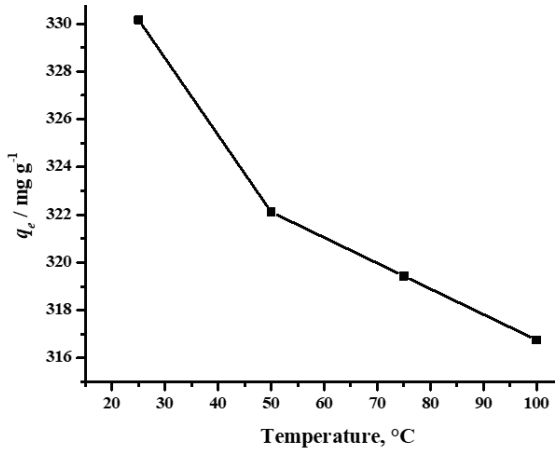

Fig. 8. Effect of the biosorbent temperature on methylene blue dye adsorption capacity. Experimental conditions: pH: 9; C_0: 5500 mg L^{-1}; biosorbent mass: 0.1 g; stirring speed: 150 rpm; contact time: 15 min; particle size: ≤36 μm; MB volume: 10 mL.

Fig. 8 shows the effect of the biosorbent's heating temperature for KH was achieved at 25 °C with an adsorption capacity of 330.16 mg g^{-1}. After the temperature was above 25 °C, the adsorption capacity decreased. This was due to damage to the biosorbent. Zein also reported the same thing for lemongrass leaves biowaste biosorbent, where the heating temperature of the biosorbent was reached at 25 °C.[10]

Equilibrium isotherm modelling

The adsorption isotherm model can describe the interaction between the adsorbent and adsorbate, which is an important factor in optimizing the use of the adsorbent[35] and the results can be seen in Fig. 9.

Based on Fig. 9, it can be seen that the R^2 value in the Langmuir isotherm model was 0.9993 for KH. The value of R^2, which was close to 1, indicates that the adsorption process follows the Langmuir isotherm model. The Langmuir isotherm applies to the adsorption of a solute from a liquid solution when it corresponds to the adsorption of a single layer (monolayer) on the surface.[36] The value of each parameter of the adsorption isotherm model was used to predict the adsorption mechanism during the process and represented in Table III.

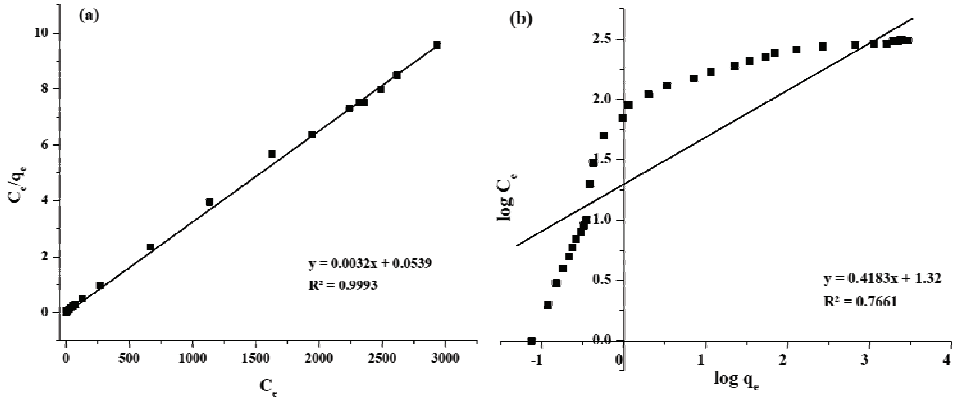

Fig. 9. Linear plots of: a) Freundlich isotherm and b) Langmuir isotherm for adsorption methylene blue dye by kapok husk.

Table III. Parameters of the adsorption isotherm model for adsorption MB dye by KH

Isotherm model	Constant	Value
Langmuir	q_m / mg g^{-1}	312.5000
	K_L / L mg^{-1}	0.0594
	R^2	0.9993
	R_L	0.0028–0.6275
	K_F	20.8929
Freundlich	1/n	0.41835
	R^2	0.7661

Kinetics modelling

In order to increase adsorption effectiveness and process scale factor, the kinetic model's definition of the adsorption mechanism has been helpful.[37] The physical and chemical characteristics of the adsorbent and the mass transmission method were crucial factors to consider when determining the adsorption mechanism.[9] The curve for pseudo-first-order, pseudo-second-order and intra-particle diffusion models to the contact time data were represented in Fig. 10 (a–c). As shown in Fig. 10a, a pseudo-first-order model allowed researchers to study the adsorption mechanism. The values of k_1 and q_e were determined from the intercept and slope of the plot of ln ($q_e - q_t$) *versus* t curve ($y = 0.0122x + 1.7576$,

R^2 = 0.046). As observed in Fig. 10b, the k_2 and q_e for the pseudo-second-order model were determined from the intercept and slope of the t/q_t *versus* t curve (y = 0.0032x – 0.001, R^2 = 0.9995). As shown in Fig. 10c, the intercept and slope of the $t^{1/2}$ *versus* q_t plot (y = 0.0566x – 12.771, R^2 = 0.064) will give information about K_{diff} and C value.[38]

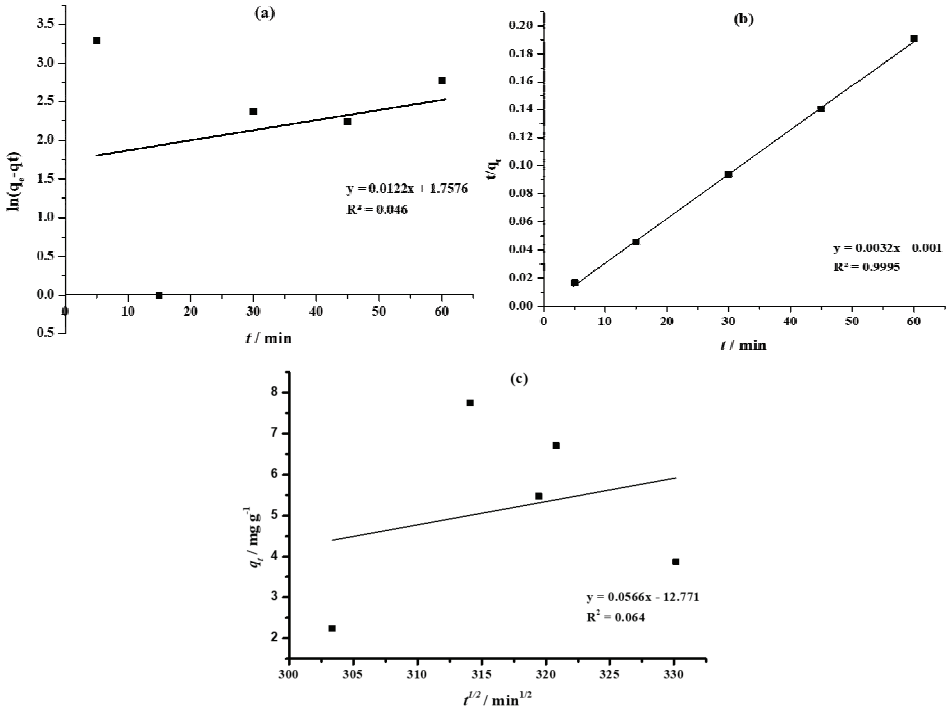

Fig. 10. Kinetic plots of: a) pseudo-first-order, b) pseudo-second-order and c) intra-particle diffusion for adsorption methylene blue dye by kapok husk.

The k_1 and k_2 were obtained with value –0.0122 and 0.0102 min^{-1}, respectively. The correlation coefficient value (R^2) obtained from pseudo-second--order kinetics (0.9995) was higher than the value from pseudo-first-order (0.046) and intra-particle diffusion (0.064). The lower value of R^2 from pseudo--first order and intra-particle diffusion models indicated that the MB dye adsorption does not occur through diffusion and multilayer formation. The pseudo-second-order kinetics can adequately describe the adsorption of methylene blue by KH by chemisorption (chemical interaction).[9]

Adsorption–desorption analysis

The adsorption–desorption analysis was an important parameter to evaluate the regeneration/reusability of a biosorbent so that it can be estimated on a large

scale.[4] Reusability study was analysed by immersing the biosorbent using a desorbing agent. The desorption agent selected must be effective, environmentally friendly, and low-cost. One of the methylene blue desorption agents reported and effectively used was 30 % acetic acid.[9] 30 % acetic acid as a desorption agent causes electrostatic repulsion between methylene blue and the surface of the biosorbent so that methylene blue is released from the surface of the adsorbent.[39] The adsorption–desorption cycle for the KH biosorbent can be seen in Fig. 11.

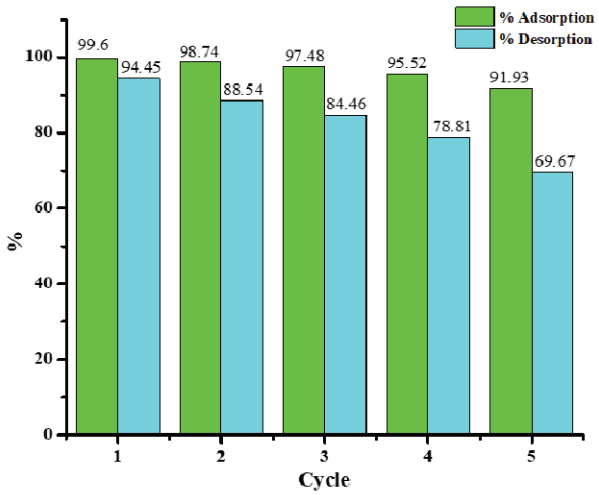

Fig. 11. Adsorption-desorption cycle of methylene blue dye onto kapok husk.

Fig. 11 shows the reusability of the biosorbent, which was reused for five cycles. The adsorption percentage decreased from the first (99.6 %) to the fifth (91.93 %) cycle. Zein *et al.* revealed that the active site on the surface of the biosorbent was saturated with methylene blue molecules, which was why the adsorption percentage declined with increasing cycles. Extreme pH circumstances trigger the degradation of biosorbent, which also exhibits blocked pores and active sites on its surface.[10]

Biosorption mechanism

The mechanism of biosorption was important to determine, which can predict how the mechanism of adsorption occurs from the data obtained. The biosorption mechanism can be predicted using the results of the influence of optimum conditions, adsorption isotherm studies, adsorption kinetics studies and biosorbent characterization using FTIR and SEM-EDS.[9,10] The adsorption mechanism can be made based on the above explanation. This is represented in Fig. 12.

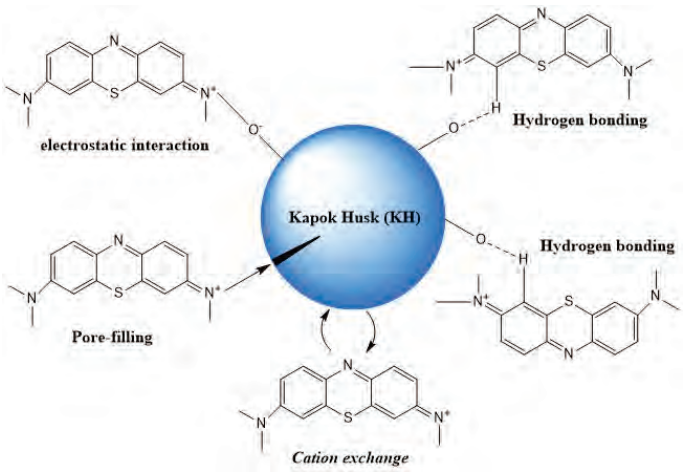

Fig. 12. Adsorption mechanism prediction of removal methylene blue dye onto kapok husk.

Based on Fig. 12, the adsorption mechanism between adsorbent and adsorbate was obtained from the data of pH_{pzc} biosorbent KH (pH_{pzc} 7.3), and the positive and negative charges on the surface of the biosorbent will be the same. For the adsorption of cationic dyes, the pH value must be greater than pH_{pzc}. It was intended that the functional groups on the surface of the biosorbent were deprotonated so that it would make the surface of the biosorbent negatively charged.[40] At the same time, the methylene blue will be protonated so that cationic exchange and electrostatic interactions occur between cationic methylene blue and negatively charged KH biosorbent. The EDS and XRF analysis results showed the cation exchange during the adsorption of methylene blue dye on the surface of the biosorbent. SEM analysis showed the results on the surface of the biosorbent before and after adsorption. A smoother surface after adsorption occurs due to the filling of biosorbent pores by methylene blue dye.

The adsorption ability of methylene blue by KH biosorbent was compared with other biosorbents. This needs to be done to see how far the research progresses and how it is positioned among the advantages and disadvantages of other biosorbents. A comparison of KH biosorbent with other biosorbents can be seen in Table IV. Table IV shows that the KH adsorption capacity value is close to the adsorption capacity value of the activated carbon from agricultural solid waste.[41,42] This could indicate that chemically activated KH performs well with high adsorption capacity, low cost, and environmental friendliness.

Application in real wastewater treatment

This work investigated kapok husk's efficiency in the biosorption of methylene blue dye removal in wastewater. Due to other competitive species in real wastewater, performance was typically lower than in experiments.[9] The waste-

water used in this study was sourced from the Environmental Chemistry Laboratory, Andalas University. Table V shows the results of applying the optimum conditions for MB adsorption in wastewater.

TABLE IV. Ability of kapok husk adsorbent for removal methylene blue dye in comparison to other adsorbents

No	Biosorbent	q_m / mg g^{-1}	Reference
1	Kapok husk	330.16	This study
2	Activated carbon from tea seed shells	324.70	[42]
3	Activated carbon derived from lignocellulosic agriculture wastes	148.80	[41]
4	Walnut shells powder	178.90	[43]
5	Coconut leaf	112.35	[44]
6	Terminalia catappa	88.62	[9]
7	Lemongrass leaves biowaste	43.15	[10]
8	*Platanus orientalis* leaf powder	114.94	[38]
9	Carbon-coated magnetic nanocomposite	110.63	[45]
10	*Streptomyces fradiae* biomass	59.63	[46]

Table V. Removal performance of kapok husk on real wastwater

Waste code	pH	Biosorbent temperature, °C	C_0 / mg L^{-1}	C_e / mg L^{-1}	R / %
Real	7.245	25	1.8445	0.2627	85.76
Optimum	9	25	2.1341	0.1877	91.21

Table V shows that good % removal was achieved for the adsorption of methylene blue dye in wastewater at optimum pH for biosorbent. At the pH of the natural solution (without adjusting the pH), the percentage of removal (%) obtained was lower than by adjusting the pH first. This informs that KH can be an excellent biosorbent to remove MB dye in aqueous solutions. Biosorbent residues can be used in concrete mixes to remove adsorbents. Another safe disposal method can be the impregnation in polymer resins and other cement mixtures.[9,15]

CONCLUSION

The MB dye adsorption process using KH has good results. The adsorption capacity of KH was 330.161 mg g^{-1} with optimum conditions at pH 9, a concentration of 5500 mg L^{-1}, a contact time of 15 min, and a heating temperature of 25 °C. The isotherm study followed the Langmuir isotherm model, as seen from the R^2 value of 0.9993, which indicated a monolayer layer in the adsorption process. The kinetic data show that KH follows a pseudo-second-order kinetic model. The adsorption-desorption results showed that the biosorbent gave an adsorption–desorption cycle of five times; this indicates that the biosorbent can be economically feasible for real wastewater treatment based on its good reuse pot-

ential. Applying biosorbent to laboratory liquid waste and textile industry waste gives a high % removal result of above 90% at optimum biosorbent conditions.

Acknowledgements. We acknowledge the Directorate of Research, Technology and Community Service, Directorate General of Higher Education, Research and Technology, Ministry of Education, Culture, Research, and Technology (Grant Numbers 086/E5/PG.02.00.PT/2022, Fiscal Year 2022).

ИЗВОД

ОЛАКШАН ПРОЦЕС ХЕМИЈСКЕ АКТИВАЦИЈЕ КАПОК ЉУСКЕ КАО ЈЕФТИНОГ БИОСОРБЕНТА ЗА УКЛАЊАЊЕ МЕТИЛЕН ПЛАВЕ БОЈЕ У ВОДЕНОМ РАСТВОРУ

RAHMIANA ZEIN[1], HAMDHAN FATHONY[1], PUTRI RAMADHANI[2] и DESWATI[3]

[1]Laboratory of Environmental Analytical Chemistry, Department of Chemistry, Andalas University, Padang 25163, Indonesia, [2]Research Center for Chemistry, National Research and Innovation Agency of Indonesia, Jakarta 10340, Indonesia и [3]Laboratory of Applied Analytical Chemistry, Department of Chemistry, Andalas University, Padang 25163, Indonesia

Ова студија разматра капок љуску (KH) активирану помоћу HNO_3, као потенцијални биосорбент за метилен плаву боју (MB), и анализира њену способност адсорпције. Капацитет адсорпције KH је 330,161 mg g^{-1} при оптималним условима: pH 9, концентрација 5500 mg L^{-1}, време контакта 15 min и температура биосорбента 25 °C. Студија изотерме је пратила Ленгмиров модел, што се види из вредности R^2 од 0,9993, и максималног капацитета адсорпције од 312,5 mg g^{-1}, што указује на монослој у процесу адсорпције. Кинетички подаци показују да KH следи модел псеудо-другог реда. Резултати TGA анализе показују да термичка стабилност утиче на перформансе биосорбената у процесу адсорпције. Резултати FTIR и SEM-EDS карактеризације су показали да електростатичке интеракције, размена катјона и попуњавање пора регулишу механизам адсорпције MB на површини KH. Поновна употреба KH кроз циклус адсорпције–десорпције постигнута је пет пута. Биосорбент може бити економски исплатив за прави третман отпадних вода на основу могућности његове добре поновне употребе и једноставног начина припреме и активирања.

(Примљено 3. марта, ревидирано 19. маја, прихваћено 29. октобра 2023)

REFERENCES

1. G. Samchetshabam, A. Hussan, T. G. Choudhury, S. Gita, *Environ. Ecol.* **35** (2017) 2349 (https://jurnal.fmipa.unila.ac.id/sains/article/view/205/pdf)
2. S. Afrin, H. R. Shuvo, B. Sultana, F. Islam, A. A. Rus'd, S. Begum, M. N. Hossain, *Heliyon* **7** (2021) e08102 (https://doi.org/10.1016/j.heliyon.2021.e08102)
3. Safni, D. F. Wulandari, Zulfarman, Maizatisna, T. Sakai, *MIPA FMIPA Univer. Lampung* **14** (2008) 143 (https://jurnal.fmipa.unila.ac.id/sains/article/view/205/pdf)
4. P. Ramadhani, R. Zein, Z. Chaidir, L. Hevira, *J. Zarah* **7** (2019) 46 (https://doi.org/10.31629/zarah.v7i2.1396)
5. Y. Rahmadani, F. Rozani, A. Rahmi, M. Suardi, *J. Katalisator* **2** (2017) 29
6. S. A. Umoren, U. J. Etim, A. U. Israel, *J. Mater. Environ. Sci.* **4** (2013) 75 (https://www.jmaterenvironsci.com/Journal/vol4-1.html)
7. K. Z. Elwakeel, A. M. Elgarahy, S. H. Mohammad, *J. Environ. Chem. Eng.* **5** (2017) 578 (https://doi.org/10.1016/j.jece.2016.12.032)

8. A. Alseddig, A. Eljiedi, A. Kamari, in *Proc. Int. Conf. Educ. Math. Sci. 2016 Conjunction with 4th Int. Postgrad. Conf. Sci. Math. 2016* **040003** (2017) (https://doi.org/10.1063/1.4983899)
9. L. Hevira, Zilfa, Rahmayeni, J. O. Ighalo, H. Aziz, R. Zein, *J. Ind. Eng. Chem.* **97** (2021) 188 (https://doi.org/10.1016/j.jiec.2021.01.028)
10. R. Zein, J. S. Purnomo, P. Ramadhani, M. F. Alif, S. Safni, *Sep. Sci. Technol.* **57** (2022) 1 (https://doi.org/10.1080/01496395.2022.2058549)
11. F. Benhachem, T. Attar, F. Bouabdallah, *Chem. Rev. Lett. 2* **2** (2019) 33 (https://doi.org/10.22034/crl.2019.87964)
12. K. Hori, M. E. Flavier, S. Kuga, T. B. T. Lam, K. Iiyama, *J. Wood Sci.* **46** (2000) 401 (https://doi.org/10.1007/BF00776404)
13. R. Zein, D. Nofita, R. Refilda, H. Aziz, *Chim. Nat. Acta* **7** (2019) 37 (https://doi.org/10.24198/cna.v7.n1.20813)
14. L. Hevira, R. Zein, E. Munaf, *J. Katalisator* **4** (2019) 42
15. L. Hevira, Zilfa, Rahmayeni, J. O. Ighalo, R. Zein, *J. Environ. Chem. Eng.* **8** (2020) 104290 (https://doi.org/10.1016/j.jece.2020.104290)
16. R. Zein, M. Suciandica, *J. Katalisator* **7** (2022) 63 (http://publikasi.lldikti10.id/index.php/katalisator/article/view/963)
17. S. Sahu, S. Pahi, S. Tripathy, S. K. Singh, A. Behera, U. K. Sahu, R. K. Patel, *J. Mol. Liq.* **315** (2020) 113743 (https://doi.org/10.1016/j.molliq.2020.113743)
18. J. Ooi, L. Y. Lee, B. Y. Z. Hiew, S. Thangalazhy-Gopakumar, S. S. Lim, S. Gan, *Bioresour. Technol.* **245** (2017) 656 (https://doi.org/10.1016/j.biortech.2017.08.153)
19. L. Bulgariu, L. Belén, O. Solomon, M. Iqbal, J. Nisar, K. Adesina, F. Alakhras, M. Kornaros, I. Anastopoulos, *J. Mol. Liq.* **276** (2019) 728 (https://doi.org/10.1016/j.molliq.2018.12.001)
20. N. K. Gupta, A. Gupta, P. Ramteke, H. Sahoo, A. Sengupta, *J. Mol. Liq.* **274** (2019) 148 (https://doi.org/10.1016/j.molliq.2018.10.134)
21. R. Zein, Z. Chaidir, S. Fauzia, P. Ramadhani, *J. Kim. Val.* **8** (2022) 10 (https://doi.org/10.15408/jkv.v8i1.22566)
22. G. Mosoarca, C. Vancea, S. Popa, M. Radulescu-Grad, S. Boran, *J. Serb. Chem. Soc.* **87** (2022) 39 (https://doi.org/10.2298/jsc220316039m)
23. D. Pathania, S. Sharma, P. Singh, *Arab. J. Chem.* **10** (2017) S1445 (https://doi.org/10.1016/j.arabjc.2013.04.021)
24. M. K. Dahri, M. R. R. Kooh, L. B. L. Lim, *Alexandria Eng. J.* **54** (2015) 1253 (https://doi.org/10.1016/j.aej.2015.07.005)
25. L. B. L. Lim, N. Priyantha, C. Hei Ing, M. Khairud Dahri, D. T. B. Tennakoon, T. Zehra, M. Suklueng, *Desalin. Water Treat.* **53** (2013) 964 (https://doi.org/10.1080/19443994.2013.852136)
26. L. Burhenne, J. Messmer, T. Aicher, M. Laborie, *J. Anal. Appl. Pyrolysis* **101** (2013) 177 (https://doi.org/10.1016/j.jaap.2013.01.012)
27. L. Hevira, Zilfa, Rahmayeni, J. O. Ighalo, H. Aziz, R. Zein, *J. Ind. Eng. Chem.* **97** (2021) 188 (https://doi.org/10.1016/j.jiec.2021.01.028)
28. W. Liu, C. Yao, M. Wang, J. Ji, L. Ying, C. Fu, *Environ. Prog. Sustain. Energy* **32** (2013) 655 (https://doi.org/10.1002/ep.11680)
29. I. Bencheikh, K. Azoulay, J. Mabrouki, S. El Hajjaji, A. Dahchour, A. Moufti, D. Dhiba, *Sci. Afr.* **9** (2020) (https://doi.org/10.1016/j.sciaf.2020.e00509)

30. M. T. Yagub, T. K. Sen, S. Afroze, & H. M. Ang, *Adv. Colloid Interface Sci.* **209** (2014) 172 (https://doi.org/10.1016/j.cis.2014.04.002)
31. W. Hassan, U. Farooq, M. Ahmad, M. Athar, M. A. Khan, *Arab. J. Chem.* **10** (2017) S1512 (https://doi.org/10.1016/j.arabjc.2013.05.002)
32. G. K. Cheruiyot, W. C. Wanyonyi, J. J. Kiplimo, E. N. Maina, *Sci. Afr.* **5** (2019) 1 (https://doi.org/10.1016/j.sciaf.2019.e00116)
33. J. Guo, B. Li, L. Liu, K. Lv, *Chemosphere* **111** (2014) 225 (https://doi.org/10.1016/j.chemosphere.2014.03.118)
34. M. M. Felista, W. C. Wanyonyi, G. Ongera, *Sci. Afr.* **7** (2020) e00283 (https://doi.org/10.1016/j.sciaf.2020.e00283)
35. P. Wang, Q. Ma, D. Hu, L. Wang, *Desalin. Water Treat.* **57** (2015) 10261 (https://doi.org/10.1080/19443994.2015.1033651)
36. M. A. Al-Ghouti, D. A. Da'ana, *J. Hazard. Mater.* **393** (2020) 122383 (https://doi.org/10.1016/j.jhazmat.2020.122383)
37. F. Batool, J. Akbar, S. Iqbal, S. Noreen, S. N. A. Bukhari, *Bioinorg. Chem. Appl.* **2018** (2018) (https://doi.org/10.1155/2018/3463724)
38. M. Peydayesh, A. Rahbar-kelishami, *J. Ind. Eng. Chem.* (2014) 1 (https://doi.org/10.1016/j.jiec.2014.05.010)
39. A. N. Labaran, Z. U. Zango, Z. N. Garba, A. Science, K. State, *Sci. World J.* **14** (2019) 66 (https://www.ajol.info/index.php/swj/article/view/208624)
40. M. Z. A. Zaimee, M. S. Sarjadi, M. L. Rahman, *Water (Switzerland)* **13** (2021) (https://doi.org/10.3390/w13192659)
41. H. M. El-Bery, M. Saleh, R. A. El-Gendy, M. R. Saleh, S. M. Thabet, *Sci. Rep.* **12** (2022) 1 (https://doi.org/10.1038/s41598-022-09475-4)
42. J. J. Gao, Y. B. Qin, T. Zhou, D. D. Cao, P. Xu, D. Hochstetter, Y. F. Wang, *J. Zhejiang Univ. Sci., B* **14** (2013) 650 (https://doi.org/10.1631/jzus.B12a0225)
43. Y. Miyah, A. Lahrichi, M. Idrissi, A. Khalil, F. Zerrouq, *Surfaces Interfaces* **11** (2018) 74 (https://doi.org/10.1016/j.surfin.2018.03.006)
44. A. H. Jawad, R. A. Rashid, R. M. A. Mahmuod, M. A. M. Ishak, N. N. Kasim, K. Ismail, *Desalin. Water Treat.* **57** (2016) 8839 (https://doi.org/10.1080/19443994.2015.1026282)
45. N. Nguyen, T. Q. Phan, C. T. Pham, H. Nguyen, S. Pham, Q. K. Nguyen, D. Ngunyen, *J. Serb. Chem. Soc.*. **88** (2023) 423 (https://doi.org/10.2298/JSC220802080N)
46. Z. Y. Velkova, G. K. Kirova, M. S. Stoytcheva, V. K. Gochev, *J. Serb. Chem. Soc.* **83** (2018) 107 (https://doi.org/10.2298/JSC170519093V).